SYNTHESIS AND CHARACTERIZATION OF SMALL MOLECULE CARBON

NANOTUBE FRAGMENTS

by

MATTHEW ROSS GOLDER

A DISSERTATION

Presented to the Department of Chemistry and Biochemistry
and the Graduate School of the University of Oregon
in partial fulfillment of the requirements
for the degree of
Doctor of Philosophy

September 2015

DISSERTATION APPROVAL PAGE

Student: Matthew Ross Golder

Title: Synthesis and Characterization of Small Molecule Carbon Nanotube Fragments

This dissertation has been accepted and approved in partial fulfillment of the requirements for the Doctor of Philosophy degree in the Department of Chemistry and Biochemistry by:

David Tyler   Chairperson
Ramesh Jasti   Advisor
Michael Haley   Core Member
John Halliwill   Institutional Representative

and

Scott L. Pratt   Dean of the Graduate School

Original approval signatures are on file with the University of Oregon Graduate School.

Degree awarded September 2015

DISSERTATION ABSTRACT

Matthew Ross Golder

Doctor of Philosophy

Department of Chemistry and Biochemistry

September 2015

Title: Synthesis and Characterization of Small Molecule Carbon Nanotube Fragments

Cycloparaphenylenes (CPPs) can be considered the smallest possible fragment of an armchair carbon nanotube (CNT), yet they were envisioned as synthetic targets almost 70 years before CNTs were discovered. Having succumbed to total synthesis in the past decade, these strained carbon-rich macrocycles, as described in Chapter **I**, have emerged as both interesting materials for applications in organic electronics as well as promising candidates to seed the "bottom-up" growth of CNTs. Herein I first report methodology that has facilitated the rapid construction of CPPs from simple building blocks as well as the current limitations to access functionalized CPPs with these strategies in Chapter **II**. With the ability to access CPPs in unprecedented quantities, some interesting physical organic properties were revealed through oxidation and subsequent optoelectronic characterization in Chapter **III**. Efforts then turned towards the synthesis of more rigid CNT fragments in Chapters **IV** and **V**, resulting in the synthesis of two [8]CPP dimers, (3,10)-dibenzo[*a,h*]anthracene-nanohoop and (2,11)-dibenzo[*c,m*]pentaphene-nanohoop. Lastly, progress towards [*n*]cyclophenacene, an aromatic belt, is presented.

This dissertation contains both previously published and unpublished co-authored material.

CURRICULUM VITAE

NAME OF AUTHOR: Matthew Ross Golder

GRADUATE AND UNDERGRADUATE SCHOOLS ATTENDED:

University of Oregon, Eugene, Oregon
Boston University, Boston, Massachusetts
University of Rochester, Rochester, New York

DEGREES AWARDED:

Doctor of Philosophy, Chemistry, 2015, University of Oregon
Master of Arts, Chemistry, 2014, Boston University
Bachelor of Science, Chemistry, 2010, University of Rochester

AREAS OF SPECIAL INTEREST:

Organic Synthesis
Physical Organic Chemistry
Organic Materials

PROFESSIONAL EXPERIENCE:

Teaching Fellow, Department of Chemistry, Boston University, Boston,
    Massachusetts, 2011 – 2013

Medicinal Chemistry Intern, GlaxoSmithKline, Waltham, Massachusetts, 2010

Target Biology Intern, Pfizer, Cambridge, Massachusetts, 2008

Research and Development Intern, Millipore, Bedford, Massachusetts, 2007

GRANTS, AWARDS, AND HONORS:

Graduate Research Symposium Speaker, Division of Organic Chemistry, 2014

Vertex Scholar Graduate Fellowship, Boston University, 2013 – 2014

Physical Organic Gordon Research Seminar Speaker, Gordon Conference, 2013

Office of Science Graduate Fellowship Finalist, U.S. Department of Energy, 2012

Feldman Travel Award, Boston University, 2012

Dean's Fellowship, Boston University, 2010 – 2011

Undergraduate Section Award, Rochester ACS Section, 2010

Ayman Amin-Salem Memorial Award, University of Rochester, 2010

RISE Scholar, Deutscher-Akademischer Austausch Dienst, 2009

PUBLICATIONS:

Golder, M. R.; Jasti, R., Synthesis and Characterization of the Smallest Carbon Nanohoops. *Acc. Chem. Res.* **2015**, *48*, 557 – 566.

Chen, H.; Golder, M. R.; Wang, F.; Doorn, S.; Jasti, R.; Tretiak, S.; Swan, A. K., Raman-active Modes of Even-numbered Cycloparaphenylenes: Comparisons between Experiments and DFT Calculations with Group Theory Arguments. *J. Phys. Chem. C* **2015**, *119*, 2879 – 2887.

Adamska, L.; Nayyar, I.; Chen, H.; Oldani, N.; Fernandez-Alberti, S.; Golder, M. R.; Jasti, R.; Doorn, S. K.; Tretiak, S. Self-trapping of Excitons, Violation of Condon Approximation and Efficient Fluorescence in Conjugated Cycloparaphenylenes. *Nano Lett.* **2014**, *14*, 6539 – 6546.

Chen, H.; Golder, M. R.; Wang, F.; Jasti, R.; Swan, A. K., Raman Spectroscopy of Carbon Nanohoops. *Carbon*, **2014**, *67*, 203 – 213.

Golder, M. R.; Wong, B. M.; Jasti, R., Photophysical and Theoretical Investigations of the [8]Cycloparaphenylene Radical Cation and its Charge-Resonance Dimer. *Chem. Sci.* **2013**, *4*, 4285 – 4291.

Cowley, R. E.; Golder, M. R.; Eckert, N. A.; Al-Afyouni, M. H.; Holland, P. L. Mechanism of Catalytic Nitrene Transfer Using Iron(I)-Isocyanide Complexes. *Organometallics*, **2013**, *32*, 5289 – 5298.

Xia, J.; Golder, M. R.; Foster, M. E.; Wong, B. M.; Jasti, R., Synthesis, Characterization, and Computational Studies of Cycloparaphenylene Dimers. *J. Am. Chem. Soc.* **2012**, *134*, 19709 – 19715.

Sisto, T. J.; Golder, M. R.; Hirst, E. S.; Jasti, R., Selective Synthesis of Strained [7]Cycloparaphenylene: An Orange-Emitting Fluorophore. *J. Am. Chem. Soc.* **2011**, *133*, 15800 – 15802.

ACKNOWLEDGMENTS

First and foremost, I must thank my advisor Professor Ramesh Jasti for his guidance, wisdom, and patience over the past five years. After arriving at Boston University in 2010, I was in the second cohort of graduate students to join the Jasti group. Since then, I have had the privilege of watching the seeds that I helped plant alongside the "OGs", Dr. Xia Tian, Dr. Elizabeth Hirst, Dr. Paul Evans, Dr. Thomas Sisto, Han Xiao, and Eric Boon, grow into the group that I am a part of today in Oregon. In the beginning, Ramesh maintained focus by constantly pushing us to be more diligent chemists and thoughtful experimentalists. Joining a young laboratory is never easy, but Ramesh's outlook, support of creative freedom, and pedagogy educated me about what could be accomplished with a true passion for science. I enjoyed the journey and wholeheartedly thank Ramesh for the opportunity to work in his laboratory and for teaching me how to be a synthetic organic chemist. I couldn't imagine flying to a conference in Morocco with any other advisor. In addition, I certainly wouldn't have gotten this far without the early support and training as an undergraduate from my former mentors, Prof. Pat Holland and Dr. Ryan Cowley.

Without my fellow colleagues in the Jasti Group, the past five years would have been excruciatingly bland. In addition to the aforementioned "OGs", thank you to my other newfound friends, Evan Darzi, Penghao Li, and Brittany White, whom I've spent countless hours with in LSEB, Klamath, or anyplace in between over the years. Their companionship, both in and out of the laboratory, is unmatched. I've learned a tremendous amount from all of them about chemistry and beyond. Yes, this includes Paul and Evan's valiant attempts to improve my mediocre knowledge of classic rock.

I am especially indebted to Dr. Jianlong Xia for his experimental guidance, friendship, and selflessness, even after he left the group. I also would like to express my gratitude to the newest members of the Jasti Lab, Dr. Evan Jackson, Jeff Van Raden, and Lisa Eytel, for their enthusiasm and dedication that will undoubtedly take the group into unchartered territory. Finally, I would like to send a special thank you to Brittany and both of the Evans for their assistance in proofreading my dissertation.

In addition to my direct co-workers, I have had the privilege of working with many other talented individuals in different groups at both Boston University and the University of Oregon. In Boston, the Porco laboratory, especially good friends Rob Ziegler and Dr. Alex Grenning, were always available to lend a hand… or some chemicals. Likewise, members of the Stephenson laboratory, Dr. Jagan Narayanam, Dr. Joe Tucker, Dr. John Nguyen, Dr. Bryan Matsuura, Mitch Keylor, and Joel Beatty, were superb scientific colleagues and made for some memorable joint group outings. Since moving to Oregon, the whole Jasti group has been welcomed with open arms by our new neighbors in Klamath and Onyx: the DWJ, Tyler, Pluth, and DeRose labs. In addition, Prof. Mike Haley, along with Gabe Rudebusch, Jon Marshall, Conerd Fredrickson, and Chris Vonnegut, were exceptionally helpful when we first arrived in Eugene and have made for insightful and aromatic-rich joint group meetings. Lastly, I wish to thank Dr. Lev Zakharov for his expertise and ability to collect data on even the most challenging of crystal samples, and Dr. Mike Strain for his constant assistance with NMR spectroscopy.

Finally, thank you to my parents for stimulating curiosity, laying the foundation upon which I have grown intellectually, and inspiring me to constantly explore all that the world has to offer. Their unwavering support prevailed during the past five years.

To my parents

TABLE OF CONTENTS

LIST OF TABLES

LIST OF FIGURES

LIST OF SCHEMES

LIST OF EQUATIONS

CHAPTER I

CYCLOPARAPHENYLENE SYNTHESIS AND CHARACTERIZATION

This chapter is based on a review published in *Accounts of Chemical Research* (February 2015). I wrote the original manuscript as it appears below, notwithstanding edits to shorten the Abstract. Editing was provided by Prof. Ramesh Jasti.

Chapter **II** is based on both published and unpublished work. Dr. Thomas Sisto was involved in **II.2.2** and was a co-author on a publication in *Journal of the American Chemical Society* (September 2011). Dr. Xia Tian, Han Xiao, and Dr. Paul Evans contributed in **II.3** as mentioned. Editing was provided by Prof. Ramesh Jasti.

Chapter **III** is based on published work in *Chemical Science* (August 2013). I performed the experiments and co-author Prof. Bryan Wong (UC Riverside) performed the majority of the computations in this chapter. Editing was provided by Prof. Ramesh Jasti.

Chapter **IV** is based on both published work in *Journal of the American Chemical Society* (November 2012) and unpublished work. Experimental work and TD-DFT computations were performed by co-author Dr. Jianlong Xia and myself. All other calculations were performed co-authors by Dr. Michael Foster (Sandia National Laboratory) and Prof. Bryan Wong (UC Riverside). Dr. Jeffery Bacon (Boston University) conducted the X-ray crystallography analysis. Editing was provided by Prof. Ramesh Jasti.

Chapter **V** is based on unpublished work. Dr. Thomas Sisto and Jessie Zhen (Boston University) provided assistance in the synthesis of starting materials for **V.4.1**. and **V.5**. In **V.5.**, Prof. Bryan Wong (UC Riverside) performed ground-state energy

1

computations and Dr. Lev N. Zakharov conducted the X-ray crystallography analyses. Editing was provided by Prof. Ramesh Jasti.

The design and construction of unique non-natural products have fascinated and perplexed organic chemists for years. Their assembly, akin to what has been accomplished for the total synthesis of natural products, has stretched the limits of what can be prepared in the laboratory. Unlike many natural products, however, carbon-rich structures often lack heteroatoms, further complicating their construction. Amongst the carbon rich structures, geodesic polycyclic aromatics such circulenes, helicenes and fullerenes share common ground due to the distortion of one or more aromatic rings out of planarity. Recently added to this group are the [n]cycloparaphenylenes ([n]CPPs), or "carbon nanohoops". Here, a linear string of benzene rings connected at the para positions is wrapped back upon itself to form a cyclic structure. Clearly a simple planar oligophenylene cannot be cyclized in this manner without extremely harsh reaction conditions. In order to access these structures using solution phase organic chemistry, clever synthetic strategies that can compensate for this severe distortion are required. Herein, we detail the long-awaited synthesis of these challenging macrocycles, which form the framework for the remainder of the dissertation, and the unique properties these nanohoops possess.

I.1. A Historical Account of [*n*]Cycloparaphenylenes

Aesthetically pleasing molecules have long captivated the interests of synthetic chemists.[1] Such targets, often displaying high degrees of symmetry, push the limits of organic synthesis despite their apparent simple structures.[2] In the transformation of complex intermediates into the striking platonic hydrocarbons cubane[3] and dodecahedrane[4] (Figure **I.1**), new boundaries were established for the assembly of molecules with atomic level precision. Like many classical natural products targeted throughout the mid-to-late 1900's,[5-7] these geometric beauties highlighted that our imagination is truly the only limit to what is available *via* organic synthesis.[8] The pursuit of structurally unique, *non-natural* products has driven the discovery of novel reactions and methodology, and perhaps most importantly, opened the door to molecules with new properties.

Several aromatics, prized for their distortion from planarity and targeted by organic chemists, fall into this category as well. The [*n*]cycloparaphenylenes ([*n*]CPPs),[9-11] comprised of benzene rings linked in the para position end-to-end, exemplify the challenges faced when targeting highly strained molecules. Although initially probed in the 1930's (*vide infra*)[12], these perplexing macrocycles did not succumb to total synthesis until recent years[13]. Over 30 years after [*n*]CPPs were first explored, the synthesis of bowl-shaped corannulene,[14-15] which has since been adapted to be both practical and scalable by Scott and Siegel,[16-17] marked yet another milestone. Unbeknownst to scientists at the time both targets would later gain additional accolades as fundamental fragments of carbon nanotubes (CNTs)[18-19] and buckminsterfullerene (C_{60})[20-21], respectively. Interestingly, it was not until the late 1980's and early 1990's, decades after the aforementioned synthetic endeavors, that these carbon allotropes were actually

discovered.[18, 20] Hence, the recent resurgence of these classical structures has been fueled by the prospect of a "bottom-up" organic synthesis of uniform carbon nanostructures (Figure **I.1**).[9-10, 22-29] What started as a quest to stretch the confines of synthesis has led us into a fascinating region of science – the merger of organic synthesis and materials science.[30]

Cubane   Dodecahedrane   Cycloparaphenylene   Corannulene
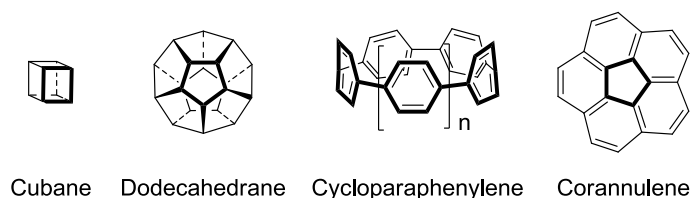
Figure I.1. Challenging hydrocarbons that have been tackled by organic synthesis.

As an initial foray into [n]CPP chemistry, Parekh and Guha first reported the synthesis of macrocyclic p,p'-diphenylenedisulfide **I.1** in 1934.[12] Unfortunately, heating with copper only led to partially desulphurized compounds, rather than the strained target molecule [2]cycloparaphenylene (**I.2**, Scheme **I.1a**). Setting their sights on less strained macrocycles, Vögtle and co-workers proposed several more targets nearly 60 years later.[31] Analogous to the methodology pursued by Parekh and Guha, pyrolysis of aryl sulfide macrocycle **I.3** also failed to furnish any [6]CPP (Scheme **I.1b**). In addition, Vögtle attempted a Cu-mediated Kumada macrocyclization of syn 1,4-diarylcyclohexane **I.4** and a Wittig macrocyclization between diphosphonium **I.5** and dialdehyde **I.6**. While the former reaction only led to polymeric byproducts (Scheme **I.1c**), which has seen been
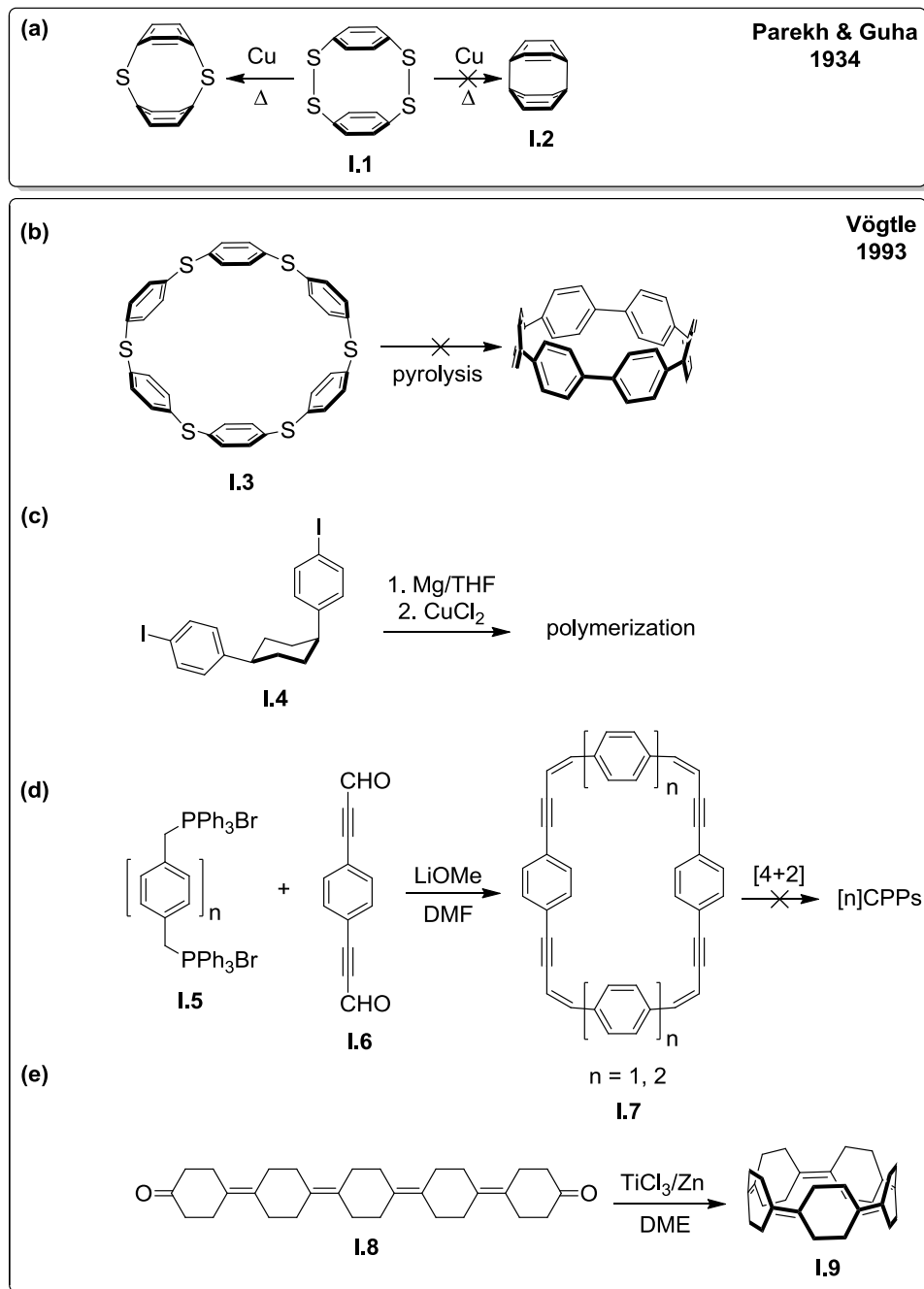
Scheme I.1. Early approaches to cycloparaphenylenes: (a) Parekh and Guha's attempts toward [2]cycloparaphenylene (**I.2**). (b) Attempted pyrolysis of macrocyclic aryl sulfide **I.3** to obtain [6]cycloparaphenylene. (c) Attempted "shotgun" Kumada macrocyclization of diiodide **I.4**. (d) "Shotgun" Wittig macrocyclization reaction followed by failed intermolecular Diels−Alder reaction. (e) Intramolecular McMurry coupling of dione **I.8** to provide trace amounts of macrocycle **I.9**.

5

addressed by the Itami group,[32] the latter afforded the desired ene-yne macrocycle **I.7** (Scheme **I.1d**). Unfortunately, intermolecular Diels-Alder reactions with **I.7** to access [*n*]CPPs were ineffective. Although conversion of **I.8** to [5]CPP precursor **I.9** was detected by mass spectrometry (Scheme **I.1e**)[31], no successful dehydrogenation conditions of **I.9** were reported. Elegant synthetic strategies had been developed to access a "picotube"[33-34] and cyclophenacene[35-36], but as of 2008 the synthesis of the [*n*]cycloparaphenylenes was still an unsolved problem.[37]

With hopes of completing the first successful [*n*]CPP synthesis over 70 years after the seminal attempt, Jasti and Bertozzi targeted macrocycles containing 1,4-syn-dimethoxy-2,5-cyclohexadiene units[38] as masked aromatic rings. Lithium-halogen exchange with diiodobenzene, followed by a two-fold nucleophilic addition reaction with 1,4-benzoquinone (1,4-BQ) allowed for facile construction of syn-cyclohexadiene moiety **I.10**. Borylation of a portion of this material generated the necessary partner **I.11** for the subsequent coupling/macrocyclization. Under Suzuki-Miyuara cross-coupling conditions, macrocycles **I.12 – I.14** were generated, albeit unselectively and in low yields (Scheme **I.2**). As in Vögtle's "shotgun" approach,[31] while intermolecular coupling to form linear oligomeric byproducts dominated, high dilution and the rigid geometry (i.e. fewer degrees of freedom) of the initial "building blocks" resulted in a small amount of desired intramolecular closure. Advantageously, the carbon framework was established in just four steps.

Conversion of macrocycles **I.12 – I.14** to their corresponding cycloparaphenylenes proved challenging due to the high strain energy that needed to be

overcome, as well as the propensity for these systems to undergo molecular

rearrangements. Following precedents for aromatization of similar systems, reductive
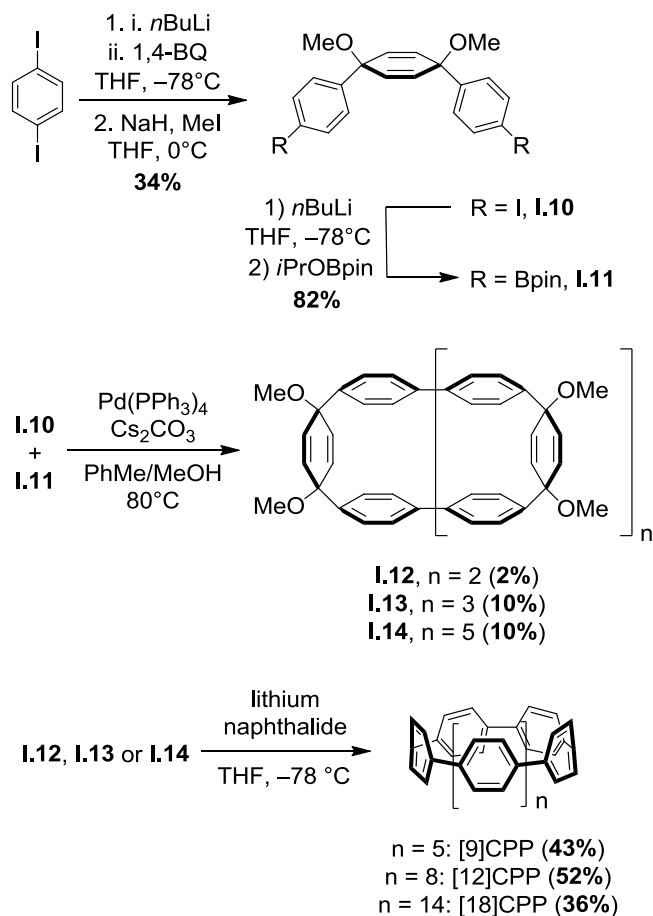
Scheme I.2. Synthesis of [9]-, [12]-, and [18]CPP by Jasti and Bertozzi.

conditions such as Stephen's reagent and low valent titanium were extensively screened

but failed to furnish [*n*]CPPs.[39-40] Under these conditions, carbocation formation (**I.15**)

followed by a rapid concomitant aryl shift to **I.16** ultimately produces undesired meta-

substituted **I.17** (Scheme **I.3**). The formation of [*n*]CPPs was finally achieved in modest

yield by treating **I.12**- **I.14** with lithium naphthalide at $-78\ ^{\circ}$C.[41] Single electron reduction

of a C-O bond to presumably form radical **I.18**, followed by a second reduction event

7

leaves the penultimate intermediate **I.19** in the correct oxidation state for the final

elimination of lithium methoxide. Impressively under these low temperature conditions,

highly strained [9]CPP can be accessed, as well as [12]- and [18]CPP.[13, 42]
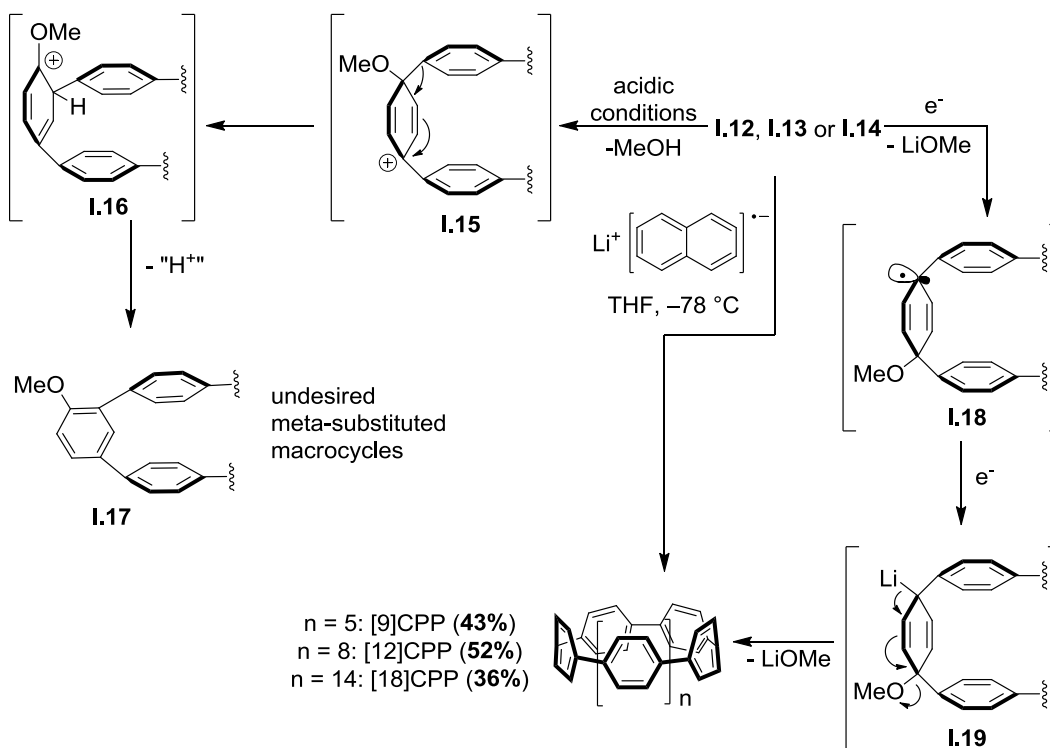
Scheme I.3. Reductive aromatization mechanism and potential decomposition pathway.

With these molecules in hand for the first time, the structures were characterized

using UV-vis and fluorescence spectroscopy. Surprisingly, all three CPPs had virtually

identical absorption maxima, but their fluorescence maxima red-shifted with decreasing

size. Preliminary computational studies indicated that the HOMO-LUMO gap of the

CPPs narrowed with decreasing size, exactly opposite to what is expected for linear *p*-

phenylenes.[43-44] Clearly, the novel architecture of these structures were leading to

optoelectronic properties that were unique, and as of yet, unexplored. Since this pivotal

report in 2008,[13] our group[45-52], as well as the groups of Itami[32, 53] and Yamago[42, 54-55],

have made significant contributions to cycloparaphenylene research. In 2009, the Itami

group reported the first selective synthesis of [12]CPP.[56] Shortly thereafter in 2010,

Yamago synthesized the smallest CPP at the time – [8]CPP.[54] In a follow-up paper,

Yamago and co-workers prepared [8]-[13]CPP characterized these structures

electrochemically.[42] These experimental results corroborated the computations that

indicated smaller CPPs would have narrower HOMO-LUMO gaps. Moreover,

computational results indicated CPPs have narrower band gaps than even the very longest

linear paraphenylenes, rendering them as new motifs in conjugated materials (Figure **I.2**,

left). Dramatic electronic structural changes from benzenoid to quinoid were also

predicted computationally for the smaller CPPs, whereby either [5]-[57] or [6]CPP[43, 58] was

foreseen as the "turning point" (Figure **I.2**, right).
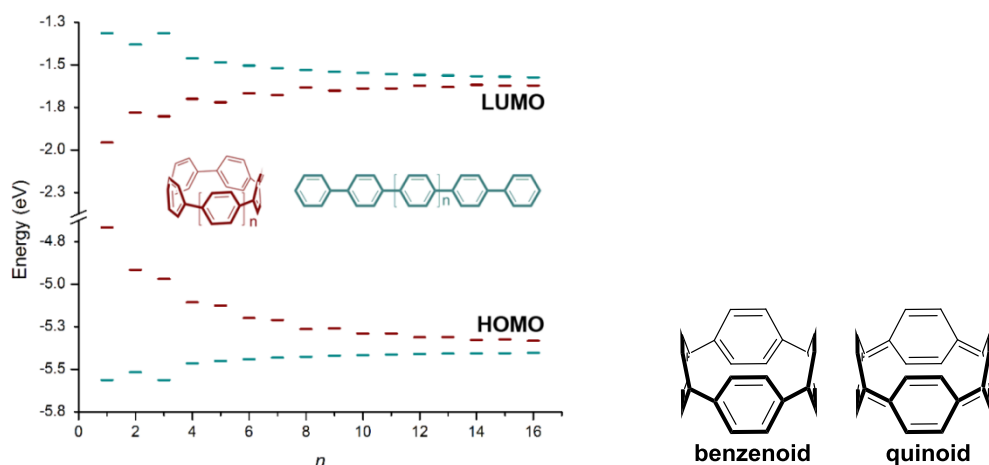
Figure I.2. Left: Calculated HOMO and LUMO levels of cyclic (red) and acyclic (blue) *p*-polyphenylenes (B3LYP/6-31G(d)).[42] Right: Benzenoid and quinoid electronic structures of [4]CPP.

To further explore these hypotheses and glean insight into the behavior of the

smaller [*n*]CPPs, we set out to apply our synthetic prowess towards these challenging

9

macrocyclic targets (Figure **I.3**).[59-60] In particular, [5]–[7]CPPs not only represented

extremely challenging synthetic targets, but also would help address the new phenomena

that was being predicted and observed for these new carbon nanohoops.[45, 48, 52]

[5]CPP	[6]CPP	[7]CPP
119 kcal/mol	97 kcal/mol	83 kcal/mol
Nature Chem.	*Angew. Chem. Int. Ed*	*J. Am. Chem. Soc.*
(2014)	*(2012)*	*(2011)*
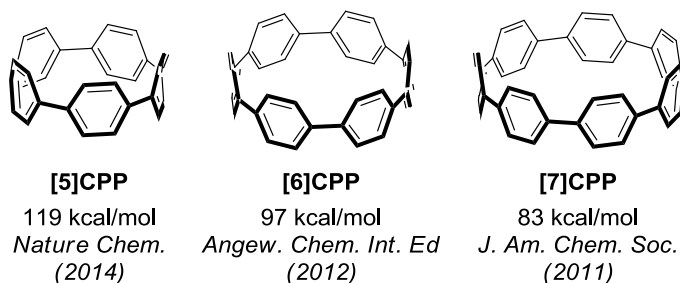
Figure I.3. Strained macrocycles accessed by the Jasti laboratory in recent years.

I.2. [7]Cycloparaphenylene

In order to access [7]CPP, we aimed to incorporate some pivotal aspects of the

original Jasti and Bertozzi synthesis, namely the use of appropriately substituted

cyclohexadiene rings to alleviate strain during a key macrocyclization step and a

reductive aromatization reaction to unveil the hidden aromatic structure in the

cyclohexadiene moieties (Scheme **I.4**). Modification of both the construction and

reactivity of these cyclohexadiene-based monomeric units, however, were essential to our

approach. Beginning with the oxidative dearomatization of biphenyl **I.20** using aqueous

phenyliodine(III) diacetate, quinol **I.21** allowed for the synthesis of unsymmetric

monomeric unit **I.22** via the nucleophilic addition of (4-chlorophenyl)lithium. Unlike the

two-fold nucleophlic additions employed by Jasti in 2008[13], we designed a system that

overwhelmingly favors the *syn* isomer over the *anti* isomer due to electrostatic control of

the incoming, anionic nucleophile.[61] Deprotonation of **I.21** with sodium hydride leads to

excellent diastereoselectivity (>19:1). The origin of the facial selectivity will be extensively discussed in Chapter **II**.

With unsymmetric **I.22** in hand, a portion of the material was borylated *via* lithium-halogen exchange conditions, followed by an (isopropoxy)pinacolborane quench to afford **I.23**. As aryl chlorides do not undergo lithium-halogen exchange under these conditions, the aryl bromide was able to be selectively transformed. After accessing both coupling partners **I.22** and **I.23**, a Suzuki-Miyuara cross-coupling reaction employing Pd(PPh$_3$)$_4$ allowed us to access the advanced dichloride intermediate **I.24**. Importantly, the aryl chlorides remained intact under these catalytic conditions, reinforcing the orthogonality we sought in this synthesis. Switching to a more reactive, electron-deficient catalyst system (Pd-SPhos[62]) allowed for facile oxidative insertion into the aryl chloride bonds, setting us up for the key macrocyclization step with 1,4-benzenediboronic acid bis(pinacol) ester as the coupling partner. Despite only an 8% isolated yield of macrocycle **I.25** upon building in 16 kcal/mol of strain energy, we were finally in a position to test the limits of our reductive aromatization conditions (Scheme **I.4**). To our delight, treatment of **I.25** with sodium naphthalide afforded [7]CPP as an orange solid in 52% yield. Impressively, the reaction was able to build in 67 kcal/mol of strain at −78 °C, allowing us to construct the smallest [*n*]CPP known at the time in 0.72% overall yield from **I.20**.
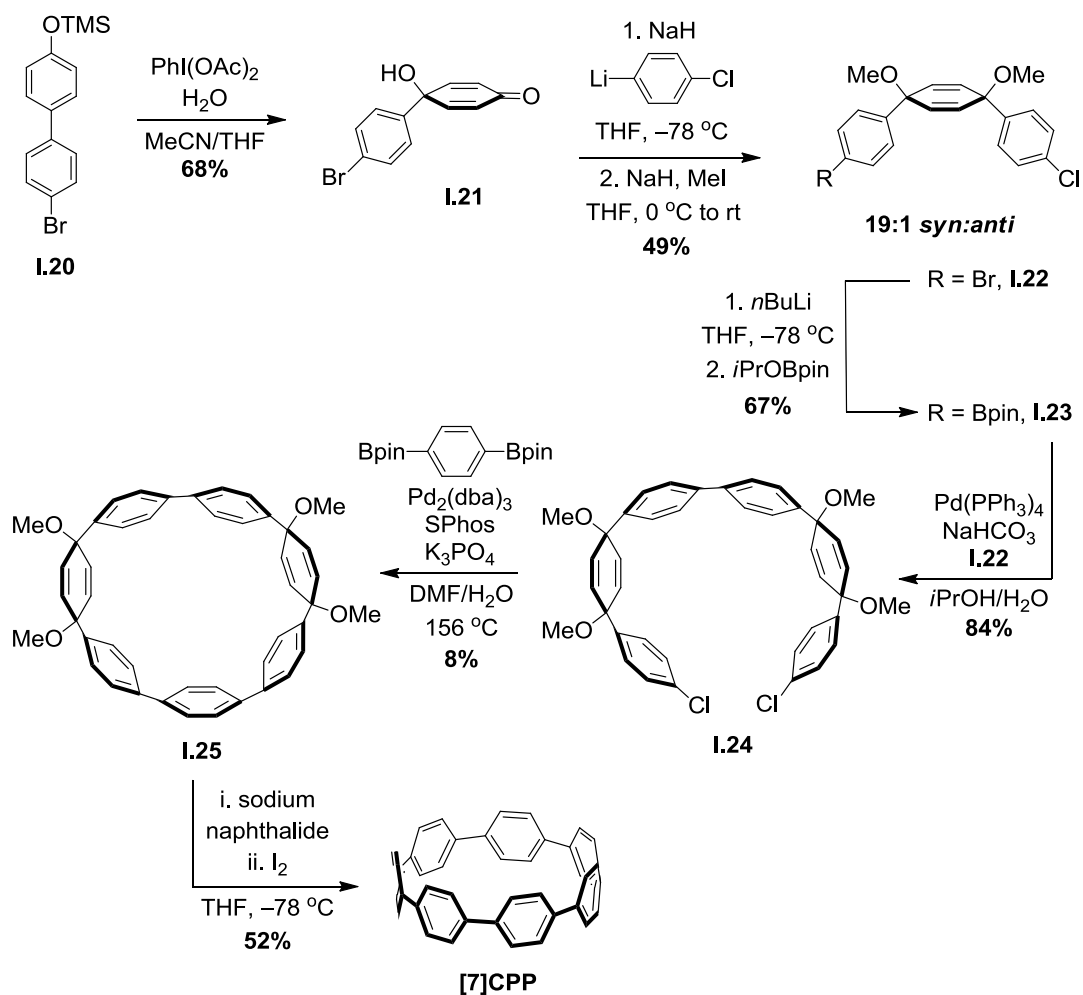
Scheme I.4. Synthesis of [7]cycloparaphenylene.

In accordance with all other [*n*]CPPs, [7]CPP also exhibits a major optical transition at 339 nm due to a combination of HOMO − 1 → LUMO and HOMO → LUMO + 1 transitions. The HOMO → LUMO transition is barely visible with a weak absorption at 410 nm, while the maximum emission shifts to 592 nm. Concurrent with the "red-shifting" emission is a dramatic decrease in quantum yield; [12]CPP has a quantum yield of 0.81, while that of [8]CPP and [7]CPP are 0.10 and 0.007, respectively. Interestingly, despite the decrease in quantum efficiency, [7]- and [8]CPPs have similar

molar extinction coefficients (Figure **I.4**). This dramatic effect on emission wavelength and quantum yield gives experimental support for size-dependent structural changes, such as increased planarization to relieve excited-state strain[63], and electronic effects such as vibronic coupling[64] and exciton localization[65]. Electrochemical measurements in tetrahydrofuran revealed an $E^{1/2}_{ox}$ of 0.53 V (vs. Fc/Fc$^+$) and a $E^{1/2}_{ox}$ and an $E^{1/2}_{red}$ of $-$ 2.57 V (vs. Fc/Fc$^+$),[66] which is consistent with the predicted trend of a narrowing HOMO-LUMO gap with decreasing [n]CPP size[42]. Intrigued with our initial findings, we sought to determine if the syntheses of [6]- and [5]CPPs would shine additional light on these phenomena.
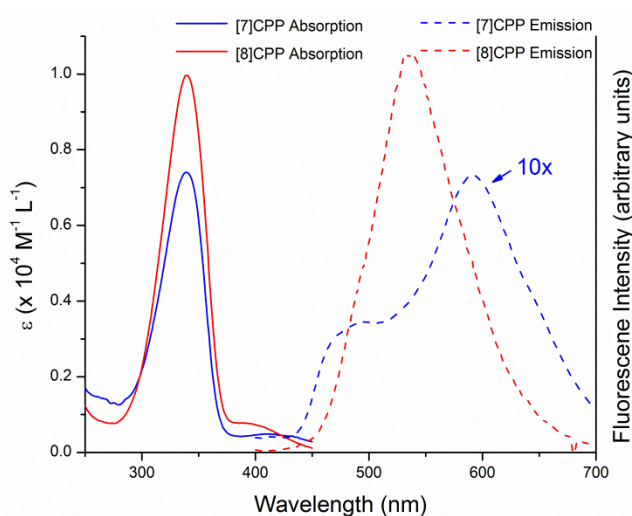
Figure I.4. Absorption and emission spectra of [7]- and [8]CPP. It should be noted that while [7]CPP is a much weaker emitter than [8]CPP, its emission spectrum has been enhanced 10-fold to allow all of the features to be shown at an appropriate scale.

I.3. [6]Cycloparaphenylene

With the synthesis of [7]cycloparaphenylene accomplished, we next set out to test the limits of our synthetic tactics. At the time, no other syntheses of [7]CPP[67], let alone

smaller, more challenging targets, had been reported in the literature. Our initial strategy

towards [6]CPP, encompassing 97 kcal/mol of strain (4.9 kcal/mol per benzene ring

greater than that of [7]CPP)[42, 48] first involved replacing a biphenyl unit with a phenyl

unit in [7]CPP macrocyclic precursor **I.25** (Scheme **I.5**). In doing so, target macrocycle

I.33 appeared, at least at first glance, to be more suitable for the geometric constraints

necessary to access [6]CPP. Thus, our route commenced with a stereoselective addition

of lithiated biphenyl **I.26** to quinol **I.21**. Desilylation of TBS-protected phenol **I.27**,

followed by oxidative dearomatization of **I.28** with aqueous PhI(OAc)$_2$ afforded highly
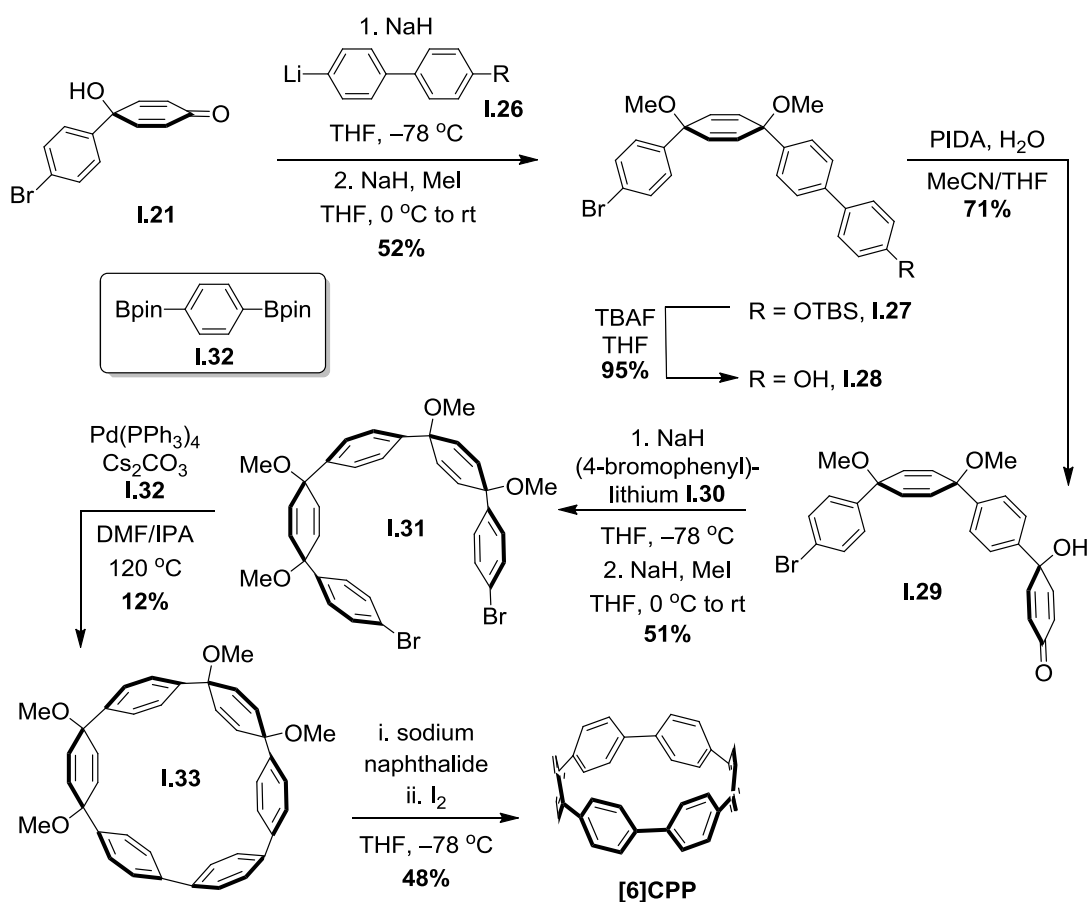
Scheme I.5. Synthesis of [6]cycloparaphenylene.

14

functionalized quinol **I.29**. Subsequent addition of lithiated arene **I.30** led to five-ring

macrocylic precursor **I.31** containing alternating arene and cyclohexadiene units.

Gratifyingly, a Suzuki-Miyaura macrocyclization reaction implementing $Pd(PPh_3)_4$ as a

catalyst and 1,4-benzenediboronic acid bis(pinacol) ester **I.32** as the coupling partner

furnished macrocycle **I.33** in 12% yield. Reductive aromatization of this strained

macrocycle with sodium naphthalide, as in our [7]CPP synthesis, gave the target

cycloparaphenylene as an orange solid in 48% yield. Before addressing the fascinating

properties of [6]CPP, it is worth noting that advanced intermediate **I.31** has become a

staple compound in our laboratory and was recently used for the first gram-scale

syntheses of [8]- and [10]CPPs[47]. In doing so, our lab recently has accessed dimeric[49],

anionic[68] and cationic[51] [8]CPP analogues.

When comparing [6]CPP to larger carbon nanohoops, there are several anomalous

physical features that immediately stand out. Most notably, unlike any of the other

[n]CPPs that were synthesized previously,[50] [6]CPP had no detectable fluorescence. As

[7]CPP showed a dramatic reduction in quantum efficiency, we were not surprised with

the continuing trend and hence the isolation of the first non-emitting cycloparaphenylene.

Our findings were supported by TD-DFT calculations that assigned no oscillator strength

($f = 0$) to the HOMO $\rightarrow$ LUMO transition.[48] The $E^{1/2}_{ox}$ of [6]CPP in dichloromethane

was shown to be 0.44 V (vs. Fc/Fc^+), which followed in accordance with preceding work

suggesting an increasing HOMO level, leading to a more facile oxidation, with

decreasing nanohoop diameter. The single ^{1}H NMR resonance 0.16 ppm *downfield* of

that observed in the case of [7]CPP ($\delta = 7.64$ ppm vs 7.48 ppm) further confirmed

Wong's NICS(1) calculations[43], predicting an increase in quinoidal character (i.e. a

decrease in aromaticity) per individual benzene ring in [n]CPPs smaller than [8]CPP. Intrigued by these solution-state results, we turned our attention to the unique behavior of [6]CPP in the crystalline state.

As in larger [n]CPPs, the average C_{ipso}-C_{ipso} bond adjoining adjacent benzene rings in [6]CPP of 1.490 Å[48] (compared to 1.488 Å in [7]CPP[69] and 1.486 Å in [8]CPP[47]) indicates a benzenoid structure with retained single bond character.[43, 57-59] The crystal packing, however, is completely unprecedented in the [n]CPP literature (Figure **I.5**). While [7]-[10]- and [12]CPPs exhibit herringbone or herringbone-like packing,[47, 69-72] [6]CPP organizes into uniform, tubular cylinders in the solid state. The predisposition for [6]CPP molecules to arrange themselves akin to how one might imagine the self-
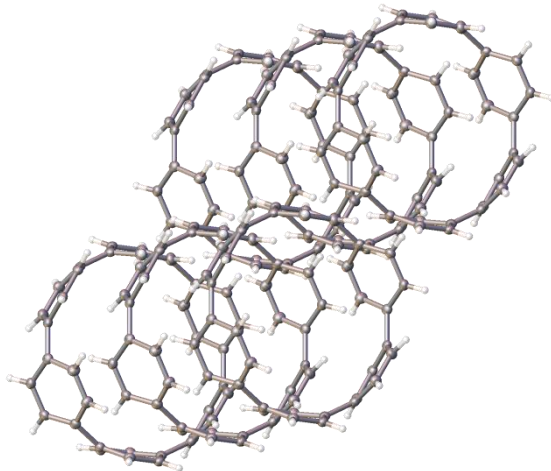
Figure I.5. ORTEP representation of [6]cycloparaphenylene (thermal ellipsoids shown at 50% probability) showing the tubular packing structure of the nanohoops in the solid state.

assembly of a (6,6) armchair CNT bodes well for the "bottom-up" synthesis of homogeneous carbon nanotubes and exploration of [*n*]CPP reactivity in the crystalline state. Furthermore, the uniform channels formed by [6]CPP ought to play a significant role in guest-host applications. We wondered, however, if these features are unique to [6]CPP or if they might be even more pronounced in smaller nanohoops. To assess these questions experimentally, our efforts naturally turned towards the synthesis of [5]CPP.

I.4. [5]Cycloparaphenylene

Our initial foray towards accessing [5]CPP, a target with 119 kcal/mol of strain energy (23.8 kcal/mol per phenyl ring), involved a serendipitous discovery upon repeating our synthetic route of [10]CPP[47]. Isolation of small amounts of a compound with a distinct singlet in its ^{1}H NMR spectrum (δ = 6.00 ppm) along with shifts similar to what was previously observed in other [*n*]CPP macrocyclic precursors prompted us to pursue the identity of this byproduct. Through mass spectrometry and X-ray crystallography, we were astonished to discover that this structure was neither a linear oligomer nor a larger macrocyclic compound, but rather the macrocyclic precursor to [5]CPP, **I.35**. We rationalized its formation through intramolecular boronate homocoupling of **I.34**, a typically undesired oxidative byproduct of Suzuki-Miyuara cross-coupling reactions. In this instance, however, we chose to exploit facile and mild carbon-carbon bond construction methodology[73] to optimize the synthesis of **I.35** *en route* to [5]CPP.

Thus treatment of **I.34**, a precursor in our selective syntheses of [8]- and [10]CPPs that is easily accessed *via* dibromide **I.31**,[47] with potassium fluoride and

bis(triphenylphosphine)palladium(II) dichloride under air at room temperature afforded macrocycle **I.35** in 44% yield on gram scale (Scheme **I.6**). Here we were in a position yet again to test the limits of our reductive aromatization chemistry. To our surprise, treatment of **I.35** at –78 $^{\circ}$C with sodium naphthalide effects reduction to dianion **I.36**, but in this case is unable to undergo two-fold elimination to [5]CPP. We anticipate that there was insufficient energy at this temperature to build in the remaining 87 kcal/mol of strain energy as no more than 67 kcal/mol of strain had previously been overcome using this methodology.[45, 48, 50] Warming above –78 $^{\circ}$C leads to decomposition as evidenced by the precipitation of insoluble, brown material. Clearly having reached the limits of our reductive aromatization reaction, we instead trapped **I.36** with a proton source to give reduced macrocycle **I.37**. Finally, treatment of **I.37** with lithium diisopropylamide (LDA) at room temperature cleanly generated deep red [5]CPP in 69% yield *via* two-fold E1cB elimination (Scheme **I.6**).[52] Yamago and co-workers also recently accessed a similar cyclohexadiene-incorporated macrocycle **I.35** through intramolecular Yamamoto coupling of **I.31**.[74] Using modified reductive aromatization methodology ultimately allowed them to isolate [5]CPP also. Counterintuitively, [5]CPP, the smallest and most strained [*n*]CPP reported to date, is now the easiest carbon nanohoop for our laboratory to access, offering mild macrocyclization conditions without exclusion of oxygen and no steps that require heating above room temperature.
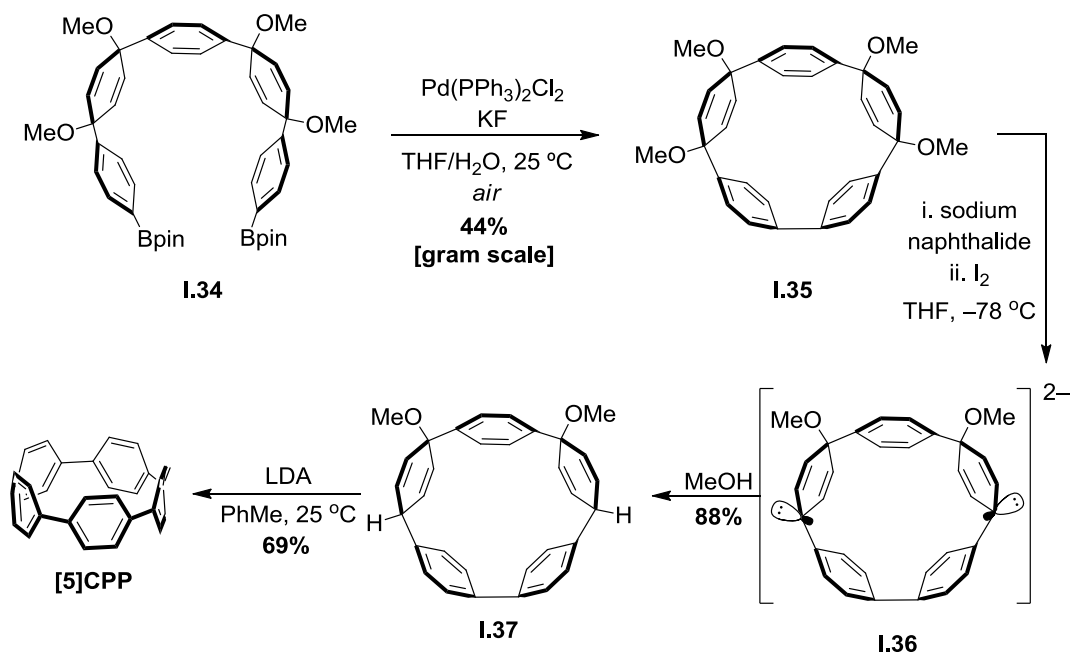
Scheme I.6. Synthesis of [5]cycloparaphenylene.

Upon analysis of [5]CPP's solid state structure[52] (Figure **I.6**), we were surprised to find that [5]CPP does not pack into uniform cylinders as [6]CPP does. Rather, it adopts the herringbone packing structure observed for other reported [*n*]CPPs (*n* = 7-10, 12),[47, 70-72] further piquing our curiosity about [6]CPP's unique behavior. Compared to the structure of [6]CPP, what truly stood out was the increased amount of distortion experienced by each benzene ring throughout the nanohoop (Table **I.1**). The *para* carbons at each tertiary center are displaced by an average of 15.6^o from planarity, which is

19
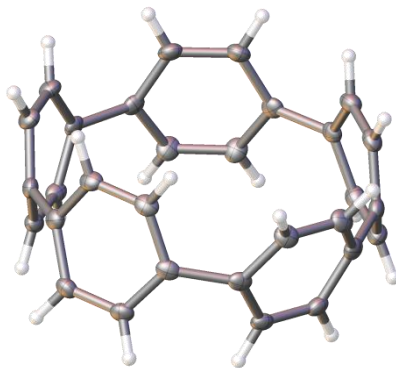
Figure I.6. ORTEP representation (thermal ellipsoids shown at 50% probability) of [5]cycloparaphenylene.

more than the lone bent aromatic ring encountered in several natural products.[52, 75-76] The

distortion found in the benzene rings of [5]CPP are trumped, however, by the single

phenyl ring of several paracyclophanes[77-79] and the pyrene moieties of

Table I.1. Deviations of benzene rings from planarity (α) seen in various organic targets as determined by crystal structure analysis.

Molecule	α (deg)
cavicularin[76]	7.9
[6]CPP[48]	12.7
haouamine A[75]	13.6
[5]CPP[52]	15.6
3-carboxy[7]paracyclophane[78]	16.8
8-carboxy[6]paracyclophane[77]	20.5
substituted [1.1]paracyclophane[79]	25

[9](2,7)pyrenophanes and 1,7-dioxa[7](2,7)pyreneophanes[80-81]. In addition, several other cyclophanes have been predicted computationally to have highly distorted aromatic rings, though the crystal structures of these compounds have not been obtained.[82-83]

The outstanding solubility of [5]CPP compared to that of other cycloparaphenylenes permitted extensive solution-state characterization, providing initial insight to the newest member of the [n]CPP family. As was observed in the case of [6]CPP, the ^{1}H NMR spectrum for [5]CPP also shows a single resonance, which is consistent with free rotation or wobbling of the phenyl rings on the NMR timescale. Furthermore, the shift of [5]CPP (δ = 7.86 ppm) is 0.24 ppm downfield from that observed for [6]CPP (δ = 7.64 ppm), giving further experimental evidence for the decrease in aromaticity seen with the smaller cycloparaphenylenes.[43] Electrochemical analysis in tetrahydrofuran revealed two quasi-reversible single-electron oxidation and reduction events ($E^{ox}_{1/2}$ = 0.25 V, 0.46 V vs Fc/Fc$^+$; $E^{red}_{1/2}$ = -2.27 V, 2.55 V vs Fc/Fc$^+$), rendering it the easiest [n]CPP to oxidize and reduce. [5]CPP is the first nanohoop that, under the experimental electrochemical conditions, showed a second oxidation wave in the solvent window. The narrowing HOMO-LUMO gap is consistent with computational data[42] and is made even more evident by the weak absorption at 502 nm. This absorption, approximately 25 nm lower in energy than that of [6]CPP,[48] again has a small oscillator strength and is responsible for [5]CPP not having any visible fluorescence. While the HOMO $\rightarrow$ LUMO transition has negligible oscillator strength for all sizes of [n]CPPs, the larger sizes are suggested to have higher quantum yields due to symmetry breaking in the excited state.[65] When [5]CPP is put side-by-side with [6]-[8]CPPs, the red shifted, visible absorption of the smaller CPPs becomes quite apparent (Figure **I.7**, left).

21

Additionally, their diminishing quantum yields are obvious under ultraviolet irradiation at 365 nm (Figure **I.7**, right). With the ability to rapidly advance the synthesis and characterization of these highly strained, hydrocarbon macrocycles, a provocative question is whether [4]CPP is accessible *via* organic synthesis.

	[5]CPP	[6]CPP	[7]CPP	[8]CPP
λ_{max} =	335 nm	338 nm	339 nm	340 nm
$E^{ox}_{1/2}$ =	0.25 V, 0.46 V	0.44 V	0.53 V	0.59 V
$E^{red}_{1/2}$ =	−2.27 V, −2.55 V	not reported	−2.57 V	not reported
$^1H\ \delta$ =	7.86 ppm	7.64 ppm	7.48 ppm	7.48 ppm
Strain/phenyl ring =	23.8 kcal/mol	16.2 kcal/mol	11.9 kcal/mol	9.18 kcal/mol
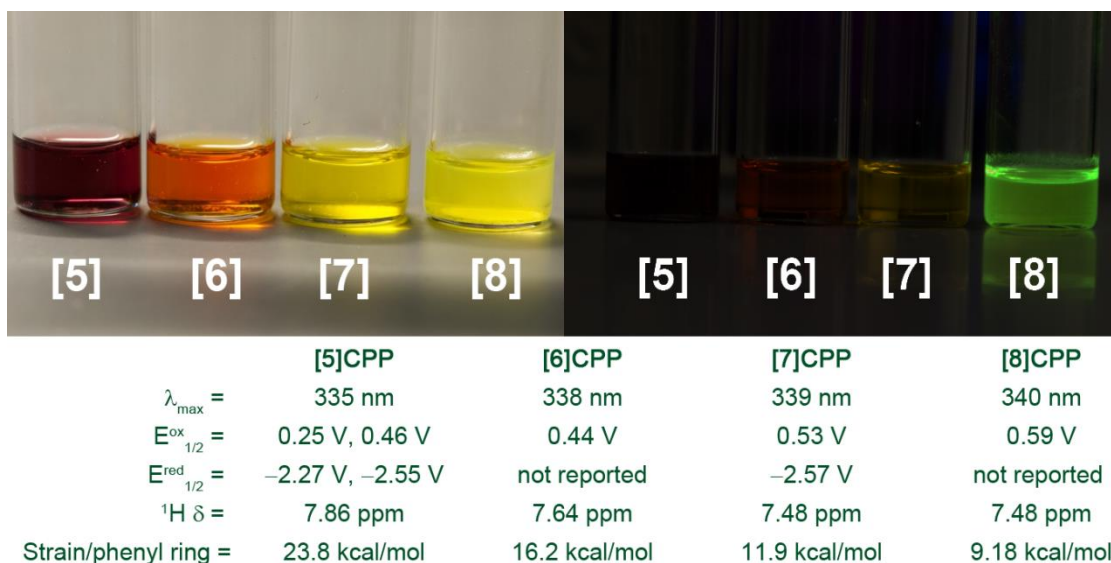
Figure I.7. [5]-[8]CPP under (left) ambient light and (right) UV irradiation (340 nm), along with a summary of selected data.[42, 45, 48-49, 66]

I.5. Conclusion

In this chapter, the Jasti laboratory's strategies to access [5]–[7]CPPs have been discussed from a historical standpoint. By tackling these organic structures as synthetic chemists, we have developed strategies to overcome tremendous amounts of molecular strain, leaving us with startlingly distorted benzene rings strung together systematically in a nanohoop. Alongside cubane, dodecahedrane and corannulene, now these small [*n*]CPPs can be added to the family of fascinating carbon-rich structures that have

succumbed to total synthesis. Aside from their prospect to function as templates for the

rational, "bottom-up" synthesis of homogeneous armchair carbon nanotubes,[25, 84-86] much

promise lies in their ability to function as stand-alone materials. With fascinating size-

dependent optoelectronic properties, reports of the implementation of

cycloparaphenylenes as organic semiconductors and sensors will surely follow. In

addition, their radially oriented pi-orbitals make them ideal candidates for applications in

a multitude of supramolecular interactions.[47, 87]

I.6. Bridge to Chapter II

Central to the Jasti laboratory's approach to synthesize the aforementioned

[*n*]CPPs is the concept of rationally constructing synthetic fragments containing 1,4-syn-

dimethoxy-2,5-cyclohexadiene moieties with predictable diastereoselectivities. In this

chapter, we briefly introduced this strategy as it related to the synthesis of [7]CPP. In

Chapter **II**, we revisit and elaborate on this concept, allowing for the exploration of an

electrostatic model to rationalize the facial selectivity when adding aryl nucleophiles to

4,4-disubstituted 2,5-cyclohexadienones. In addition, this motif is expanded to address

more complicated cases where the nucleophile and/or the dienone have functionality. The

implications of functionality on the stereochemical outcome of this class of reactions will

be the subject of Chapter **II** in an attempt to synthesize highly derivatized

cycloparaphenylenes.

CHAPTER II

DIASTEREOSELECTIVE ADDITION OF ARYL NUCLEOPHILES TO 4,4'-

DISUBSTITUTED 2,5-DIENONES

This chapter is based on both published and unpublished work. As mentioned

below, Dr. Thomas Sisto was involved in **II.2.2** and was a co-author on a publication in

Journal of the American Chemical Society (September 2011). Dr. Xia Tian, Han Xiao,

and Dr. Paul Evans contributed in **II.3**. Dr. Lev N. Zakharov collected the X-ray

crystallographic data. Editing was provided by Prof. Ramesh Jasti.

The synthesis of [*n*]cycloparaphenylenes in the Jasti laboratory has relied heavily

on construction 1,4-syn-dimethoxycyclohexa-2,5-dienes. These systems act as masked,

oxidized terphenyl units, which can be fully aromatized under reducing conditions.

Although they have been previously synthesized via the two-fold nucleophilic addition of

aryl lithium reagents to *p*-benzoquinone, we sought more efficient methods to generate

1,4-syn-dimethoxycyclohexa-2,5-dienes, as well as techniques that would allow for

unsymmetric systems to be made. Herein, we present the underlying physical organic

principles governing diastereoselective additions to 4,4-disubstituted 2,5-

cyclohexadienones, as well as the direct implications in attempting to synthesize

functionalized 1,4-syn-dimethoxycyclohexa-2,5-dienes.

II.1. Background

Despite advances allowing for the stereoselective addition of nucleophiles to

acyclic carbonyls[1-3] less is known about the origin of selectivity for additions to cyclic

conjugated ketones.[4] Of particular interest to the Jasti laboratory are diastereoselective additions of aryl nucleophiles to 4,4-disubstituted 2,5-cyclohexadienones to form 1,4-dihydroxycyclohexa-2,5-diene systems, which are the formal addition products of a two-fold nucleophilic addition to *p*-benzoquinone (Scheme **I.2**). Related studies by Liotta and co-workers[5-6] provided precedence for controlling the facial selectivity of 1,4-addition to *in situ* generated quinol alkoxides (Scheme **II.1**). Addition of methylmagnesium chloride to **II.1** afforded **II.2**, where the Grignard reagent was directed to the same face as the alkoxide.[5] Substituting a more basic (and coordinatively saturated) organocuprate for the Grignard reagent left one face of the quinol electrostatically shielded, forcing the incoming nucleophile to add in a 1,4 fashion from the opposite face, affording the opposite diastereomer **II.3**[6].
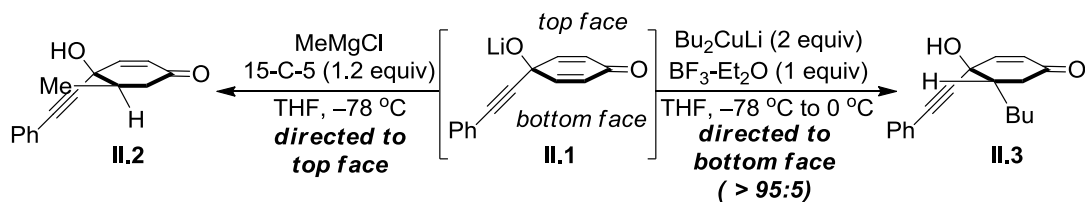
Scheme II.1. Diasereoselective 1,4-additions to *p*-quinol **II.1** controlled by electrostatics.

Wipf and co-workers then used the latter findings from the Liotta group to control facial selectivity of 1,2-additions to 4,4-disubstituted 2,5-cyclohexadienones.[4, 7] They initially observed a stark difference in facial selectivity for a variety of 4-alkoxy and 4-aceyloxy substituted *p*-quinols (Figure **II.1**). In almost all of the cases studied, anti addition that positioned the nucleophile on the face opposite the polar substituent dominated.

25

syn:anti ratio with MeMgBr	4.8:1	8.6:1	10.1:1	17.7:1	32:1
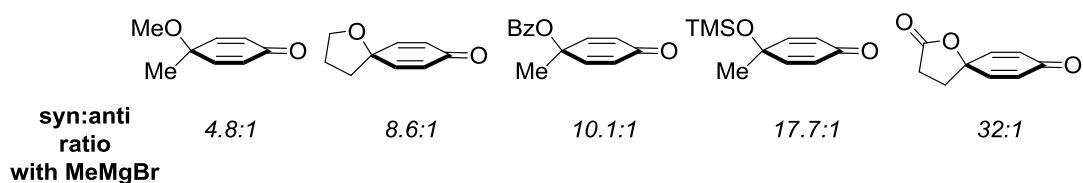
Figure II.1. Facial selectivity for the syn diastereomer increases with larger dipole moments.

Two models were initially considered, but neither one accounted for both the facial selectivity and the dramatic differences in diastereomeric ratios between the different substrates. A modified Anh-Eisenstein model would actually predict preference for addition to the same face as the polar 4-alkoxy or 4-aceyloxy substituent due to favorable overlap between the forming σ_{Nu-C} bond and the σ^{*}_{C-O} of the polar group. While this model can discern between 4-alkoxy and 4-aceyloxy substituents, again it fails to predict the correct facial selectivity (Figure **II.2**). A modified Cieplak effect where donation of the 4-alkyl or 4-aryl σ_{C-C} stabilizes the antiperiplanar σ^{*} of the forming Nu-C bond. Despite explaining the correct facial selectivity, changing the polar substituent should not dramatically affect the donation ability of σ_{C-C} (Figure **II.2**). Thus, this model too fails to completely explain the observed experimental results.[4]

vinylogous Anh-Eisenstein model
(*predicts top face addition*)

vinylogous Cieplak model
(*predicts bottom face addition*)
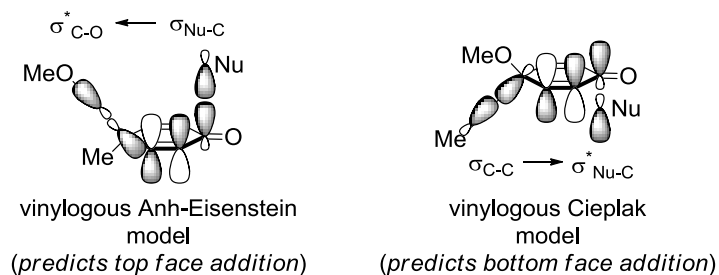
Figure II.2. Neither model accurately predicts the stereoselectivity of 1,2-additions to 4,4-disubstituted 2,5-cyclohexadienones.

The Wipf group then turned to an inherent difference between their 4,4-disubstituted 2,5-cyclohexadienones: dipole moment. As in Liotta's previous examples, electrostatics alone can dramatically bias the facial selectivity of dienone addition reactions. The dipole moments for a subset of the dienones studied were determined computationally, and a linear relationship was found between the logarithim of the diastereomeric ratio and the computed dipole (μ).[7] With this "dipole effect" (Figure **II.3**) model in hand, increasing amounts of the desired syn addition product (with respect to the 4-alkyl substituent) could be obtained by increasing the dipole moment of the polar group.
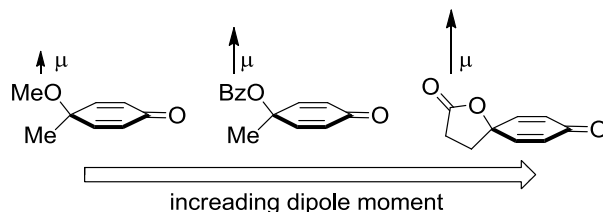
Figure II.3. 4,4-disubstituted 2,5-cyclohexadienones with larger dipole moments led to increasing amounts of the syn 1,2-addition product.

II.2. Development of an Electrostatic Model for 1,4-Addition to Dienones

Following work from the Liotta and Wipf laboratories, we speculated that it might be possible to combine the two previously discussed methods to impart facial selectivity for 1,4 dieneone additions of aryl lithium reagents by slowing down the rate of addition to one face of the ketone. While 1,4-syn-dimethoxycyclohexa-2,5-diene systems can be synthesized in two steps from *p*-benzoquinone, the yields and diastereoselectivity are both poor.[8] In addition, this method does not allow access to unsymmetrical systems

where the two aromatic rings bear different substituents. We envisioned a stepwise

addition procedure that would address all three of these issues.

II.2.1. Synthesis of 1,4-syn-dimethoxycyclohexa-2,5-dienes

Bromoquinol **II.4** was used as the primary substrates for our initial studies

(Scheme **II.2**). We hypothesized that we would obtain excellent diastereocontrol by first

deprotonating *p*-quinol **II.4** with a base to afford a metal alkoxide. Cooling a solution of

II.4 to –78°C, followed by addition of either NaH or KHMDS then one equivalent of (4-

bromophenyl)lithium gave a 1:1 mixture of **II.4** and diol **II.5**[8], even after prolonged

reaction time (Scheme **II.2**). Warming the reaction slowly to room temperature did not

afford additional product and just lead to an intractable mixture of decomposed material.[*]

Clearly, only a portion of the (4-bromophenyl)lithium reagent was reacting with **II.4**,

causing the reaction to stall at ~50% conversion.
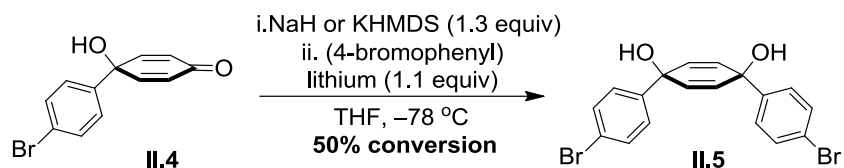
Scheme II.2. Attempted diastereoselective synthesis of diol **II.5**. In the absence of excess
aryl lithium reagent, only 50% conversion is observed to **II.5**.

Gratifyingly, when we simply used excess (4-bromophenyl)lithium (2.4 equiv),

we observed complete consumption of starting material, as well as a good diastereomeric

ratio (syn:anti = 10:1). Our facial selectivity improved (syn:anti = 19:1) by employing

NaH as a base, presumably due to the presence of an even more ionic bond (NaO > LiO)

---

[*] Attempts to deprotonate quinol **II.4** at 0 °C also led to an untraceable mixture of decomposed material.

(Scheme **II.3**). Decreasing the electrostatic effect further by methylating the alcohol of

II.4 before addition of (4-bromophenyl)lithium caused the diastereometric ratio to drop

precipitously (syn:anti = 3:1).[9]
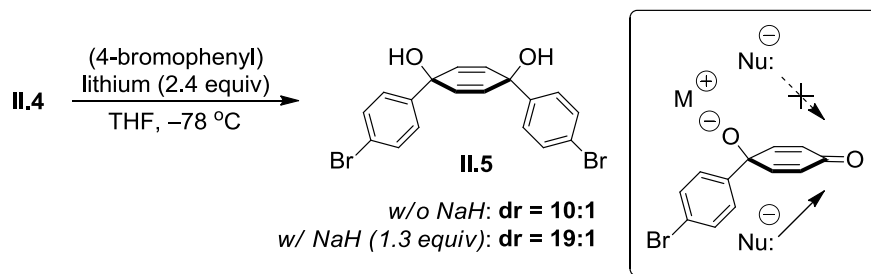
Scheme II.3. Diastereoselective synthesis of **II.5** under electrostatic control. This model (inset) can explain the observed diastereomeric ratios for addition of aryl lithium reagents to **II.4**.

These results are indeed consistent with an electrostatic model where the

stereoselectivity of the addition reaction is highly dependent on the strength of the

negative charge on one face of the dienone (Scheme **II.3**, inset). It is still unclear,

however, what the actual role of sodium hydride is in the reaction. One would expect that

NaH (1.3 equiv) should fully deprotonate the tertiary alcohol of **II.4**. If the alcohol was

fully deprotonated by sodium hydride, full conversion to **II.5** ought to have been

observed upon the addition of aryl lithium (1.0 equiv). That was not the case, however,

and excess aryl lithium (2.4 equiv) was necessary to drive the formation of diol **II.5** to

completion. We found it interesting that one equivalent of aryl lithium led to any

conversion at all. If the sodium hydride was simply a spectator in the reaction and the

tertiary alcohol was simply quenching the aryl lithium reagent, we would expect

quantitative recovery of quinol **II.4**. Instead, the situation appears to be more

complicated, as the addition of one equivalent of aryl lithium to **II.4** leads to 50%

conversion. Additional studies are required to fully understand this process.

II.2.2. Utility in the Total Synthesis of [7]Cycloparaphenylene

      With the ability to begin with **II.4** and add any (4-halophenyl)lithium reagent

diastereoselectively, we chose to apply this methodology towards the synthesis of [7]CPP

II.7. Specifically, stereoselective addition of (4-chlorophenyl)lithium to **II.4**, followed by

methylation afforded unsymmetric 1,4-syn-dimethoxycyclohexa-2,5-diene **II.6** in good

yield (49%) and excellent diastereoselectivity (syn:anti = 19:1). This easily accessible

intermediate was then elaborated further by Dr. Thomas Sisto to deliver [7]CPP **II.7** in an

additional four steps (2.3% yield from **II.6**) (Schemes **I.4** and **II.4**). At the time of

synthesis, [7]CPP **II.7** was the smallest and most strained member of the [n]CPP family.[9]
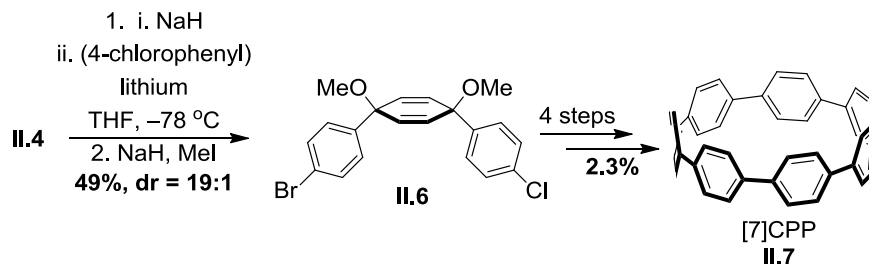
Scheme II.4. A general synthetic route to [7]CPP **II.7** taking advantage of a dipole controlled diastereoselective addition to **II.4**.

Since then, this methodology to construct 1,4-syn-dimethoxycyclohexa-2,5-dienes has

been exploited by our laboratory to synthesize both [5][10]- and [6]CPP[11], as well as [8] –

[12]CPP[12], as previously discussed in Chapter **I**.

II.3. Selectivity of Aryl Lithium Nucleophiles to Larger Quinones

While the two-fold nucleophilic addition of (4-halophenyl)lithium reagents to *p*-benzoquinone allowed facile access to the desired syn diastereomer for Jasti and Bertozzi's seminal syntheses of [9]-, [12]-, and [18]CPP,[8] a compilation of results from our own laboratory and the Itami laboratory shows that the general stereochemical outcome of this type of reaction is highly dependent on both the substitution patterns of both the quinone fragment and the nucleophile. Han Xiao showed that addition of (4-bromophenyl)lithium to 9,10-anthraquinone gives the syn diastereomer (**II.8**, Figure **II.4**). However, Dr. Xia Tian showed that increasing the substitution on the aryl lithium species by substituting (4-bromonaphthyl)lithium for (4-bromophenyl)lithium afforded the anti diastereomer (**II.9**) as the only isolable compound. Interestingly, using the same nucleophile as Dr. Xia Tian, the Itami laboratory switched 9,10-anthraquinone to 1,4-napthaquinone and obtained the desired syn diastereomer (syn:anti = 3:1) as confirmed by X-ray crystallographic analysis (**II.10**) .[13] Lastly, Dr. Paul Evans attempted the two-fold addition of (4-bromo-2,5-dimethylphenyl)lithium to 2,5-dimethyl-1,4-benzoquinone and obtained the anti diastereomer (**II.11**) as confirmed by X-ray crystallographic analysis. Although it is still unclear how particular combinations of quinone and aryl lithium components dictate the observed diastereoselectivities, this is all that was known about additions to more complex quinones at the time as we embarked on the problems presented below in Chapter **II.4**.

31
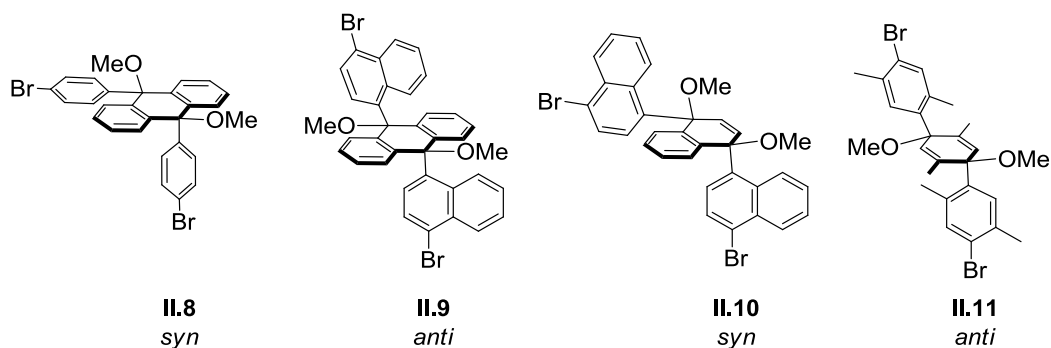
Figure II.4. Various examples of products from the two-fold addition of aryl lithium reagents to substituted quinones from our group and the Itami laboratory.

II.4. Effects of Nucleophile Substitution on Facial Selectivity to Functionalized Dienones

In order to explore the synthesis of derivatized cycloparaphenylenes, we were intrigued by the possibility of adding functionality to both the cyclohexadiene component and the aryl components of our 1,4-dimethoxycyclohexa-2,5-diene systems. To begin, we imagined olefins as simple, yet versatile handles that could easily be installed through allylation reactions. Ostensibly, we could begin with a prefunctionalized quinone monoketal and a prefunctionalized 1,4-dibromoarene and employ our newfound methodology to rapidly access highly functionalized 1,4-syn-dimethoxycyclohexa-2,5-dienes. To access the necessary substituted quinone monoketal **II.14**, we synthesized **II.12** via allylation and two-fold Claisen rearrangement of hydroquinone (Scheme **II.5**).[14-15] Monomethylation was affected with catalytic sodium nitrite in acidic methanol to afford **II.13** in 52% yield.[16] Interestingly, while small amounts of the corresponding quinone ($< 10\%$) were formed during the reaction, presumably due to the competing oxidation of **II.12** with NO_2,[17] the diether was never observed. Initial mechanistic studies suggest that the hydroquinone is oxidized to a reactive, acidic semiquinone that is capable

32

of being alkylated, while the monoalkylated product is more basic and less reactive.[16]

Oxidative dearomatization of **II.13** in methanol then delivered ketal **II.14** 67% yield.
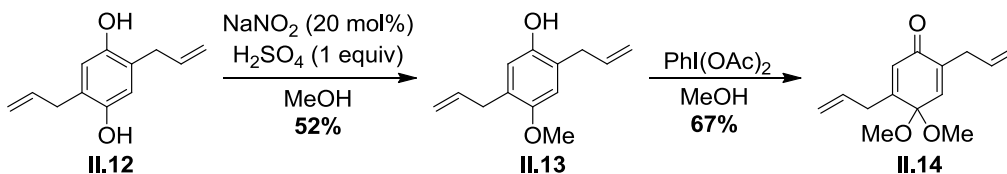
Scheme II.5. Synthesis of ketal **II.14** via monoalkylation and oxidation of **II.12**.

To synthesize the necessary arene component, two-fold benzylic bromination of 1,4-dibromo-*p*-xylene[18] afforded **II.15**, which then underwent a two-fold copper-mediated Kumada coupling with vinylmagnesium chloride at the benzylic positions to deliver **II.16** in 43% yield . Lithium-halogen exchange of **II.16** with *n*BuLi (**II.17**), followed by quenching with either **II.14** or **II.14**/MeI afforded **II.18** and **II.19**, respectively, after ketal deprotection (Scheme **II.6**).
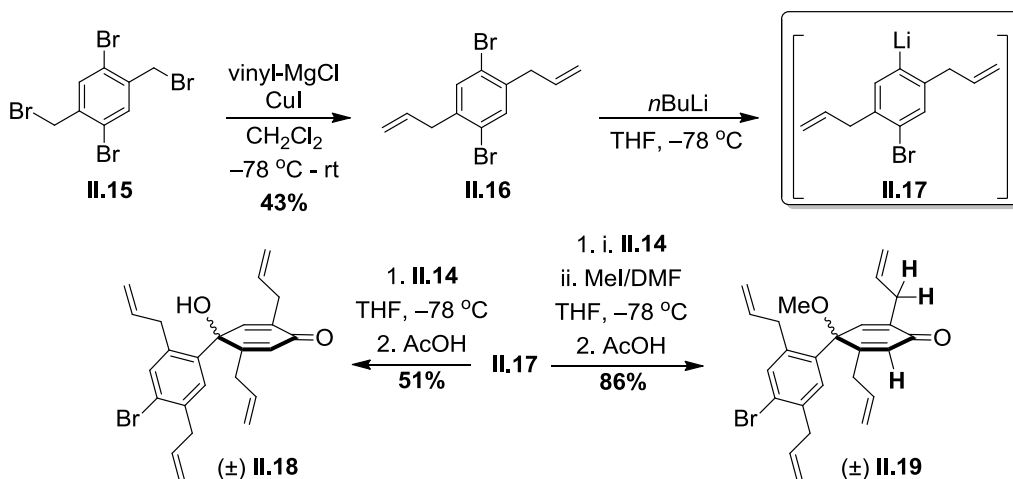
Scheme II.6. Synthesis of tetra-allylated ketones **II.18** and **II.19** from aryl lithium **II.17**.

33

We immediately noticed that both **II.18** and **II.19** exhibited extremely broad resonances in their ^{1}H NMR spectrum at room temperature. Many of these resonances sharpened at 70 °C, and we attribute this dynamic behavior to a rare form of atropisomerism between sp^2-sp^3 hybridized carbons.[19-21] For example, at room temperature we observed broadening of the more downfield aromatic singlet of **II.19**, which is presumably the hydrogen closest to the quaternary center (Figure **II.5**). Surprisingly, however, the broadened allylic sp^3 hydrogens and broadened sp^2 olefinic hydrogen on the cyclohexadiene ring (Scheme **II.6**, shown in bold) are located closest to the carbonyl group, as determined by ^{1}H-^{13}C HMBC NMR experiments on related analog **II.26** (Figure **II.6**), as well as ^{1}H-^{1}H COSY NMR experiments of **II.19** (Figure **II.7**). Specifically, we determined the carbonyl ^{13}C resonance (184.8 ppm) has a cross-peak with the more upfield vinyl ^{1}H resonance and the quaternary carbon ^{13}C resonance (77.5 ppm) has a cross-peak with the more downfield vinyl ^{1}H resonance. In general, the substituted to 4,4-disubstituted 2,5-cyclohexadienones discussed thus far, as well as the ones addressed in the remainder of Chapter **II**, behaved similarly on the NMR timescale. Figures **II.5** – **II.7** serve as representative examples for these class of compounds at both room temperature and 70 °C.

Unfortunately, addition of aryl lithium **II.17** to quinol **II.18** (after treatment with sodium hydride) led to rapid decomposition (Scheme **II.7**). On the other hand, methylated quinol **II.19** allowed for clean addition of **II.17** (60% yield, albeit with a reversal of diastereoselectivity (anti/syn > 19:1) as predicted by our electrostatic model (Scheme **II.3**, inset).

34
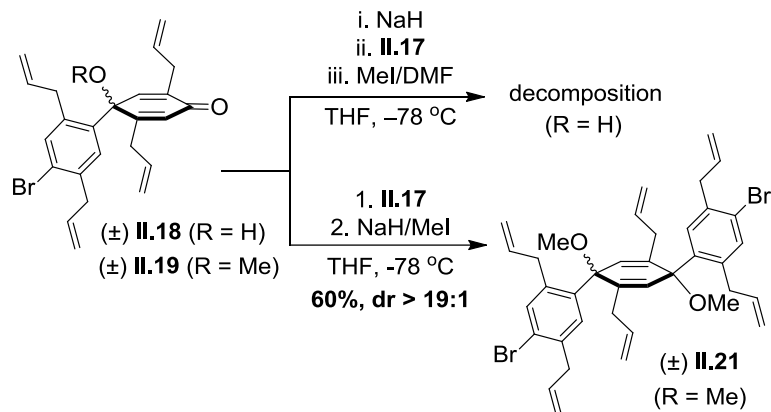
Scheme II.7. Two approaches towards the synthesis of **II.21**. Rates of nucleophilic addition were competitive with decomposition (R = H) unless the dipole moment of the electrophile was diminished via methylation (R = Me).

We rationalized these results with both electrostatic and steric arguments. In the case of quinol **II.18**, addition to the top face (leading to the anti addition product) is slow due to the large dipole from the latent sodium alkoxide. Addition to the bottom face, however, may also be slow due to the sterics imposed by the appended aromatic ring. Regardless of the ring conformation, one of the allyl groups will lie directly underneath the bottom face of the ketone (assuming that the phenyl ring bisects the cyclohexadiene ring). Hence, addition to either face becomes slower than unfavorable pathways, such as decomposition via allylic deprotonation (pK_a ~33 for allylbenzene[22]) by the aryl lithium reagent. On the other hand, methylation of the alcohol (**II.19**) minimizes the electrostatic effect and increases the rate of addition to the top face, while addition to the bottom face remains slow, resulting in sole addition to afford the anti product (Figure **II.10**). This result is consistent with adduct **II.11** that was synthesized by Dr. Paul Evans.

Probing the dominant conformations of **II.18** and **II.19** with low temperature NOE experiments were unfortunately unsuccessful and did not provide us with any additional insight to the orientation of the aryl ring with respect to the cyclohexadiene ring. Cooling to −40 °C, however, did lead to sharpening of the ^{1}H NMR resonances for dienones **II.18** and **II.19**, suggestive of a major conformation being adopted at lower temperatures (for **II.19**, Figure **II.8**). Since the dienones discussed in this section were introduced to the aryl lithium species at room temperature, rather than at −78 °C, multiple conformations could have been present under the actual reaction conditions. In the future, it may be useful to precool the ketones to −78 °C, although there is the obvious possibility that the dominant atropisomer may not improve the status quo.

To study the effect of nucleophile substitution on facial selectivity, (4-bromophenyl)lithium was added to methylated quinol **II.19** and TMS-protected quinol **II.22** (Scheme **II.8**). In the former example, unsymmetric 1,4-syn-dimethoxycyclohexa-2,5-diene **II.23** was isolated in 46% yield (syn:anti ~ 4:1), while the latter example afforded **II.24** in 55% yield[†] (syn:anti ~ 3:1). In the case of **II.24**, the tertiary silyl ether was somewhat sensitive to the aryl lithium reagent, leading to recovery of both TMS-quinol **II.22** and deprotected **II.18**. For both systems, the diastereomers could not be separated and the diastereomeric ratios were determined by ^{1}H NMR integrations of either the methyl ether or silyl ether regions, respectively. We have tentatively assigned the more upfield, shielded methyl ether and trimethylsilyl resonances to the anti diastereomer, as it is plausible to assume that, at least based on the X-ray crystallographic data for similar adduct **II.21** (Figure **II.10**), these groups are situated in the shielding

---

[†] The yield is based on recovered starting material **II.22** (brsm).

cone of the arene directly across the cyclohexadiene ring. Surprisingly, unlike Wipf's systems,[7] there was almost no difference in selectivity between the methylated (**II.19**) and silylated analog (**II.22**). Thus, while the substitution pattern of the dienone is certainly important, the size of the incoming nucleophile plays a key role as well, since the use of less sterically demanding nucleophile (4-bromophenyl)lithium gave a reversal in selectivity in both cases presented.
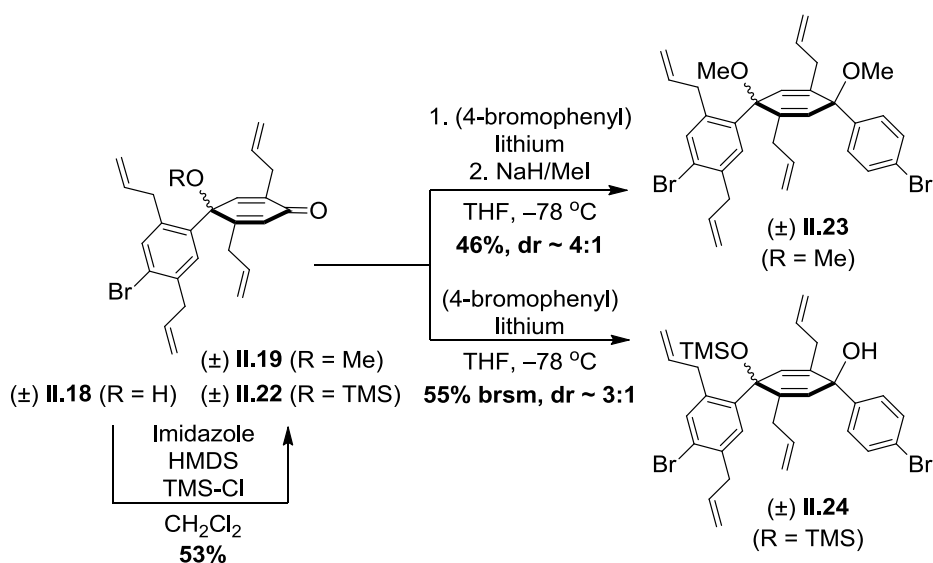
Scheme II.8. Use of an unsubstituted nucleophile increased rate of addition to the bottom face, affording syn stereoisomers **II.23** and **II.24**.

To follow up on these observations, we next wanted to examine the effect of arene substitution pattern on both the dienone and the nucleophile components. We first synthesized a methyl ether derived from *p*-dibromoxylene (**II.26**, 76% yield) (Scheme **II.9**) by nucleophilic addition of (4-bromo-2,5-dimethylphenyl)lithium **II.25** to ketal **II.14**, followed by *in situ* methylation. Upon acid catalyzed deprotection, a nucleophilic

addition of another equivalent of **II.25** to ketone **II.26** afforded **II.27** in 62% yield after *in situ* methylation. Not surprisingly, we observed a diastereomeric ratio of >19:1 in favor of the anti stereoisomer, which is consistent with what was observed for a similar system with larger allyl substituents on the arene components (**II.20**, Scheme **II.7**). The stereochemical configuration of the major diastereomer was unequivocally determined by X-ray crystallographic analysis (Figure **II.11**).
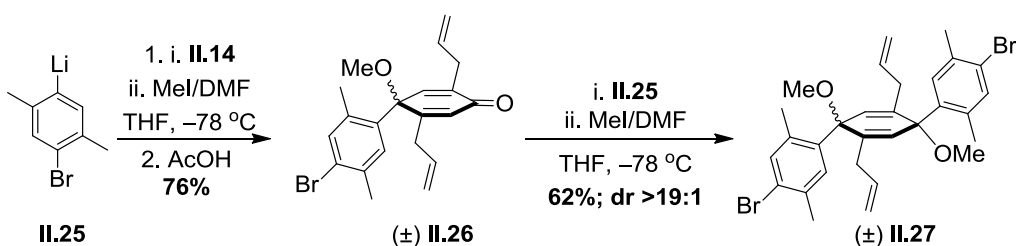
Scheme II.9. Smaller *p*-substituents also resulted in exclusive top face addition to deliver anti adduct **II.27**.

It was hypothesized that use of ortho substitution, rather than para substitution, would increase the rate of addition to the bottom face by alleviating sterics, thus leading to the desired syn diastereomer. Addition of (4-bromo-2,3-dimethylphenyl)lithium **II.28**, derived from 1,4-dibromo-*o*-xylene[23] and *n*BuLi, to ketal **II.14** delivered methyl ether **II.29** in 71% yield after *in situ* methylation and acid catalyzed deprotection (Scheme **II.10**). In line with our expectations, addition of another equivalent of **II.28** to methyl ether **II.28** and methylation of the resulting alkoxide gave **II.30** in 49% yield with a much lower anti/syn diastereomeric ratio (2:1) as determined by ^{1}H NMR spectroscopy (Figure **II.9**). Isolation of both compounds allowed us to obtain crystal structures of both the anti (Figure **II.12**) and syn (Figure **II.13**) diastereomers. Indeed, ortho substitution allowed

for the formation of the desired 1,4-syn-dimethoxycyclohexa-2,5-diene, albeit as the minor stereoisomer. The NMR spectra for the two diastereomers (Figure **II.9**) are consistent with our original assertion that the ethereal groups of the anti isomer resonate more upfield (shielded) and those of the syn isomer resonate more downfield (deshielded).
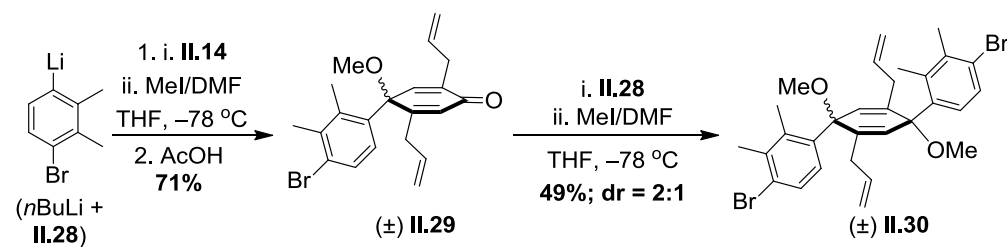
Scheme II.10. Use of *o*-substitution increased addition rate to the bottom face and delivered **II.30** with a diastereomeric ratio of 2:1 (anti/syn).

Notwithstanding optimization, we then examined the diastereoselectivity of an elaborated model that would provide more functionality than a simple methyl group. Inclusion of a single propenyl substituent into both the dienone and the nucleophile components provided additional insight to the stereoselectivity of this class of nucleophilic addition reactions. Beginning with benzylic bromide **II.31**[24], a copper-catalyzed Kumada cross-coupling with vinylmagnesium chloride (**II.32**) followed by olefin isomerization afforded **II.33** (Scheme **II.11**). After lithium-halogen exchange, addition to ketal **II.14**, and *in situ* methylation, dienone **II.34** was easily accessed with functionality on only one side of the arene. In this example, however, the substituent in the lone ortho position is larger than a methyl group. Accordingly, the diastereomeric

39

ratio upon nucleophilic addition to deliver symmetric **II.35** (66% yield) was affected by switching to the bulkier propenyl group, increasing the preference for anti addition to 6:1. The stereochemistry of the major diastereomer was determined by X-ray crystallographic analysis (Figure **II.14**). It seems that while para substitution on the aryl rings leads to high selectivity for the anti isomer, simply increasing the size of the ortho substituent closest to the quaternary center also favors addition to form the anti product (i.e. **II.29** to **II.34**). Although the exact synergy between the different variables that lead to the observed diastereoselectivities is not completely clear at this time, additional experiments to probe the intricacies of the stereochemical outcomes in this class of reactions are currently ongoing.
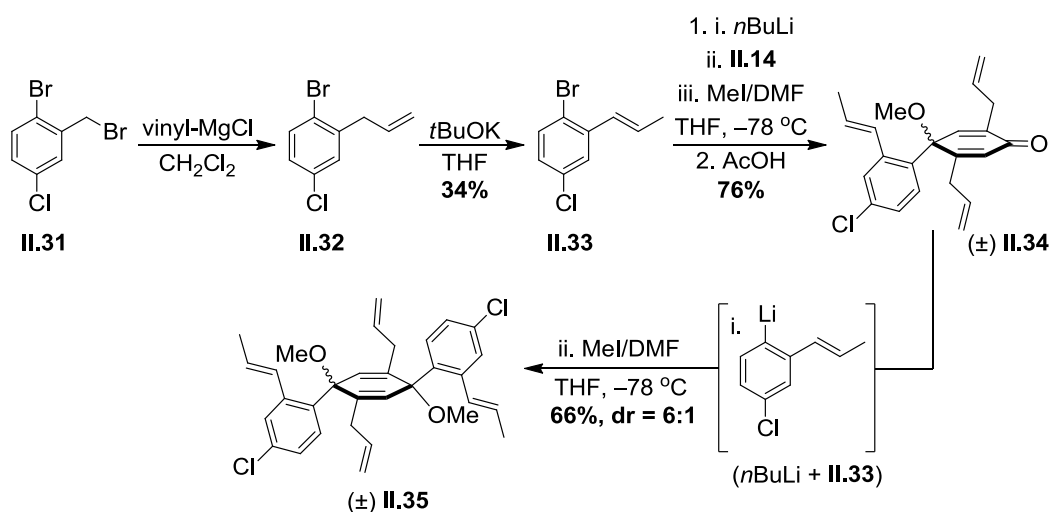
Scheme II.11. Propenyl groups on each aryl component led to an erosion of diastereoselectivity in the formation of **II.35** (anti/syn = 6:1).

40

II.5. Experimental

II.5.1. General Experimental Considerations

All glassware was oven (140 $^\circ$C) or flame dried and cooled under an inert atmosphere of nitrogen unless otherwise noted. Moisture sensitive reactions were carried out under an inert atmosphere of nitrogen using standard syringe/septa technique. Tetrahydrofuran, diethyl ether, dichloromethane, and dimethylformamide were dried by filtration through alumina according to the methods described by Grubbs (JC Meyer).[25] Silica column chromatography was conducted with Zeochem Zeoprep 60 Eco 40-63 μm silica gel. Thin Layer Chromatography (TLC) was performed using Sorbent Technologies Silica Gel XHT TLC plates. Developed plates were visualized using UV light at wavelengths of 254 and 365 nm. ^{1}H NMR spectra were recorded at 500 MHz on a Varian VNMRS, 500 MHz on a Varian INOVA-500, 400 MHz on a Varian VNMRS, or 300 MHz on a Varian INOVA-300. ^{13}C NMR spectra were recorded at 125 MHz on a Varian VNMRS, 125 MHz on a Varian INOVA-500, or 100 MHz on a Varian VNMRS. All ^{1}H NMR spectra were taken in $CDCl_3$ (referenced to TMS, δ 0.00 ppm) or benzene-d_6 (referenced to residual C_6H_6, δ 7.16 ppm). All ^{13}C NMR spectra were taken in $CDCl_3$ (referenced to chloroform δ 77.16 ppm), or benzene-d_6 (referenced to benzene, δ 128.06 ppm). IR spectra were recorded on a Thermo Nicolet 6700 FT-IR. Microwave reactions were conducted with a Biotage Initiator+. All reagents were obtained commercially unless otherwise noted.

II.5.2. Synthetic Details

II.4
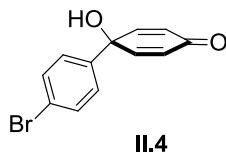
4'-bromo-1-hydroxy-[1,1'-biphenyl]-4(1H)-one **II.4**. To a dry 500 mL round bottom flask

charged with a magnetic stir bar, 4'-bromo-(1,1'-biphenyl)-4-ol (51 g, 200 mmol, 1.0

equiv), imidazole (22 g, 320 mmol, 1.6 equiv) and dichloromethane (300 mL) was added

neat chlorotrimethylsilane (33 mL, 260 mmol, 1.3 equiv) at 0 °C. The mixture was then

allowed to warm rt and stirred for 16 h. With stirring, 1 M aq sodium bicarbonate (150

mL) was added and the layers were separated. The organic layer was washed one

additional time with 1 M aq sodium bicarbonate (150 mL) followed by a saturated brine

solution (150 mL). The organic layer was then was dried over sodium sulfate and

concentrated under reduced pressure to afford off-white solid TMS-biphenol that was

used without further purification. To a 250 mL round bottom flask charged with a

magnetic stir bar, crude white TMS-biphenol (5.0 g, 16 mmol, 1.0 equiv), THF (80 mL),

distilled water (35 mL) and MeCN (20 mL) was added (diacetoxyiodo)benzene (7.5 g,

23 mmol, 1.5 equiv) slowly as a solid over the course of 30 minutes. The reaction

mixture was allowed to stir for 16 h before concentrating under reduced pressure to

afford a crude orange solid. This solid was passed through a short pad of silica (EtOAc)

to afford **II.4** (2.8 g, 68%) as a yellow solid. ^{1}H NMR (400 MHz, CDCl$_3$) δ 7.51 (d, *J* =

8.6 Hz, 2H), 7.36 (d, *J* = 8.6 Hz, 2H), 6.85 (d, *J* = 10.0 Hz, 2H), 6.25 (d, *J* = 10.0 Hz,

2H), 2.38 (s, 1H); ^{13}C (125 MHz, CDCl$_3$) δ 185.31, 150.08, 137.73, 132.04, 127.20,

127.11, 122.58, 70.73; HRMS (Q-TOF ES+) *m/z* calcd for $C_{12}H_9BrO_2$ (M)$^+$ 264.9864; found, 264.9867; IR (neat) 3393, 2360, 1665, 1398, 827 cm^{-1}.
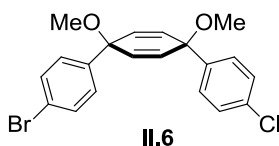
(1's,4's)-syn-4-bromo-4''-chloro-1',4'-dimethoxy-1',4'-dihydro-1,1':4',1''-terphenyl **II.6**.

To a dry 2 L round bottom flask was added sodium hydride (3.9 g, 98 mmol, 1.3 equiv) and THF (400 mL). The slurry was cooled to −78 °C, at which point **II.4** (20 g, 75 mmol, 1.0 equiv) was added slowly as a solution in THF (200 mL) and stirred for 2 h. In a separate, dry 500 mL round bottom flask charged with a magnetic stir bar, 4-bromochlorobenzene (35 g, 180 mmol, 2.4 equiv) and THF (200 mL) was added *n*BuLi (74 mL, 180 mmol, 2.4 equiv, 2.5 M in hexanes) over the course of 25 min at −78 °C. The reaction mixture containing the aryl lithium reagent was allowed to stir for 30 min before it was transferred via cannula to the slurry containing deprotonated **II.4**. This reaction mixture was stirred for 2 h at -78 °C before it was quenched with water (50 mL) and allowed to warm to rt. Upon separation of the layers, the aqueous layer was extracted with diethyl ether (3 x 200 mL) and the combined organic layers were washed with a saturated brine solution (150 mL) and dried over sodium sulfate. Concentration under reduced pressure afforded a crude brown diol that was used without further purification. To a dry 1 L round bottom flask was added sodium hydride (7.8 g, 200 mmol, 2.6 equiv) and THF (400 mL). The slurry was cooled to 0 °C, the crude diol was added as a solution in THF (200 mL) and the reaction mixture was allowed to stir for 30 min. Neat methyl

iodide was then injected (19 mL, 300 mmol, 4.0 equiv) and the reaction mixture was allowed to warm to rt and stirred for 16 h. The excess sodium hydride was quenched by the addition of water (150 mL). The layers were separated and the aqueous layer was extracted with ethyl acetate (3 x 150 mL). The combined organic layers were washed with a saturated brine solution (100 mL), dried over sodium sulfate and concentrated under reduced pressure. The brown solid was washed with hot hexanes to afford a yellow solid that was recrystallized from hexanes to afford white, crystalline **II.6** (15 g, 49%). ^{1}H NMR (400 MHz, CDCl$_3$) δ 7.43 (d, J = 8.5 Hz, 2H), 7.32 – 7.29 (overlap, 4H), 7.24 (d, J = 8.5 Hz, 2H), 6.07 (s, 4H), 3.41 (s, 6H); ^{13}C (125 MHz, CDCl$_3$) δ 142.33, 141.78, 133.39, 133.30, 131.49, 128.55, 127.75, 127.40, 121.70, 74.43, 74.38, 52.03; HRMS (Q-TOF ES+) m/z calcd for C$_{20}$H$_{18}$BrClO$_2$ (M)$^+$ 405.0257; found, 405.0239; IR (neat) 2982, 2826, 2360, 1484, 1081, 1009, 820 cm^{-1}.
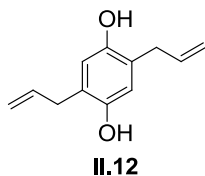
II.12

2,5-diallylbenzene-1,4-diol **II.12**. Hydroquinone (50 g, 0.45 mol, 1.0 equiv), allyl bromide (120 g, 1.0 mol, 2.2 equiv), and potassium carbonate (140 g, 1.0 mmol, 2.3 equiv) were suspended in acetone (650 mL) and heated to 60 ^{o}C for 19 h. The crude reaction mixture was cooled to rt and filtered through a short pad of celite topped with activated carbon (hexanes). The filtrate was concentrated and crystallized from hexanes at –5 ^{o}C. The resulting white crystalline solid was washed with cold hexanes to afford 1,4-bis(allyloxy)benzene, which was used without further purification (48 g). This solid

was then dissolved in minimal DMF (~ 25 mL) and portioned into microwave tubes.

Each tube was heated to 235 $^{\circ}$C for 1 h. The contents of all of the tubes (viscous brown

oil) were combined and layered with chloroform (20 mL) at −5 $^{\circ}$C. The resulting tan solid

was filtered and recrystallized from hot chloroform to afford **II.12** as the para

regioisomer (>20:1) (10 g, 25% for para regioisomer). ^{1}H NMR (300 MHz, acetone-d_6)

δ(ppm) 7.50 (s, 2H), 6.58 (s, 2H), 5.95 (ddt, J = 17.2, 10.0, 6.5 Hz, 2H), 5.03 (d, J = 17.2

Hz, 2H), 4.97 (d, J = 10.0 Hz), 3.28 (d, J = 6.5 Hz, 4H); ^{13}C NMR (150 MHz, acetone-

d_6) δ(ppm) 147.65, 137.39, 124.71, 116.39, 114.43. Characterization was consistent with

the literature.[14-15]
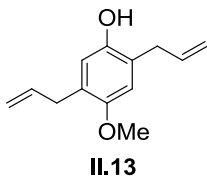
II.13

2,5-diallyl-4-methoxyphenol **II.13**. 2,5-diallylbenzene-1,4-diol **II.12** (2.7 g, 14 mmol, 1.0

equiv) and NaNO$_2$ (98 mg, 1.4 mmol, 10 mol%) were dissolved in methanol (50 mL) and

the solution was sparged with N$_2$ for 15 min. Sulfuric acid (1.4 g, 0.76 mL, 14 mmol, 1.0

equiv) was added via syringe while still sparging. The reaction mixture was then placed

under an N$_2$ atmosphere and was allowed to stir at rt for 16 h. An addition portion of

NaNO$_2$ (98 mg, 1.4 mmol, 10 mol%) was added at this time and stirring was continued

for an addition 4 h. The reaction was quenched by the addition of water (30 mL) and was

extracted with EtOAc (2 x 30 mL). The combined organics were washed with brine (20

mL), dried over sodium sulfate, and concentrated on Celite. Purification on silica gel (4

cm x 4 cm, hexanes then 10% acetone/hexanes) and washing the resulting solid with cold

hexanes (5 mL) afforded **II.13** as a yellow solid (1.5 g, 52%). ^{1}H NMR (300 MHz,

CDCl$_3$) δ(ppm) 6.63 (s, 1H), 6.61 (s, 1H), 6.08 – 5.85 (overlap, 2H), 5.26 – 4.90 (overlap, 4H), 4.58 (s, 1H), 3.77 (s, 4H), 3.38 (d, J = 6.3 Hz, 1H), 3.31 (d, J = 6.5 Hz, 1H); ^{13}C NMR (150 MHz, CDCl$_3$) δ(ppm) 151.44, 147.62, 136.87, 136.50, 128.11, 123.50, 117.55, 116.33, 115.58, 113.02, 56.26, 35.17, 33.82.
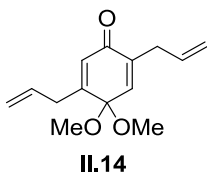
II.14

2,5-diallyl-4,4-dimethoxycyclohexa-2,5-dienone **II.14**. To a methanolic solution (45 mL) of **II.13** (3.3 g, 16 mmol, 1.0 equiv) at 0 °C under an N$_2$ atmosphere was added PhI(OAc)$_2$ (6.1 g, 19 mmol, 1.2 equiv) portionwise over 5 h. The reaction was allowed to stir for an additional 30 min at 0 °C, whereupon sat. aq NaHCO$_3$ (50 mL) was added and the resulting solution was extracted with EtOAc (3 x 50 mL). The combined organics were washed with sat. aq NaHCO$_3$ (50 mL), water (2 x 50 mL), and brine, then dried over sodium sulfate and concentrated under vacuum. Purification on silica gel (0 – 10% EtOAc/hexanes) afforded **II.14** as a yellow oil (2.5 g, 67%). ^{1}H NMR (500 MHz, CDCl$_3$) δ(ppm) 6.51 (t, J = 1.3 Hz, 1H), 6.24 (t, J = 1.5 Hz, 1H), 5.91 – 5.77 (overlap, 2H), 5.27 – 5.08 (overlap, 4H), 3.21 (s, 6H), 3.11 (br d, J = 6.8 Hz, 1H), 3.03 (br d, J = 7.1 Hz, 2H); ^{13}C NMR (125 MHz, CDCl$_3$) δ(ppm) 184.86, 157.64, 141.69, 139.09, 134.46, 132.98, 129.03, 118.91, 117.60, 96.03, 51.05, 32.90, 32.76.
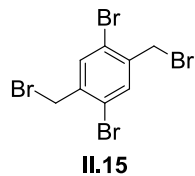
II.15

1,4-dibromo-2,5-bis(bromomethyl)benzene **II.15**. To a slurry of 1,4-dibromo-*p*-xylene

(25 g, 95 mmol, 1.0 equiv) and NBS (37 g, 210 mmol, 2.2 equiv) in benzene (400 mL)

was added AIBN (0.31 g, 1.9 mmol, 0.02 equiv). The mixture was heated to 80 $^{\circ}$C for 25

h whereupon an additional portion of AIBN (80 mg) was added and stirring continued for

another 16 h. Upon cooling to rt, the crude reaction mixture was filtered through a short

pad of Celite (EtOAc) and the filtrate was washed with 1 M aq NaOH (3 x 100 mL). The

organic phase was then washed with water (100 mL) and brine (100 mL). After

concentrating under vacuum to a pale yellow solid, washing with ethanol (4 x 50 mL)

afforded **II.15** as a white solid (23 g, 59%). Characterization data was consistent with

previous reports in the literature.[18]
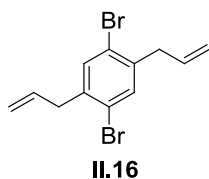
II.16

1,4-diallyl-2,5-dibromobenzene **II.16**. To a suspension of 1,4-dibromo-2,5-

bis(bromomethyl)benzene **II.15** (10 g, 24 mmol, 1.0 equiv) and copper(I) iodide (4.5 g,

24 mmol, 1.0 equiv) in anhydrous DCM (240 mL) at –78 $^{\circ}$C was added vinyl magnesium

bromide (140 mL, 100 mmol, 4.2 equiv, 0.7 M in THF) as a stream via cannula. After

cannulation, the resulting yellow suspension was allowed to gradually warm to rt for 18

h. The reaction was quenched by the addition of sat. aq NH$_4$Cl (150 mL). After filtering

through a pad of Celite, the filtrate was extracted with EtOAc (2 x 100 mL) and the

47

combined organics were washed with brine (50 mL), dried over sodium sulfate, and concentrated on Celite. Purification on silica gel (4 cm x 15 cm, hexanes) afforded **II.16** as a white solid (3.2 g, 43%). ^{1}H NMR (300 MHz, CDCl$_3$) δ(ppm) 7.39 (s, 2H), 5.92 (ddt, J = 16.8, 10.1, 6.4 Hz, 2H), 5.23 – 5.00 (overlap, 4H), 3.44 (d, J = 6.4 Hz, 4H); ^{13}C NMR (150 MHz, CDCl$_3$) δ(ppm) 139.22, 134.85, 133.99, 123.37, 117.23, 39.53.
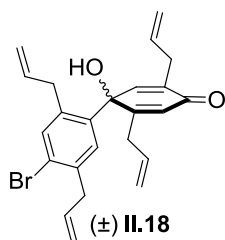
(±) **II.18**

(±)-2,2',5,5'-tetraallyl-4'-bromo-1-hydroxy-[1,1'-biphenyl]-4(1H)-one **II.18**. To a slurry of **II.16** (1.0 g, 3.3 mmol, 0.75 equiv) in anhydrous THF (6 mL) at −78 ^{o}C was added *n*BuLi (1.9 mL, 4.5 mmol, 1.1 equiv, 2.4 M in hexanes) dropwise to form lithiate **II.17**. The pale orange aryl lithium reagent was stirred for 10 min before adding **II.14** (1.0 g, 4.3 mmol, 1.0 equiv) in anhydrous THF (2 mL) dropwise via cannula. After stirring for 45 min, the reaction was quenched by the addition of water (5 mL) and the biphasic mixture was extracted with EtOAc (2 x 15 mL). Upon concentrating the combined organics, the resulting crude yellow oil was dissolved in acetone (4 mL) and 10% aq AcOH (5 mL) was added. After stirring for 30 min, the reaction was quenched with sat. aq NaHCO$_3$ (5 mL) and was extracted with EtOAc (3 x 10 mL). The combined organics were washed with brine (5 mL), dried over sodium sulfate, and concentrated on Celite. Purification on silica gel (3 cm x 12 cm, 0 – 20% EtOAc/hexanes) afforded **II.18** as a white solid after washing with minimal hexanes (0.70 g, 51%). ^{1}H NMR (500 MHz, C$_6$D$_6$, 70 ^{o}C) δ(ppm) 7.81 (br s, 1H), 7.37 (s, 1H), 6.25 (s, 1H), 6.19 (s, 1H), 5.91 (m,

1H), 5.78 (m, 1H), 5.59 (m, 1H), 5.51 (dddd, J = 17.1, 10.1, 7.1, 7.0 Hz, 1H), 5.05 − 4.97

(m, 3H), 4.98 (d, J = 10.1 Hz, 1H), 4.91 (dd, J = 10.0, 1.5 Hz, 1H), 4.85 (dd, J = 10.1, 1.5

Hz, 1H), 4.82 − 4.73 (overlap, 2H), 3.52 − 3.36 (m, 2H), 3.19 − 3.00 (m, 4H), 2.80 (ddd, J

= 17.4, 7.0, 1.3 Hz, 1H), 2.40 (dd, J = 17.4, 7.1 Hz, 1H); ^{13}C NMR (125 MHz, C_6D_6, 70

^{o}C) δ(ppm) 184.26, 160.41, 144.39, 137.96, 136.36, 135.40, 135.13, 134.61, 133.26,

128.91, 127.37, 126.16, 124.47, 117.88, 116.78, 116.13, 115.98, 39.83, 35.33, 34.98,

32.79.

(±)-2,2′,5,5′-tetraallyl-4′-bromo-1-methoxy-[1,1′-biphenyl]-4(1H)-one **II.19**. To a slurry

of **II.16** (1.0 g, 3.3 mmol, 0.75 equiv) in anhydrous THF (15 mL) at −78 ^{o}C was added

*n*BuLi (1.8 mL, 4.4 mmol, 1.1 equiv, 2.4 M in hexanes) dropwise. The pale orange aryl

lithium reagent (**II.17**) was stirred for 5 min before adding **II.14** (1.0 g, 4.3 equiv, 1.0

mmol) in anhydrous THF (4 mL) via cannula. After stirring for 2 h, MeI (1.8 g, 0.79 mL,

13 mmol, 3.0 equiv) and anhydrous DMF (4 mL) were added and the reaction mixture

was allowed to warm to rt over 16 h. The reaction was quenched with water (20 mL) and

the biphasic mixture was extracted with EtOAc (2 x 20 mL). The combined organics

were washed with 5% aq LiCl (5 x 4 mL). Upon concentrating under vacuum, the

resulting crude yellow oil was dissolved in acetone (5 mL) and 10% aq AcOH (5 mL)

was added. After stirring for 1 h, the reaction was quenched with sat. aq $NaHCO_3$ (15

mL) and was extracted with EtOAc (3 x 10 mL). The combined organics were washed

with brine (10 mL), dried over sodium sulfate, and concentrated on Celite. Purification on silica gel (4 cm x 12 cm, 0 – 5% EtOAc/hexanes) afforded **II.19** as a yellow oil (1.2 g, 86%). Solid white dione **II.20** was also isolated as a byproduct of this reaction (0.20 g, 11%, dr > 19:1). Major product **II.19**: ^{1}H NMR (500 MHz, C_6D_6, 70 ^{o}C) δ(ppm) 7.84 (br s, 1H), 7.40 (s, 1H), 6.45 (s, 1H), 6.16 (s, 1H), 5.96 – 5.87 (m, 1H), 5.78 (dddd, J = 17.0, 10.2, 6.9, 6.9 Hz, 1H), 5.69 – 5.59 (br m, 1H), 5.47 (dddd, J = 17.1, 10.2, 7.2, 7.0 Hz, 1H), 5.05 – 4.84 (overlap, 6H), 4.84 – 4.74 (overlap, 2H), 3.52 – 3.38 (m, 2H), 3.29 – 3.20 (br m, 2H), 3.16 (ddd, J = 15.7, 6.p, 1.4 Hz, 1H), 3.06 (ddd, J = 15.7, 6.9, 1.3 Hz, 1H), 2.86 (s, 3H), 2.64 (dd, J = 17.6, 7.0 Hz, 1H), 2.42 (dd, J = 17.6, 7.2 Hz, 1H); ^{13}C NMR (125 MHz, C_6D_6, 70 ^{o}C) δ(ppm) 184.12, 157.73, 142.42, 139.66, 137.83, 136.42, 135.43, 135.33, 134.76, 132.80, 129.68, 129.16, 124.42, 118.00, 116.64, 116.10, 115.85, 49.63, 39.84, 35.21, 32.81. Byproduct **II.20**: ^{1}H NMR (500 MHz, C_6D_6, 70 ^{o}C) δ(ppm) 7.83 (br s, 1H), 6.46 (s, 1H), 6.25 (s, 1H), 5.93 – 5.81 (m, 1H), 5.73 (dddd, J = 16.9, 10.0, 7.1, 6.8 Hz, 1H), 5.54 – 5.43 (m, 1H), 4.99 – 4.84 (m, 5H), 4.75 (d, J = 16.9 Hz, 1H), 3.44 (br s, 2H), 3.15 (dd, J = 15.8, 6.8 Hz, 1H), 3.00 (dd, J = 15.8, 7.3 Hz, 1H), 2.70 (dd, J = 17.4, 7.0 Hz, 1H), 2.51 (dd, J = 17.4, 6.5 Hz, 1H); ^{13}C NMR (125 MHz, C_6D_6, 70 ^{o}C) δ(ppm) 184.24, 158.11, 142.95, 142.91, 139.42, 137.55, 136.73, 134.84, 134.82, 133.03, 133.01, 130.61, 129.70, 129.64, 117.81, 117.79, 116.53, 115.28, 49.78, 36.24, 35.31, 32.82.
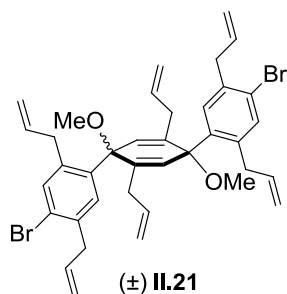
(±) **II.21**

(±)-anti-2,2',2'',5,5',5''-hexaallyl-4,4''-dibromo-1',4'-dimethoxy-1',4'-dihydro-1,1':4',1''-terphenyl **II.21**. To a slurry of **II.16** in anhydrous THF (3 mL) was added *n*BuLi (0.17 mL, 0.41 mmol, 1.1 equiv, 2.4 M in hexanes) at –78 °C. The light orange aryl lithium (**II.17**) solution was stirred for 20 min before adding **II.14** (0.17 g, 0.39 mmol, 1.0 equiv) in anhydrous THF (3 mL). The reaction mixture was stirred for 90 min before quenching with water (5 mL) and extracting with EtOAc (2 x 10 mL). The combined organics were washed with brine (5 mL), dried over sodium sulfate, and concentrated on Celite. Purification on silica gel (2 cm x 10 cm, 0 – 5% EtOAc/hexanes) afforded semi-pure alcohol (0.17 g) that was used directly without further purification. A portion of this alcohol (52 mg, 0.077 mmol, 1.0 equiv) in anhydrous THF (3 mL) was added to a slurry of sodium hydride (37 mg, 0.93 mmol, 12 equiv) at 0 °C in anhydrous THF (1.5 mL), After stirring for 20 min, MeI (0.24 mL, 3.9 mmol, 50 equiv) was added and the reaction was allow to warm to rt for 16 h. The reaction mixture was then quenched with water (2 mL) and extracted with EtOAc (2 x 10 mL). The combined organics were washed with brine (10 mL), dried over sodium sulfate, and concentrated on Celite. Purification on silica gel (2 cm x 15 cm, hexanes then 10% EtOAc/hexanes) afforded **II.21**as a colorless solid (50 mg, 60%, anti/syn > 19:1). ^{1}H NMR (500 MHz, C_6D_6, 70 °C) δ(ppm) 7.54 (s, 1H), 7.18 (s, 1H), 6.25 (s, 1H), 6.02 (dddd, *J* = 16.7, 10.1, 6.8, 6.2 Hz, 1H), 5.83 – 5.69 (m, 2H), 5.08 – 4.86 (m, 8H), 3.85 (dd, *J* = 15.3, 6.2 Hz, 1H), 3.76 (dd, *J* = 15.3, 6.8 Hz,

51

1H), 3.36 (d, $J = 6.5$ Hz, 2H), 3.05 (s, 3H), 2.82 – 2.68 (m, 3H); ^{13}C NMR (125 MHz, C_6D_6, 70 ^{o}C) δ(ppm) 140.84, 139.95, 139.92, 138.40, 138.38, 136.56, 136.39, 135.49, 135.04, 131.75, 131.72, 129.93, 123.58, 117.04, 117.01, 116.12, 116.10, 115.25, 80.59, 51.07, 39.66, 38.09, 35.41.
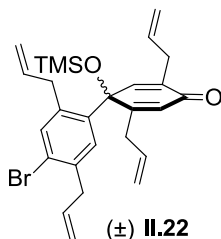
(±) **II.22**

(±)-2,2',5,5'-tetraallyl-4'-bromo-1-((trimethylsilyl)oxy)-[1,1'-biphenyl]-4(1H)-one **II.22**.
To a solution of **II.18** (0.36 g, 0.84 mmol, 1.0 equiv) in anhydrous DCM (5 mL) was added imidazole (0.17 g, 2.5 mmol, 3.0 equiv), and trimethylsilylchloride (9.1 mg, 0.011 mL, 0.084 mmol, 10 mol%). Hexamethyldisilazane (0.20 g, 0.26 mL, 1.3 mmol, 1.5 equiv) was added dropwise and the resulting white suspension was stirred for 15 h. The reaction was quenched with water (5 mL) and extracted with EtOAc (2 x 10 mL). The combined organics were washed with brine (5 mL), dried over sodium sulfate, and concentrated on Celite. Purification on silica gel (3 cm x 8 cm, 0 – 5% EtOAc/hexanes) afforded **II.22** as a pale yellow oil (0.22 g, 53%). ^{1}H NMR (300 MHz, C_6D_6) δ(ppm) 7.90 (br s, 1H), 7.37 (s, 1H), 6.32 (s, 1H), 6.01 – 5.71 (overlap, 2H), 5.63 – 5.37 (overlap, 2H), 5.15 – 4.67 (overlap, 8H), 3.45 (br, 2H), 3.21 – 3.04 (overlap, 4H), 2.87 (dd, $J = 17.8, 6.5$ Hz, 1H), 2.42 (d, $J = 17.8$ Hz, 1H), 0.05 (s 9H).
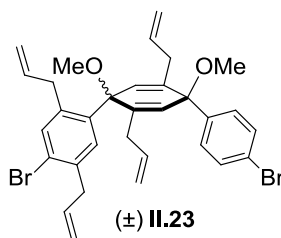
(±) **II.23**

(±)-2,2',5,5'-tetraallyl-4,4''-dibromo-1',4'-dimethoxy-1',4'-dihydro-1,1':4',1''-terphenyl

II.23. To a solution of 1,4-dibromobenzene (96 mg, 0.41 mmol, 1.1 equiv) in anhydrous

THF (3 mL) was added *n*BuLi (0.16 mL, 0.39 mmol, 1.1 equiv, 2.4 M in hexanes) at −78

°C. The aryl lithium reagent was stirred for 10 min before adding **II.19** (0.16 g, 0.37

mmol, 1.0 equiv). The reaction mixture was stirred for 90 min before quenching with

water (5 mL) and extracting with EtOAc (2 x 10 mL). The combined organics were

washed with brine (5 mL), dried over sodium sulfate, and concentrated on Celite.

Purification on silica gel (2 cm x 10 cm, 0 − 5% EtOAc/hexanes) afforded semi-pure

alcohol (0.15 g) that was used directly without further purification. A portion of this

alcohol (0.10 g, 0.077 mmol, 1.0 equiv) in anhydrous THF (4 mL) was added to a slurry

of sodium hydride (0.10 g, 2.6 mmol, 15 equiv) at 0 °C in anhydrous THF (2 mL), After

stirring for 20 min, MeI (0.53 mL, 8.5 mmol, 50 equiv) was added and the reaction was

allow to warm to rt for 16 h. The reaction mixture was then quenched with water (2 mL)

and extracted with EtOAc (2 x 10 mL). The combined organics were washed with brine

(10 mL), dried over sodium sulfate, and concentrated on Celite. Purification on silica gel

(2 cm x 14 cm, hexanes then 10% EtOAc/hexanes) afforded **II.23** as a thick yellow oil

(50 mg, 60%, syn:anti ~ 4:1). Major Diastereomer, resonances selected from 4:1 mixture:

^{1}H NMR (500 MHz, C_6D_6, 70 °C) δ(ppm) 7.53 (s, 1H), 7.40 − 7.35 (overlap, 2H), 7.33 −

7.24 (overlap, 3H), 6.09 (s, 1H), 6.06 − 5.91 (m, 1H), 5.88 (s, 1H), 5.86 − 5.66 (m, 2H),

5.59 − 5.48 (m, 1H), 5.07 − 4.71 (m, 8H), 3.79 (dd, *J* = 15.5, 6.0 Hz, 1H), 3.70 (dd, *J* =

15.5, 6.9 Hz, 1H), 3.37 (d, J = 6.7 Hz, 2H), 3.10 (s, 6H), 2.77 (d, J = 6.7 Hz, 5H), 2.67 (dd, J = 16.6, 7.2 Hz, 1H), 2.52 (dd, J = 16.6, 7.4 Hz, 1H); ^{13}C NMR (125 MHz, C$_6$D$_6$, 70 ^{o}C) δ(ppm) 142.74, 141.24, 140.87, 139.81, 139.70, 138.23, 136.58, 136.28, 136.24, 135.48, 135.05, 134.95, 132.59, 131.22, 131.06, 130.90, 129.81, 128.20, 123.63, 121.33, 117.00, 116.66, 116.15, 115.31, 77.74, 76.36, 51.71, 50.60, 39.68, 39.66, 37.77, 35.30, 34.41, 33.36, 26.35, 23.07, 13.59.
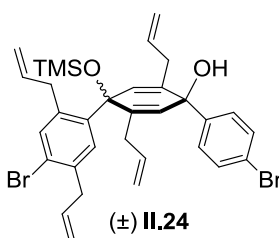
(±) **II.24**

trimethyl(((±)-2,2',5,5'-tetraallyl-4,4''-dibromo-4'-hydroxy-1',4'-dihydro-[1,1':4',1''-terphenyl]-1'-yl)oxy)silane **II.24**. To a solution of 1,4-dibromobenzene (80 mg, 0.34 mmol, 1.2 equiv) in anhydrous THF (2 mL) was added *n*BuLi (0.13 mL, 0.31 mmol, 1.1 equiv, 2.4 M in hexanes) dropwise at –78 ^{o}C. After stirring the aryl lithium reagent for 10 min, **II.22** (0.14 g, 0.28 mmol, 1.0 equiv) was added in anhydrous THF (4 mL). After stirring for 2 h, the reaction was quenched with water (5 mL) and was extracted with EtOAc (2 x 10 mL). The combined organics were washed with brine (5 mL), dried over sodium sulfate, and concentrated on Celite. Purification on silica gel (2 cm x 10 cm, 0 – 5% EtOAc/hexanes) afforded a semi-pure product (0.10 g) that was further purified by preparative TLC (5% EtOAc/hexanes) to afford **II.24** as a colorless oil (17 mg, 55% brsm, syn:anti ~ 3:1). Major Diastereomer, resonances selected from mixture: ^{1}H NMR (500 MHz, C$_6$D$_6$) δ(ppm) 7.53 (s, 1H), 7.33 (s, 1H), 7.28 (d, J = 8.6 Hz, 2H), 7.11 (d, J = 8.6 Hz, 2H), 6.13 (s, 1H), 5.97 (br, 1H), 5.78 – 5.49 (overlap, 4H), 5.11 – 5.00 (m, 8H),

3.84 (br d, 1H), 3.37 – 3.22 (m, 2H), 2.98 (dd, J = 17.3, 7.8 Hz, 2H), 2.85 (ddd, J = 16.6, 7.1, 1.3 Hz, 1H), 2.73 (dd, J = 17.3, 7.0 Hz, 1H), 2.51 – 2.41 (overlap, 2H), 0.21 (s, 9H); ^{13}C NMR (150 MHz, CDCl$_3$) δ(ppm) 142.64, 140.61, 138.18, 136.65, 136.08, 135.81, 135.38, 135.12, 134.80, 131.49, 131.22, 130.15, 129.26, 128.07, 127.57, 123.27, 121.28, 117.89, 117.73, 116.82, 116.63, 115.88, 72.78, 39.70, 35.01, 34.85, 34.65, 2.23 (only one C-O resonance observed).
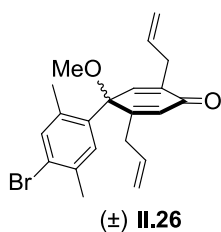
(±) **II.26**

(±)-2,5-diallyl-4'-bromo-1-methoxy-2',5'-dimethyl-[1,1'-biphenyl]-4(1H)-one **II.26**. To a solution of 1,4-dibromo-2,5-dimethylbenzene (0.17 g, 0.64 mmol, 1.1 equiv) in anhydrous THF (3 mL) at −78 ^{o}C was added *n*BuLi (0.26 mL, 0.61 mmol, 1.1 equiv, 2.4 M in hexanes) dropwise. The pink aryl lithium reagent (**II.25**) was stirred for 10 min before adding **II.14** (0.14 g, 0.58 mmol, 1.0 equiv) in anhydrous THF (2 mL) via cannula. After stirring for 3 h, MeI (0.25 g, 0.10 mL, 1.7 mmol, 3.0 equiv) and anhydrous DMF (1 mL) were added and the reaction mixture was allowed to warm to rt over 20 h. The reaction was quenched with water (10 mL) and the biphasic mixture was extracted with EtOAc (2 x 10 mL). The combined organics were washed with 5% aq LiCl (5 x 2 mL). Upon concentrating under vacuum, the resulting crude yellow oil was dissolved in acetone (3 mL) and 10% aq AcOH (3 mL) was added. After stirring for 3 h, the reaction was quenched with sat. aq NaHCO$_3$ (5 mL) and was extracted with EtOAc (2 x 10 mL). The combined organics were washed with brine (5 mL), dried over sodium sulfate, and

concentrated on Celite. Purification on silica gel (2 cm x 7 cm, 0 – 5% EtOAc/hexanes) afforded **II.26** as a yellow oil (0.17 g, 76%). ^{1}H NMR (300 MHz, CDCl$_3$) δ(ppm) 7.77 (br s, 1H), 7.24 (s, 1H), 6.42 (t, J = 1.6 Hz, 1H), 6.24 (s, 1H), 5.89 – 5.73 (m, 1H), 5.75 – 5.57 (m, 1H), 5.20 – 4.93 (m, 4H), 3.16 (s, 3H), 3.14 – 3.07 (overlap, 1H), 2.77 (dd, J = 18.0, 6.9 Hz, 1H), 2.45 (overlap, 1H), 2.40 (s, 3H), 2.02 (br s, 3H); ^{13}C NMR (125 MHz, CDCl$_3$) δ(ppm) 185.70, 158.72, 142.71, 136.02, 135.84, 135.30, 134.58, 132.67, 129.74, 129.15, 124.36, 118.98, 117.46, 77.28, 77.02, 76.77, 71.14, 50.40, 35.14, 32.77, 22.62, 19.24.
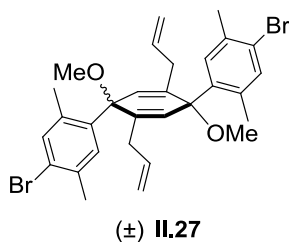
(±) **II.27**

(±)-anti-2',5'-diallyl-4,4''-dibromo-1',4'-dimethoxy-2,2'',5,5''-tetramethyl-1',4'-dihydro-1,1':4',1''-terphenyl **II.27**. To a solution of 1,4-dibromo-2,5-dimethylbenzene (73 mg, 0.28 mmol, 1.1 equiv) in anhydrous THF (2 mL) was added *n*BuLi (0.11 mL, 0.27 mmol, 1.1 equiv, 2.4 M in hexanes) at –78 ^{o}C. The aryl lithium reagent (**II.25**) was stirred for 10 min before adding **II.14** (98 mg, 0.25 mmol, 1.0 equiv) in anhydrous THF (3 mL). The reaction mixture was stirred for 2.5 h before MeI (0.18 g, 0.080 mL, 1.3 mmol, 5.0 equiv) and anhydrous DMF (1 mL) were added and the reaction mixture was allowed to warm to rt over 16 h. The reaction was quenched with water (10 mL) and the biphasic mixture was extracted with EtOAc (2 x 10 mL). The combined organics were washed with 5% aq LiCl (5 x 2 mL) and brine (10 mL), then dried over sodium sulfate and concentrated on Celite. Purification on silica gel (1 cm x 8 cm, 0 – 2 – 5% EtOAc/hexanes) afforded **II.27**

as a white solid after washing with minimal hexanes (ca. 3 mL) (90 mg, 62%, anti/syn >

19:1). ^{1}H NMR (500 MHz, CDCl$_3$) δ(ppm) 7.34 (s, 1H), 7.10 (br s, 1H), 6.13 (t, *J* = 1.6

Hz, 1H), 5.78 (ddd, *J* = 17.1, 10.0, 7.1 Hz, 1H), 5.07 (dd, *J* = 10.0, 1.8 Hz, 1H), 5.00 (dd,

J = 16.9, 1.8 Hz, 0H), 3.12 (s, 3H), 2.77 – 2.63 (m, 3H), 2.51 (s, 3H), 2.28 (s, 3H); [13]C

NMR (125 MHz, CDCl$_3$) δ(ppm) 141.04, 139.62, 136.83, 136.20, 135.04, 134.31,

130.47, 130.14, 123.33, 117.58, 79.80, 51.43, 35.28, 22.44, 21.47.
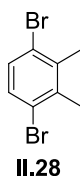
II.28

1,4-dibromo-2,3-dimethylbenzene **II.28**. To a solution of 2,3-dimethylaniline (6.6 mL,

6.5 g, 53 mmol, 1.0 equiv) in anhydrous DCM (150 mL) at 0 °C was added freshly

ground *n*Bu$_4$Br$_3$ (27 g, 56 mmol, 1.1 equiv). The reaction mixture was stirred for 2 h,

whereupon the resulting HBr salt was filtered under vacuum and washed with Et$_2$O (100

mL). After drying under high vacuum, the crude salt was freebased by first suspending it

in Et$_2$O (100 mL), followed by adding sat aq. NaHCO$_3$ (50 mL). The resulting mixture

was stirred rapidly for 15 h under air. The biphasic reaction mixture was then extracted

with Et$_2$O (1 x 40 mL) and the organics were washed with brine (40 mL) then dried over

sodium sulfate. Concentration under vacuum afforded 4-bromo-2,3-dimethylaniline (7.1

g) as a pale orange oil that was used without further purification. This crude product was

then taken up in HBr (20 mL) and cooled to 0 °C. Crushed ice was also added to the

reaction mixture. NaNO$_2$ (2.4 g, 35 mmol, 1 equiv) was added as a solution in water (10

mL) slowly via pipette while continuing to stir the reaction mixture rapidly. The resulting

yellow diazonium solution was kept at 0 °C while CuBr (3.1 g, 26 mmol, 0.6 equiv) in

HBr (10 mL) was heated to reflux (ca. 120 $^{\circ}$C). To this refluxing solution was added the cold diazonium solution portionwise (as a fast drip) via an addition funnel packed with crushed ice. Upon completion of addition of the diazonium solution, the resulting brown mixture was heated for an addition 90 min. Upon cooling to rt, the crude reaction mixture was extracted with hexanes (2 x 50 mL) and the combined organics were concentrated onto Celite. Purification on silica gel (5 cm x 9 cm, hexanes) afforded a semi-pure oily white solid that was further purified by distillation (50 $^{\circ}$C, high vacuum). The solid remaining in the pot was crystalline **II.28** (1.3 g, 9.4%). Characterization data was consistent to previous reports in the literature.[23]
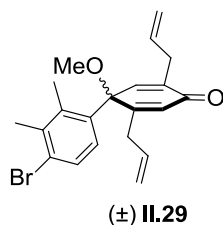
(±) **II.29**

(±)-2,5-diallyl-4'-bromo-1-methoxy-2',3'-dimethyl-[1,1'-biphenyl]-4(1H)-one **II.29.** To a solution of **II.28** (0.12 g, 0.51 mmol, 1.1 equiv) in anhydrous THF (3 mL) at –78 $^{\circ}$C was added *n*BuLi (0.25 mL, 0.61 mmol, 1.2 equiv, 2.4 M in hexanes) dropwise. The aryl lithium reagent was stirred for 10 min before adding **II.14** (0.12 g, 0.51 mmol, 1.0 equiv) in anhydrous THF (2 mL) via cannula. After stirring for 1 h, MeI (0.36 g, 0.16 mL, 2.6 mmol, 5.0 equiv) and anhydrous DMF (1 mL) were added and the reaction mixture was allowed to warm to rt over 20 h. The reaction was quenched with water (3 mL) and the biphasic mixture was extracted with EtOAc (2 x 10 mL). The combined organics were washed with 5% aq LiCl (5 x 2 mL). Upon concentrating under vacuum, the resulting

58

crude yellow oil was dissolved in acetone (2 mL) and 10% aq AcOH (2 mL) was added. After stirring for 1 h, the reaction was quenched with sat. aq NaHCO$_3$ (10 mL) and was extracted with EtOAc (2 x 10 mL). The combined organics were washed with brine (5 mL), dried over sodium sulfate, and concentrated on Celite. Purification on silica gel (2 cm x 7 cm, 0 – 5% EtOAc/hexanes) afforded **II.29** as a yellow oil (0.14 g, 71%). ^{1}H NMR (500 MHz, C$_6$D$_6$) δ(ppm) 7.80 (br s, 1H), 7.50 (br s, 1H), 6.50 (s, 1H), 6.02 (br s, 1H), 5.79 (dddd, J = 17.1, 10.0, 6.9, 6.9 Hz, 1H), 5.47 – 5.35 (m, 1H), 5.02 (dd, J = 17.1, 1.7 Hz, 1H), 4.96 (dd, J = 10.0, 1.5 Hz, 1H), 4.88 (d, J = 10.1 Hz, 1H), 4.73 (d, J = 17.1 Hz, 1H), 3.15 (d, J = 6.9 Hz, 2H), 2.81 (s, 3H), 2.57 (dd, J = 17.8, 6.6 Hz, 1H), 2.30 – 2.21 (br m, 1H), 2.11 (s, 3H), 1.82 (br s, 3H); ^{13}C NMR (125 MHz, C$_6$D$_6$) δ(ppm) 184.48, 157.92, 142.03, 137.07, 136.76, 135.05, 134.90, 132.76, 130.24, 129.91, 129.60, 129.51, 127.96, 127.86, 127.77, 127.76, 127.67, 127.58, 127.48, 126.04, 125.85, 124.87, 118.23, 118.03, 116.85, 116.69, 49.45, 35.18, 33.04, 19.80, 15.99.
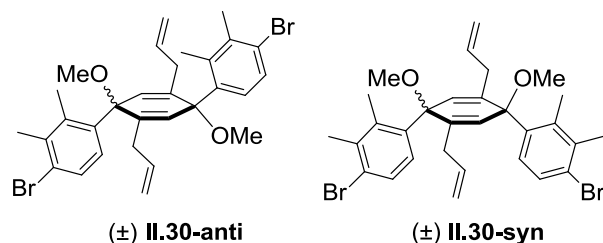
(±) **II.30-anti**   (±) **II.30-syn**

(±)-anti-2',5'-diallyl-4,4''-dibromo-1',4'-dimethoxy-2,2'',3,3''-tetramethyl-1',4'-dihydro-1,1':4',1''-terphenyl **II.30-anti** and *(±)-syn-2',5'-diallyl-4,4''-dibromo-1',4'-dimethoxy-2,2'',3,3''-tetramethyl-1',4'-dihydro-1,1':4',1''-terphenyl* **II.30-syn.** To a solution of **II.28** (90 mg, 0.33 mmol, 1.2 equiv) in anhydrous THF (2 mL) was added *n*BuLi (0.15 mL, 0.36 mmol, 1.1 equiv, 2.4 M in hexanes) at −78 °C. The aryl lithium reagent was stirred

for 10 min before adding **II.29** (98 mg, 0.25 mmol, 1.0 equiv) in anhydrous THF (3 mL).

The reaction mixture was stirred for 1.5 h before MeI (0.64 g, 0.28 mL, 4.5 mmol, 15

equiv) and anhydrous DMF (1 mL) were added and the reaction mixture was allowed to

warm to rt over 16 h. The reaction was quenched with water (10 mL) and the biphasic

mixture was extracted with EtOAc (2 x 10 mL). The combined organics were washed

with 5% aq LiCl (5 x 2 mL) and brine (10 mL), then dried over sodium sulfate and

concentrated on Celite. Purification on silica gel (1 cm x 15 cm, 0 – 2% EtOAc/hexanes)

afforded semi-pure **II.30** (0.13 g) as a 2:1 mixture of diastereomers. Some of the major

diastereomer could be purified completely by washing semi-pure **II.30** with hexanes and

keeping the resulting solid **II.30-anti** (22 mg). The supernatant, which still contained

both diastereomers, was purified again on basic alumina (1 cm x 7 cm, hexanes then 2%

EtOAc/hexanes). From the resulting solid, additional **II.30-anti** could be crystalized from

cold hexanes, each time removing the supernatant, concentrating under vacuum,

dissolving in minimal hexanes, and allowing to sit overnight at –5 ^{o}C. This process was

repeated two times to afford additional **II.30-anti** (17 mg) and a crop of **II.30** that was a

2:1 mixture of **II.30-anti**:**II.30-syn** (24 mg). The supernatant contained only **II.30-syn**

and was purified further by preparative TLC (2% EtOAc/hexanes) to yield an analytically

pure sample of **II.30-syn** (15 mg). Thus, the following white solids were isolated: **II.30-anti** (41 mg, 22%), **II.30-syn** (15 mg, 9%), and **II.30** (24 mg, 14%, anti/syn = 2:1). **II.30-anti**: ^{1}H NMR (500 MHz, C$_6$D$_6$, 70 ^{o}C) δ(ppm) 7.33 (d, J = 9.1 Hz, 2H), 7.11 (br d, J = 9.1 Hz, 2H), 6.30 (s, 2H), 5.75 (ddd, J = 17.1, 10.2, 7.1 Hz, 2H), 4.96 (d, J = 10.2 Hz, 2H), 4.91 (dd, J = 17.1, 1.8 Hz, 2H), 3.06 (s, 6H), 2.80 (d, J = 7.1 Hz, 4H), 2.52 (s, 6H), 2.26 (s, 6H); ^{13}C NMR (125 MHz, C$_6$D$_6$, 70 ^{o}C) δ(ppm) 141.49, 139.96, 138.39, 137.97,

135.25, 130.63, 129.21, 127.85, 127.75, 127.67, 127.56, 127.47, 127.36, 126.90, 125.13, 116.82, 109.99, 79.93, 71.49, 51.03, 35.60, 19.87, 18.45. **II.30-syn**: ^{1}H NMR (500 MHz, C$_6$D$_6$, 70 ^{o}C) δ(ppm) 7.12 (d, J = 8.7 Hz, 2H), 6.52 (d, J = 8.7 Hz, 2H), 6.38 (s, 2H), 5.78 (dddd, J = 17.0, 10.2, 7.0, 7.0 Hz, 2H), 5.01 (dd, J = 10.2, 1.7 Hz, 2H), 4.96 (dd, J = 17.0, 1.7 Hz, 2H), 3.14 (s, 6H), 2.85 (dd, J = 16.9, 7.0 Hz, 2H), 2.71 (dd, J = 16.9, 7.0 Hz, 2H), 2.54 (s, 6H), 2.23 (s, 6H); ^{13}C NMR (125 MHz, C$_6$D$_6$, 70 ^{o}C) δ(ppm) 140.61, 138.73, 138.49, 138.11, 135.33, 130.32, 129.13, 128.07, 127.85, 127.75, 127.66, 127.56, 127.46, 127.37, 126.96, 125.23, 116.86, 80.64, 50.27, 35.05, 19.89, 18.56.
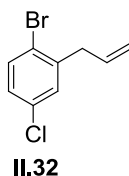
II.32

2-allyl-1-bromo-4-chlorobenzene **II.32**. To a dry RBF charged with a large stirbar, 1-bromo-2-(bromomethyl)-4-chlorobenzene[24] (9.0 g, 32 mmol, 1.0 equiv) and copper(I) iodide (3.0 g, 16 mmol, 0.5 equiv) were suspended in anhydrous dichloromethane (315 mL) and cooled to −78 ^{o}C. Vinylmagnesium bromide (95 mL, 67 mmol, 2.1 equiv, 0.7 M in THF) was then added as a stream via cannula and the reaction mixture was allowed to warm to rt for 16 h. The reaction was quenched by the careful addition of water (100 mL) and was then extracted with ethyl acetate (3 x 200 mL). The combined organics were washed with brine (100 mL), dried over sodium sulfate, and concentrated onto Celite. Purification on silica gel (hexanes) afforded **II.32** as a colorless oil (4.5 g, 61%). ^{1}H NMR (300 MHz, CDCl$_3$) δ(ppm) 7.46 (dd, J = 8.5, 1.2 Hz, 1H), 7.21 (d, J = 2.6 Hz, 1H), 7.05 (dd, J = 8.5, 2.6 Hz, 1H), 5.92 (ddd, J = 16.5, 10.0, 6.3 Hz, 1H), 5.22 – 5.00

(overlap, 2H), 3.46 (d, *J* = 6.3 Hz, 3H); ^{13}C NMR (150 MHz, CDCl$_3$) δ(ppm) 141.24, 134.63, 133.73, 133.39, 130.28, 127.90, 122.36, 117.39, 40.04.
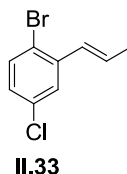
II.33

(E)-1-bromo-4-chloro-2-(prop-1-en-1-yl)benzene **II.33**. To a solution of **II.32** (1.4 g, 6.1 mmol, 1.0 equiv) in anhydrous THF (20 mL) was added solid potassium *tert*-butoxide (3.4 g, 30 mmol, 5.0 equiv). The reaction mixture was stirred under N$_2$ for 21 h. The reaction was quenched by the addition of sat. aq NH$_4$Cl (5 mL), acidified with 1 M aq HCl, and extracted with EtOAc (3 x 20 mL). The combined organics were washed with brine (10 mL), dried over sodium sulfate, and concentrated on Celite. Purification on silica gel (2 cm x 6 cm, hexanes) afforded **II.33** as a colorless oil (0.47 g, 34%). ^{1}H NMR (300 MHz, CDCl$_3$) δ(ppm) 7.44 (d, *J* = 8.4 Hz, 1H), 7.43 (d, *J* = 2.6 Hz, 1H), 7.02 (dd, *J* = 8.4, 2.6 Hz, 1H), 6.65 (dd, *J* = 15.7, 2.0 Hz, 1H), 6.20 (dq, *J* = 15.7, 6.7 Hz, 0H), 1.93 (dd, *J* = 6.7, 2.0 Hz, 2H).
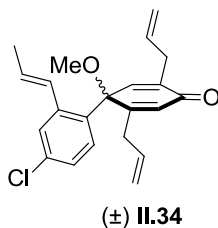
(±) **II.34**

(±)-(E)-2,5-diallyl-4'-chloro-1-methoxy-2'-(prop-1-en-1-yl)-[1,1'-biphenyl]-4(1H)-one **II.34**. To a solution of **II.33** (0.20 g, 0.86 mmol, 1.1 equiv) in anhydrous THF (5 mL) at −78 °C was added *n*BuLi (0.43 mL, 1.0 mmol, 1.3 equiv, 2.4 M in hexanes) dropwise.

The aryl lithium reagent was stirred for 20 min before adding **II.14** (0.18 g, 0.79 mmol, 1.0 equiv) in anhydrous THF (1.5 mL) via syringe. After stirring for 45 min, MeI (0.45 g, 0.20 mL, 3.2 mmol, 4.0 equiv) and anhydrous DMF (1 mL) were added and the reaction mixture was allowed to warm to rt over 16 h. The reaction was quenched with water (3 mL) and the biphasic mixture was extracted with EtOAc (2 x 10 mL). The combined organics were washed with 5% aq LiCl (5 x 2 mL). Upon concentrating under vacuum, the resulting crude yellow oil was dissolved in acetone (1.5 mL) and 10% aq AcOH (1.5 mL) was added. After stirring for 1 h, the reaction was quenched with sat. aq $NaHCO_3$ (10 mL) and was extracted with EtOAc (2 x 10 mL). The combined organics were washed with brine (5 mL), dried over sodium sulfate, and concentrated on Celite. Purification on silica gel (2 cm x 14 cm, $0-5\%$ EtOAc/hexanes) afforded **II.34** as a thick pale yellow oil (0.19 g, 66%). ^{1}H NMR (300 MHz, C_6D_6) δ(ppm) 7.79 (br s, 1H), 7.12 (overlap, 1H), 6.42 (t, $J = 1.7$ Hz, 1H), 6.32 (br d, $J = 15.1$ Hz, 1H), 5.98 (s, 1H), 5.72 (ddt, $J = 17.0, 10.0, 6.8$ Hz, 1H), 5.35 (overlap, 2H), $5.03 - 4.79$ (overlap, 4H), 4.70 (dd, $J = 16.9, 1.7$ Hz, 1H), 3.08 (d, $J = 6.8$ Hz, 2H), 2.79 (s, 3H), 2.53 (dd, $J = 17.7, 6.6$ Hz, 1H), 2.23 (dd, $J = 17.7, 6.8$ Hz, 1H), 1.41 (dd, $J = 6.6, 1.8$ Hz, 3H); ^{13}C NMR (150 MHz, $CDCl_3$) δ(ppm) 185.65, 159.39, 143.32, 134.62, 134.04, 133.98, 132.75, 129.71, 129.39, 128.39, 128.25, 128.10, 127.21, 118.88, 117.38, 50.48, 35.16, 32.80, 18.54.
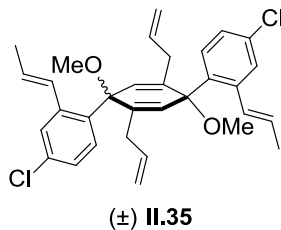
(±) **II.35**

(±)-anti-2',5'-diallyl-4,4''-dichloro-1',4'-dimethoxy-2,2''-di((E)-prop-1-en-1-yl)-1',4'-dihydro-1,1':4',1''-terphenyl **II.35**. To a solution of **II.33** (94 mg, 0.41 mmol, 1.1 equiv) in anhydrous THF (2.5 mL) was added *n*BuLi (0.17 mL, 0.41 mmol, 1.1 equiv, 2.4 M in hexanes) at −78 °C. The aryl lithium reagent was stirred for 20 min before adding **II.35** (0.31 g, 0.37 mmol, 1.0 equiv) in anhydrous THF (1.5 mL). The reaction mixture was stirred for 50 min before MeI (0.21 g, 0.10 mL, 1.5 mmol, 4.0 equiv) and anhydrous DMF (0.5 mL) were added and the reaction mixture was allowed to warm to rt over 16 h. The reaction was quenched with water (10 mL) and the biphasic mixture was extracted with EtOAc (2 x 10 mL). The combined organics were washed with water (5 x 5 mL) and brine (5 mL), then dried over sodium sulfate and concentrated on Celite. Purification on silica gel (2 cm x 6 cm, 0 − 2% EtOAc/hexanes) afforded **II.35** as a white solid (0.15 g, 78%, anti/syn ~ 6:1). An analytically pure sample of the major diastereomer could be isolated by crystallizing the diastereomeric mixture from hot acetone. Major Diastereomer: ^{1}H NMR (300 MHz, C$_6$D$_6$) δ(ppm) 7.51 (d, *J* = 2.4 Hz, 2H), 7.40 (d, *J* = 15.1 Hz, 2H), 6.25 (d, *J* = 8.6 Hz, 2H), 7.03 (dd, *J* = 8.6, 2.4 Hz, 2H), 6.24 (s, 2H), 5.73 − 5.60 (overlap, 4H), 4.94 (d, *J* = 10.5 Hz, 2H), 4.88 (d, *J* = 16.5 Hz, 2H), 3.01 (s, 6H), 2.89 − 2.6 (m, 4H), 1.71 (dd, *J* = 6.6, 1.8 Hz, 6H); ^{13}C NMR (125 MHz, CDCl$_3$) δ(ppm) 140.72, 137.58, 137.55, 135.09, 133.40, 131.47, 130.94, 128.93, 128.90, 128.09, 126.28, 117.63, 79.75, 51.64, 35.46, 18.86.

II.5.3. Selected NMR Spectra

The following NMR spectra are representative examples of certain key intermediates and products that were introduced throughout Chapter **II**. They serve to provide additional structural information about connectivity and insight to dynamic behavior at various temperatures.
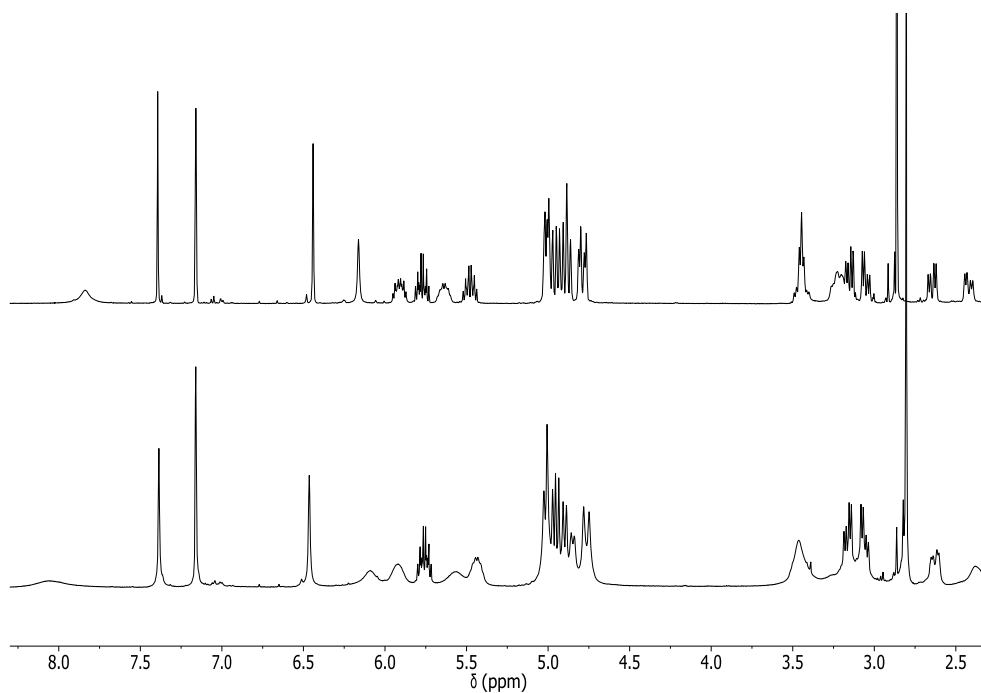
Figure II.5. ^{1}H NMR spectra of **II.19** at 25 $^\mathrm{o}$C (bottom) and 70 $^\mathrm{o}$C (top) in C$_6$D$_6$ (500 MHz).
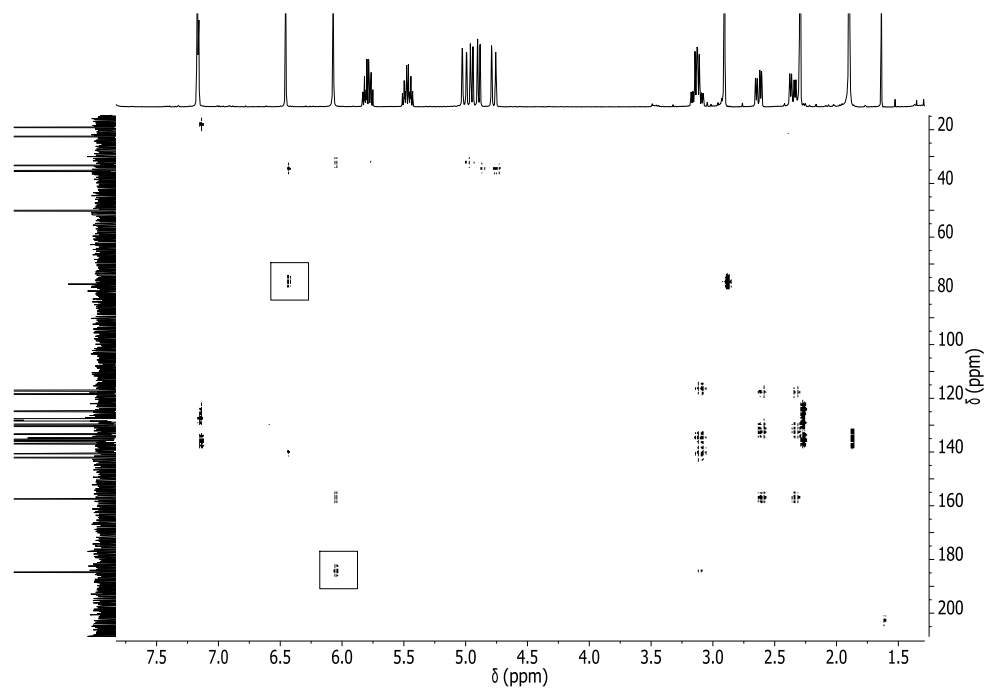
Figure II.6. ^{1}H-^{13}C HMBC NMR spectrum of **II.26** at 70 ^{o}C in C$_6$D$_6$. Relevant cross-peaks are enclosed in a box (500 MHz).
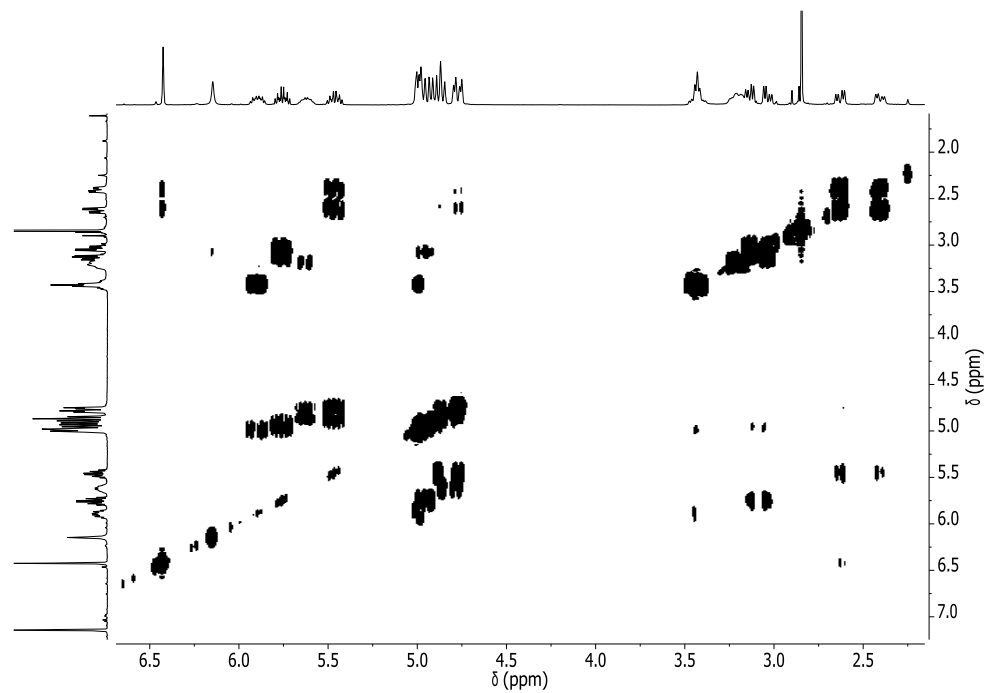
Figure II.7. ^{1}H-^{1}H COSY NMR spectrum of **II.19** at 70 ^{o}C in C$_6$D$_6$ (500 MHz).
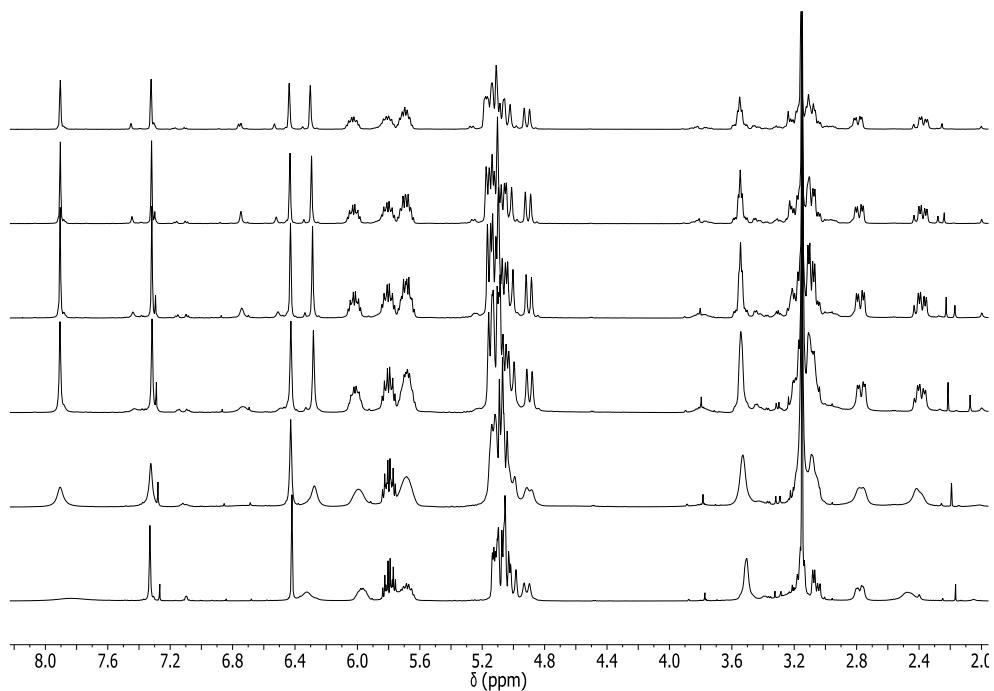
Figure II.8. ^{1}H NMR spectra of **II.19** at 25 ^{o}C, 0 ^{o}C, −10 ^{o}C, −20 ^{o}C, −30 ^{o}C, −40 ^{o}C (bottom - top) in CDCl$_3$ (500 MHz).
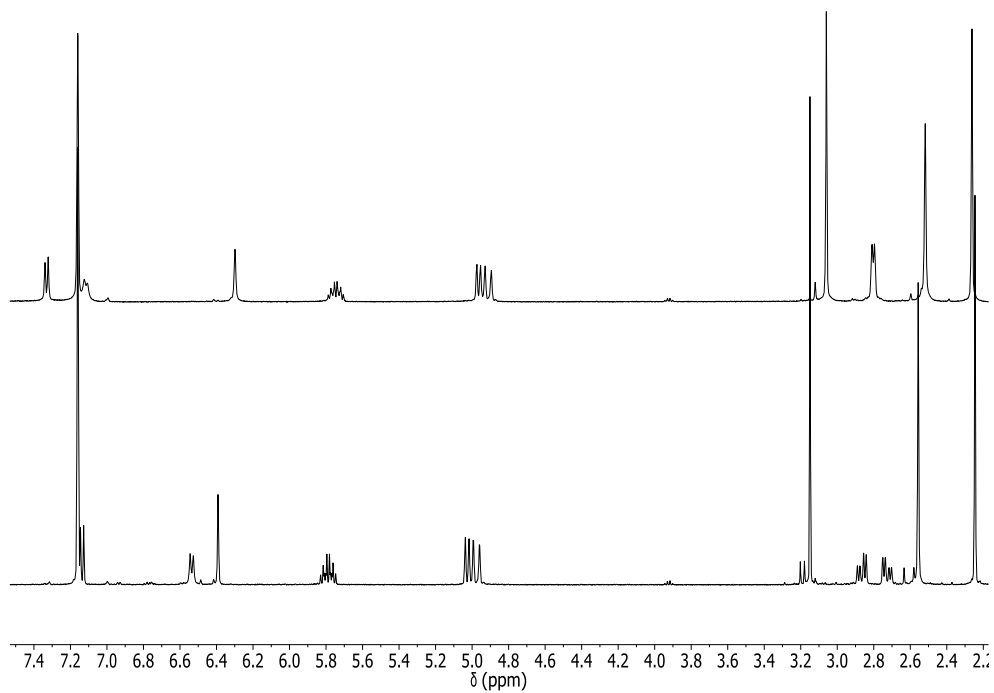
Figure II.9. ^{1}H NMR spectra of **II.30**: syn (bottom) and anti (top) at 70 ^{o}C in C$_6$D$_6$ (500 MHz)

II.5.4. X-ray Crystallographic Data

Data were collected on a Bruker AXS Smart APEX instrument or a Enraf-Nonius CAD-4 Turbo Diffractometer instrument at the University of Oregon. Relevant structures and data used to assign the stereochemistry of **II.21**, **II.27**, **II.30-anti**, **II.30-syn**, and **II.35** are provided below in Figures **II.10** – **II.14** and Tables **II.1** – **II.5**.
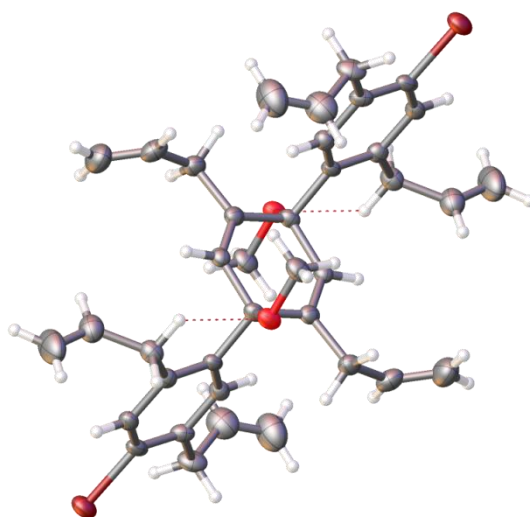
Figure II.10. ORTEP representation of **II.21** (thermal ellipsoids shown at 50% probability).

Table II.1. X-ray crystallographic parameters for **II.21**.

Identification code	cu_jasti7_0m
Empirical formula	$C_{19}H_{22}BrO$
Formula weight	346.28
Temperature/K	173(2)
Crystal system	N/A
Space group	P-1
a/Å	11.0188(4)
b/Å	11.4339(5)
c/Å	14.2012(6)
a/°	74.001(3)
ß/°	77.671(3)

$\gamma/°$	88.154(2)
Volume/Å^3	1679.54(12)
Z	4
ρ_{calc}g/cm^3	1.369
μ/mm^{-1}	3.293
F(000)	716
Crystal size/mm^3	$0.13 \times 0.09 \times 0.04$
Radiation	CuKα (λ = 1.54178)
2Θ range for data collection/°	14.4 to 133.24
Index ranges	$-12 \leq h \leq 13, -13 \leq k \leq 13, -16 \leq l \leq 16$
Reflections collected	10294
Independent reflections	5619 [R_{int} = 0.0491, R_{sigma} = N/A]
Data/restraints/parameters	5619/0/389
Goodness-of-fit on F^2	1.054
Final R indexes [I>=2σ (I)]	R_1 = 0.0578, wR_2 = 0.1726
Final R indexes [all data]	R_1 = 0.0679, wR_2 = 0.1824
Largest diff. peak/hole / e Å^{-3}	0.95/-0.68
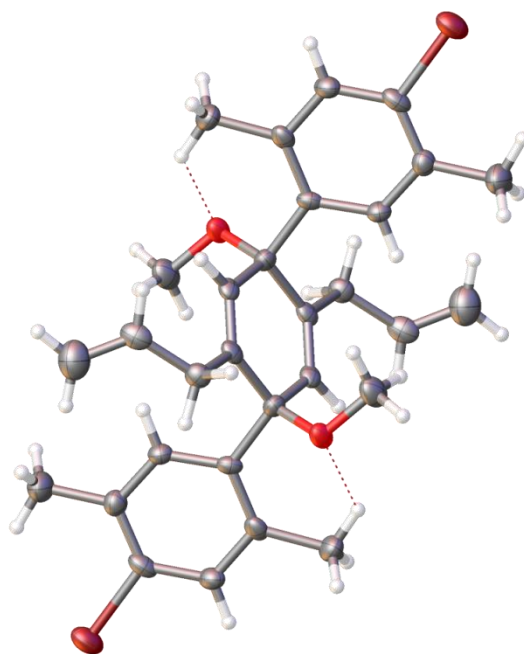
Figure II.11. ORTEP representation of **II.27** (thermal ellipsoids shown at 50% probability).

Table II.2. X-ray crystallographic parameters for **II.27.**

Identification code	mo_jasti15_0m
Empirical formula	$C_{30}H_{34}Br_2O_2$
Formula weight	586.39
Temperature/K	173(2)
Crystal system	triclinic
Space group	P-1
a/Å	9.4294(13)
b/Å	15.874(2)
c/Å	16.066(2)
α/°	117.847(4)
β/°	95.271(4)
γ/°	90.619(4)
Volume/Å^3	2113.4(5)
Z	3
ρ_{calc}g/cm^3	1.382
μ/mm^{-1}	2.9
F(000)	900
Crystal size/mm^3	$0.100 \times 0.090 \times 0.060$
Radiation	MoKα ($\lambda = 0.71073$)
2Θ range for data collection/°	2.884 to 56.392
Index ranges	$-12 \leq h \leq 12$, $-21 \leq k \leq 18$, $-20 \leq l \leq 21$
Reflections collected	28327
Independent reflections	10330 [$R_{int} = 0.1134$, $R_{sigma} = 0.1853$]
Data/restraints/parameters	10330/4/460
Goodness-of-fit on F^2	1.013
Final R indexes [I>=2σ (I)]	$R_1 = 0.0654$, $wR_2 = 0.0986$
Final R indexes [all data]	$R_1 = 0.1823$, $wR_2 = 0.1254$
Largest diff. peak/hole / e Å^{-3}	0.55/-0.61
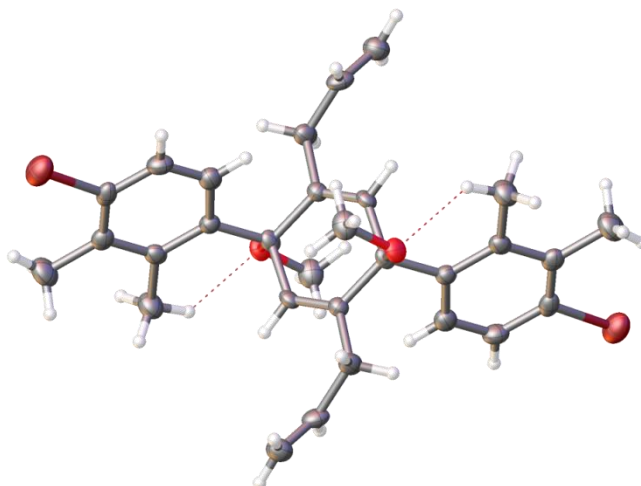
Figure II.12. ORTEP representation of **II.30-anti** (thermal ellipsoids shown at 50% probability).

Table II.3. X-ray crystallographic parameters for **II.30-anti**.

Identification code	mo_jasti16_0m
Empirical formula	$C_{30}H_{34}Br_2O_2$
Formula weight	586.39
Temperature/K	296(2)
Crystal system	triclinic
Space group	P-1
a/Å	10.749(2)
b/Å	10.911(2)
c/Å	14.052(3)
α/°	71.614(4)
β/°	76.361(4)
γ/°	60.928(4)
Volume/Å3	1360.1(5)
Z	2
$\rho_{calc}g/cm^3$	1.432
μ/mm^{-1}	3.004
F(000)	600
Crystal size/mm^3	$0.220 \times 0.190 \times 0.100$
Radiation	MoKα ($\lambda = 0.71073$)
2Θ range for data collection/°	3.07 to 49.994
Index ranges	$-12 \leq h \leq 12$, $-12 \leq k \leq 12$, $-16 \leq l \leq 16$

Reflections collected	19338
Independent reflections	4782 [$R_{int} = 0.0911$, $R_{sigma} = 0.0827$]
Data/restraints/parameters	4782/0/307
Goodness-of-fit on F^2	1.01
Final R indexes [$I>=2\sigma (I)$]	$R_1 = 0.0536$, $wR_2 = 0.1314$
Final R indexes [all data]	$R_1 = 0.0911$, $wR_2 = 0.1525$
Largest diff. peak/hole / e Å^{-3}	1.87/-0.73
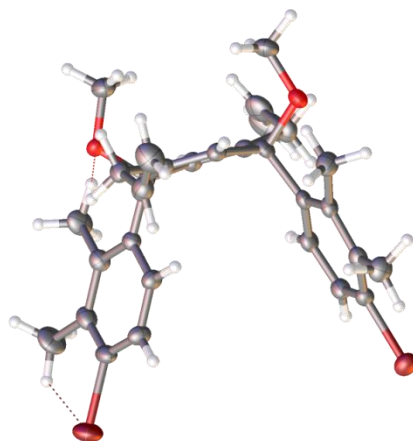
Figure II.13. ORTEP representation of **II.30-syn** (thermal ellipsoids shown at 50% probability).

Table II.4. X-ray crystallographic parameters for **II.30-syn**.

Identification code	cu_jasti17_0m
Empirical formula	$C_{30}H_{34}Br_2O_2$
Formula weight	586.39
Temperature/K	173(2)
Crystal system	monoclinic
Space group	$P2_1/n$
a/Å	8.2099(3)
b/Å	27.6344(9)
c/Å	12.0993(4)
α/°	90
β/°	104.117(2)
γ/°	90

Volume/Å^3	2662.14(16)
Z	4
ρ_{calc}g/cm^3	1.463
μ/mm^{-1}	4.046
F(000)	1200
Crystal size/mm^3	$0.150 \times 0.140 \times 0.060$
Radiation	CuKα ($\lambda = 1.54178$)
2Θ range for data collection/°	6.396 to 133.404
Index ranges	$-9 \leq h \leq 9$, $-32 \leq k \leq 25$, $-14 \leq l \leq 14$
Reflections collected	15756
Independent reflections	4696 [$R_{int} = 0.0680$, $R_{sigma} = 0.0660$]
Data/restraints/parameters	4696/0/307
Goodness-of-fit on F^2	1.049
Final R indexes [I>=2σ (I)]	$R_1 = 0.0621$, wR$_2 = 0.1894$
Final R indexes [all data]	$R_1 = 0.0675$, wR$_2 = 0.1949$
Largest diff. peak/hole / e Å^{-3}	0.64/-1.42
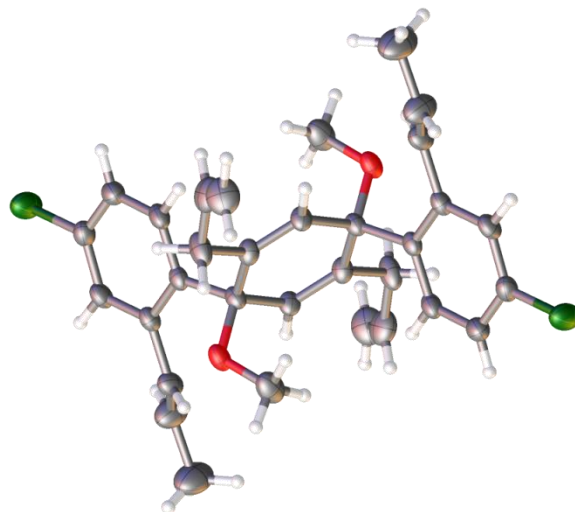
Figure II.14. ORTEP representation of **II.35** (thermal ellipsoids shown at 50% probability).

Table II.5. X-ray crystallographic parameters for **II.35**.

Identification code	mo_jasti26_0m
Empirical formula	$C_{32}H_{34}Cl_2O_2$
Formula weight	521.49
Temperature/K	173(2)
Crystal system	monoclinic
Space group	$P2_1/n$
a/Å	9.856(3)
b/Å	8.573(3)
c/Å	17.254(5)
α/°	90
β/°	94.163(6)
γ/°	90
Volume/Å^3	1454.1(8)
Z	2
$\rho_{calc}g/cm^3$	1.191
μ/mm^{-1}	0.249
F(000)	552
Crystal size/mm^3	$0.210 \times 0.180 \times 0.060$
Radiation	MoKα ($\lambda = 0.71073$)
2Θ range for data collection/°	4.62 to 49.974
Index ranges	$-11 \leq h \leq 11, -10 \leq k \leq 10, -20 \leq l \leq 20$
Reflections collected	10008
Independent reflections	2567 [$R_{int} = 0.0692$, $R_{sigma} = 0.0682$]
Data/restraints/parameters	2567/0/163
Goodness-of-fit on F^2	1.01
Final R indexes [I>=2σ (I)]	$R_1 = 0.0547$, $wR_2 = 0.1204$
Final R indexes [all data]	$R_1 = 0.1032$, $wR_2 = 0.1453$
Largest diff. peak/hole / e Å^{-3}	0.35/-0.28

II.6. Conclusion

Herein, we have discussed the scope of substrates that we have used to synthesize both unfunctionalized and functionalized 1,4-dimethoxycyclohexa-2,5-dienes. Based on the seminal work of Liotta and Wipf, we have successfully developed an electrostatic

model to control the facial selectivity for the addition of aryl lithum nucleophiles to 4,4-disubstituted 2,5-cyclohexadienones. In cases where the components have neither alkyl nor alkenyl substituents, electrostatic shielding of the top face by the newly formed metal alkoxide is effective in reliably delivering the desired syn diastereomer, such as **II.6**. On the contrary, two-fold addition to various quinones with either (4-bromophenyl)lithium or (4-bromonaphthyl)lithium to afford **II.8** – **II.11** gave vastly different stereochemical outcomes. It is still unclear at this time how the size and substitution patterns of the two components dictate the diastereomeric ratio. These results also had implications in the stepwise formation of substituted 1,4-dimethoxycyclohexa-2,5-diene adducts. In general, we found that para substitution on the aryl ring of our 4,4-disubstituted 2,5-cyclohexadienones in combination with para substitution on the aryl lithium component overwhelmingly gave anti products (**II.21** and **II.27**) . Removing substitution from the aryl lithium nucleophile tentatively appears to switch the selectivity to syn (**II.23** and **II.24**), while utilizing ortho aryl substitution on both components (**II.30**) lowers the anti/syn ratio to 2:1. Increasing the size of the substituent closest to the stereocenter of the 4,4-disubstituted 2,5-cyclohexadienone and on the incoming aryl nucleophile causes this selectivity to erode to 6:1 (**II.35**). Work is underway to hone in on the various factors that dictate the diastereomeric ratio for these types of adducts, such that functionalized 1,4-dimethoxycyclohexa-2,5-dienes with predictable stereochemistry can be readily synthesized.

II.7. Bridge to Chapter III

In Chapter **II**, we have discussed the development of methodology to reliably synthesize 1,4-syn-dimethoxycyclohexa-2,5-dienes with excellent diastereomeric ratios, thus leading to numerous [*n*]cycloparaphenylene products. This methodology has been exploited to allow for the synthesis of [8]CPP on gram-scale, allowing for a more thorough study of its physical and electronic properties. With large quantities of [8]CPP available, we studied the controlled oxidation of this carbon nanohoop, as well as its novel photophysical properties. In addition, the implications of the substrates chosen in this chapter in an attempt to predictably synthesize substituted 1,4-syn-dimethoxycyclohexa-2,5-dienes will be made clear later in Chapter **V**.

CHAPTER III

INVESTIGATIONS OF THE [8]CPP RADICAL CATION

This chapter is based on published work in *Chemical Science* (August 2013). I performed the experiments and Prof. Bryan Wong (UC Riverside) performed the majority of the computations in this chapter. Assistance was provided by Dr. Sébastien Rochat (spectroelectrochemistry, Massachusetts Institute of Technology), Dr. Jeffrey W. Bacon (X-ray crystallography, Boston University), and Dr. Paul Ralifo and Dr. Mehkala Pati (EPR spectroscopy, Boston University). Editing was provided by Prof. Ramesh Jasti.

Treatment of [8]cycloparaphenylene (CPP) with the oxidant triethyloxonium hexachloroantimonate afforded an isolable radical cation of the parent carbon nanohoop. The photophysical properties of $[8]CPP^{\cdot+} SbCl_6^-$ were investigated, showing the presence of two absorptions at 535 nm and 1115 nm. Time-dependent density functional theory (DFT) calculations were used to examine these optical absorptions, revealing a delocalized, quinoidal carbon nanohoop. Upon mixing with neutral [8]cycloparaphenylene, the formation of an unusually strong charge-resonance complex $([8]CPP_2)^{\cdot+}$ was observed. Spectroscopic and computational studies were indicative of extensive intermolecular charge delocalization between the two carbon nanohoops as well.

III.1. Introduction

Understanding intramolecular[1] and intermolecular[2] charge transfer phenomena in π-conjugated materials is important for design of better performing organic electronic materials and photovoltaics.[3-5] The study of small molecule aromatic radical cations can

serve as excellent model systems for charge transfer processes in more complex *p*-type materials.[6-9] Seminal work by Kochi[10-11] and Rathore[12-15] allowed for the isolation and characterization of a variety of electron-rich aromatic radical cation salts. Unequivocal analyses of these compounds in the solid state and in solution allowed for direct structural and electronic comparisons between the charged compounds and the neutral parent compounds, providing insight into the behavior of polyphenylene materials. Furthermore, open-shell fragments of conducting polymers such as tetrathiafulvalene[16-19] and oligothiophene[20-23] have been studied as *p*-doped models of conducting polymers.

Radicals derived from polycyclic aromatic hydrocarbons (PAHs) are of particular importance due to their structural similarities to carbon materials such as graphene, fullerenes and carbon nanotubes (CNTs) (Figure **III.1**).[24-25] Numerous charged and uncharged radical planar polycyclic aromatic hydrocarbon compounds have been extensively studied,[1, 25-26] suggesting varying amounts of charge delocalization throughout the respective π-systems. Additionally, studies of *in situ* generated corannulene radical cations and anions have provided insight to the structural and electronic properties of a bent PAH with unpaired electrons.[24, 27-29] Although these systems were observed spectroscopically, it was not until recently that highly distorted, open-shell aromatic compounds were isolated by chemists.[30-32] These nonplanar compounds have been shown to have intriguing electronic and structural properties owing to their non-planar π-systems with three-dimensional spin delocalization.

Lawton, 1967:

Open-shell fullerene fragment

Morita, 2011:

Open-shell graphene fragment

This work:

Open-shell CNT fragment
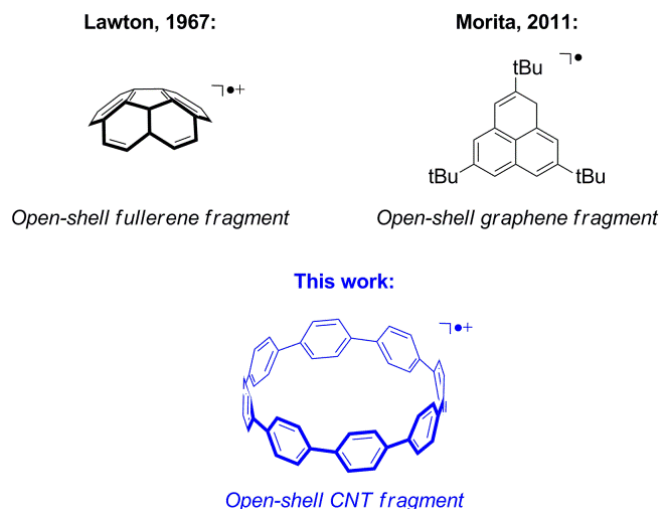
Figure III.1. The [*n*]cycloparaphenylene radical cation represents a rare example of a distorted, open-shell graphitic material.

Over the past several years, our group,[33-34] as well as the groups of Itami[35-36] Yamago,[37-38] Isobe,[39] and Müllen[40] have developed syntheses of short, neutral [*n,n*] armchair CNT fragments. These segments, [*n*]cycloparaphenylenes ([*n*]CPPs),[41-43] have attracted ample interest due to their radially-oriented π-systems, tuneable optical properties and supramolecular capabilities.[34, 44] With our group's ability to access carbon nanohoops on gram-scale,[34] the study of their reactivity has become increasingly viable. For example, in a recent collaboration with the Petrukhina group we have reported on the multi-electron reduction of [8]CPP to a tetraanion, an extremely distorted structure in the solid-state.[45] Herein, we report the first synthesis, theoretical analysis and photophysical characterization of quinoidal $[8]CPP^{\bullet+} \, SbCl_6^-$, as well as the formation of the corresponding unusually strong charge-resonance complex, $([8]CPP_2)^{\bullet+}$.

79

III.2. Experimental Results

III.2.1. Synthesis

Triethyloxonium hexachloroantimonate ($Et_3O^+SbCl_6^-$) (E_{red} = 1.5 V vs. SCE)[11] is a reagent that has previously been used for the generation of numerous aromatic radical cations[11, 13, 46] as well as the oxidation of single-walled CNTs.[8, 47] Treatment of an anhydrous dichloromethane solution of [8]CPP (**III.1**) at 0 °C with $Et_3O^+SbCl_6^-$ immediately led to the formation of a dark orange solution that slowly became deep purple over time (Scheme **III.1**). Upon cooling to −50 °C, the addition of anhydrous pentane led to the precipitation of a purple solid that was isolated in 67% yield. The radical cation **III.1**$^{\cdot+}$ was stable on the order of days at ambient temperature if excluded from excessive moisture. Additionally, exposure to zinc dust allowed for the nearly quantitative reduction back to neutral [8]CPP **III.1**.

Scheme III.1. Single electron oxidation of [8]CPP **III.1**.

III.2.2. Structural Analysis

We anticipated that EPR spectroscopy would provide insight to the electronic nature of the nanohoop radical cation **III.1**$^{\cdot+}$ (Figure **III.18**, Table **III.3**). Charge delocalization has been extensively studied via analysis of EPR hyperfine structures, indicating spin-orbit coupling between the unpaired electron and atoms in the π-system.[10-11, 46, 48-50] Unfortunately in our hands, no hyperfine structure was observed for a dilute (10^{-3} M) solution of **III.1**$^{\cdot+}$ in dichloromethane at 25 $^{\circ}$C. Rather, only a single, broad line (g = 2.007) was obtained, which is consistent with the presence of a delocalized organic radical.[51] The spectrum remained unchanged upon further dilution (10^{-5} M) and cooling to below –263 $^{\circ}$C. In addition, the spectrum remained unchanged even after the addition of 5 equivalents of oxidant. As no EPR signal was observed for either neutral **III.1** or Et$_3$O$^+$SbCl$_6^-$ reagent in CH$_2$Cl$_2$, we cannot attribute the observed signal to a paramagnetic impurity introduced into the experiment (Figure **III.20**). A number of other delocalized aromatic radical cations, such as coronene, biphenyl, phenanthrene,[1] and azacoronene[52] portray unresolved signals as well. Additionally, attempts at characterizing **III.1**$^{\cdot+}$ via single crystal X-ray crystallography have to date been unsuccessful. Twinned crystals were obtained by slowly cooing the crude reaction mixture to –30 $^{\circ}$C in a nitrogen-filled glovebox over the course of 7 days. Unfortunately, refinement of the crystal structure was unsuccessful. Since a stoichiometric amount of antimony trichloride byproduct was present during crystallization it is likely that the SbCl$_6^-$ anion sites were partially occupied by disordered SbCl$_3$. The antimony trichloride could be removed as described in Chapter **III.4.2**, but attempts at crystallizing the purified compound under numerous conditions were unsuccessful.

III.2.3. Photophysical and Electrochemical Characterization of Radical Cation

Aromatic radical cations often have characteristic features in the near-IR (NIR) as observed in the twin absorption bands of the quaterphenyl[15] and biphenyl[53-54] radical cations. As seen in Figure **III.2**, **III.1**$^{\bullet+}$ has two major absorptions at 535 nm ($\varepsilon = 0.81$ ($\pm$ 0.03) x 10^4 M^{-1} cm^{-1}) and 1115 nm ($\varepsilon = 1.03$ ($\pm$ 0.03) x 10^4 M^{-1} cm^{-1}), which is consistent with similar aromatic radical cations. These data are in stark contrast to neutral **III.1**, which has an absorption at 340 nm ($\varepsilon = 1.00$ x 10^5 M^{-1} cm^{-1}) and a broad shoulder around 400 nm.[38] The presence of the two red-shifted absorptions closely matches the values estimated by TD-DFT calculations (*vide infra*).

Spectroelectrochemical experiments (performed in 0.1 M n-Bu$_4$PF$_6$ in CH$_2$Cl$_2$ under ambient conditions) allowed us to monitor the formation of radical cation **III.1**$^{\bullet+}$ *in situ* by applying a constant potential to the sample (Figure **III.17**). Use of slightly higher potentials than the sole observed $E^{ox}_{1/2}$ (0.65 V vs. Fc/Fc$^+$) in the cyclic voltammogram (Figure **III.14**) led to an increase in absorption at 535 nm and a decrease in absorption at 340 nm over 10 minutes. An isosbestic point at 368 nm strongly supports our hypothesis that a single oxidation step occurs from neutral **III.1** to radical cation **III.1**$^{\bullet+}$. This observation is consistent with the absorption in the visible region from both chemical oxidation of neutral **III.1** and the calculated TD-DFT spectrum (*vide infra*). Importantly, this also provides evidence against formation of radical cation **III.1**$^{\bullet+}$ via a disproportionation mechanism involving a dicationic species or interaction between two radical cation species to form a π-dimer.[52, 55-56] Cyclic voltammetry with one equivalent of both neutral **III.1** and ferrocene (Figure **III.15**) revealed almost identical integrated peak areas (A$_1$ / A$_{Fc}$ = 1.06). To further support this claim, differential pulse voltammetry experiments confirmed that the single wave observed in the cyclic voltammogram

corresponds to the transfer of a single electron as evidenced by just one peak in current differential (Figure **III.16**).[52] Lastly, evidence against a dication species is seen in the calculated TD-DFT spectrum for a **III.1**$^{2+}$ species, which is inconsistent with our experimental data (Tables **III.8** – **III.10**). These data, along with the EPR signal, absence of an absorption at 340 nm (Figure **III.2**), and nearly quantitative reduction back to neutral **III.1** confirms the identity and isolation of radical cation **III.1**$^{\cdot+}$.
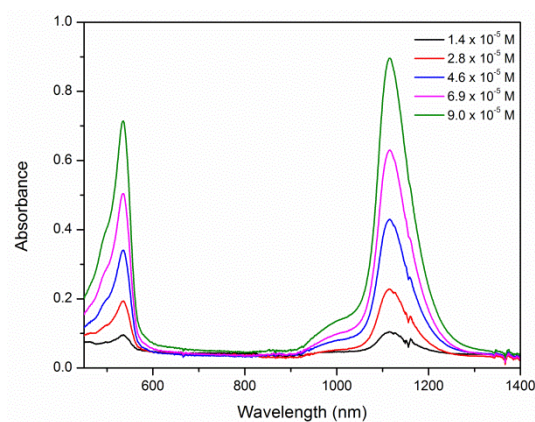
Figure III.2. UV-vis-NIR spectrum of **III.1**$^{\cdot+}$ at increasing concentrations.

III.2.4. Characterization of Charge-Resonance Dimer

Charge-resonance (CR) dimers can be prepared by mixing an aromatic radical cation with its neutral counterpart, giving rise to an intense band in the NIR that results from intermolecular charge transfer (Figure **III.3**). The titration of a yellow dichloromethane solution of **III.1** (8.2 x 10^{-3} M) into a purple dichloromethane
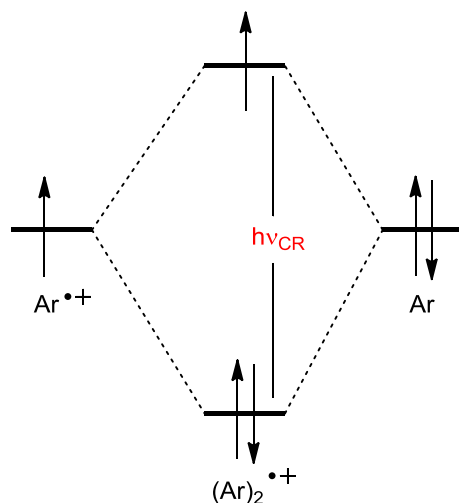
Figure III.3. Diagram showing orbital interactions during the formation of a charge-resonance dimer.

solution of **III.1**$^{\bullet+}$ (1.0 x 10^{-4} M) resulted in the formation of an orange CR dimer,[19] **III.(1)$_2$**$^{\bullet+}$. Concomitant with the gradual decrease in absorbance at 535 nm (loss of purple color) and 1115 nm was the growth of new bands at 687 nm and 1747 nm (Figure **III.4**). We attribute the broad absorption at 1747 nm to a CR transition that has been observed in other mixed valence dimer systems.[19, 46] Specifically, this characteristic near-IR band can be ascribed to the delocalization of positive charge throughout both [8]CPP moieties. In addition, the EPR spectrum of the CR dimer **III.(1)$_2$**$^{\bullet+}$ exhibits a broad, unresolved line as well, confirming its paramagnetic character (Figure **III.19**).
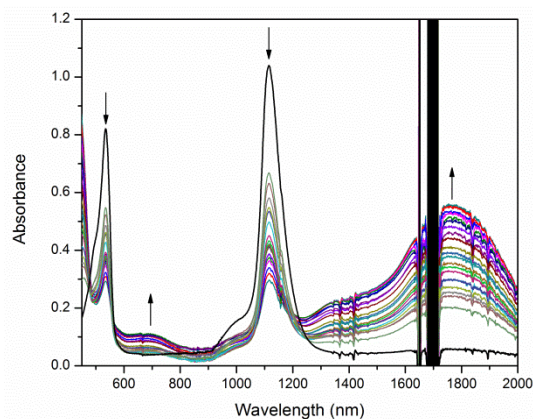
Figure III.4. Titration of neutral **III.1** into solution (Table **III.2**) of **III.1**[.+] leads to a charge-resonance band at 1747 nm.

With the ability to observe the CR complex **III.(1)$_2$**[.+] under ambient conditions, we next sought to investigate the dimerization process quantitatively. The Benesi-Hildebrand procedure (Equation **III.1**)[57] was first used to evaluate the electron transfer process between iodine and benzene[58] and later applied to mixed valence organic paramagnetic complexes.[19, 46, 50] Thus, we used this technique to extrapolate values for the binding constant of **(1)$_2$**[.+], K_{dimer}, as well as the extinction coefficient of its CR band, ε_{1747}:

$$\frac{[\text{III.1}^{\cdot+}]}{A_{1747}} = \frac{1}{\varepsilon_{1747}} + \frac{1}{K_{dimer}\varepsilon_{1747}} \frac{1}{[\text{III.1}]}$$

Equation III.1. Benesi-Hildebrand equation used to determine binding strength.

In order to employ this procedure, we have made the assumption that **III.1**, **III.1**[.+], and **III.(1)$_2$**[.+] are the only three species that exist in solution.[57] Using the data from Figure **III.4** and Equation **III.1**, a linear plot of [(**III.1**)[.+]]/A_{1747} vs **III.1**/[**III.1**] was constructed (Figure **III.5**). The slope and intercept allowed us to extract values of 1.15 ($\pm$ 0.03) x 10^4 M^{-1} and 2.99 ($\pm$ 0.06) x 10^4 M^{-1} cm^{-1} for K_{dimer} and ε_{CR}, respectively.

Unexpectedly, the binding constant calculated is two orders of magnitude larger than that of charge-resonance dimers formed from octamethylbiphenylene (OMB),[46] naphthalene and pyrene.[59] "Sandwich-like" complexes from non-planar PAHs have been observed previously,[60-63] however, *a priori* one might expect planar polycyclic aromatic hydrocarbons to engage in more efficient π-π interactions than the highly distorted nanohoops. The high binding constant suggests that the interaction between the two nanohoops in **III.(1)$_2$**$^{\cdot+}$ is unusually strong compared to other known mixed valence dimers of planar aromatic systems. As pointed out by an insightful reviewer after submission of the material found in this chapter, aggregates formed from a 1:1 ratio of **III.1** and **III.1**$^{\cdot+}$ or "hoop-in-hoop" complexes could also lead to a high binding constant. Further studies are warranted to differentiate between these alternate hypotheses.
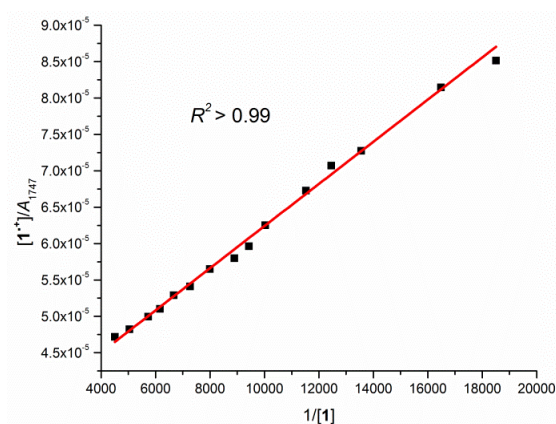
Figure III.5. Benesi-Hildebrand plot of **III.1**$^{\cdot+}$.

With a binding constant in hand, ΔG^o for the formation of dimer **III.(1)$_2$**$^{\cdot+}$ was estimated ($\Delta G^o = -RT \ln K_{dimer}$). By relating the change in Gibbs free energy with the equilibrium constant, K_{dimer}, we calculated that the dimerization process is exothermic by 5.55 kcal/mol. This value, however, should underestimate the true binding energy as no

diffusional entropic parameters are considered for this intermolecular process. This process is in contrast to charge-transfer dimers formed by cyclophane-like radical cations where the entropic changes are negligible due to the rigidity and intramolecularity of the system.[50]

III.3. Computational Analysis and Discussion

III.3.1. Structural Analysis of Radical Cation

Since we were unable to gain any detailed structural information from EPR spectroscopy and X-ray crystallographic analysis, density functional theory (DFT) calculations were performed[49, 64] using the Gaussian 09 package.[65] Previous X-ray crystal structure analysis[34] and theoretical results unequivocally prove the benzenoid character of closed-shell **1**. In contrast, DFT analysis of **III.1**[.+] provides evidence for a delocalized quinoidal structure (Figure **III.6** and **III.22**). This quinoidal nature is evident in the shortening of C_{ipso}-C_{ipso} bonds (**a**) by 1.5 pm and the C_{ortho}-C_{ortho} bonds (**c**) by 0.7 pm, as well as the elongation of the C_{ispo}-C_{ortho} bonds (**b**) by 0.6 pm. Interestingly, the arene rings in neutral **1** are non-uniformly canted to various degrees, ranging from 15° to 33°. In contrast, the benzene rings in **1**[.+] all flatten to a uniform torsional angle of 23° (Table **III.1**).
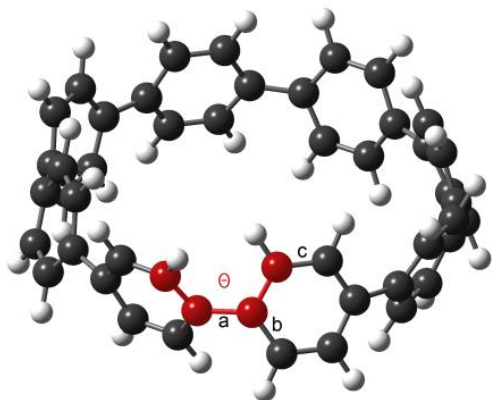
Figure III.6. DFT optimized geometry of **III.1**[·+] performed at the UB3LYP/6-31G(d,p) level of theory. Labels refer to the C_{ipso}-C_{ipso} (a), C_{ispo}-C_{ortho} (b) and C_{ortho}-C_{ortho} (c) bonds. Torsional angle (θ) between aryl rings is depicted in red.

Table III.1. Theoretical[a] bond lengths (pm) and torsional angles (°)[b] of **III.1** and **III.1**[·+].

Parameter	1	1[·+]
a	148.7(1)	147.2(0)
b	140.8(1)	141.4(2)
c	139.1(2)	138.4(0)
θ	26(7)	23(0)

[a] DFT calculations performed at the RB3LYP/6-31G(d,p) or UB3LYP/6-31G(d,p) level of theory for **III.1** and **III.1**[·+], respectively.
[b] Bond lengths are an average of symmetrically equivalent bonds; torsional angles are an average of symmetrically equivalent four-atom angles (*vide supra,* Figure **III.6**)

III.3.2. TD-DFT Calculations for Radical Cation

In order to probe the origins of the optical transitions of **III.1**[·+], time-dependent

(TD) DFT calculations were performed at the UB3LYP/6-31G(d,p) level of theory

(Figure **III.7** and Table **III.4**). Consistent with our experimental data, these calculations

predict an absorption in the near-IR at 1414 nm ($f = 0.2601$) and in the visible region at

644 nm ($f = 0.0021$). The lower energy A-type[66] transition corresponds to a mixture of

degenerate SOMO-1 β → SOMO β and SOMO-2 β → SOMO β, while the higher energy

transition corresponds to a mixture of SOMO-5 β → SOMO β and SOMO-6 β → SOMO

β. As a comparison, the sole predicted absorption for **III.1** at 340 nm (f = 1.4872, 1.3057) at the same level of theory involves the combination of HOMO-1 → LUMO, HOMO → LUMO+1, HOMO-2 → LUMO and HOMO → LUMO+2.[67] The small, broad shoulder around 400 nm present in neutral **III.1** arises from the symmetry-forbidden HOMO → LUMO transition.[38] Of particular significance is the decreased HOMO-LUMO gap (1.1 eV) for **III.1**[·+] compared to that of neutral **III.1** (3.2 eV).

Additionally, the frontier molecular orbitals encompassing these transitions (Figure **III.7**) were analyzed to further understand the electronic nature of **III.1**[·+]. The occupied β orbitals involved show increased electron density along the C_{ipso}-C_{ipso} and C_{ipso}-C_{ortho} bonds, further confirming a delocalized quinoidal character. This electron
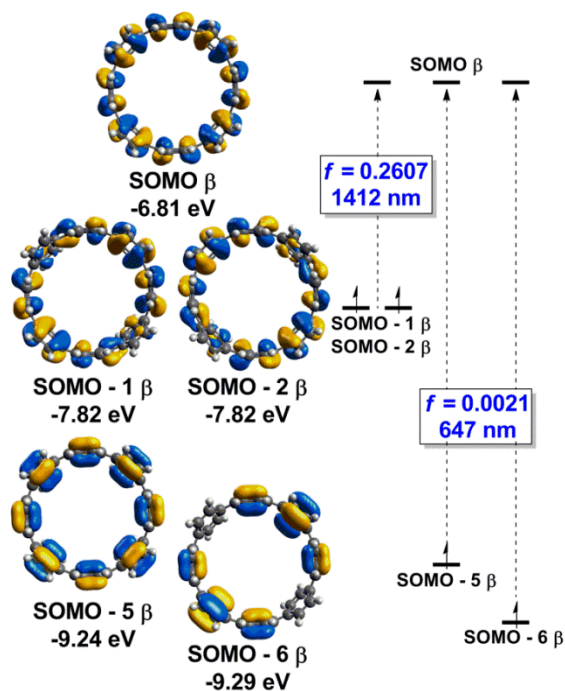
Figure III.7. Electronic transitions (TD-DFT) for **III.1**[·+] calculated at the UB3LYP/6-31G(d,p) level of theory with associated frontier molecular orbitals.[68]

89

distribution is also in good agreement with the shortened C_{ipso}-C_{ipso} (**a**) and C_{ortho}-C_{ortho} (**c**) bonds, as well as the lengthened C_{ipso}-C_{ortho} (**b**) bonds observed in the DFT optimized geometry (*vide supra,* Table **III.1**).

III.3.3. DFT Analysis of Charge-Resonance Dimer

In order to gain further insight to the interactions that contribute to the high stability of **III**.**(1)$_2$**$^{\cdot+}$, DFT calculations were performed at the UωB97X-D/6-31G(d,p)[69-70] level of theory in the gas phase. The UωB97X-D functional has been successfully shown to model charge-transfer complexes, despite the inherent difficulty in modelling their interaction energies with DFT calculations.[71] TD-DFT calculations on the optimized geometry at the same level of theory are consistent with the experimentally observed broad charge-resonance band in the NIR (Table **III.5**). In the optimized geometry (Figure **III.8**), we observe a π→π* interaction between a significantly shortened C_{ipso}-C_{ipso} bond of one quinoidal nanohoop and the face of an aryl ring on the adjacent nanohoop 3.10 Å away. The donating C_{ipso}-C_{ipso} bond has shortened to 144.5 pm, while the torsional angle of this specific C_{ipso}-C_{ipso} bond further decreased to 13°. These structural deformations may contribute to the enhanced interaction in the nanohoop charge-resonance dimer.

We also computationally investigated the charge-resonance dimers arising from ([6]CPP)$^{\cdot+}$**,** ([10]CPP)$^{\cdot+}$ and ([12]CPP)$^{\cdot+}$ to explore the relationship between [*n*]CPP size and binding strength. The geometries of the four nanohoop charge-resonance complexes were optimized after choosing a consistent set of Euler angles to orient one CPP ring relative to the other. This configuration was held constant in all four of the radical cation dimers. The restriction provided a consistent set of geometries for different sized [*n*]CPP charge-resonance dimers for comparison.
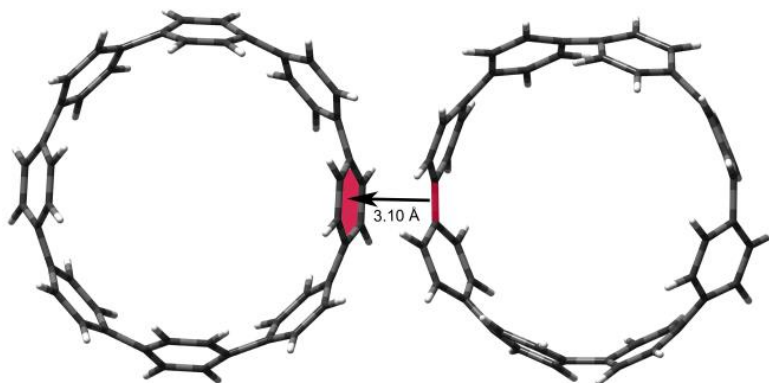
Figure III.8. Optimized geometry of **III.(1)$_2$**$^{\cdot +}$ at the UωB97X-D/6-31G(d,p) level of theory (gas phase) depicting the π→π* interaction (highlighted in red).

The binding energies were determined by subtracting the energies of two individual components (i.e **III.1** and **III.1**$^{\cdot +}$) from the energy of a dimeric structure (i.e **III.(1)$_2$**$^{\cdot +}$) (Figure **III.9** and Table **III.6**). From these data, a general trend emerges relating the size of the nanohoops in a charge-resonance dimer to the binding energy. Specifically, as the nanohoops become larger, the binding energy increases. Presumably, the positive charge is more delocalized throughout the quinoidal π-system in the larger nanohoops than in the smaller nanohoops, giving rise to the observed trend.

To begin investigating this trend experimentally, we attempted to characterize the charge-resonance complex of [12]CPP using the Benesi-Hildebrand procedure. However, even upon treating [12]CPP with a large excess of oxidant (20 equivalents) and prolonging the reaction time, we were never able to isolate or observe [12]CPP$^{\cdot +}$. Rather, only the paramagnetic charge-resonance complex ([12]CPP)$_2$$^{\cdot +}$ was detected by EPR (Figure **III.21**) and UV-vis-NIR (Figure **III.13**) spectroscopy. Both the charge-resonance band in the NIR and the band in the visible region increased in intensity upon addition of neutral [12]CPP (Figure **III.13**). These experimentally observed absorptions are

consistent with the bands observed for **III.(1)$_2$**$^{\cdot+}$. Since [12]CPP$^{\cdot+}$ was not detectable under our experimental conditions, we were not able to measure the exact binding constant for this larger cycloparaphenylene. The experimental observation, however, is consistent with larger carbon nanohoops forming stronger charge-resonance dimers.

Figure III.9. Theoretical binding energies of [n]CPP charge-resonance dimers (n = 6, 8, 10, 12) calculated at the UωB97X-D/6-31G(d,p) level of theory (gas phase).

The study of intermolecular charge transfer in cycloparphenylenes may have implications in analogous phenomena in single-walled CNTs. Prior theoretical[72] and experimental work on systems consisting of two crossed nanotubes has showed that metal-metal nanotube junctions have a very high conductance (0.1 – 0.2 e^2/h).[73-75] In addition, studies have shown a relationship between diameter and conductance in networks made exclusively of CNT bundles.[76] To our knowledge, however, there has been no single study explicitly relating CNT diameter and conductance across CNT-CNT

junctions. Based on our results comparing differing sized [n]CPP charge-resonance dimers, carbon nanotube diameter should dramatically affect hole transport across intermolecular CNT junctions.

III.4. Other Relevant Work

Around the same time as our work outlined in this chapter, the Yamago laboratory published conflicting results concerning the synthesis and characterization of [8]CPP's radical cation and dication.[77] They begin by treating [8]CPP **III.1** with a different oxidant than we used, $NOSbF_6$ in dichloromethane. Using 1.0 equivalents of the reagent afforded what was assigned as [8]CPP$^{\cdot+}$ SbF_6^-, while using excess (5.0 equiv) of reagent delivered what was assigned as [8]CPP^{2+} $(SbF_6^-)_2$. Interestingly, the UV/vis/NIR spectra that they report for these two compounds are fairly consistent with our "charge-resonance" and "radical-cation" spectra, respectively. By adding 1.0 equivalent of [8]CPP **III.1** to over-oxidized [8]CPP^{2+} $(SbF_6^-)_2$, the formation of [8]CPP$^{\cdot+}$ SbF_6^- by optical and EPR spectroscopy was observed. Based on our own experiments, this result seems odd as we should have seen multiple species under our reaction conditions if such a disproportionation mechanism was operative. That is, with the 1.5 equivalents of oxidant that we used (Scheme **III.1**), if we were actually forming [8]CPP^{2+} $(SbCl_6^-)_2$ rather than [8]CPP$^{\cdot+}$ $SbCl_6^-$ **III.1**$^{\cdot+}$, the remaining 0.5 equivalents of [8]CPP **III.1** should have caused some degree of disproportionation to afford a mixture of species with all three oxidation states.

In addition, treatment of [8]CPP **III.1** with $SbCl_5$ (1.5 equiv), which is the parent reagent to the Meerwein salt $Et_3O^+SbCl_6^-$ used by our group, $[8]CPP^{2+}(SbCl_6^-)_2$ was obtained in greater than 50% yield. Based on the stoichiometry of this oxidation, which is identical to the stoichiometry for reactions using $SbCl_5$, (Scheme **III.1**), it is impossible to perform a two-electron oxidation and obtain a 58% yield. Nonetheless, a highly disordered crystal structure of $[8]CPP^{2+}(SbCl_6^-)_2$ was obtained, which potentially faces some of the same difficulties that we encountered in our crystallization attempts (*vide supra*, Chapter **III.2.2**). A ^{1}H NMR spectrum of $[8]CPP^{2+}(SbCl_6^-)_2$ has also been reported, with a single resonance extremely far upfield at approximately 5.1 ppm.[77] There has been additional evidence proposed for an extremely stable "cycloparaphenylene-dication" by magnetic circular dichroism,[78] suggesting stabilization by a special type of in-plane aromaticity, akin to what is observed for *cis*-[32]annulene^{2+}.[79] The NMR spectrum of $[8]CPP^{2+}(SbCl_6^-)_2$ is consistent with what is observed in the aromatic *cis*-[*n*]annulenes.

Based on the stoichiometry of the single-electron oxidation process (Scheme **III.1**), alongside our electrochemical measurements (*vide infra,* Chapter **III.5.3.2**), we were unsure of how a cycloparaphenylene dication could be proposed. Since our initial communication, however,[80] we have been involved in a collaboration with Prof. Rajendra Rathore's group at Marquette University. Their laboratory has preliminary evidence that the first and second cathodic potentials for [8]CPP are actually overlapping, but can be resolved under specialized conditions. Thus, the interplay between [8]CPP and the two aforementioned oxidized species is not entirely clear at this point.

III.5. Experimental

III.5.1. General Experimental Considerations

All glassware was oven dried and cooled under an inert atmosphere of N_2 before usage. Triethoxonium hexachloroantimonate was purchased from Sigma-Aldrich and stored at -30 ^{o}C in an MBraun glovebox filled with N_2. All other manipulations were performed under standard Schlenk technique under an N_2 atmosphere. [8]Cycloparaphenylene (**III.1**) and [12]cycloparaphenylene were synthesized as described in the literature.[34, 81] Dichloromethane and toluene were dried by filtration through alumina according to the methods described by Grubbs (JC Meyer).[82] Anhydrous pentane was purchased from Sigma-Aldrich.

Optical spectra were recorded in screw-top quartz cuvettes using a Shimadzu UV-3600 UV-vis-NIR spectrophotometer under ambient conditions. Spectroelectrochemistry experiments were performed using a honeycomb spectroelectrochemical cell (Pine Instruments) connected to an AUTOLAB PGSTAT 10 potentiostat (Eco Chemie), using 0.1 M nBu$_4$NPF$_6$ in dichloromethane as solvent. UV-Vis spectra were recorded on a Cary 4000 spectrophotometer (Agilent) under ambient conditions with the electrochemical cell inserted into a quartz cuvette. Differential potential voltammetry experiments were performed on a Princeton Applied Research Potentiostat/Galvanastat Model 273 running M270/250 Electrochemical Software (Princeton Applied Research) with a glassy carbon working electrode, platinum counter electrode and silver wire reference electrode. Measurements were conducted in 0.1 M n-Bu$_4$NPF$_6$ in dichloromethane in an MBraun glovebox filled with N_2. Cyclic voltammetry experiments were performed using an CH Instruments 1200B potentiostat running CH Instruments software. Measurements were

conducted in degassed 0.1 M n-Bu$_4$NPF$_6$ in dichloromethane under an N$_2$ atmosphere with a glassy carbon working electrode, platinum counter electrode and Ag/AgCl reference electrode. The ferrocene/ferrocenium couple was used as an internal reference for all electrochemical experiments. nBu$_4$NPF$_6$ was recrystallized from EtOH before use. X-band EPR spectra were recorded on a Bruker ELEXSYS-II E500 CW-EPR equipped with a cryo-cooled cavity using a flame-sealed capillary tube containing a dichloromethane solution of sample placed inside a quartz EPR tube. Spectra were collected with a 100 kHz modulation frequency and 1 G modulation amplitude.

III.5.2. Synthetic Details

Oxidation of [8]CPP (**III.1**): To a 20 mL glass vial with a septum screwcap and stirbar was added triethyloxonium hexachloroantimonate (24 mg, 0.054 mmol) in a glovebox. The vial was sealed, removed from the glovebox and placed under a stream of N$_2$. To the vial was then added dichloromethane (1 mL) and the gold solution was cooled to 0 °C. Then, a bright yellow dichloromethane solution (6 mL) of **1** (21 mg, 0.034 mmol) was added via cannula and the reaction mixture immediately darkened to brown/orange. The solution was stirred at 0 °C for 3 h, then cooled to – 50 °C whereupon anhydrous pentane (10 mL) was added to precipitate out a dark purple solid. The solvent was removed via cannula under N$_2$ pressure and the solid was washed with an additional aliquot of pentane (10 mL). The solid was redissolved in dichloromethane (5 mL) and the process (precipitation then washing) was repeated two additional times (three times total). The dark purple solid was then washed with toluene (10 mL) and pentane (3 x 10 mL), then dried under vacuum to afford highly pure **III.1**$^{\cdot+}$ (22 mg, 69%). UV-vis-NIR

(CH$_2$Cl$_2$): 535 (ε = 0.81 ($\pm$ 0.03) x 10^4 M^{-1} cm^{-1}), 1115 (ε = 1.03 ($\pm$ 0.03) x 10^4 M^{-1} cm^{-1}) nm.

Oxidation of [12]CPP: To a 20 mL glass vial with a septum screwcap and stirbar was added triethyloxonium hexachloroantimonate (240 mg, 0.55 mmol) in a glovebox. The vial was sealed, removed from the glovebox and placed under a stream of N$_2$. To the vial was then added dichloromethane (2 mL) and the gold solution was cooled to 0 ^{o}C. Then, a dichloromethane solution (5 mL) of [12]CPP (25 mg, 0.027 mmol) was added via cannula and the reaction mixture immediately darkened to dark blue. The solution was stirred at 0 ^{o}C for 3 h, then warmed to room temperature for another 14 h. The solution was then cooled to –50 ^{o}C whereupon anhydrous pentane (10 mL) was added to precipitate out a dark blue solid. The solvent was removed via cannula under N$_2$ pressure and the solid was washed with an addition aliquot of pentane (10 mL). The solid was redissolved in dichloromethane (5 mL) and the process (precipitation then washing) was repeated two additional times (three times total). The dark purple solid was then washed with toluene (2 x 10 mL) and pentane (3 x 10 mL), then dried under vacuum to afford 33 mg of a dark blue solid. The compound is EPR active (g = 2.006) and has a broad absorption in the near-IR region, which is reminiscent of a charge-resonance dimer.

The dark blue solid was dissolved to a final concentration of 0.78 mg/mL in CH$_2$Cl$_2$. To 2.4 mL of this solution was added 0.15 mL of neutral [12]CPP (1.9 mM in CH$_2$Cl$_2$) in three separate aliquots (3 x 0.05 mL). A UV-vis-NIR spectrum was recorded after each increment. Figure **III.13** shows bands increasing in intensity at 585 nm and beyond 2000 nm in the NIR.

III.5.3. Optoelectronic Characterization

III.5.3.1. Photophysics

The binding constant, K_{dimer}, for $III.(1)_2{}^{\cdot+}$ was determined by gradually titrating a

dichloromethane solution (8.2 x 10^{-3} M) of **1** into a cuvette containing a dichloromethane

solution of $1^{\cdot+}$ (1.0 x 10^{-4} M). After each aliquot of **1** was added, a spectrum was

recorded, carefully noting the absorption at 1747 nm. From these data, a Benesi-

Hildebrand plot was constructed (Figure **III.5**). The data extracted from the plot is

summarized below in Table **III.2** based on the Benesi-Hildebrand equation (Equation

III.1). Other relevant photophysical data are presented in Figure **III.10** – **III.12**.

Table III.2. Data extracted from UV-vis-NIR spectrum (Figure **III.4**) used to construct a
Benesi-Hildebrand plot (Figure **III.5**).

Total Volume of III.1 Added (μL)	1/[III.1]	$[III.1^{\cdot+}]/A_{1747}$
39	18503.58423	8.5153E-5
44	16487.4552	8.14598E-5
49	13554.90388	7.2748E-5
54	12455.19713	7.07127E-5
59	11524.67604	6.72664E-5
69	10035.84229	6.25136E-5
74	9431.00358	5.96417E-5
79	8897.32237	5.79812E-5
89	7998.49085	5.65055E-5
99	7270.86534	5.40988E-5
109	6669.78339	5.2892E-5
119	6164.87455	5.10385E-5
129	5734.76703	4.99444E-5
149	5041.04521	4.82196E-5
169	4505.88838	4.71776E-5

Figure III.10. UV-vis-NIR spectrum of **III.1**$^{\cdot+}$ (2.7 x 10^{-4} M) and **1** (6.4 x 10^{-6} M). The absence of an absorption at 340 nm and a CR band in the NIR confirms the purity of **III.1**$^{\cdot+}$.

Figure III.11. Beer-Lambert plot of **III.1**$^{\cdot+}$ at 535 nm ($\varepsilon = 0.81$ ($\pm$ 0.03) x 10^4 M^{-1} cm^{-1}).

Figure III.12. Beer-Lambert plot of **III.1**[.+] at 1115 nm ($\varepsilon = 1.03$ (± 0.03) x 10^4 M^{-1} cm^{-1}).

Figure III.13. UV-vis-NIR spectra after the oxidation of [12]CPP (with increasing concentrations of neutral [12]CPP added).

III.5.3.2. Electrochemistry

Cyclic voltammetry of **III.1** (1×10^{-3} M) was performed at increasing scan rates (25 mV/s → 700 mV/s). At a scan rate of 50 mV/s, $E^{ox}_{1/2} = 0.68$ V (vs. Fc/Fc$^+$). The addition of 1 equivalent of ferrocene revealed nearly identical integrated oxidation peak areas for the two species, confirming that **III.1** is oxidized to **III.1**$^{\cdot+}$ via a one-electron process.

Figure III.14. Cyclic voltammograms of **III.1** (1×10^{-3} M) at increasing scan rates (25 mV/s → 700 mV/s) (0.1 M n-Bu$_4$PF$_6$ in CH$_2$Cl$_2$).

Figure III.15. Cyclic voltammogram of **III.1** (1 x 10^{-3} M) containing 1 equivalent of ferrocene (0.1 M n-Bu$_4$PF$_6$ in CH$_2$Cl$_2$, scan rate = 50 mV/s). A$_1$ / A$_{Fc}$ = 1.06.

Differential potential voltammetry was used to achieve maximum sensitivity in current changes and confirmed that the single wave in the cyclic voltammogram corresponds to a single electron oxidation process.

Figure III.16. Differential pulse voltammogram of radical cation **III.1**$^{\cdot+}$ (0.1 M n-Bu$_4$PF$_6$ in CH$_2$Cl$_2$) (pulse height = 25 mV, scan increment = 2 mV).

102

Spectroelectrochemistry experiments were performed in order to probe the behavior of neutral **1** close to its oxidation potential. Thus, based on the cyclic voltammogram (Figure **III.14**), a constant potential of 0.8 V was applied for minutes 0 – 8. The potential was then increased to 0.9 V for another two minutes (minutes 8 – 10). At each time point, a UV-vis spectrum was recorded, showing a gradual increase in absorption at 535 nm (radical cation **III.1**$^{\cdot+}$) and a gradual decrease in absorption at 340 nm (neutral **1**). An isosbestic point was also observed at 368 nm, suggesting direct oxidation from **III.1** to radical cation **III.1**$^{\cdot+}$.

Figure III.17. UV-vis spectrum (in CH_2Cl_2) depicting the gradual oxidation over time of neutral **1** to radical cation **III.1**$^{\cdot+}$ with an applied potential. Applied potentials are all relative to the Fc/Fc$^+$ couple for consistency when referring to cyclic voltammogram (Figure **III.15**)

III.5.4. EPR Spectroscopy

Figure III.18. X-band EPR spectra of **III.1**$^{\cdot+}$ (10^{-3} M) recorded at: (a) 293 K. (b) 167 K. (c) 8 K. (d) 8 K (10^{-5} M) (e) 293 K (after 5 equiv oxidant).

Table III.3. Parameters associated with the five EPR spectra of **III.1**$^{\cdot+}$ shown in Figure **III.18**.

	a	b	c	d	e
Frequency (GHz)	9.389310	9.388179	9.389615	9.389778	9.867088
g	2.007	2.006	2.007	2.008	2.007

Figure III.19. X-band EPR spectrum of charge-resonance dimer **III.(1)$_2$$^{\cdot+}$** in CH$_2Cl_2$ after the completion of titration experiments (Frequency = 9.389929 GHz, g = 2.007 G)
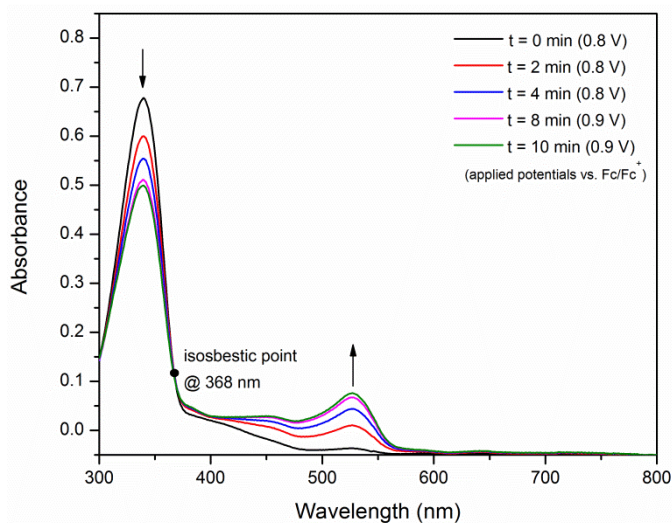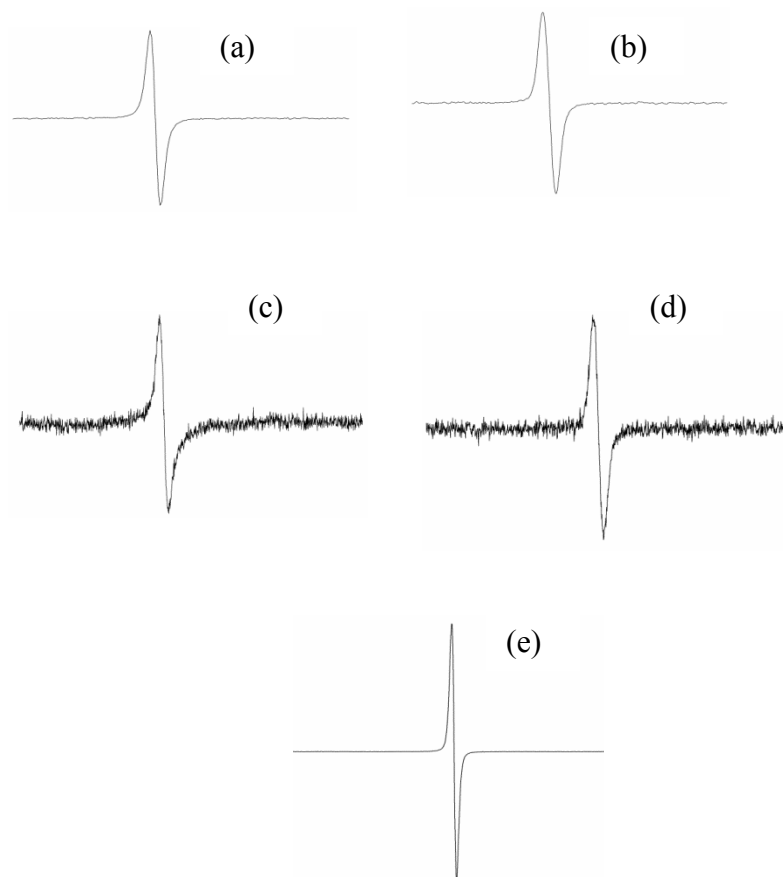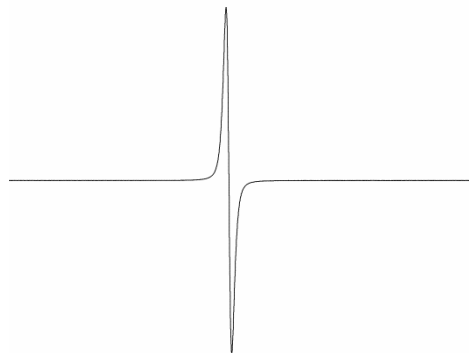
Figure III.20. Control X-band EPR spectra (CH$_2$Cl$_2$) of (left) triethyloxonium hexachloroantimonate and (right) [8]Cycloparaphenylene **III.1** from 3000 – 4000 G. The absence of signal confirms that the experimentally observed signals come from **III.1**$^{\cdot+}$ and **III.(1)$_2$$^{\cdot+}$**.

Figure III.21. X-band EPR spectrum of ([12]CPP)$_2$$^{\cdot+}$ after optical titration experiments (CH$_2$Cl$_2$) (Frequency = 9.857404 GHz, g = 2.006)
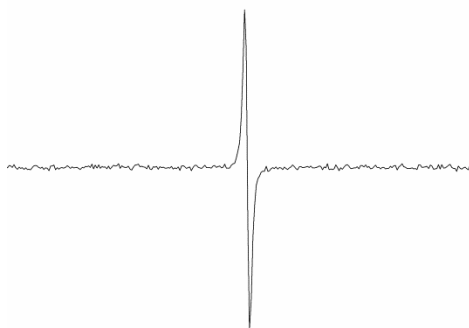
III.5.5. Computational Details

All calculations were carried out with the Gaussian 09 package.[65] Calculations

performed on **III.1** and **III.1**[·+] used the B3LYP exchange-correlation functional[83] and a

polarized 6-31G(d,p) basis set[84] using default SCF convergence criteria (density matrix

converged to at least 10^{-8}) and the default DFT integration grid (75 radial and 302 angular

quadrature points). Calculations performed on the four [n]CPP charge-resonance dimers

used the long-range corrected hybrid ωB97x functional[69] with an empirical dispersion

term (ωB97xD).[70] Calculations performed on the hypothetical **III.1**[2+] dication species

were performed at the RB3LYP/6-31G(d) level of theory (closed-shell singlet) or

UB3LYP/6-31G(d) level of theory (open-shell singlet and triplet). All excited state

calculations (TD-DFT) were performed on fully optimized structures. The fully

optimized structures were confirmed to be true minima by vibrational analysis.

III.5.5.1. Analysis of Radical Cation

Figure III.22. Spin density distribution of **III.1**[·+] calculated at the UB3LYP/6-31G(d,p) level of theory showing complete delocalization of positive spin (blue).

Table III.4. Predicted absorptions of radical cation **III.1**$^{\cdot+}$ via TD-DFT calculations (UB3LYP/6-31G(d,p)).

Energy (cm^{-1})	Wavelength (nm)	Osc. Strength	Major contributions
7071.11152	1414.204821	0.2601	H (B)→L (B) (100%)
7071.11152	1414.204821	0.2601	H-1(B)→L (B) (100%)
14679.392	681.2271244	0	H-2(B)→L (B) (97%)
14681.81168	681.1148527	0	H-3(B)→L (B) (97%)
15085.89824	662.8707049	0	H-4(B)→L (B) (99%)
15508.53568	644.8062026	0.0021	H-5(B)→L (B) (99%)
15508.53568	644.8062026	0.0021	H-6(B)→L (B) (99%)
16478.82736	606.8392964	0	H-7(B)→ L (B) (98%)
16480.44048	606.7798984	0	H-8(B)→L (B) (98%)
17091.81296	585.0754407	0	H-9(B)→L (B) (99%)
17091.81296	585.0754407	0	H-10(B)→L (B) (99%)
17423.30912	573.9437859	0	H-11(B)→L (B) (99%)

Table III.5. Predicted absorptions of charge-resonance dimer **III.(1)$_2$**$^{\cdot+}$ via TD-DFT calculations (UωB97xD /6-31G(d,p)).

Energy (cm^{-1})	Wavelength (nm)	Osc. Strength	Major contributions
6035.48848	1656.86672	0.3842	H-3(B)→L (B) (29%), H-1(B) →L(B) (24%), H(B) →L(B) (39%)
8745.53008	1143.441268	0.2844	H-14(B) →L(B) (10%), H-4(B) →L(B) (75%)
11524.93584	867.6837892	0.1009	H-1(B) →L(B) (63%), H(B) →L(B) (18%)
11925.79616	838.5184407	0.009	H-2(B) →L(B) (79%)
12743.648	784.7046623	0.0113	H-3(B) →L(B) (47%), H(B) →L(B) (42%)
16678.85424	599.561568	0.002	H-22(B) →L(B) (12%), H-20(B) →L(B) (68%)
18579.1096	538.2389262	0.0003	H-27(B) →L(B) (82%)
19057.39968	524.7305597	0.0156	H-15(B) →L(B) (11%), H-13(B) →L(B) (14%), H-9(B) →L(B) (10%), H-6(B) →L(B) (22%), H-1(B) →L(B) (11%)
19346.95472	516.8772112	0.0002	H-14(B) →L(B) (28%), H-4(B) →L(B) (11%)
19914.77296	502.1397944	0.1406	H-5(A) →L(A) (20%), H-1(A) →L(A) (21%)
20626.15888	484.8212437	0.0029	H-13(B) →L(B) (11%), H-6(B) →L(B) (14%)

III.5.5.2. Analysis of Charge-Resonance Dimers

We analyzed a series of charge-resonance dimers for several different [n]CPP systems. For each value of "n", the geometries of the neutral monomer ([n]CPP) and radical cation monomer ([n]CPP)$^{\cdot+}$ were minimized. The energy of the charge-resonance complex was then minimized using the same level of theory. The binding energy was calculated by subtracting the sum of the energies of the two monomers from the energy of the charge-resonance dimer.

Table III.6. Energies (in Hartress) of the components making up four charge-resonance [n]cycloparaphenylene dimers (([n]CPP)$_2^{\cdot+}$) (n = 6, 8, 10, 12). Calculations were done at the UωB97xD/6-31G(d,p) level of theory.

n	Neutral	Radical Cation	Charge-Resonance Dimer	Binding Energy
6	-1385.75873228	-1385.51883903	-2771.29690059	-0.01932928
8	-1847.76942719	-1847.52228711	-3695.31447870	-0.0227644
10	-2309.76555675	-2309.50991553	-4619.30549827	-0.03002599
12	-2771.75393372	-2771.49492278	-5543.28222063	-0.03336413

III.5.5.3. Analysis of a Dication

In order to probe the predicted absorption spectrum of the **III.1**$^{2+}$ dication (arising from an oxidation of the radical cation **III.1**$^{\cdot+}$ or over-oxidation of neutral **1**), the ground-state energies of the closed-shell singlet (R), open-shell singlet (U) and triplet (T) were calculated. It was found that the ground-state energies of the closed-shell singlet and the open-shell singlet are nearly equal and have predicted absorptions at 922 nm, which are inconsistent with the experimentally determined values from the oxidation of **III.1**.

Table III.7. Difference in ground-state energies between the three configurations of **III.1^{2+}**.

	Energy (kcal/mol)
ΔU-R	0.01
ΔT-R	7.49
ΔT-U	7.50

Table III.8. Predicted absorptions for **III.1^{2+}** (closed-shell singlet) via TD-DFT calculations (RB3LYP/6-31G(d)).

Energy (cm^{-1})	Wavelength (nm)	Osc. Strength	Major contributions
10839.35984	922.5637074	0.4944	H→L (100%)
10840.1664	922.4950643	0.4943	H-1→L (100%)
16681.27392	599.4745994	0	H-4→L (100%)
17183.7608	581.9447859	0.0009	H-5→L (100%)
17184.56736	581.9174723	0.0009	H-6→L (100%)
18024.19632	554.8097581	0	H-7→L (53%), H-3→L (43%)
18024.19632	554.8097581	0	H-8→L (53%), H-2→L (43%)
18629.11632	536.7941146	0	H-8→L (40%), H-2→L (48%)
18630.72944	536.7476369	0	H-7→L (40%), H-3→L (48%)
19192.0952	521.0478531	0	H-9→L (100%)
19192.90176	521.0259566	0	H-10→L (100%)
19568.75872	511.0186161	0	H-11→L (100%)

Table III.9. Predicted absorptions for **III.1^{2+}** (open-shell singlet) via TD-DFT calculations (UB3LYP/6-31G(d)).

Energy (cm^{-1})	Wavelength (nm)	Osc. Strength	Major contributions
1829.27808	5466.637418	0	H (A)→L (A) (70%), H (B)→L (B) (70%)
1835.73056	5447.422524	0	H-1(A)→L (A) (70%), H-1(B)→L (B) (70%)
10840.1664	922.4950643	0.4941	H (A)→L (A) (50%), H (B)→L (B) (50%)
10840.97296	922.4264314	0.4938	H-1(A)→L (A) (50%), H-1(B)→L (B) (50%)
13816.3728	723.7789646	0	H-2(A)→L (A) (49%), H-2(B)→L (B) (49%)
13817.98592	723.6944702	0	H-3(A)→L (A) (49%), H-3(B)→L (B) (49%)
15164.13456	659.450756	0	H-4(A)→L (A) (49%), H-4(B)→L (B) (49%)
15681.13952	637.7087575	0	H-5(A)→L (A) (49%), H-5(B)→L (B) (49%)
15681.94608	637.6759586	0	H-6(A)→L (A) (49%), H-6(B)→L (B) (49%)

16683.6936	599.387656	0	H-4(A)→L (A) (50%), H-4(B)→L (B) (50%)
16811.13008	594.8440083	0	H-7(A)→L (A) (49%), H-7(B)→L (B) (49%)
16815.96944	594.6728219	0	H-8(A)→L (A) (49%), H-8(B)→L (B) (49%)

Table III.10. Predicted absorptions for **III.1^{2+}** (triplet) via TD-DFT calculations (UB3LYP/6-31G(d)).

Energy (cm^{-1})	Wavelength (nm)	Osc. Strength	Major contributions
2467.26704	4053.067559	0	H (B)→L (B) (99%)
9318.18768	1073.170057	0.1331	H (B)→L+1(B) (91%)
12169.37728	821.7347338	0.2469	H-2(B)→L (B) (13%), H-1(B)→L (B) (71%)
12183.89536	820.7555716	0.2184	H-2(B)→L (B) (80%), H-1(B)→L (B) (11%)
12465.3848	802.2215247	0.0133	H-7(B)→L (B) (11%), H-3(B)→L (B) (77%)
12757.35952	783.8612672	0	H-4(B)→L (B) (94%)
12876.7304	776.5946548	0.0001	H-8(B)→L (B) (22%), H-5(B)→L (B) (64%)
13574.4048	736.6805504	0.018	H-6(B)→L (B) (86%)
13900.25504	719.4112605	0.0088	H-8(B)→L+1(B) (11%), H-7(B)→L (B) (73%), H-3(B)→L (B) (14%)
14180.13136	705.2120849	0.0025	H-8(B)→L (B) (62%), H-5(B)→L (B) (26%)
15097.99664	662.3395301	0	H-10(B)→L+1(B) (14%), H-9(B)→L (B) (81%)
15194.78384	658.120583	0.0003	H-10(B)→L (B) (81%), H-9(B)→L+1(B) (14%)

III.6. Conclusion

In summary, [8]CPP **III.1** was successfully chemically oxidized for the first time and isolated as a cationic hexachloroantimonate salt. A thorough comparison of bond lengths and angles derived via DFT calculations illustrate the delocalized quinoidal character of **III.1**$^{·+}$. The optical properties of this novel radical cation were further explored, displaying transitions in both the visible region and in the near-IR. TD-DFT calculations and an FMO analysis allowed us to relate the quinoidal structural data with the observed optical transitions, revealing four A-type transitions from singly-occupied β

orbitals with varying quinoid-like character. The spectroscopic properties of **III.1**$^{•+}$ were then exploited to observe an *in situ* CR dimer with an unusually large binding constant, K_{dimer}. The charge-resonance band at 1747 nm was characteristic of extensive charge delocalization throughout both cycloparaphenylene rings. Furthermore, DFT calculations showed that a general trend exists relating nanohoop size and charge-resonance binding strength. The highly delocalized nature of the [*n*]CPP radical cations – both intramolecularly and intermolecularly – bodes well for their use in advanced organic electronics and photovoltic devices. We are continuing to investigate these species in collaboration with Professor Rajendra Rathore's group at Marquette University.

III.7. Bridge to Chapter IV

In this chapter, we began to explore many of the physical organic properties that our newly found carbon nanohoops possess. Through an oxidation reaction, a whole new class of important organic compounds was realized. While [*n*]CPPs and structurally related molecules, including but not limited to the aforementioned compounds, have potential applications directly as organic materials, we have also been interested in using the structural backbone offered by [*n*]CPPs as building-blocks for homogeneous armchair CNTs. Thus, Chapter **IV** begins our foray into extended [*n*]CPP-related structures. Through the synthesis of dimeric cycloparaphenylenes, as will be discussed in the next chapter, we begin to develop methodology and tools to link [*n*]CPPs and study their structural and optoelectronic properties.

CHAPTER IV

SYNTHESIS, CHARACTERIZATION, AND COMPUTATIONAL STUDIES OF

CYCLOPARAPHENYLENE DIMERS

This chapter is based on both published work in *Journal of the American Chemical Society* (November 2012) and unpublished work. Experimental work and TD-DFT computations were performed by Dr. Jianlong Xia and myself. All other calculations were performed by Dr. Michael Foster (Sandia National Laboratory) and Prof. Bryan Wong (UC Riverside). Dr. Jeffrey Bacon (Boston University) collected the X-ray crystallographic data. Editing was provided by Prof. Ramesh Jasti.

Two novel arene-bridged cycloparaphenylene dimers (**IV.1** and **IV.2**) were prepared using a vinyl bromide functionalized precursor. The preferred conformations of these dimeric structures were evaluated computationally in the solid-state, as well as in the gas and solution phases. In the solid-state, the "trans" configuration is preferred by 34 kcal/mol due to the denser crystal packing structure that is achieved. In contrast, in the gas phase and solution phase, the cis conformation is favored by 7 kcal/mol (**IV.1**) and 10 kcal/mol (**IV.2**), with a cis to trans activation barrier of 20 kcal/mol. The stabilization seen in the cis conformations is attributed to the increased van der Waals interactions between the two cycloparaphenylene rings. Together, these calculations indicate that that the cis conformation is accessible in solution, which is promising for future efforts towards the synthesis of short carbon nanotubes (CNTs) via cycloparaphenylene monomers. In addition, work towards the synthesis of a directly linked cycloparaphenylene dimer is presented.

IV.1. Background

Since their discovery in 1991,[1] carbon nanotubes (CNTs) have captured the

interest of physicists, engineers, and chemists due to their unique architecture, desirable

optoelectronic properties, as well as their high tensile strength.[2] Over the last two

decades, chemical vapor deposition[3] and laser ablation methods[4] have been developed

further, allowing for the scalable production of carbon nanotubes. These synthetic

methods, however, provide very little control over CNT diameter or chirality—the two

structural features that determine the band gap of CNTs.[2, 5] In order to take advantage of

the unique properties of CNTs for applications in nanotechnology, new synthetic

approaches to circumvent these shortcomings must be pursued.[6-9]

The [*n*]cycloparaphenylenes ([*n*]CPPs) represent the shortest possible fragment of

an armchair CNT. Due to this structural relationship, the CPPs have recently attracted

significant attention due to their potential as monomeric precursors or seeds for the

"bottom-up" synthesis of uniform armchair CNTs.[5-8, 10-19] Additionally, CPPs exhibit size-

dependent, tunable optoelectronic properties[16, 20-26] which position them as novel "carbon

quantum dots" for optoelectronic applications.[23] Furthermore, the cycloparaphenylenes

possess unique nanosized cavities which can be exploited for supramolecular

assemblies[25, 27] or as components of novel graphitic materials and porous organic

frameworks. With these promising features in mind, the CPPs have become highly touted

non-natural synthetic targets.

Only recently have the cycloparaphenylenes succumbed to synthesis. As early as

1934, well before the discovery of CNTs, the [*n*]CPPs were first conceptualized and the

initial attempts were made at their preparation.[28] These highly strained aromatic

macrocycles were later revisited by Vögtle and co-workers in 1993, but they too were unsuccessful in synthesizing the desired [n]CPPs.[29] It was not until 2008 that the CPPs were finally prepared by Jasti and Bertozzi utilizing novel reductive aromatization methodology.[22] Since then, our group,[22-25, 30] as well as the groups of Itami[16, 31-35] and Yamago[21, 36-37] have made the synthetic availability of [n]CPPs (n = 6 – 16, 18) possible. Most recently, our group has developed the gram-scale synthesis of two different sized CPPs, heightening the interest in using these fascinating structures in materials science applications and as possible precursors to uniform CNTs.[38-50]

Despite recent contributions by Itami,[16, 31-35] Yamago,[21, 36-37] and our group,[22-25, 30] a synthetic procedure towards the functionalization of cycloparaphenylenes had not been reported prior to this work. In particular, synthetic methods that can connect CPP units may allow access to wider polyaromatic hydrocarbon belts and ultimately CNTs. Herein, we describe the first synthesis of arene-bridged cycloparaphenylene dimers (Figure **IV.1**, **IV.1** and **IV.2**) as well as their optoelectronic characterization (Figure **IV.2**). We also report computational studies indicating that in the gas phase and in solution these arene-bridged cycloparaphenylene dimers prefer cis conformations in which the two cycloparaphenylene units are stacked on top of each other in a nanotube-like geometry. Related to this work is a recent report from the Anderson laboratory where two porphyrin nanorings are linked together such that a short nanotube structure is formed.[51] Our results, along with synthetic access to linked CPP structures, open up the possibility of using **IV.1** and **IV.2** to synthesize short CNT fragments via cycloparaphenylene monomers. More broadly, the synthetic methodology developed in this work will be

amenable to preparing a wide variety of monofunctionalized CPPs for use in materials science applications.
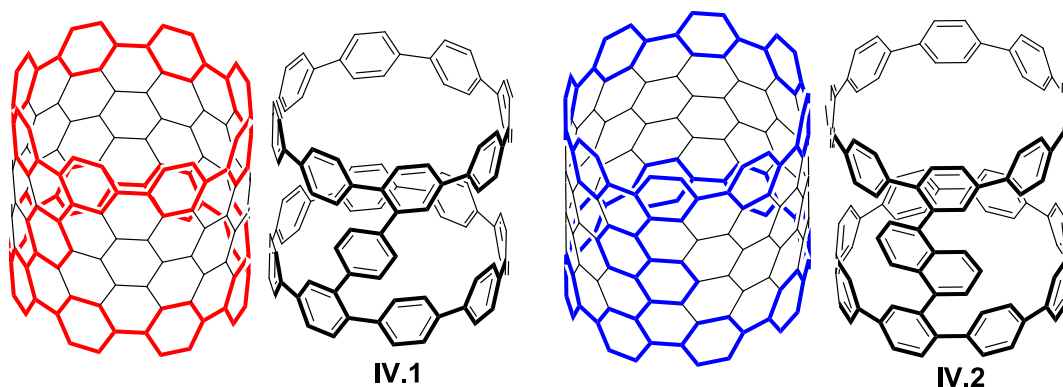
Figure IV.1. Cycloparaphenylene dimers are short segments of armchair carbon nanotubes (CNT double bonds omitted for clarity).

IV.2. Synthesis of Aryl-Linked Cycloparaphenylenes

In order to couple two cycloparaphenylene molecules, installation of a functional handle for dimerization was required. We hypothesized that a late-stage functionalization reaction of CPP would likely lead to mixtures so we turned our attention to preparing a mono-functionalized macrocyclic precursor. We envisioned bromo-substituted macrocycle **IV.7** as a key intermediate—a structure that could be further derivatized through transition metal catalyzed cross-coupling reactions (Scheme **IV.1**). Recently, we reported a sequential oxidative dearomatization/addition procedure using cyclohexadiene units as masked benzene rings to prepare compound **IV.6** on multi-gram scale. This building block was successfully used in the synthesis of [6]cycloparaphenylene,[24] the smallest CPP to date, as well as the first gram-scale synthesis of [8]CPP and [10]CPP.[25]

We expected that bromo-substituted macrocycle **IV.7** could be prepared efficiently by taking advantage of readily available building block **IV.6**.

Diiodide **IV.5** (Scheme **IV.1**), which bears a vinyl bromide functionality within the cyclohexadiene unit, is easily prepared in two steps. The synthesis started from 2-bromo-4,4-dimethoxycyclohexa-2,5-dienone **IV.3**,[52] which underwent an addition of (4-iodophenyl)lithium, and subsequent deprotection with 10% AcOH to generate bromodieneone **IV.4** in 90% yield. Deprotonation of alcohol **IV.4** with sodium hydride followed by addition of (4-iodophenyl)lithium, and subsequent methylation in a one-pot sequence[25] produced brominated monomer **IV.5** in 78% yield and in high diastereoselectivity. Diiodide **IV.5** and diboronate **IV.6**[24-25] underwent Suzuki coupling/macrocyclization in the presence of Pd(OAc)$_2$ (10 mol%.) and Cs$_2$CO$_3$ (4 equiv) in DMF/iPrOH (10:1) at 100 °C for 24 h to deliver macrocycle **IV.7** in 30% isolated yield. Notably, the less reactive vinyl bromide remained intact under these reaction conditions.
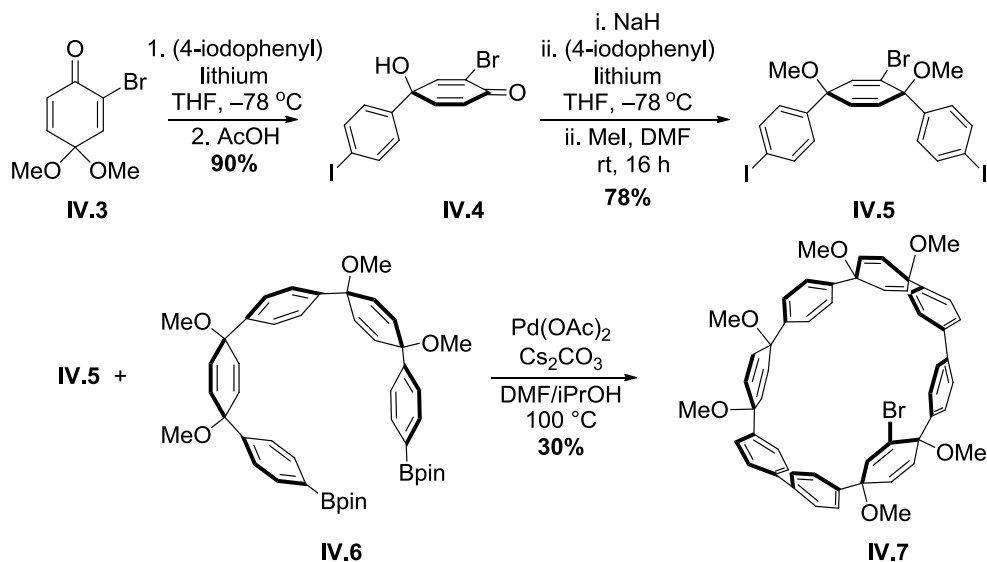
Scheme IV.1. Synthesis of bromo-substituted macrocycle **IV.7**.

116

With bromo-substituted macrocycle **IV.7** in hand, we next investigated the reactivity of the vinyl bromide for metal-catalyzed cross-coupling reactions to prepare macrocyclic precursors to arene-bridged dimers **IV.1** and **IV.2** (Scheme **IV.2**). After careful exploration, we found that macrocycle **IV.7** and commercially available 1,4-benzenediboronic acid bis(pinacol) ester **IV.8** underwent an efficient Pd-catalyzed cross-coupling reaction in the presence of $Pd(PPh_3)_4/Cs_2CO_3$ in toluene/H_2O at 80 °C for 24 h to deliver the dimeric macrocycle **IV.10** in 66% isolated yield. Under the same conditions, the 1,5-naphthalene bridged dimeric macrocycle **IV.11** was also assembled by coupling of **IV.7** with 1,5-naphthalenediboronic acid bis(pinacol) ester[53] **IV.9** in 49% yield. A careful analysis of the ^{1}H and ^{13}C NMR data of the macrocycles **IV.10** and **IV.11** reveal the high level of C_2 symmetry in these two molecules. Both compounds only show four types of methyl ethers, suggesting high levels of asymmetry close to the arene bridge, and greater equivalence further away from the bridge. This symmetry is confirmed by the 30 and 33 sp^2 resonances observed in the ^{13}C spectra of **IV.10** and **IV.11** respectively, suggesting symmetry about the two macrocycles. Additionally, **IV.10** and **IV.11** show further evidence of substitution in the alkene region of their ^{1}H NMR spectra, with one or more resonances shifted downfield of δ 6.0 ppm. A MALDI-TOF analysis of both **IV.10** and **IV.11** confirms their structures with masses of 1664.3682 *m/z* and 1713.4715 *m/z*, respectively.
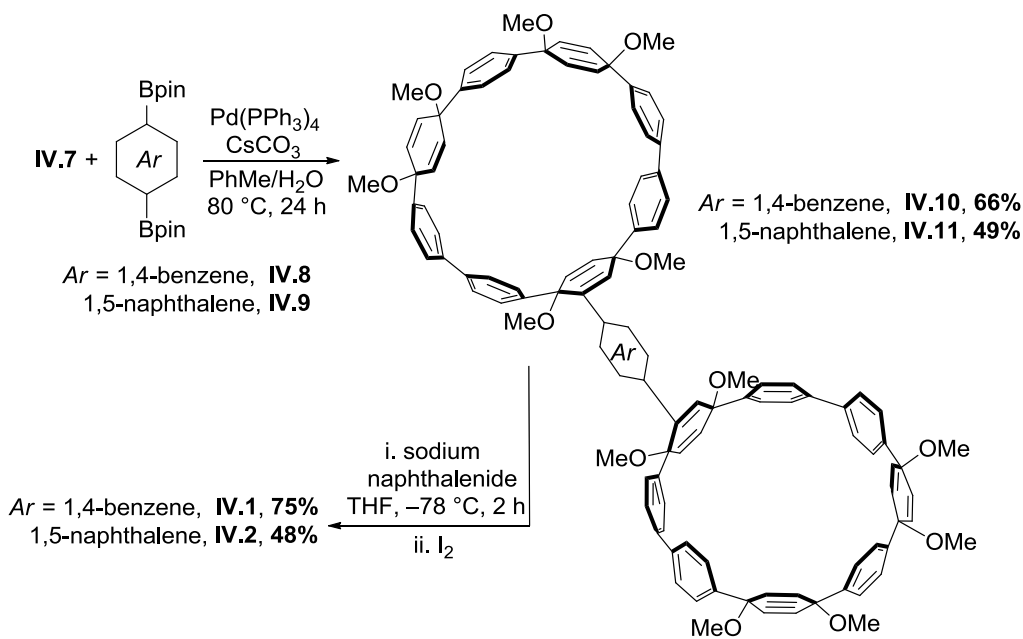
Scheme IV.2. Dimerization and reductive aromatization to synthesize **IV.1** and **IV.2**.

Subjecting **IV.10** and **IV.11** to sodium naphthalenide[25] at −78 °C for 2 h and then quenching with I_2 led to the arene-bridged CPPs **IV.1** and **IV.2** in 75% and 48% isolated yield, respectively. Both compounds exhibit clusters of overlapping peaks around 127.4 and 137.8 ppm in the ^{13}C NMR spectra—consistent with the chemical shifts observed for [8]CPP.[21] The ^{1}H NMR spectra of both compounds are complex with multiple overlapping peaks ranging from 7− 8 ppm as expected. The MALDI spectra of **IV.1** and **IV.2** show single peaks at 1291.5924 and 1341.1713, respectively.

IV.3. Optoelectronic Characterization

With the CPPs possessing unique optoelectronic properties, we were curious about the behavior of these novel dimeric structures. Both **IV.1** and **IV.2** exhibit an absorption maximum at 340 nm, similar to that of [8]CPP and other CPPs (Figure **IV.2**).

118

The extinction coefficient (ε) of dimer **IV.1** is 0.87 x 10^{-5} M^{-1} cm^{-1}, which is slightly

smaller than that of [8]CPP (ε = 1.0 x 10^{-5} M^{-1} cm^{-1}),[21] while dimer **IV.2** exhibits an

increased ε value of 1.7 x 10^{-5} M^{-1} cm^{-1} (Figures **IV.7** and **IV.8**). The corresponding

emission spectra have the same maximum as [8]CPP at about 540 nm (Figure **IV.2**), with

improved fluorescence quantum yields of 0.18 and 0.15 (Figures **IV.9** and **IV.10**),
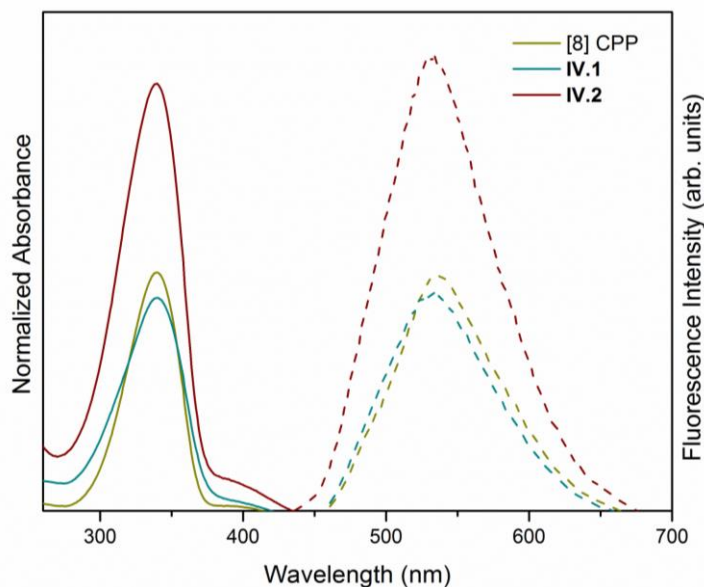
Figure IV.2. Normalized UV-Vis absorption (solid line) and fluorescence spectra (dot line) of **IV.1**, **IV.2** and [8]CPP in dichloromethane.

respectively, in contrast to that of [8]CPP (0.10).[30] The enhanced quantum yields may

indicate a more rigid structure. Cyclic voltammetry analysis showed that the half-wave

oxidation potentials of **IV.1** and **IV.2** are 0.64 V and 0.68 V (vs. Fc/Fc^+), which are larger

than that of [8]CPP (0.59 V) (Figures **IV.11** and **IV.12**).[21]

IV.4. Computational Studies

IV.4.1. Conformational Analyses

With the first cycloparaphenylene dimers in hand, we were interested in the conformational dynamics of these molecules in solution. One can envision two extreme orientations—a trans conformer in which the two CPP rings are positioned as far apart as possible from each other or a cis conformer in which the CPP rings are oriented on top of each other in a nanotube-like arrangement (Figure **IV.1**). If the cis conformer is accessible in solution, further carbon-carbon bond forming reactions using functionalized dimers may be feasible to "lock" the molecule into a nanotube-like geometry. In addition to this enticing possibility, the dimeric CPPs can also be envisioned as supramolecular host molecules which can readily switch orientation.[54-60] The energetics and pathways for this conformational isomerization are relevant for both types of future studies. In an effort to unravel the conformational dynamics of these molecules, we first considered NMR analysis. Unfortunately, the high levels of symmetry in these molecules impede this type of study. Therefore, we decided to investigate these issues *in silico* (*vide infra*).

As an initial starting point for our investigations, we decided to examine the solid-state structure of these dimeric CPPs. Accordingly, several attempts were made to acquire the crystal structures of dimers **IV.1** and **IV.2**. Unfortunately, due to the insolubility of these compounds, our attempts to acquire a refined structure were not successful. However, we were able to obtain preliminary X-ray crystallographic data for dimer **IV.1**, indicating that the trans conformation is preferred in the crystalline state (Figure **IV.18**).

Due to the uncertainty in the crystallographic data, we sought to verify this result computationally by performing periodic boundary condition calculations using the PBE-

D functional with projector augmented wave pseudopotential on the experimental crystal structure (trans) (Figure **IV.3**) and a representative cis crystal structure (Figure **IV.15**). Upon optimization of the unit cell and atomic positions, the trans crystal structure is predicted to be lower in energy by 34 kcal/mol per molecule. In addition, the unit cell volume of the optimized trans structure is smaller by 16% resulting in a denser crystal packing. This computational result is consistent with the preliminary X-ray data that was acquired.
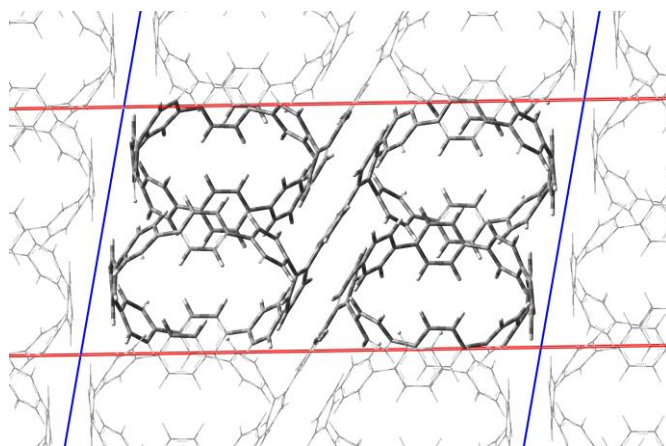
Figure IV.3. Optimized (PBE-D functional) solid-state packing of trans **IV.1**.

Next, we examined the dynamics of the CPP dimer systems in both the gas phase and in solution. An analysis of the conformational barrier from trans to cis in the gas-phase was conducted for **IV.1** using density functional theory (DFT) based *ab initio* calculations.[61-62] It is important to note that to properly model these nanohoop systems, a computational method capable of modeling van der Waals interactions must be used, such as the B3LYP-D functional. The B3LYP functional alone is incapable of modeling van

der Waals interactions and is therefore quantitatively incapable of modeling these types of systems. We also investigated these systems using the M06-2X functional, which like B3LYP-D, is designed for modeling van der Waals interactions. For both types of calculations, the same quantitative results were achieved.

The potential energy curve (PEC) (Figure **IV.14**) corresponding to the trans to cis conformational change in compound **IV.1** was calculated by starting with the optimized trans geometry and creating a series of structures mapping the conformational change. These structures were optimized, minimizing the total energy, while constraining two dihedral angles (Figure **IV.13**). At the B3LYP-D/6-31G(d,p) level of theory, the energy barrier from trans to trans (i.e. left to right) is 13 kcal/mol. The energy barrier from cis to trans (i.e. right to left) is 20 kcal/mol, in which the lowest energy pathway is that in which one CPP ring flips on top of the other as opposed to a rotating motion around the aryl linker axis (Figure **IV.4**). In contrast to the solid-state structure, the cis conformation is found to be 7 kcal/mol more stable in energy in the gas phase because of the increased van der Waals interactions between the two rings. The cis conformation of dimer **IV.2** is predicted to be 10 kcal/mol lower in energy than the trans conformation (Figure **IV.14**). Furthermore, SCRF calculations using a polarizable continuum model (PCM) and the B3LYP-D functional showed no changes in the preferred conformation or relative stability of **IV.1** and **IV.2** via the inclusion of dichloromethane solvent effects. These results together are very promising for future efforts towards the synthesis of short carbon nanotubes via cycloparaphenylene monomers.
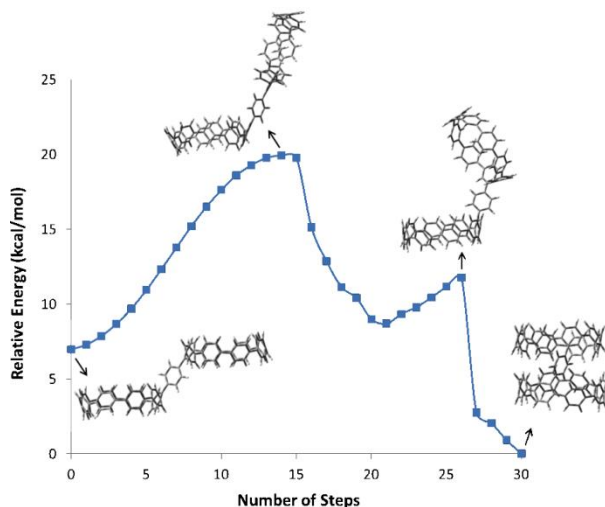
Figure IV.4. The potential energy curve (B3LYP-D/6-31G(d,p)) of the trans to cis transition for **IV.1**.

IV.4.2. Time-Dependent DFT Calculations

To gain a more in depth understanding of the optical data for the CPP dimers, we carried out TD-DFT calculations at the B3LYP-D/6-31G(d,p) level of theory (Table **IV.1**) for both the cis and trans conformations of **IV.1** and **IV.2**. The calculations revealed that although the HOMO→LUMO transition is forbidden for [8]CPP ($f = 0$), the HOMO→LUMO transition of dimers **IV.1** and **IV.2** have non-zero oscillator strengths.[*] Consistent with this result, we observe weak shoulder peaks centered around 400 nm for both dimers **IV.1** and **IV.2** that is not present in the absorption spectrum of [8]CPP (*vide supra*, Figure **IV.2**). Furthermore, TD-DFT results indicate that the maximum absorption of the cis conformation of **IV.1** can be assigned to a combination of HOMO-3→LUMO, HOMO→LUMO+2 and HOMO→LUMO+3 transitions, while the maximum absorption for cis **IV.1** can be assigned to HOMO-4→LUMO, HOMO-3→LUMO, and HOMO→LUMO+3. The maximum absorption of the trans conformation at

---

[*] For a full analysis of all optical transitions for dimers **IV.1** and **IV.2**, see Tables **IV.3** – **IV.7**.

123

Table IV.1. Significant optical contributions of **IV.1** and **IV.2** obtained via TD-DFT calculations.[a]

	Major Contributions[b]	Oscillator Strength	Wavelength (nm)
[8] CPP	H→L	0	473
	H-1→L	1.4872	356
	H→L+1	1.4872	356
	H-2→L	1.3057	345
	H→L+2	1.3057	345
cis	H→L	0.0084	481
	H→L+2	0.2574	365
Dimer **IV.1**	H→L+3	0.2574	365
	H→L	0.0085	467
	H→L+2	1.0170	379
trans	H-2→L	0.7106	373
cis	H→L	0.0146	479
	H–4→L	0.1236	368
	H–3→L	0.1236	368
Dimer **IV.2**	H→L+3	0.1236	368
	H→L	0.0199	465
	H→L+2	0.4018	379
trans	H–2→L	0.6321	373

[a]Calculations were performed at the B3LYP-D/6-31G(d,p) level of theory. [b]H = HOMO, L = LUMO.

approximately 375 nm can attributed to a blending of HOMO-2→LUMO and HOMO→LUMO+2 transitions for both **IV.1** and **IV.2**. TD-DFT calculations predict very similar optical absorption spectra for both the cis and trans conformers of dimers **IV.1** and **IV.2**. Hence, we were not able to differentiate the preferred conformations of **IV.1** or **IV.2** by analysis of the UV-vis data.

In addition to the TD-DFT calculations, we also analyzed the frontier molecular orbitals of dimer **IV.1** (Figure **IV.5**). In contrast to the predicted absorption spectra, the frontier molecular orbitals of the cis and trans configurations of **IV.1** are localized quite differently. Most notably, in the cis configuration, the HOMO and LUMO lie almost

exclusively on one cycloparaphenylene ring on either side of the arene bridge. On the other hand, the HOMO and LUMO are more evenly distributed across the arene bridge in the trans configuration. An FMO analysis on dimer **IV.2** led to similar results (Figure **IV.17**).
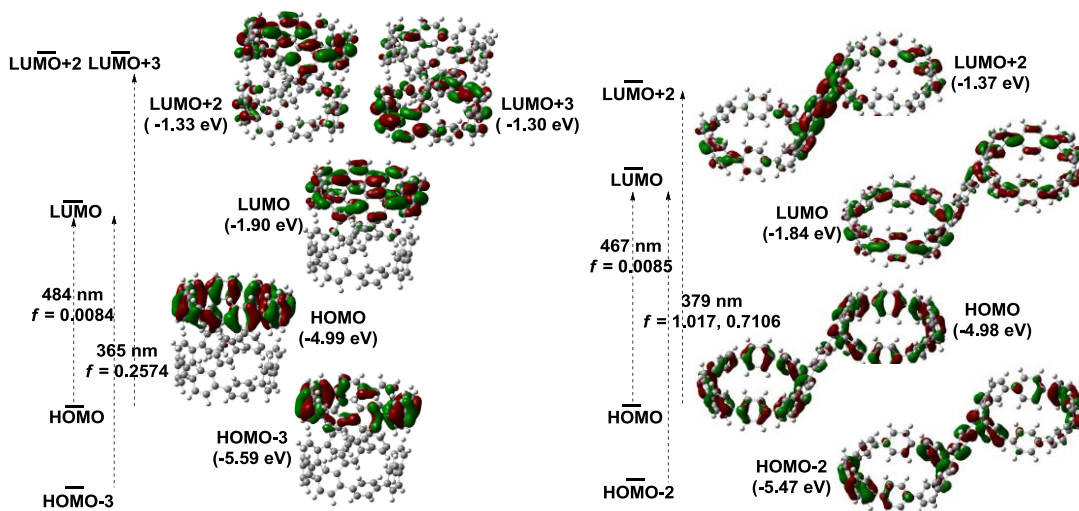
Figure IV.5. Major electronic transitions (TD-DFT) and representative FMOs for **IV.1** cis (left) and trans (right), calculated at the B3LYP/6-31G(d,p) level of theory.

IV.5. Towards the Synthesis of a Directly Linked Cycloparaphenylene Dimer

IV.5.1. Motivation

Inspired by arene-bridged cycloparaphenylene dimers **IV.1** and **IV.2**, we were also interested in the conformational dynamics of a direct CPP dimer (i.e. no arene-linker) (Figure **IV.6**). This molecule is especially fascinating because if it can be prepared, successful cyclodehydrogenation would deliver an ultra-short CNT in one step. To probe this type of structure further, we again analyzed the potential energy surface of the corresponding cis to trans conformational change by DFT calculations (Figure **IV.16**). Surprisingly, the trans conformation is predicted to be a relatively unstable local

minimum in comparison to the cis conformation, which is predicted to be 30 kcal/mol lower in energy.
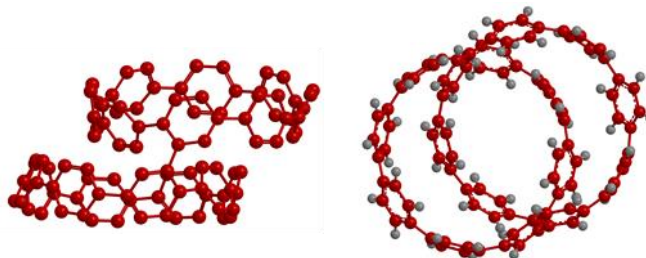
Figure IV.6. Side-view (left) and top-view (right) of lowest-energy conformation of directly-linked [8]CPP dimer.

IV.5.2. Synthetic Attempts

Having synthesized two different aryl-bridged [8]CPP dimers, we envisioned a directly-linked dimer arising from a coupling reaction involving the vinyl bromide functional handle. Dr. Jianlong Xia first synthesized model compound **IV.13** in two steps from **IV.3** in 63% yield. So we could evaluate coupling conditions, portions of **IV.13** were also either borylated (**IV.14**, 80% yield) or stanylated (**IV.15**, used crude) (Scheme **IV.3**). In addition, **IV.13** was used directly under reductive homocoupling conditions. Under the seven different cross-coupling conditions that we screened (Table **IV.2**), we always observed various mixtures of starting materials, unidentifiable decomposition products, and dehalogenated **IV.13**. Interestingly, the nucleophile coupling partner **IV.14** or **IV.15** was almost always observed by crude ^{1}H NMR. In only one case, an attempted Stille coupling using Pd(PPh$_3$)$_4$ / AsPh$_3$ in DMF (Table **IV.2**, entry 6), did we observe
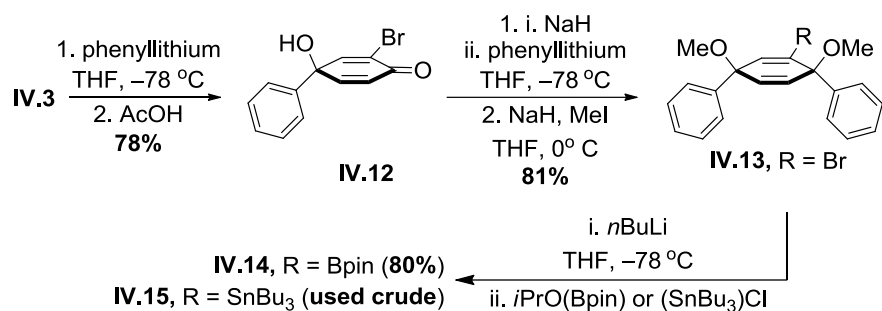
Scheme IV.3. Synthesis of coupling partners **V.13** – **V.15** for attempted direct-dimer formation.

decomposition of the vinyl nucleophile. Additionally, reductive homocoupling conditions either returned starting material (Table **IV.2**, entry 8) or led to reductive aromatization, presumably via electron transfer, as evidenced by the loss of olefin and methyl ether resonances in the crude ^{1}H NMR spectrum (Table **IV.2**, entry 9). We attribute these results partially to the sterics around the vinyl substituent, but probably more significantly to the electron deficiency of the cyclohexadiene. The appended phenyl rings and methyl ethers could be inductively withdrawing electron density from the central ring, rendering **IV.14** and **IV.15** significantly less nucleophilic than expected. The two reductive homocoupling conditions[63-65] have precedence on sterically similar systems, but do not possess inductively electron withdrawing groups.

Table IV.2. Coupling conditions screened towards a direct-dimer.

Entry	Coupling Partner[a]	Catalyst[b]	Base or Additives	Solvent, Temp, Time	Outcome
1	IV.14	5 mol% $Pd(PPh_3)_2Cl_2$ / PPh_3 (1:10)	KOAc	PhMe, 80 °C, 14 h	IV.13, IV.14
2	IV.14	5 mol% Pd_2dba_3 / SPhos (1:2)	K_3PO_4	DMF/H_2O, 100 °C, 24 h	IV.14, decomposition
3	IV.14	10 mol% $Pd(PPh_3)_4$	Cs_2CO_3	PhMe/H_2O, 80 °C, 21 h	dehalogenated IV.13, IV.14
4	IV.15	15 mol% $Pd(PPh_3)_4$	none	DMF, 90 °C, 22 h	IV.13, IV.15, decomposition
5	IV.15	15 mol% $Pd(PPh_3)_4$	none	PhMe, 90 °C, 22 h	IV.13, IV.15
6	IV.15	20 mol% $Pd(PPh_3)_4$ / $AsPh_3$ (1:2)	none	DMF, 110 °C, 40 h	IV.13, destanylated IV.15
7	IV.15	20 mol% Pd_2dba_3 / $AsPh_3$ (1:2)	none	DMF, 110 °C, 40 h	IV.13, IV.15
8	IV.13	10 mol% $Pd(OAc)_2$ / PPh_3 (1:2)	DABCO NBu$_4$Br 4Å MS	DMF, 90 °C, 40 h	IV.13
9	IV.13	100 mol% CuI	nBuLi THF	PhMe, −25 °C – rt, 45 h	aromatized decomposition of IV.13

[a] The second coupling partner was always vinyl bromide IV.13. [b] Catalyst loadings are based on mols of Pd (entries 1 − 8); in cases where external ligand is added, ligand:Pd is indicated.

IV.5.3. Itami's Synthesis and Dimerization of Chloro[10]cycloparaphenylene

Since our experiments, a directly-linked [10]CPP dimer has been accessed by the Itami laboratory using other methodology.[66] Although we were unsuccessfully able to dimerize model IV.13 under a variety of conditions, Itami and co-workers found conditions that allowed an aryl chloride to be carried through the synthetic route (Scheme IV.4). Beginning from previously accessed dibromide IV.16, mild palladium-mediated macrocyclization conditions with IV.17 kept the functional handle intact to afford macrocycle IV.18 in 41% yield. Oxidative aromatization delivered chloro[10]CPP IV.19 in 31% yield, which could then be dimerized to IV.20 under Yamamoto-type conditions

with super-stoichiometric Ni(cod)$_2$/2,2'-bpy.[66] The group computationally determined

that the cis conformation of the [10]CPP direct-dimer is favored by approximately 5

kcal/mol over the trans conformation, which is consistent with our results for the [8]CPP

direct-dimer (Figure **IV.16**).
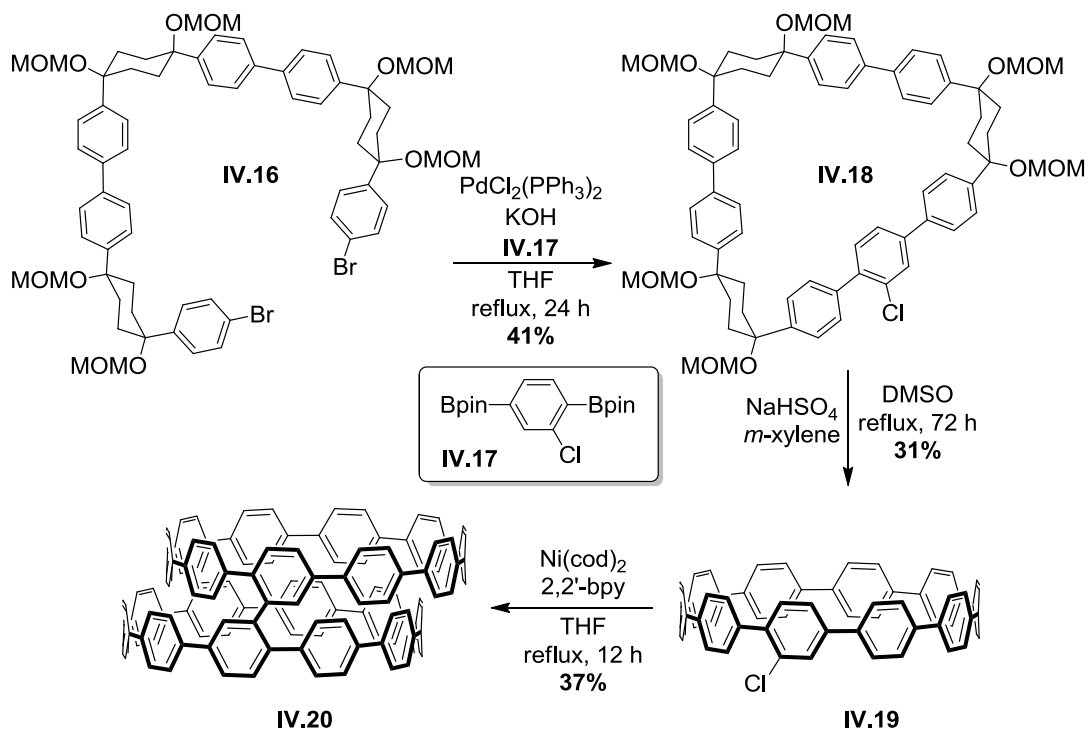
Scheme IV.4. Itami's synthesis of a directly-linked [10]CPP dimer.

IV.6. Experimental

IV.6.1. General Experimental Considerations

All glassware was oven (140 ^{o}C) or flame dried and cooled under an inert

atmosphere of nitrogen unless otherwise noted. Moisture sensitive reactions were carried

out under an inert atmosphere of nitrogen using standard syringe/septa technique. Tetrahydrofuran and dimethylformamide were dried by filtration through alumina according to the methods described by Grubbs (JC Meyer).[67] Silica column chromatography was conducted with Zeochem Zeoprep 60 Eco 40-63 μm silica gel. Thin Layer Chromatography (TLC) was performed using Sorbent Technologies Silica Gel XHT TLC plates. Developed plates were visualized using UV light at wavelengths of 254 and 365 nm. ^{1}H NMR spectra were recorded at 500 MHz on a Varian VNMRS or at 400 MHz on a Varian VNMRS. ^{13}C NMR spectra were recorded at 125 MHz on a Varian VNMRS or 100 MHz on a Varian VNMRS. All ^{1}H NMR spectra were taken in $CDCl_3$ unless otherwise noted and are referenced to TMS (δ 0.00 ppm). All ^{13}C NMR spectra were taken in $CDCl_3$ and were referenced to residual $CHCl_3$ (δ 77.16 ppm). The MALDI matrix (10 mg/ml of 7,7,8,8-tetracyanquinodimethane in THF with 1% silver trifluoroacetate as a promoter) was prepared according to the literature procedure.[22] IR spectra were recorded on a Thermo Nicolet FT-IR. Absorbance and fluorescence spectra were obtained in a 1 cm Quartz cuvette with dichloromethane using a Varian Cary 100 Bio UV-vis spectrometer and a Horiba Jobin Yvon Fluoromax 3 fluorimeter. Fluorescence was measured by excitation at 340 nm. All reagents were obtained commercially unless otherwise noted.

IV.6.2. Synthetic Details

IV.3
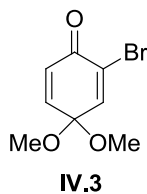
2-bromo-4,4-dimethoxycyclohexa-2,5-dienone **IV.3**. Quinone monoketal **IV.3** was prepared from commercially available 4-methoxyphenol.[68]

IV.4
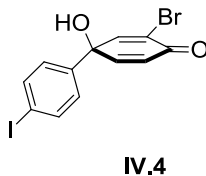
(±)-3-bromo-1-hydroxy-4'-iodo-[1,1'-biphenyl]-4(1H)-one **IV.4**. Quinone monoketal **IV.3** (11 g, 47 mmol) was dissolved in THF (150 mL) in a 500 mL flask, the resulting solution was cooled down to −78 °C. A separate 250 mL flask was charged with 1,4-iodobenzene (16 g, 47 mmol) and THF (150 mL). This solution was cooled down to −78 °C, and *n*BuLi (21 mL, 52 mmol, 2.5 M in hexane) was added slowly by syringe. The reaction mixture was allowed to stir at −78 °C for 30 min. This lithium reagent was then transferred to the flask containing ketone **IV.3** via cannula. The resulting mixture was allowed to stir for 2 h before it was warmed up to room temperature and quenched with water (100 mL) and extracted with diethyl ether (3 × 100 mL). The combined organic phase was washed with brine (60 mL) and dried over sodium sulfate.

After removing the solvent under vacuum, the brown residue was dissolved in acetone

(100 mL), and 10% aq AcOH (50 mL) was added. The resulting mixture was refluxed

overnight before it was cooled to room temperature and quenched with sat. aq NaHCO$_3$

(50 mL). The mixture was then extracted with DCM (3×100 mL), the organic phase was

separated and washed with water (3×150 mL) and dried over sodium sulfate. After

removing solvent under reduced pressure, the crude product was purified by on silica gel

(25% EtOAc/hexanes) to give compound **IV.4** as a white solid (17 g, 90%, m.p. 148 °C.).

^{1}H NMR (400 MHz, CDCl$_3$): δ(ppm) 7.73 (d, J = 8.8 Hz, 2H), 7.18 (d, J = 8.8 Hz, 2H),

6.80 (d, J = 2.0 Hz, 1H,), 6.95 (d, J = 10.0 Hz, 1H), 6.22 (dd, J = 8.0 Hz, 1H), 2.91 (s,

1H). ^{13}C NMR (100 MHz, CDCl$_3$): δ(ppm) 183.44, 149.78, 149.73, 141.78, 138.07,

137.87, 132.32, 127.32, 125.29, 94.84, 74.24; HRMS (Q-TOF ES+) (*m/z*) calc'd for

C$_{12}$H$_8$BrIO$_2$ [M]$^+$: 390.8831. Found: 390.8742; IR (neat): 732, 817, 933, 959, 1006, 1062,

1298, 1375, 1395, 1480, 1615, 1644, 1668, 2853, 2924, 3320 cm^{-1}.
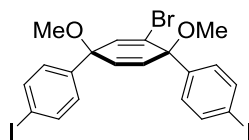
IV.5

(±)-syn-2'-bromo-4,4''-diiodo-1',4'-dimethoxy-1',4'-dihydro-1,1':4',1''-terphenyl **IV.5**. To

a slurry of sodium hydride (1.1 g, 27 mmol, 60% in mineral oil) in THF (100 mL) was

added slowly a solution of ketone **IV.4** (8.0 g, 21 mmol) in THF (100 mL) at −78 °C, the

reaction mixture was stirred for another 2 h at −78 °C to generate the alkoxide.

In a separate 250 mL round flask, 1,4-iodobenzene (15 g, 45 mmol) was dissolved in

THF (120 mL), this solution was cooled down to −78 °C, and then *n*BuLi (20 mL, 50

mmol, 2.5 M in hexane) was added slowly to this solution. After the addition, the resulting mixture was stirred for 30 min at –78 °C. This lithium reagent was then transferred to a slurry of the deprotonated ketone **IV.4** via cannula, and the resulting mixture was allowed to stir for another 2 h at –78 °C. Methyl iodide (5.10 mL, 81.8 mmol) and dry DMF (80 mL) were then added to quench the addition reaction, the reaction mixture was allowed to warm up to room temperature and stir overnight. Water (150 mL) was then added carefully to quench the methylation reaction, and the resulting mixture was extracted with DCM (3 × 100 mL). The combined organic layer was washed with water (3 × 100 mL) and brine (100 mL) and dried over sodium sulfate. After concentrating under reduced pressure, the crude off-white solid was purified by column on silica gel (20% EtOAc/hexanes) to give diiodide **IV.5** as a white solid (10 g, 78%, m.p. 135 °C.) ^{1}H NMR (400 MHz, CDCl$_3$): δ(ppm) 7.70 (dd, J = 8.8 Hz, 2H), 7.63 (dd, J = 8.8 Hz, 2H), 7.15 (dd, J = 8.8 Hz, 2H), 7.08 (dd, J = 8.8 Hz, 2H), 6.57 (d, J = 2.0 Hz, 1H), 6.07 (dd, J = 10.2, 2.0 Hz, 1H), 6.02 (d, J = 10.2 Hz, 1H), 3.43 (s, 3H), 3.41 (s, 3H). ^{13}C NMR (100 MHz, CDCl$_3$): δ(ppm) 141.86, 140.93, 137.77, 137.73, 137.35, 133.89, 131.21, 128.85, 128.15, 127.90, 94.11, 93.91, 77.67, 77.51, 52.29, 51.85. HRMS (Q-TOF ES+) (*m/z*) calc'd for C$_{20}$H$_{17}$BrI$_2$O$_2$ [M-CH$_3$]$^+$: 606.8399. Found: 606.8267, 606.8289; IR (neat): 706, 736, 772, 816, 951, 1004, 1022, 1084, 1173, 1264, 1391, 1482, 1583, 2824, 2939 cm^{-1}.

IV.7
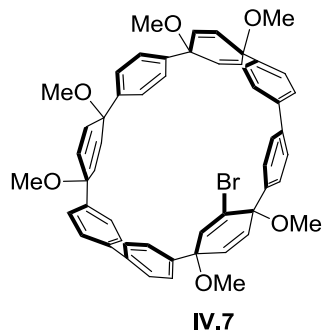
bromo-macrocycle **IV.7**. Diiodide **IV.5** (1.25 g, 2.00 mmol), diboronate **IV.6** (1.5 g, 2.0 mmol), Pd(OAc)$_2$ (0.14 g, 0.20 mmol, 0.10 equiv) and Cs$_2$CO$_3$ (2.6 g, 8.0 mmol, 4.0 equiv) were charged in a 500 mL Schlenk flask under nitrogen, then degassed DMF (350 mL) and 2-isopropanol (35 mL) was added. The resulting mixture was heated to 100 $^\circ$C and stirred for 24 h. After cooling down to room temperature, the mixture was filtered through a short plug of Celite, and water (250 mL) was added to the filtrate. After extraction with dichloromethane (3 × 100 mL), the combined organic phase was washed with water (8 × 100 mL) and dried over sodium sulfate. After removing the solvent under vacuum, the crude mixture was purified on silica gel (40% EtOAc/hexanes) to give brominated [8]macrocycle **IV.7** as a white solid (0.53 g, 30%, m.p. 155 $^\circ$C.) ^{1}H NMR (400 MHz, CDCl$_3$): δ(ppm) 7.45-7.53 (overlap, 14H), 7.35 (d, J = 8.4 Hz, 2H), 7.23 (t, J = 8.8 Hz, 2H), 7.08 (d, J = 8.0 Hz, 2H), 6.79 (d, J = 1.6 Hz, 1H), 6.23-6.26 (overlap, 2H), 6.12-6.15 (overlap, 4H), 6.04-6.08 (overlap, 4H), 3.47-3.49 (overlap, 12H), 3.40 (s, 6H). ^{13}C NMR (100 MHz, CDCl$_3$): δ(ppm) 143.35, 143.31, 143.02, 142.85, 140.53, 140.11, 139.46, 139.43, 139.40, 138.70, 138.30, 134.55, 133.72, 133.48, 133.46, 133.30, 132.98, 132.80, 132.76, 132.61, 131.32, 128.10, 127.30, 127.18, 127.15, 126.87, 126.79, 126.38, 126.31, 126.24, 104.96, 78.83, 78.78, 74.59, 74.51, 74.02, 73.96, 52.43 (OMe), 52.12, 52.09, 51.80. MALDI-TOF (*m/z*) calc'd for C$_{54}$H$_{49}$BrO$_6$ [M]$^+$: 873.87, found (isotopic

pattern): 872.1226, 874.1280, 875.1285. IR (neat): 736, 772, 820, 949, 1005, 1016, 1080, 1174, 1265, 1397, 1449, 1491, 2823, 2932 cm^{-1}.

IV.9
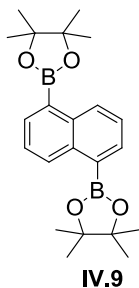
1,5-bis(4,4,5,5-tetramethyl-1,3,2-dioxaborolan-2-yl)naphthalene **IV.9**. To a round-bottom flask charged with a stirbar, bis(pinacolato)diboron (0.51 g, 2.0 mmol), benzoyl peroxide (10 mg, 0.040 mmol) and acetonitrile (6 mL) was added 1,5-naphthalenediamine (320 mg, 2.0 mmol). *Tert*-butyl nitrite (0.31 g, 0.36 mL, 3.0 mmol) was then added dropwise to the stirring reaction mixture. The reaction mixture was allowed to stir for 16 h before concentrating under reduced pressure. The crude residue was then purified by silica gel chromatography (hexanes), followed by recrystallization from hot hexanes to afford **IV.9** as a light orange solid (0.12 g, 16%, m.p. 281 – 283 °C). ^{1}H NMR (400 MHz, CDCl$_3$): δ(ppm) 8.88 (d, *J* = 8.4 Hz, 2H), 8.06 (d, *J* = 6.8, 2H), 7.51 (dd, *J* = 8.4, 6.8 Hz, 2H), 1.42 (s, 24H); ^{13}C NMR (125 MHz, CDCl$_3$): δ(ppm) 136.7, 135.3, 132.0, 125.4, 83.7, 25.0 (C-B signal not observed); HRMS (Q-TOF, ES+) (*m/z*) calc'd for C$_{22}$H$_{30}$B$_2$O$_4$ [M]$^{+}$: 379.2481, Found: 380.2338; IR (neat): 802, 936, 1205, 1331, 1371, 1510, 2975 cm^{-1}.
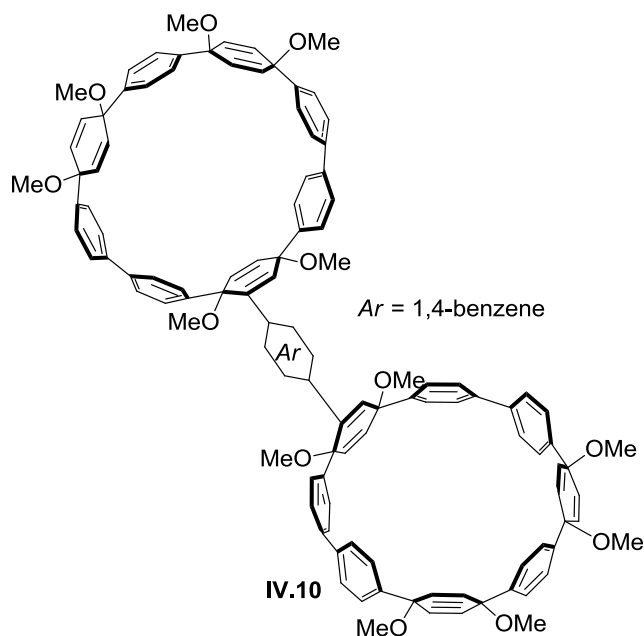
Ar = 1,4-benzene

IV.10

phenyl macrocycle dimer **IV.10.** A mixture of brominated [8]macrocycle **IV.7** (0.29 g, 0.33 mmol), 1,4-benzenediboronic acid bis(pinacol) ester (50 mg, 0.15 mmol), Pd(PPh$_3$)$_4$ (38 mg, 0.033 mmol) and Cs$_2$CO$_3$ (0.43 g, 1.3 mmol) was dissolved in PhMe/H$_2$O (7 mL, 6:1) and stirred at 80 $^\circ$C for 24 h under nitrogen. After cooling down to room temperature, water (10 mL) was added**.** The aqueous phase was extracted with dichloromethane (3 × 10 mL) and the combined organics were washed with water (3 × 10 mL) and dried over sodium sulfate. After removing the solvent under vacuum, the crude mixture was purified on silica gel (50% EtOAc/hexane) to give **IV.10** as a white solid (0.17 g, 66%, d.p. > 300 °C.). ^{1}H NMR (400 MHz, CDCl$_3$): δ (ppm) 7.47-7.52 (overlap, 20H), 7.40 (d, *J* = 8.4 Hz, 4H), 7.27 (d, *J* = 6.0 Hz, 8H), 7.20 (d, *J* = 6.0 Hz, 8H), 7.04 (d, *J* = 8.8 Hz, 4H, Ar), 6.68 (d, *J* = 2.0 Hz, 2H), 6.02-6.21 (overlap, 20H), 3.40-3.48 (overlap, 30), 3.12 (s, 6H). ^{13}C NMR (100 MHz, CDCl$_3$): δ (ppm) 143.30, 142.80, 142.72, 140.86, 140.25, 140.21, 139.67, 139.49, 139.45, 139.34, 138.18, 136.69, 135.57, 134.00, 133.51, 133.40, 133.19, 133.10, 132.81, 132.32, 128.82, 127.58, 127.22, 126.97,

136

126.83, 126.73, 126.59, 126.49, 126.23, 126.18, 78.78, 76.30, 74.58, 74.54, 74.05, 74.03, 52.10, 51.97, 51.84, 51.69. MALDI-TOF (*m/z*) calc'd for $C_{114}H_{102}O_{12}$ [M]$^+$: 1664.02. Found: 1664.3682. IR (neat): 819, 950, 1016, 1079, 1174, 1491, 2822, 2931 cm^{-1}.

Ar = 1,5-naphthalene
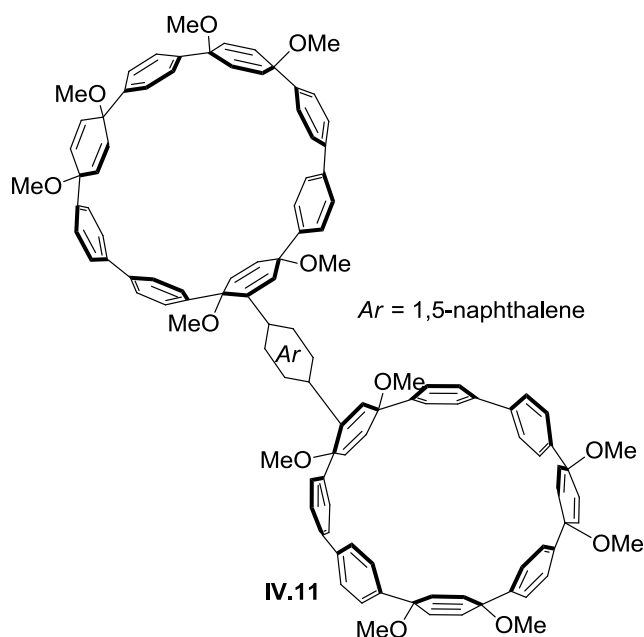
IV.11

naphthyl-macrocycle dimer **IV.11.** A mixture of brominated [8]macrocycle **IV.7** (73 mg, 0.084 mmol), 1,5-naphthalenediboronic acid bis(pinacol) ester **IV.9** (16 mg, 0.042 mmol), Pd(PPh$_3$)$_4$ (9.7 mg, 0.0084 mmol) and Cs$_2$CO$_3$ (110 mg, 0.34 mmol) was dissolved in PhMe/H$_2$O (2 mL, 6:1) and stirred at 90 °C for 24 h under nitrogen. After cooling down to room temperature, 5 mL water was added. The aqueous phase was extracted with DCM (3 × 5 mL) and the combined organics were washed with water (3 × 5 mL) and brine (5 mL) and dried over sodium sulfate. After removing the solvent under vacuum, the crude mixture was purified on silica gel (30% - 50% EtOAc/hexanes) to give compound **IV.11** as an off-white solid (35 mg, 49%, d.p. > 300 ^{o}C). ^{1}H NMR (400 MHz,

CDCl$_3$): δ(ppm) 8.28 (br s, 1H), 7.53-7.47 (overlap, 28H), 7.29-7.27 (overlap, 8H), 7.12-7.00 (overlap, 9H), 6.61 (br d, 2H), 6.46 (d, J = 10.5 Hz, 2H), 6.36 (d, J = 10.5 Hz, 2H), 6.17-6.05 (overlap, 16H), 3.59 (overlap, 6H), 3.49 (overlap, 12H), 3.48 (overlap, 12H), 3.26 (overlap, 6H); ^{13}C NMR (125 MHz, CDCl$_3$): δ(ppm) 143.32, 142.96, 142.87, 140.77, 140.40, 140.36, 139.78, 139.52, 139.41, 137.04, 136.14, 135.47, 133.94, 133.55, 133.50, 133.25, 133.12, 133.05, 132.87, 132.75, 132.37, 128.05, 127.62, 127.44, 126.94, 126.76, 126.36, 126.32, 126.28, 126.24, 126.22, 125.42, 124.26, 79.81, 76.41, 74.63, 74.52, 74.13, 74.10, 52.76, 52.51, 52.11, 51.86. MALDI-TOF (*m/z*) calc'd for C$_{118}$H$_{104}$O$_{12}$ [M]$^+$: 1714.08, Found: 1713.4715. IR(neat): 729, 819, 950, 1016, 1079, 1174, 1490, 2822, 2934 cm^{-1}.

Preparation of Sodium Naphthalenide (1.0 M in THF): To a 25 mL dry roundbottom flask charged with a solution of naphthalene (770 mg, 6.0 mmol) in dry THF (6 mL) was added sodium metal (210 mg, 9.0 mmol) under nitrogen. The reaction mixture was stirred for 18 h at room temperature. After this time, a green solution containing sodium naphthalenide (1.0 M in THF) was formed.
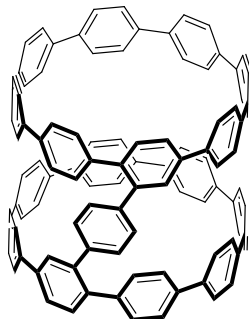
IV.1

[8]CPP phenyl dimer **IV.1.** Compound **IV.10** (150 mg, 0.090 mmol) was dissolved in THF (15 mL) under nitrogen and cooled down to −78 °C. At this point, the freshly prepared sodium naphthalenide (1.6 mL, 1.6 mmol, 1.0 M in THF) was added. The reaction mixture was stirred for 2 h at −78 °C before the addition of I_2 (1.5 mL, 1 M solution in THF). Then the resulting mixture was warmed up to room temperature and sodium thiosulfate (saturated solution) was carefully added to remove excess I_2. Water (30 mL) was then added and the mixture was extracted with dichloromethane (3 x 20 mL). The combined organics were washed with brine (30 mL) and dried over sodium sulfate. After removing the solvent under reduced pressure, the crude yellow solid was purified on silica gel (20% hexanes/chlorobenzene) to give compound **IV.1** as a yellow solid (88 mg, 75%, d.p. > 350 °C). ^{1}H NMR (400 MHz, CDCl3): δ (ppm) 7.93 (overlap, 2H), 7.75 (s, 4H), 7.55 (overlap, 14H), 7.47 (overlap, 34H), 7.38 (overlap, 4H), 7.09 (overlap, 8H). ^{13}C NMR (100 MHz, CDCl3+CS2): δ (ppm) 140.19, 137.33 (multiple overlapping peaks), 127.11 (multiple overlapping peaks). MALDI-TOF (*m/z*) calc'd for $C_{102}H_{66}$ [M]$^+$: 1291.62. Found: 1291.5924. IR (neat): 735, 815, 1261, 1482, 1587, 2335, 2360, 2851, 2924, 3018 cm^{-1}.
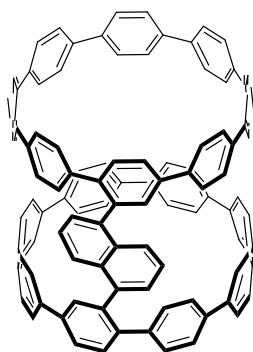
IV.2

[8]CPP naphthyl dimer **IV.2.** Compound **IV.11** (35 mg, 0.020 mmol) was dissolved in 3

mL THF under nitrogen and cooled down to −78 °C. At this point, the freshly prepared

sodium naphthalenide (0.36 mL, 0.36 mmol, 1.0 M in THF) was added. The reaction

mixture was stirred for 2 h at −78 °C before the addition of I_2 (1 mL, 1 M solution in

THF). Then the resulting mixture was warmed up to room temperature and sodium

thiosulfate (saturated solution) was carefully added to remove excess I_2. Water (30 mL)

was then added and the mixture was extracted with dichloromethane (3×20 mL), which

was combined and washed brine (30 mL) and dried over sodium sulfate. The crude

yellow solid was purified on silica gel (40% hexanes/DCM) to give compound **IV.2** as a

yellow solid (13 mg, 48%, d.p. > 350 °C). ^{1}H NMR (400 MHz, CDCl$_3$): δ (ppm) 8.00

(m, 1H), 7.82 (overlap, 2H), 7.68 (br s, 1H) 7.49 (overlap, 54H), 7.14 (overlap, 8H), 7.01

(overlap, 2H). ^{13}C NMR (100 MHz, CDCl$_3$): δ (ppm) 137.38-138.23 (multiple

overlapping peaks), 127.38 (multiple overlapping peaks). MALDI-TOF (*m/z*) calc'd for

$C_{106}H_{68}$ [M]$^+$: 1341.67, Found: 1341.1713. IR(neat): 729, 815, 1074, 1262, 1482, 1586,

2364, 2980, 3021.
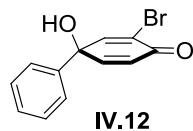
IV.12

(±)-3-bromo-1-hydroxy-[1,1'-biphenyl]-4(1H)-one **IV.12**. To a solution of

bromobenzene (6.1 g, 39 mmol, 1.0 equiv) in THF (100 mL) at −78 °C was added *n*BuLi

(16 mL, 39 mmol, 1.0 equiv, 2.5 M in hexanes). The mixture was stirred for 45 min

before adding neat **IV.3** (9.0 g, 39 mmol, 1.0 equiv) via syringe. The resulting solution

was stirred for 2 h before quenching with water (100 mL) and extracting with diethyl

ether (3 × 100 mL). The combined organics were washed with brine (60 mL) and dried

over sodium sulfate. After removing the solvent under vacuum, the brown residue was

dissolved in acetone (100 mL), and 10% aq AcOH (50 mL) was added. The resulting

mixture was refluxed overnight before it was cooled to room temperature and quenched

with sat. aq NaHCO$_3$ (50 mL). The mixture was then extracted with DCM (3 × 100 mL),

the organic phase was separated and washed with water (3 × 150 mL) and dried over

sodium sulfate. After removing solvent under reduced pressure, the crude product was

washed with DCM (50 mL) and hexanes (60 mL) to afford **IV.12** as a while solid (8.0 g,

78%). ^{1}H NMR (400 MHz, CDCl$_3$) δ(ppm) 7.50 − 7.29 (overlap, 5H), 6.99 (d, *J* = 9.9 Hz,

1H), 6.81 (s, 1H), 6.21 (d, *J* = 9.9 Hz, 1H), 3.08 (s, 1H).
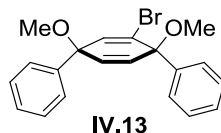
IV.13

(±)-syn-2'-bromo-1',4'-dimethoxy-1',4'-dihydro-1,1':4',1''-terphenyl **IV.13**. To a slurry of sodium hydride (1.3 g, 31 mmol, 1.3 equiv, 60% in mineral oil) in THF (150 mL) was added slowly a solution of ketone **IV.12** (6.4 g, 24 mmol, 1.0 equiv) in THF (100 mL) at −78 °C, the reaction mixture was stirred for another 2 h at −78 °C to generate the alkoxide.

In a separate 250 mL round flask, bromobenzene (8.3 g, 53 mmol, 1.0 equiv) was dissolved in THF (120 mL), this solution was cooled down to −78 °C, and then *n*BuLi (23 mL, 58 mmol, 1.1 equiv, 2.5 M in hexane) was added slowly to this solution. After the addition, the resulting mixture was stirred for 30 min at −78 °C. This lithium reagent was then transferred to a slurry of the deprotonated ketone **IV.12** via cannula, and the resulting mixture was allowed to stir for another 2 h at −78 °C. Methyl iodide (6.3 mL, 97 mmol, 4.0 equiv) and dry DMF (80 mL) were then added to quench the addition reaction, the reaction mixture was allowed to warm up to room temperature and stir overnight. Water (150 mL) was then added carefully to quench the methylation reaction, and the resulting mixture was extracted with DCM (3 × 100 mL). The combined organics were washed with water (3 × 100 mL) and brine (100 mL) and dried over sodium sulfate. After concentrating under reduced pressure, the crude oil was purified on silica gel (20% EtOAc/hexanes) to give a pale yellow oil that solidified with standing. After washing with hexanes, **IV.13** was recovered as a white solid (7.3 g, 81%). ^{1}H NMR (400 MHz,

CDCl$_3$) δ(ppm) 7.52 – 7.11 (overlap, 10H), 6.66 (d, J = 2.1 Hz, 1H), 6.13 (dd, J = 10.0, 2.1 Hz, 1H), 6.08 (d, J = 10.0 Hz, 1H), 3.49 (s, 3H), 3.47 (s, 3H).
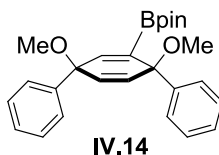
IV.14

2-((±)-syn-1',4'-dimethoxy-1',4'-dihydro-[1,1':4',1''-terphenyl]-2'-yl)-4,4,5,5-tetramethyl-1,3,2-dioxaborolane **IV.14**. To a solution of **IV.13** (1.9 g, 5.0 mmol, 1 equiv) in THF (80 mL) at −78 °C was added *n*BuLi (2.2 mL, 5.5 mmol, 1.1 equiv, 2.5 M in hexanes). After stirring for 5 min, 2-isopropoxy-4,4,5,5-tetramethyl-1,3,2-dioxaborolane (2.0 mL, 10 mmol, 2.0 equiv) was added and the reaction was stirred an additional 1 h before warming to rt. The reaction was then quenched with water (40 mL) and the resulting mixture was extracted with DCM (3 x 50 mL). The combined organics were washed with water (3 x 50 mL) and brine (50 mL) and dried over sodium sulfate. After concentrating under reduced pressure, the crude product was passed through a short plug of silica gel (20% EtOAc/hexanes) that was triturated with hexanes and dried under high vacuum to afford **IV.14** was a white solid (1.7 g, 80%). ^{1}H NMR (400 MHz, CDCl$_3$) δ(ppm) 7.45 (d, J = 7.2 Hz, 2H), 7.40 (d, J = 7.1 Hz, 2H), 7.38 – 7.27 (overlap, 3H), 7.27 – 7.18 (overlap, 3H), 6.91 (d, J = 2.5 Hz, 1H), 6.14 (d, J = 10.2 Hz, 1H), 6.07 (dd, J = 10.2, 2.5 Hz, 1H), 3.45 (s, 3H), 3.43 (s, 3H), 1.17 (s, 6H), 1.08 (s, 6H); ^{13}C NMR (100 MHz, CDCl$_3$) δ(ppm) 147.37, 144.21, 143.11, 136.68, 130.46, 128.42, 127.95, 127.61, 127.01, 126.50, 126.23, 83.33, 76.55, 74.38, 52.17, 51.78, 24.81, 24.15.
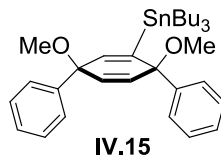
IV.15

tributyl((±)-syn-1',4'-dimethoxy-1',4'-dihydro-[1,1':4',1''-terphenyl]-2'-yl)stannane

IV.15. To a solution of **IV.13** (0.50 g, 1.3 mmol, 1.0 equiv) in THF (5 mL) at −78 °C was added *n*BuLi (0.62 mL, 1.4 mmol, 1.1 equiv, 2.3 M in hexanes). After stirring for 25 min, tributyltin chloride (0.35 mL, 1.3 mmol, 1.0 equiv) was added and the reaction was stirred an additional 30 min before warming to rt. After 16 h, the reaction was then quenched with water (40 mL) and the resulting mixture was extracted with DCM (3 x 20 mL). The combined organics were washed with water (3 x 20 mL) and brine (20 mL) and dried over sodium sulfate. After concentrating under reduced pressure, the resulting crude yellow oil **IV.15** was used without further purification (0.80 g). ^{1}H NMR (400 MHz, CDCl$_3$) δ(ppm) 7.50 (d, J = 7.1 Hz, 2H), 7.34 (d, J = 7.9 Hz, 2H), 7.33 – 7.23 (overlap, 3H), 7.26 – 7.15 (overlap, 3H), 6.27 (s, 1H), 6.11 – 6.05 (overlap, 2H), 3.49 (s, 1H), 3.43 (s, 1H), 1.37 – 1.22 (m, 6H), 1.24 – 1.06 (m, 6H), 0.95 – 0.86 (m, 3H), 0.71 (t, J = 7.1 Hz, 9H), 0.68 (ddd, J = 12.6, 9.8, 6.1 Hz, 3H).

IV.6.3. Optical Characterization

The extinction coefficients for **IV.1** and **IV.2** were calculated by measuring the slope of Beer-Lambert plots (absorbance at 340 nm) and averaging over three independent trials. The quantum yields of **IV.1** and **IV.2** were determined using the methods described by Williams[69] using anthracene (ethanol) and quinine (10% H$_2$SO$_4$) as external standards. The fluorescence of **IV.1** and **IV.2** was integrated from 450 – 680 nm. The fluorescence

of anthracene was integrated from 360 – 480 nm. The fluorescence of quinine was integrated from 400 – 600 nm.
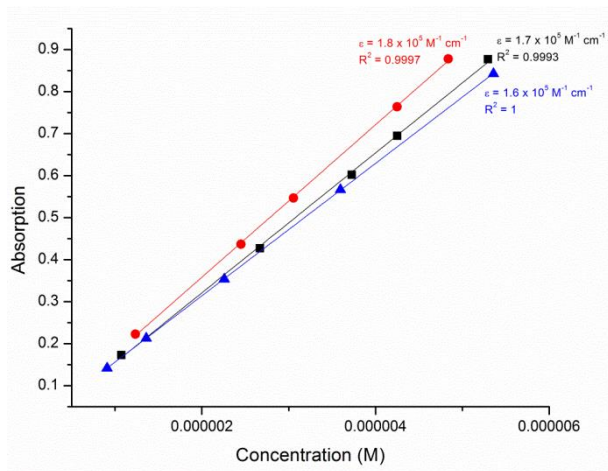
Figure IV.7. Beer-Lambert plots for the determination of the extinction coefficient of **IV.1** ($\varepsilon = 0.88 \times 10^5$ M^{-1} cm^{-1} (12%)).
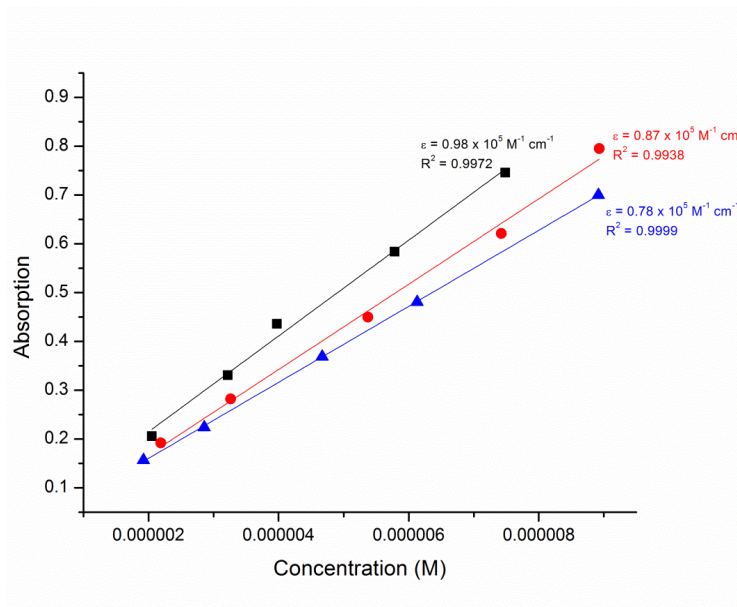
Figure IV.8. Beer-Lambert plots for the determination of the extinction coefficient of **IV.2** ($\varepsilon = 1.7 \times 10^5$ M^{-1} cm^{-1} (7.2%)).
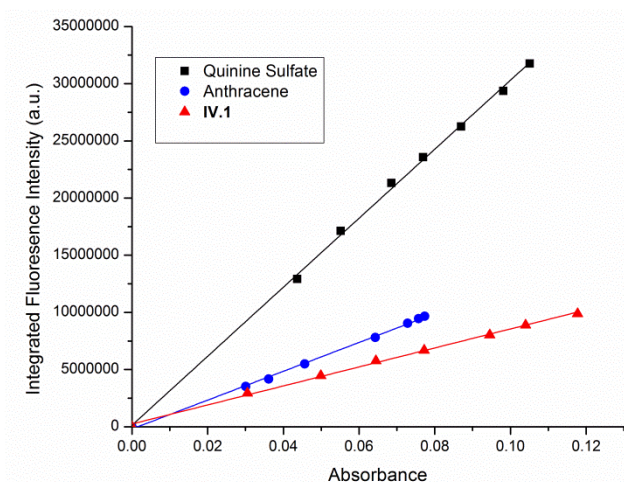
Figure IV.9. Quantum yield measurement of **IV.1** ($\Phi = 0.18$).
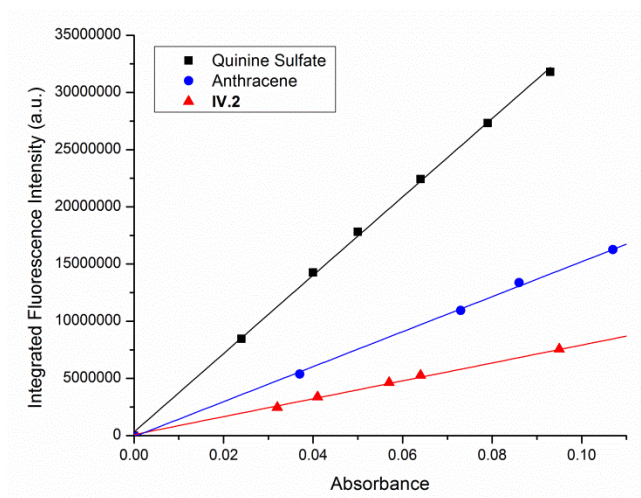
Figure IV.10. Quantum yield measurement of **IV.2** ($\Phi = 0.15$).

IV.6.4. Electrochemical Analysis

Electrochemical measurements were performed on a Princeton Applied Research

Potentiostat/Galvanastat Model 273 running M270/250 Electrochemical Software

(Princeton Applied Research) with a silver wire reference electrode, a glassy carbon

146

working electrode, and a platinum counter electrode. The ferrocene/ferrocenium couple

was used as an internal reference. The scan rate for data acquisition was 100 mV/s. The

electrolyte (nBu$_4$NPF$_6$) was received from Sigma-Aldrich and was recrystallized from

methylene chloride three times. Dichloromethane for the electrochemical analysis was

obtained from Fisher and was distilled over calcium hydride before use. The

dichloromethane was thoroughly degassed by subjecting it to at least six successive

freeze-pump-thaw cycles, after which they were transferred to a glove box under an N$_2$

atmosphere.
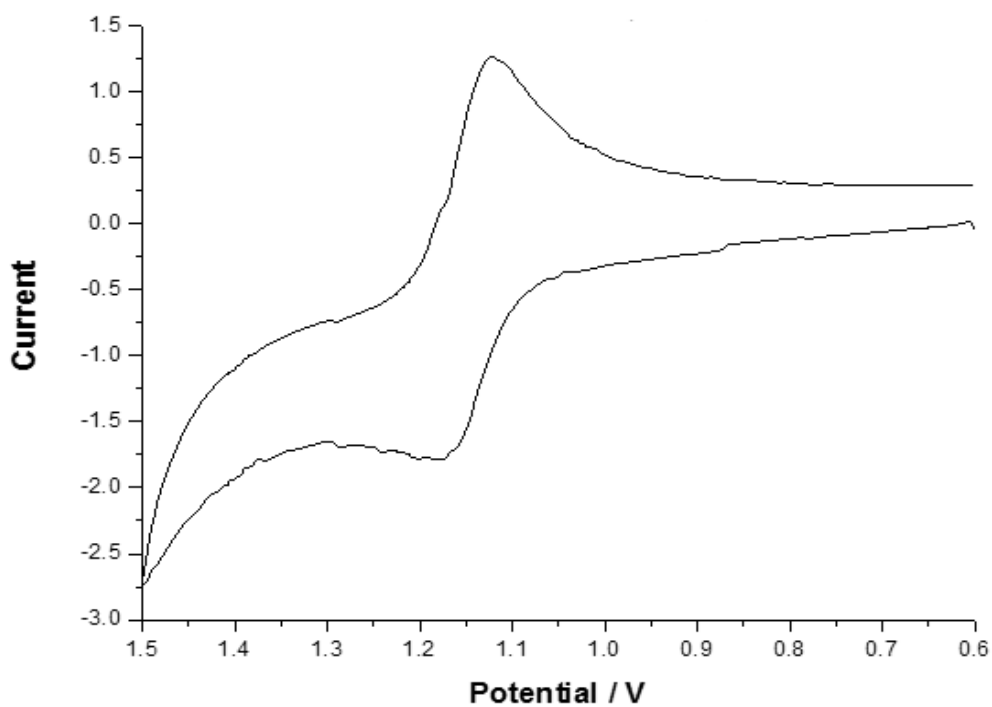
Figure IV.11. Cyclic voltammetry plot of **IV.1**.
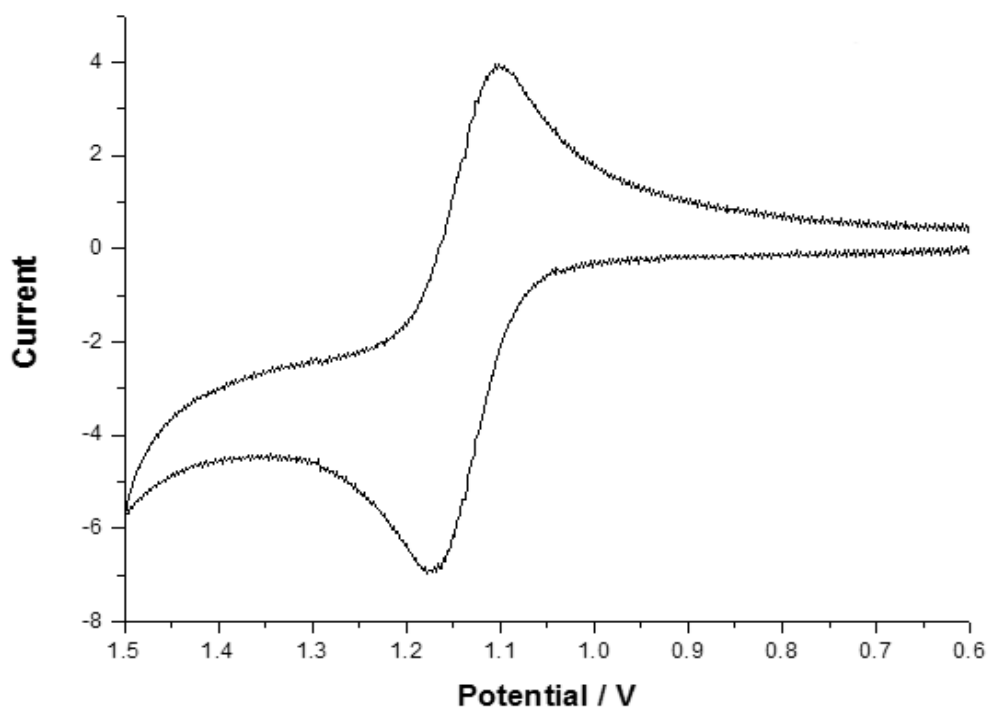
Figure IV.12. Cyclic voltammetry plot of **IV.2**.

IV.6.5. Computational Details

All calculations were carried out with the Gaussian 09 package[70] using the B3LYP exchange-correlation functional[71] augmented with an empirical dispersion term (B3LYP-D) and a polarized 6-31G(d,p) basis[72] using default SCF convergence criteria (density matrix converged to at least 10^{-8}) and the default DFT integration grid (75 radial and 302 angular quadrature points). All excited state calculations (TD-DFT) were performed on fully optimized structures. The fully optimized structures were confirmed to be true minima by vibrational analysis.

Solid State Crystal Calculation: VASP was used for all periodic boundary condition calculations using the PBE-D functional with an energy cutoff of 500 eV. The projector-

augmented-wave (PAW) pseudo-potentials were used to describe the interactions

between the ions and electrons. A gamma-point was sufficient for sampling the Brillouin

zone during all calculations since the no metal atoms are present in the systems. No

constraints were applied to the atoms positions or unit cell parameters during the

geometry optimizations.

Table IV.3. Major electronic transitions for [8]CPP determined by TD-DFT methods using B3LYP/6-31G(d, p).

Energy (cm^{-1})	Wavelength (nm)	Osc. Strength (f)	Major contribs
21106	473	0	HOMO→LUMO (97%)
26741	374	0.0001	HOMO-1→LUMO (51%), HOMO→LUMO+1 (-49%)
27827	359	0.0302	HOMO-2→LUMO (64%), HOMO→LUMO+2 (-35%)
28031	356	1.4872	HOMO-1→LUMO (49%), HOMO→LUMO+1 (51%)
28958	345	1.3057	HOMO-2→LUMO (35%), HOMO→LUMO+2 (65%)
31622	316	0.0018	HOMO-5→LUMO (-10%), HOMO→LUMO+3 (77%)

Table IV.4. Major electronic transitions for dimer **IV.1** (cis) determined by TD-DFT methods using B3LYP/6-31G(d, p).

Energy (cm^{-1})	Wavelength (nm)	Osc. Strength (f)	Major contribs
20777	481	0.0084	HOMO→LUMO (92%)
22409	446	0.0142	HOMO-1→LUMO+1 (53%), HOMO→LUMO+1 (-36%)
22640	441	0.0112	HOMO-1→LUMO+1 (33%), HOMO→LUMO+1 (58%)
23879	418	0.0039	HOMO-1→LUMO (88%), HOMO-1→LUMO+1 (-11%)
26514	377	0.0497	HOMO-2→LUMO (82%)
26625	375	0.0125	HOMO-2→LUMO+1 (45%), HOMO→LUMO+2 (-38%)
26744	374	0.0768	HOMO-3→LUMO (47%), HOMO-2→LUMO+1 (16%), HOMO→LUMO+2 (19%)
27060	369	0.0162	HOMO-3→LUMO+1 (28%), HOMO→LUMO+3 (19%), HOMO→LUMO+4 (42%)
27247	367	0.0708	HOMO→LUMO+3 (15%), HOMO→LUMO+5 (46%)
27383	365	0.2574	HOMO-3→LUMO (31%), HOMO→LUMO+2 (-18%), HOMO→LUMO+3 (11%)

Table IV.5. Major electronic transitions for dimer IV.1 (trans) determined by TD-DFT methods using B3LYP/6-31G(d, p).

Energy (cm^{-1})	Wavelength (nm)	Osc. Strength (f)	Major contribs
21411	467	0.0085	HOMO-1→LUMO+1 (37%), HOMO→LUMO (60%)
24080	415	0.1266	HOMO-1→LUMO+1 (59%), HOMO→LUMO (-37%)
26360	379	1.017	HOMO→LUMO+2 (81%)
26785	373	0.7106	HOMO-2→LUMO (80%)
27401	365	0.0008	HOMO-4→LUMO (32%), HOMO-3→LUMO+1 (14%), HOMO-1→LUMO+3 (-17%), HOMO→LUMO+4 (-31%)

Table IV.6. Major electronic transitions for dimer IV.2 (cis) determined by TD-DFT methods using B3LYP/6-31G(d, p).

Energy (cm^{-1})	Wavelength (nm)	Osc. Strength (f)	Major contribs
20870	479	0.0146	HOMO→LUMO (81%), HOMO→LUMO+1 (-16%)
22670	441	0.0003	HOMO→LUMO (17%), HOMO→LUMO+1 (82%)
22830	438	0.0219	HOMO-1→LUMO (38%), HOMO-1→LUMO+1 (58%)

Energy (cm⁻¹)	Wavelength (nm)	Osc. Strength (f)	Major contribs
24294	411	0.0007	HOMO-1→LUMO (60%), HOMO-1→LUMO+1 (-38%)
25869	386	0.0946	HOMO-2→LUMO (76%)
26210	381	0.0029	HOMO-2→LUMO (-15%), HOMO-2→LUMO+1 (29%), HOMO→LUMO+2 (48%)
26555	376	0.0501	HOMO-2→LUMO+1 (54%), HOMO→LUMO+2 (-36%)
26726	374	0.0068	HOMO-3→LUMO (40%), HOMO→LUMO+3 (37%), HOMO→LUMO+4 (21%)
27044	369	0.0233	HOMO-3→LUMO+1 (-21%), HOMO→LUMO+3 (-25%), HOMO→LUMO+4 (47%)
27175	368	0.1236	HOMO-4→LUMO (-15%), HOMO-3→LUMO (33%), HOMO→LUMO+3 (-12%)

Table IV.7. Major electronic transitions for dimer **IV.2** (trans) determined by TD-DFT methods using B3LYP/6-31G(d, p).

Energy (cm⁻¹)	Wavelength (nm)	Osc. Strength (f)	Major contribs
21503	465	0.0199	HOMO-1→LUMO+1 (-43%), HOMO→LUMO (50%)
21505	465	0.0007	HOMO-1→LUMO (49%), HOMO→LUMO+1 (-45%)
24135	414	0.0156	HOMO-1→LUMO+1 (52%), HOMO→LUMO (45%)

24137	414	0.0001	HOMO-1→LUMO (47%), HOMO→LUMO+1 (51%)
26388	379	0.4018	HOMO→LUMO+2 (85%)
26769	373	0.6321	HOMO-2→LUMO (80%)
27492	363	0.0094	HOMO-5→LUMO+1 (-16%), HOMO-4→LUMO (29%), HOMO-1→LUMO+3 (-21%), HOMO→LUMO+4 (24%)
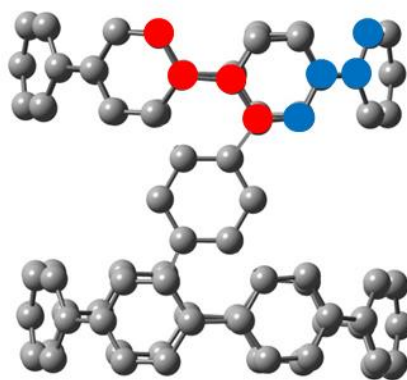
Figure IV.13. A schematic of the CPP dimer **IV.1** indicating the dihedral angles that were frozen during the constrained optimizations which were required to map the potential energy between the cis and trans conformations.
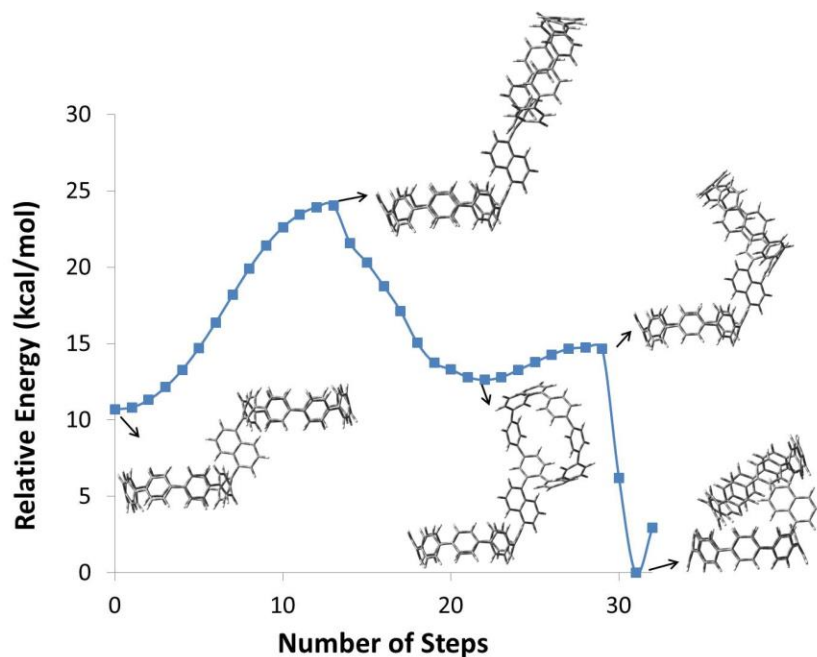
Figure IV.14. The potential energy curve of the trans to cis transition for dimer **IV.2**. The potential energy curve was calculated by starting with the optimized trans geometry and creating a series of structures mapping the conformational change. These structures were optimized, minimizing the total energy, while constraining two dihedral angles (Figure **IV.13**).
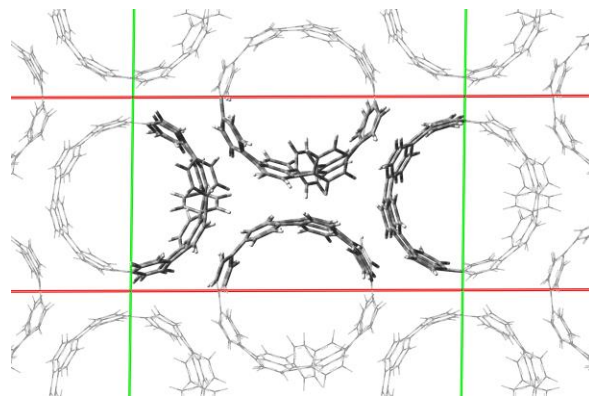
Figure IV.15. Optimized (PBE-D functional) solid-state packing of cis **IV.1**, which was found to be higher in energy than trans packing in the solid state (Figure **IV.3**).
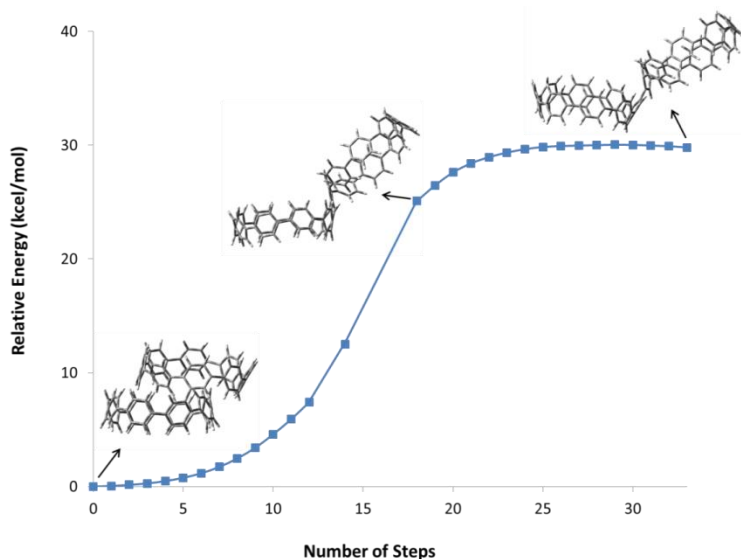
Figure IV.16. The potential energy curve of the cis to trans transition for the direct dimer (i.e. no arene-linker). The potential energy curve was calculated by starting with the optimized cis geometry and creating a series of structures mapping the conformational change. These structures were optimized, minimizing the total energy, while constraining two dihedral angles; the dihedral angles frozen are equivalent to those shown in Figure **IV.13**.
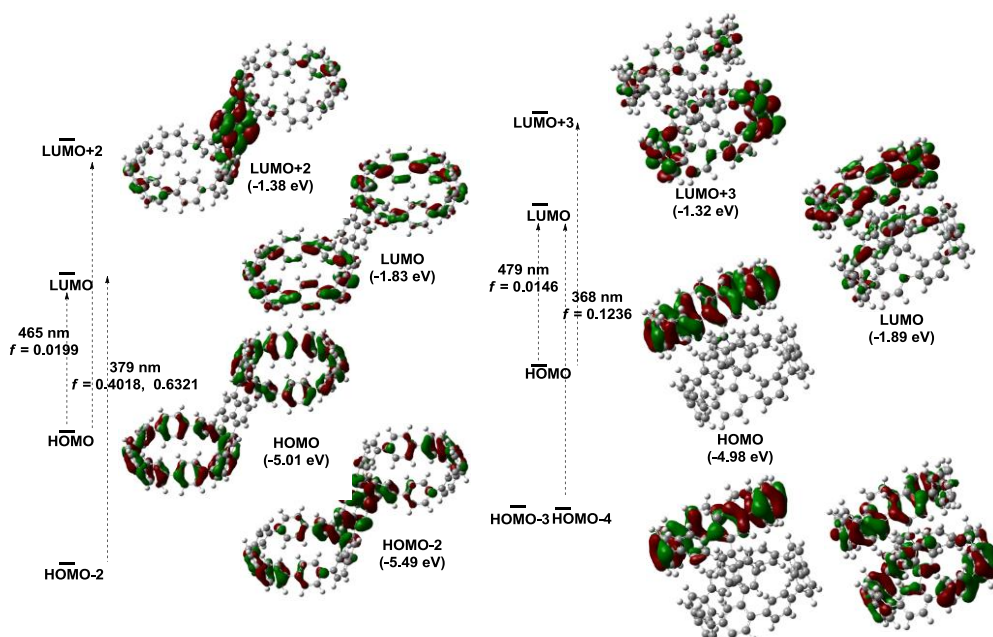
Figure IV.17. Major electronic transitions (TD-DFT) and representative FMOs for **IV.2** trans (left) and cis (right), calculated at the B3LYP/6-31G(d,p) level of theory.

IV.6.6. Preliminary X-ray Crystallographic Data

Data were collected on a Bruker AXS Proteum-R instrument at Boston University. The structure and data in Figure **IV.18** and Table **IV.8** are not fully refined due to instability of the crystal sample during data collection, but can be used to preliminarily show the trans conformation of **IV.1** in the solid state.
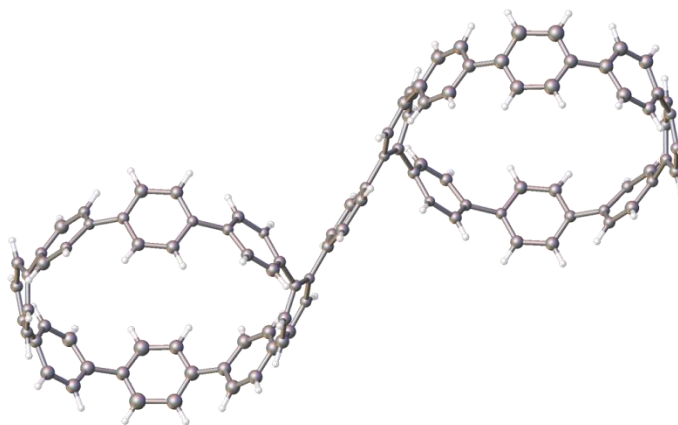
Figure IV.18. ORTEP representation (ellipsoids shown at 50% probability) of the preliminary (not fully refined) solid state structure of **IV.1**.

Table IV.8. Preliminary X-ray crystallographic parameters **IV.1**.

Identification code	jxia07a
Empirical formula	$C_{120}HCl_{0.5}$
Formula weight	1458.93
Temperature/K	100(2)
Crystal system	N/A
Space group	$P2_1/c$
a/Å	27.259(7)
b/Å	9.494(3)
c/Å	15.463(4)
$\alpha/°$	90
$\beta/°$	98.934(15)
$\gamma/°$	90
Volume/Å^3	3953.0(19)

Z	2
$\rho_{calc}g/cm^3$	1.226
μ/mm^{-1}	0.704
F(000)	1457
Crystal size/mm^3	none
Radiation	CuKα (λ = 1.54178)
2Θ range for data collection/°	9.4 to 132.54
Index ranges	-30 ≤ h ≤ 32, -10 ≤ k ≤ 11, -18 ≤ l ≤ 15
Reflections collected	20845
Independent reflections	5974 [R_{int} = 0.0965, R_{sigma} = N/A]
Data/restraints/parameters	5974/0/234
Goodness-of-fit on F^2	1.113
Final R indexes [I>=2σ (I)]	R_1 = 0.2754, wR_2 = 0.6091
Final R indexes [all data]	R_1 = 0.2903, wR_2 = 0.6168
Largest diff. peak/hole / e Å^{-3}	1.06/-1.16

IV.7. Conclusion

In summary, the syntheses of arene-bridged CPP dimers **IV.1** and **IV.2** were accomplished using macrocycle precursor **IV.7**. More broadly, this general synthetic route will be useful for the preparation of a variety of mono-functionalized CPPs via cross-coupling reactions. From computational analyses, we find that **IV.1** and **IV.2** can adopt the favored cis conformations in the gas phase and in solution, although the trans is the preferred conformer in the solid-state. As a result, further carbon-carbon bond forming reactions (e.g. cyclodehydrogenations) that lock the cis conformation and generate a nanotube-like structure are possible. With the ability to selectively functionalize cycloparaphenylenes and link them together, undoubtedly there is potential to exploit the desired cis conformation in interesting supramolecular and polymer chemistry applications

IV.8. Bridge to Chapter V

In Chapter **IV**, the synthesis and characterization of two cycloparaphenylene dimers were discussed. Perhaps most importantly, we have shown by DFT calculations that these two dimers prefer to adopt the cis conformation in solution. In the long term, these results could have implications in the synthesis of ultra-short CNTs if appropriate chemistry is developed to oxidatively dehydrogenate carbons between the aryl linker and the CPP backbone. Despite accessing a rigid structure, our laboratory has not had success thus far with Scholl-type reactions in the context of [*n*]CPPs, as will be introduced in Chapter **V**. While still realizing that the dimers have a real potential to act as models for extended CPP-based organic materials, we turned our efforts towards the synthesis of rigid graphitic belts from other types of [*n*]CPP precursors. Specifically, Chapter **V** will detail our work in developing ring-closing metathesis as a methodology for relatively strain-free benzannulations during the synthesis of two different fragments of [*n*]cyclophenacene.

CHAPTER V

TOWARDS THE SYNTHESIS OF AN AROMATIC BELT

This chapter is based on unpublished work. In addition to experimental assistance mentioned below in **V.4.1.** by Dr. Thomas Sisto, Jessie Zhen (Boston University) also provided assistance in the synthesis of starting materials for **V.4.1**. In **V.5.**, Prof. Bryan Wong (UC Riverside) performed ground-state energy computations and Dr. Lev N. Zakharov conducted the X-ray crystallographic analyses.

The construction of aromatic belts has been an ongoing challenge in the chemistry community, even before the discovery of carbon nanotubes. Despite numerous attempts, these double-stranded macrocycles, which include [*n*]cyclacenes and [*n*]cyclophenacenes, are still outstanding synthetic challenges. Typically, prior approaches relied on late-state, strain-building oxidation steps that were incapable of accessing the fully conjugated envisaged targets. In this chapter, we describe our efforts towards using appropriately functionalized [*n*]cycloparaphenylene precursors capable of undergoing one or more ring-closing metathesis events, thereby separating the strain-building event from the ring-forming reaction. In addition to detailing the successes and failures of incorporating olefins into [*n*]CPPs, we also report on the synthesis and characterization of (3,10)-dibenzo[*a,h*]anthracenyl-nanohoop and (2,11)-dibenzo[*c,m*]pentapheneyl-nanohoop. These two molecules not only provide proof of principle that [*n*]cyclophenacenes can potentially be derived from the bottom-up via functionalized [*n*]CPPs, but are also one of the largest fully conjugated belt fragments reported to date.

V.1. Background

Long before the discovery of carbon nanotubes in the early 1990's, significant efforts were made to synthesize rigid, double-stranded CNT fragments that are commonly referred to as "aromatic belts".[1-4] Like members of the [n]cycloparaphenylene family, the envisaged [n]cyclacene and [n]cyclophenacene targets (Figures **V.1**, marked in red) are the smallest rigid unit cycles of zigzag and armchair CNTs, respectively (Figure **V.1**, left). These molecules are prized for their severely distorted and strained aromatic systems with inward facing pi-orbitals
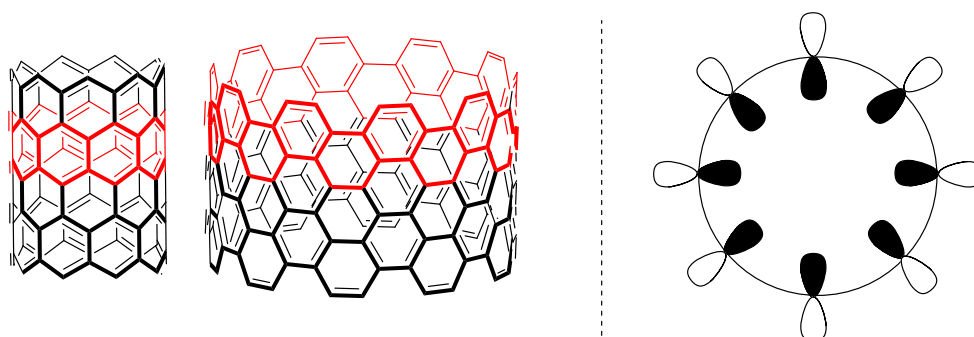
Figure V.1. Zigzag and armchair nanotubes (left), radially oriented p-orbitals (right).

(Figure **V.1**, right). Elegant work from the Nakamura group has allowed access to a fullerene-derived [10]cyclophenacene (**V.1**) through systematic, top-down degradation of C_{60} fullerene (Scheme **V.1**)[5]. While the phenacene in this example is electronically equivalent to a cyclophenancene, structurally it differs due to the lack of an open cavity.
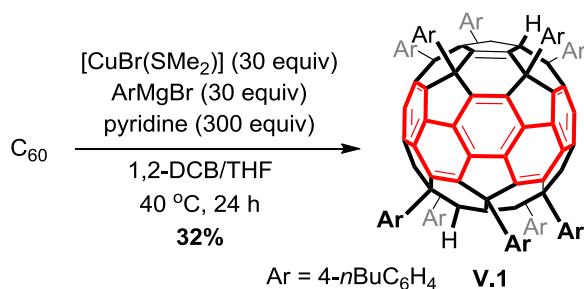
Scheme V.1. Nakamura's top-down approach to C_{60} derived [10]cyclophenacene **V.1**.

Predictions of instability stemming from low singlet-triplet gaps have not dissuaded synthetic chemists from pursuing $[n]_x$cyclacenes, where n defines the ring size(s) and x defines the number of units in the macrocycle, as several accounts on the synthesis of their macrocyclic precursors have been reported.[3, 6] Work from the Stoddart,[7-9] Cory,[10-11] and Schlüter[12-13] laboratories describe the assembly of several oxygenated macrocycles via Diels-Alder cycloaddition reactions en route to various cyclacene targets. Upon assembly of kohnkene **V.4**[7] from **V.2** and **V.3**, Stoddart was able to affect partial deoxygenation[8] with TiCl$_4$ and LiAlH$_4$ to deliver **V.5**. Further dehydration with acetic anhydride and HCl led to **V.6** (after *in situ* isomerization), which could not be further oxidized to $[6]_{12}$cyclacene **V.7**, presumably due to the inability to build in the remainder of the required strain or the instability of the product under the reaction conditions (Scheme **V.2**).
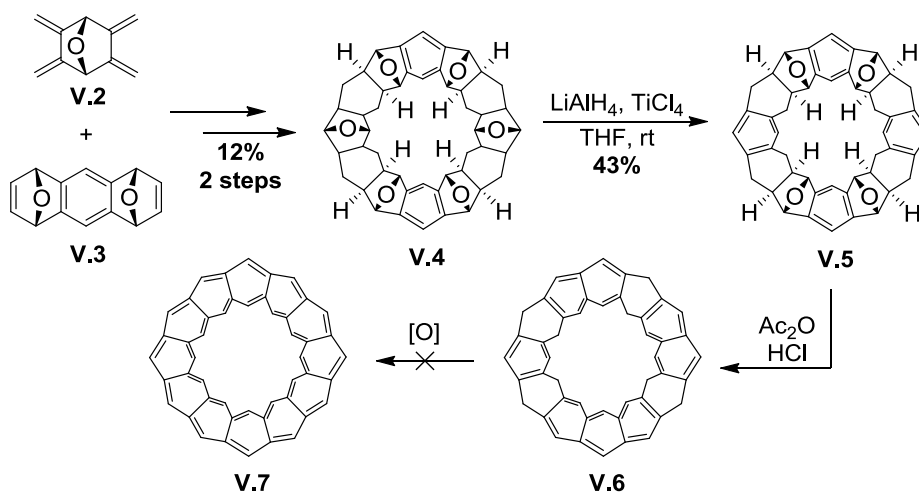
Scheme V.2. Stoddart's attempt towards $[6]_{12}$cyclacene.

The Cory group was also plagued by the same type of issues with late stage oxidations encountered by the Stoddart lab (Scheme **V.3**). Upon assembling **V.10** in 69%

from **V.8** and **V.9**,[10] treatment with a variety of oxidants, such as DDQ, *m*CPBA/*p*TsOH, or PCC only lead to partially dehydrogenated products rather than [6]$_8$cyclacene **V.11**.[11] No other reports on further manipulations of this scaffold have been reported.
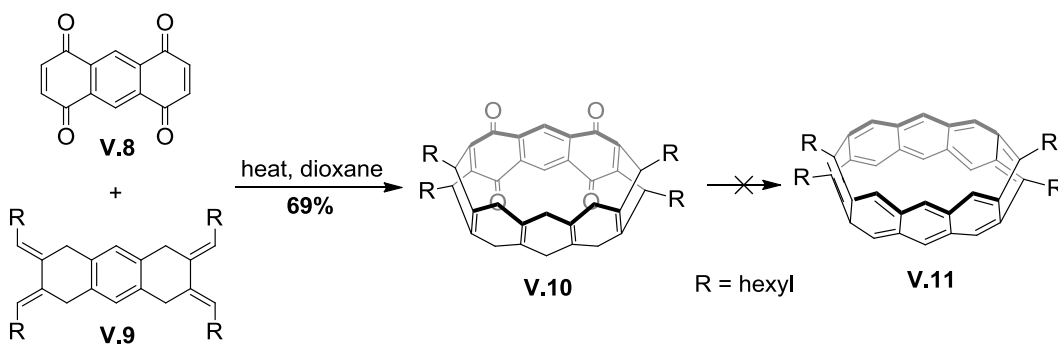
Scheme V.3. Cory's attempt towards [6]$_8$cyclacene.

In Schlüter's system, Diels-Alder assembly of **V.14** proceeded in high yield from **V.12** and **V.13**. Following several transformations and separation of the resulting diastereomers, macrocyclization afforded **V.15** in 25-45% yield. *p*TsOH was effective in dehydrating **V.15** to **V.16**,[12] but further oxidation could not be affected with a variety of Brønstead and Lewis acids[13-14] (Scheme **V.4**). The Schlüter laboratory reports observing the target C$_{84}$ fragment **V.17** via mass spectrometry after pyrolysis of an aceylated derivative of **V.16**,[15] but no solution-state characterization of **V.17** has been reported to date.[14] The observed molecular ion could also simply arise from a rearranged isomer due to the harsh experimental conditions.[15]
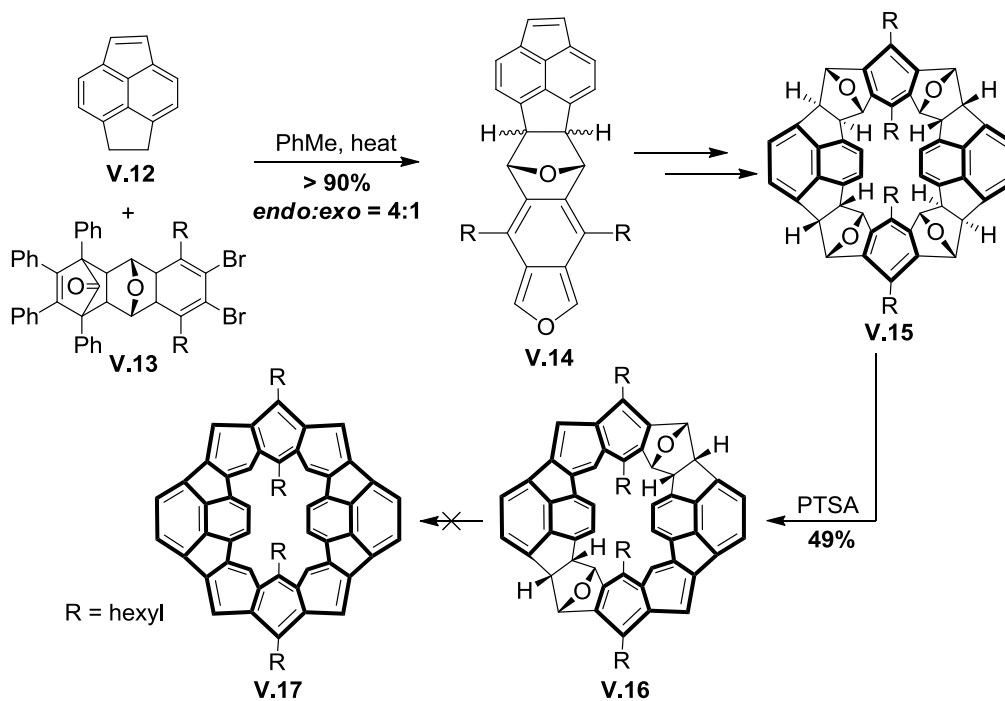
Scheme V.4. Schlüter's attempt towards buckybelt **V.17**.

Likewise, attempts towards the bottom-up syntheses of [*n*]cyclophenacenes have also been unsuccessful. One strategy employed by the Iyoda and Vollhardt laboratories stems from attempted oxidative couplings to stitch together the fjord regions of benzoannulenes (Scheme **V.5**). Initially, Iyoda and Vollhardt were able to independently access the all cis-isomer of **V.20** via a a nickel-catalyzed trimerization of **V.18**[16] or cobalt-mediated [2+2+2] cyclotrimerization between **V.19** and bis(trimethylsilyl)acetylene[17], respectively. Both laboratories also reported the thermal isomerization to benzoannulene **V.21**.[16, 18] Despite the macrocyclic rigidity of **V.21**, dehydrogenative cyclizations to form the desired [*n*]cyclophenacenes have been unsuccessful to date. Additionally, Herges and co-workers reported on the failure of both flash vacuum pyrolysis (FVP) and oxidative conditions[19] to close the walls of his group's advanced "picotube" **V.22** to nanotube **V.23**[20-21] (Scheme **V.5**).

Scheme V.5. Attempts from Vollhardt, Iyoda, and Herges towards rigid armchair CNT fragments.

V.2. Motivation

Due to overwhelming precedence for late-stage, strain-building oxidations to be detrimental in the synthesis of [*n*]cyclacenes and [*n*]cyclophenacenes, we opted to apply our own strain-building methodology as previously applied in the synthesis of [*n*]CPPs. For example, in the synthesis of [7]CPP, 16 kcal/mol of strain energy was built up during the macrocyclization step, followed by a late-state *reductive* aromatization event that added an additional 67 kcal/mol of strain energy (Scheme **I.4**). The Müllen group,[22-24] as well as our own laboratory, have explored the Scholl reaction extensively on substituted [*n*]CPPs. While Müllen and co-workers have shown evidence for oxidative C-C bond formation on extremely large [*n*]CPP backbones (*n* = 21) (**V.24**), these systems are almost completely unstrained (**V.25**) and contain substitution patterns to prevent strain-relieving cationic 1,2-phenyl shifts (**V.26**, Scheme **V.6**).[24] Hence, we sought a model system to explore milder methodology in the context of functionalized [*n*]CPP macrocyclic precursors.

164

Scheme V.6. The variable reactivity of Müllen's large arylated CPPs under Scholl conditions; products depend on the substitution pattern (**V.25** versus **V.26**).

We hypothesized that we could access the [*n*]cyclophenacenes through macrocyclization of olefin functionalized building blocks, followed by ring-closing metathesis and reductive aromatization. Importantly, unlike in the synthetic attempts from Vollhardt and Iyoda (Scheme **V.5**) we would be separating the ring-forming step (RCM) from the strain-building step (reductive aromatization). In addition, RCM is a redox-neutral process and should not cause cationic, strain-relieving rearrangements. Ring-closing metathesis has been shown to be effective in the synthesis of simple polycyclic aromatic hydrocarbons[25], as well as complex ones such as sumanene[26] and septulene[27] (Figure **V.2**).
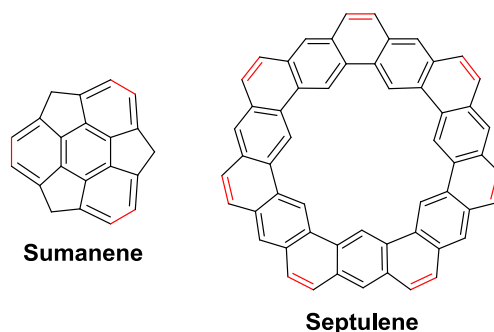
Figure V.2. Examples from Sakurai and King of PAHs accessed through multifold RCM reactions.

V.3. Progress Towards [*n*]Cyclophenacenes

V.3.1. Retrosynthetic Analysis

When considering how to assemble a cyclophenacene such as **V.27**, one must be conscientious of the cyclohexadiene stereochemistry in the corresponding macrocyclic precursor (Scheme **V.7**). In the case of **V.28**, all of the stereocenters are (*S*) and "matched", predisposing all the olefins to undergo productive ring closing metathesis. In a "mismatched" case, however, where cyclohexadiene rings with opposite stereochemical configurations (i.e. **V.29**) are in a macrocycle, not all of the necessary ring formations can occur. In such a case, partially closed products such as **V.30** will form, preventing belt formation upon reductive aromatization. Thus, only cyclohexadiene rings with the same stereochemical configuration, either (*S*,*S*) or (*R*,*R*) ought to be assembled together, to avoid scenarios such as **V.30** where complete ring closure is not possible. In order to build the appropriate macrocycle, one needs to synthesize the necessary chiral building blocks in an optically pure fashion.

166

Scheme V.7. Retrosynthetic analysis of [*n*]cyclophenacene **V.27**. To access **V.27**, cyclohexadiene rings in the macrocyclic precursor must be of the same stereochemical configuration (**V.28**) to ensure all of the olefins can undergo productive RCM reactions.

V.3.2. Initial Efforts in Controlling Stereochemistry

Despite the vast array of asymmetric transformations reported on achiral 2,5-cyclohexadienones,[28] no asymmetric 1,2-additions have been reported to date. In addition, the synthesis of chiral 2,5-cyclohexadienones via an asymmetric oxidative dearomatization reaction of a functionalized phenol is also not well understood.[29] Upon the synthesis of **II.19** (Scheme **II.6**), however, the formation of minor byproduct **II.20** was observed as a single diastereomer due to a slight excess of *n*BuLi. We believed that this result could have implications in controlling the cyclohexadiene stereochemistry (Scheme **V.8**).

167

Scheme V.8. Synthesis of **II.20**, an interesting byproduct with significant stereochemical implications.

It seems possible that the reactive atropisomer is determined by the stereochemical configuration of the cyclohexadiene ring. For example, a pre-determined (*R*) center in the racemic mixture of lithiate during diketone **II.14** formation (Scheme **V.9**, top) causes the top aromatic allyl group to swing away from the proximal allyl group appended to the cyclohexadiene ring. As a result, attack of electrophile **II.14** on the pro-(*R*) face minimizes steric clashing between allyl groups. In the case of attack on the pro-(*R*) face (Scheme **V.9**, bottom), sterics prevent formation of the other "mismatched" diastereomer. This relay of stereochemical information may be responsible for the formation of only a single diastereomer, **II.20**, which is conveniently poised to undergo two C-C bond formations via RCM upon olefin isomerization (Scheme **V.9**). Only the olefins that are aligned to form new 6-membered rings via RCM are marked in red in Scheme **V.9**.
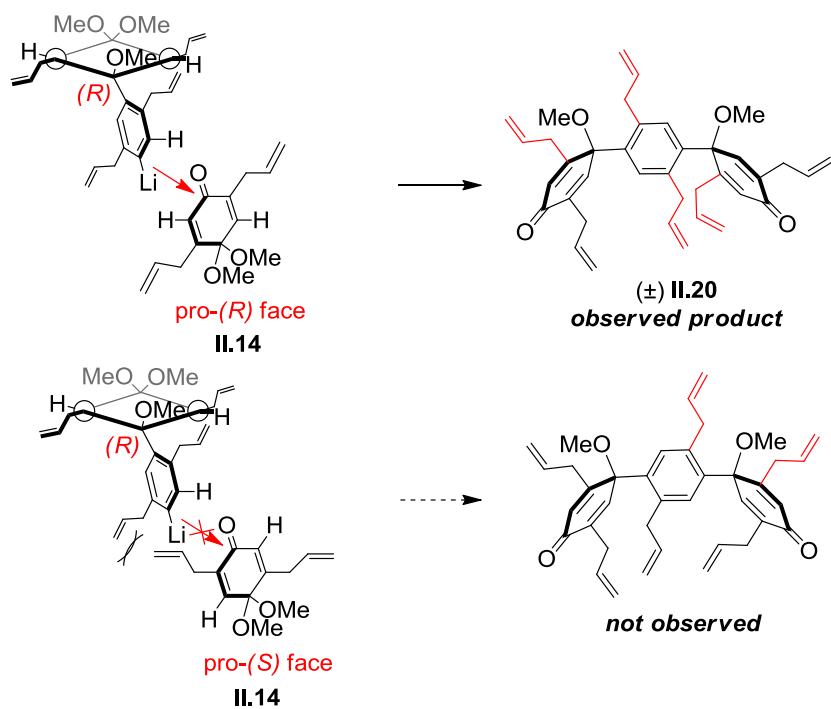
Scheme V.9. Stereochemical transfer occurs from the *in situ* generated organolithium compound to **II.14** such that all of the necessary olefins of **II.20** are predisposed to close.

Thus to control the cyclohexadiene stereochemistry in our system, we envisioned beginning with prochiral ketal **II.20** (originally introduced in Scheme **II.5**). Transketalization with **V.31** with $BF_3 \cdot Et_2O$ (Scheme **V.10**) afforded **V.32** in 55% yield. Upon nucleophilic addition, however, the two diastereomeric adducts **V.22** (dr = 1:1) were inseparable under a plethora of chromatographic and crystallization conditions.
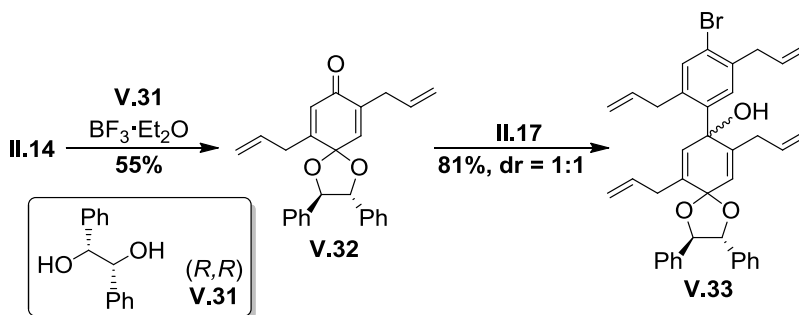
Scheme V.10. Attempted synthesis of an optically pure quinol via **V.33**.

Around this same time, we learned more about the facial selectivity of the addition of aryl lithium reagents to functionalized 4,4-disubstituted 2,5-cyclohexadienones, as described in Chapter **II.4.** It soon became obvious that our current methodology was insufficient to synthesize the desired functionalized building blocks, with high amounts of the necessary syn diastereomer. While continuing to investigate the problems posed in Chapter **II**, we concurrently began to examine other means of functionalizing the cyclohexadiene rings such that we could begin to examine ring closing methathesis methodology in the context of these systems.

V.4. Synthesis of Difunctionalized 1,4-syn-Dimethoxycyclohexa-2,5-dienes: Model Systems for Ring-Closing Metathesis

The majority of our next efforts towards the synthesis of a model system to explore RCM reactions on difunctionalized 1,4-syn-dimethoxycyclohexa-2,5-dienes relied on methodology to vinylate the central diene ring. In addition, we briefly explored a potential two-fold Claisen rearrangement of 1,4-syn-dihydroxycyclohexa-2,5-diene under *O*-vinylation conditions to affect functionalization and concurrent aromatization of the system.

170

V.4.1. Vinylation of Central Diene Ring

We first envisioned that brominated benzoquinone monoketal **IV.3** (Scheme **IV.1**) would serve as a useful functional handle for vinylation of the central diene ring in our model system. Lithium-halogen exchange of styrene **V.34**, followed by nucleophilic addition to **IV.3** and acid-catalyzed deprotection afforded *p*-quinol **V.35** in 47% yield (Scheme **V.11**). It should be noted that lithium halogen exchange of **V.34** was only possible with *t*BuLi in Et$_2$O. Other conditions led to polymeric byproducts even before the addition of **IV.3**. Brominated diene **V.36** was synthesized by a stereoselective nucleophilic addition of (4-chlorophenyl)lithium and subsequent methylation reaction in 63% yield.
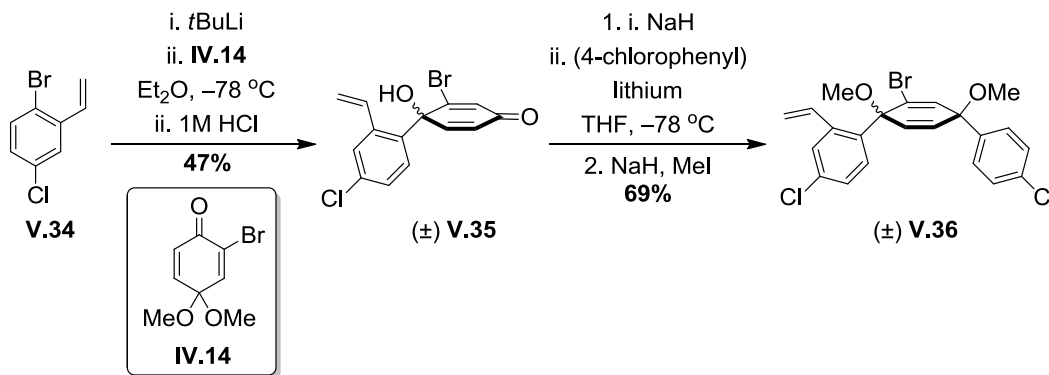
Scheme V.11. Synthesis of vinylated **V.36** with a bromide functional handle.

Unexpectedly, treatment of **V.36** with vinyl-BF$_3$K[30-32] and Pd(PPh$_3$)$_4$ only afforded *5-exo-trig* Heck cyclization product **V.37** (Scheme **V.12**), rather than a vinylated diene, as assessed by crude ^{1}H NMR spectroscopy (Figure **V.14**, bottom), where two new terminal olefinic protons appear around 5.5 ppm. Attempts to isolate **V.37** from the crude

reaction mixture tentatively afforded a ~1:1 mixture of anisole products (Scheme **V.12**), presumably via acid-catalyzed degradation on silica gel (Figure **V.14**, top), as evidenced by the downfield shift of the two methyl ether resonances and the loss of the cyclohexadiene *ABX* system.
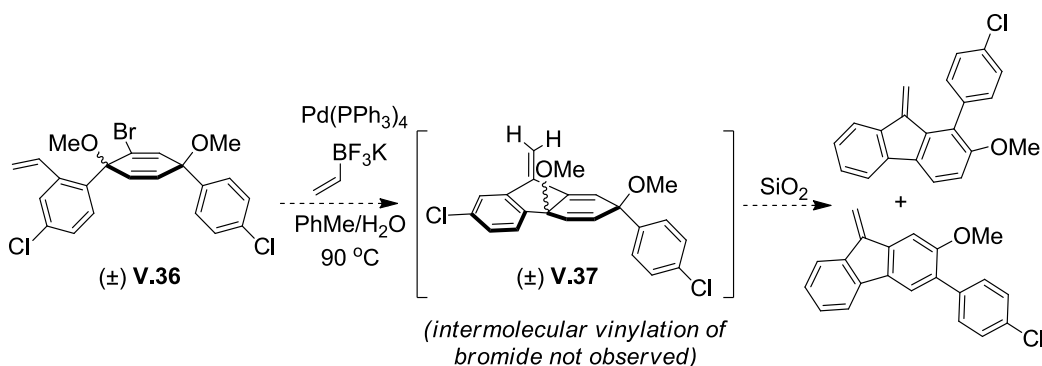
Scheme V.12. Attempted vinylation of **V.36** led to an unexpected 5-*exo-trig* cyclization to **V.37**.

To overcome this challenge, we planned a new synthetic route where vinyl bromide **V.36** was formylated with *n*BuLi and DMF in 26% yield (**V.38**) followed by olefinating with Wittig conditions to afford diolefin **V.39** in 60% yield (Scheme **V.13**). With model **V.39** in hand, we began to examine RCM conditions to form a new 6-membered ring (Table **V.1**) using ruthenium catalysis in CH_2Cl_2. In general, we were able to observe the disappearance of both terminal olefins (**V.39**) and the appearance of a new pair of doublets (J = 9.6 Hz) in the putative ring-closed product **V.40** (Figure **V.15**). Similar to **V.37**, however, **V.40** proved to be extremely unstable on silica gel and we were unable to cleanly isolate it without observing new anisole resonances from 1,2-phenyl shift degradation products. In addition, Grubbs II in CH_2Cl_2 (entry 3) proved to be the most efficient catalyst system, showing > 95% conversion to the tentative product

V.40. Although the ring-closed product **V.40** was not isolable, it is worth noting that none of the catalysts employed decomposed the cyclohexadiene internal olefins during the course of the reaction, while only one set of conditions (entry 1) led to small amounts of Lewis acid catalyzed rearrangement. While the conversions reported are certainly not indicative of the actual reaction yield, they did give us a benchmark for future systems.
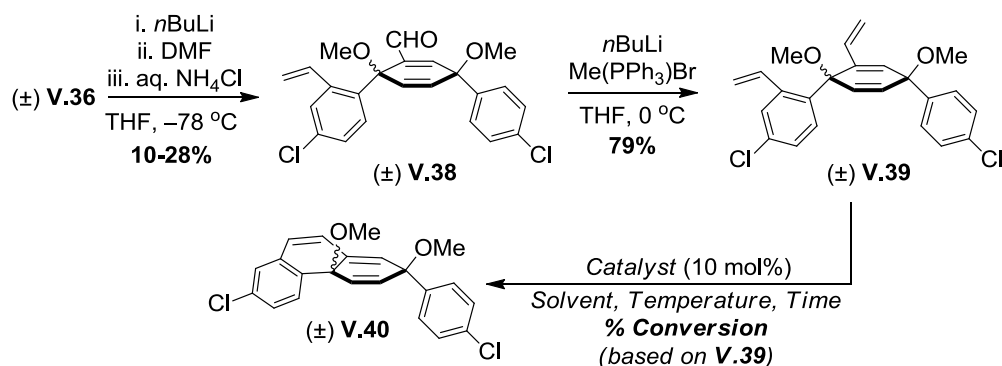
Scheme V.13. Development of model system **V.40** for ring closing metathesis.

Table V.1. Conditions for ring closing metathesis of **V.39**.

Entry	Catalyst	Solvent, Temp, Time	% Conversion to V.40 from V.39
1	Grubbs I	CH$_2$Cl$_2$, 35 $^{\circ}$C, 18 h	56%[a]
2	Grubbs I	PhMe, 65 $^{\circ}$C, 17 h	20%
3	Grubbs II	CH$_2$Cl$_2$, 35 $^{\circ}$C, 16 h	> 95 %
4	Grubbs-Hoveyda II	CH$_2$Cl$_2$, 35 $^{\circ}$C, 16 h	80%

[a] Small amounts of aromatized **V.40** isomers were also observed in the crude mixture.

To assess the efficiency of RCM in the context of an [*n*]CPP macrocyclic precursor, we first wanted a more streamlined approach to incorporate both of the required vinyl groups. Lithiation of **V.34** with *t*BuLi in Et$_2$O, followed by addition of ketal **V.41** and acid-catalyzed deprotection delivered *p*-quinol **V.42** in 45% yield.

Attempted stereoselective addition to **V.42** with (4-chlorophenyl)lithium delivered the

desired 1,2-addition product, which could not be completely purified (Scheme **V.14**).

Additionally, 25% of phenol **V.43** was isolated, resulting from initial 1,4-addition/*5-exo-*

trig cyclization of the latent alkoxide, followed by base catalyzed rearrangement and

trapping of the benzylic aldehyde with (4-chlorophenyl)lithium (Scheme **V.14**).
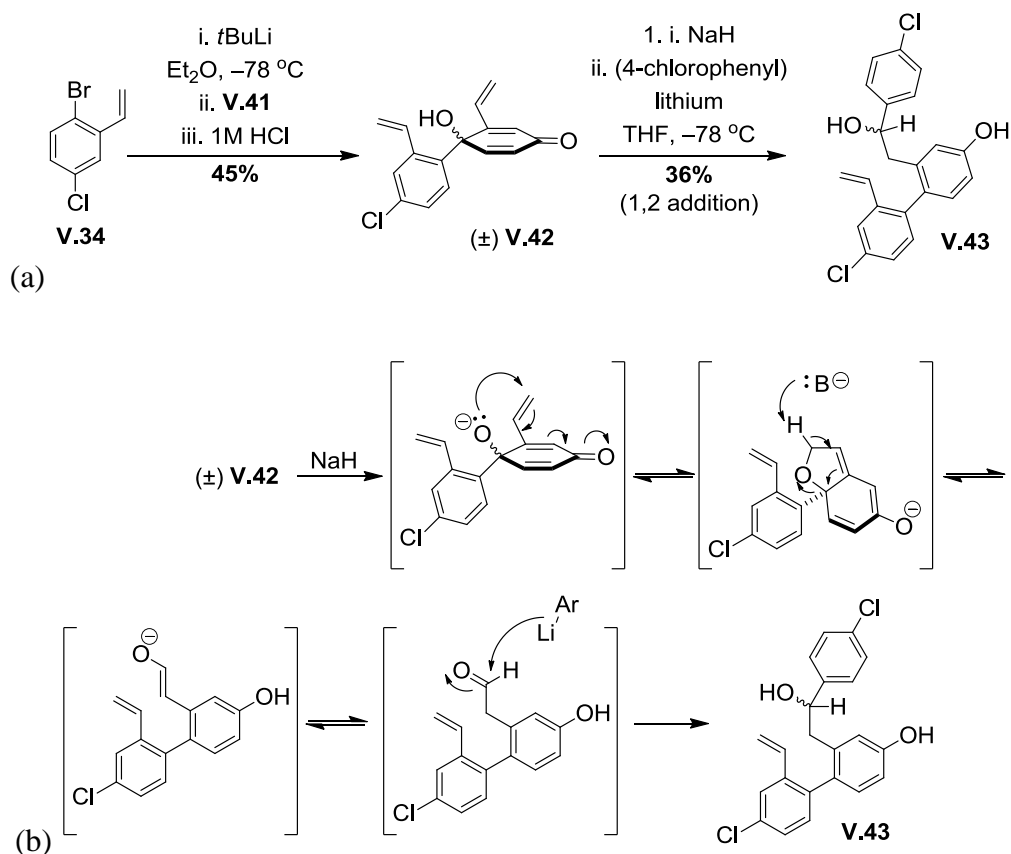
Scheme V.14. (a) Unexpected cyclization of **V.42** to phenol **V.43** via 5-*exo-trig*
cyclization. (b) Proposed mechanism of phenol **V.43** formation.

Hence, methylated **V.44** was synthesized instead to circumvent the undesired

cyclization event. To **V.44** was added **V.45**, derived from **II.6**, to rapidly deliver 5-ring

dichloride **V.46** in 49% yield, a key coupling partner in a potential macrocyclization reaction. The facial selectivity of this reaction has not been unequivocally determined, although **V.46** appears to be one diastereomer by ^{1}H NMR spectroscopy (Scheme **V.15**).
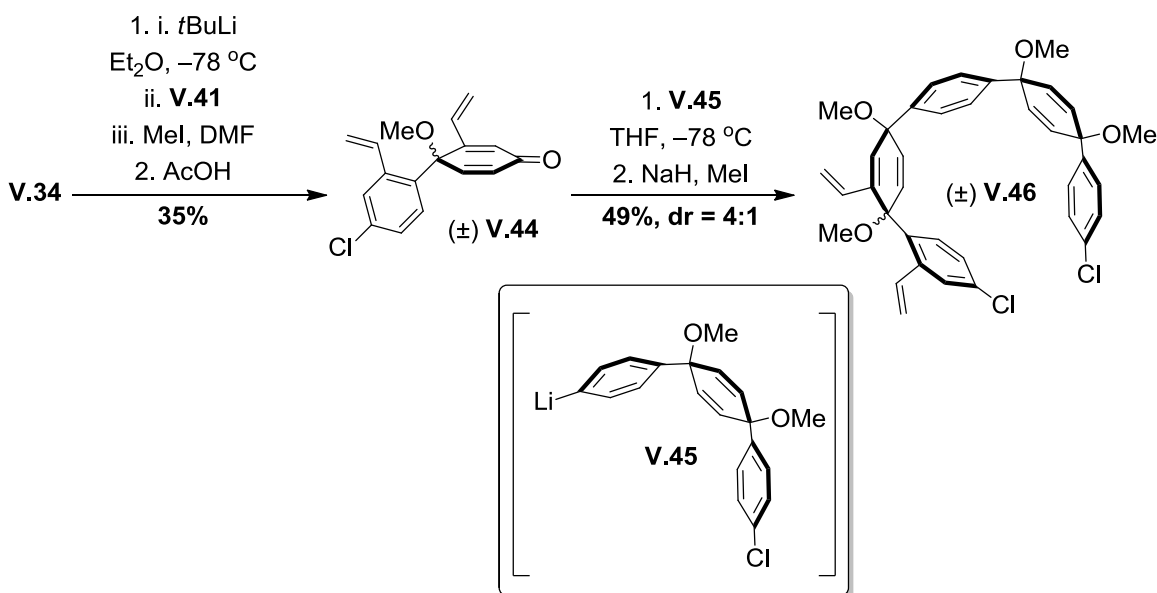
Scheme V.15. Synthesis of 5-ring **V.46** as a macrocyclic precursor.

Having accessed this advanced intermediate, we wanted to probe the competency of **V.46** to undergo a two-fold Suzuki-Miyuara cross-coupling reaction, as would be required in a subsequent macrocyclization step (Scheme **V.16**). In collaboration with Dr. Thomas Sisto, we screened a variety of conditions to couple **V.46** with 4-methylphenylboronic acid bis(pinacol)ester and rapidly concluded that the vinylated cyclohexadiene was unable to undergo successful cross-coupling (Table **V.2**). While we predominately observed extensive decomposition in the crude ^{1}H NMR spectra, in

several cases (Table **V.2**, entries 7 and 10) we could isolate small amounts of material

arising from aromatization of the substituted cyclohexadiene ring (**V.47** and **V.48**). Key

in identifying this specific
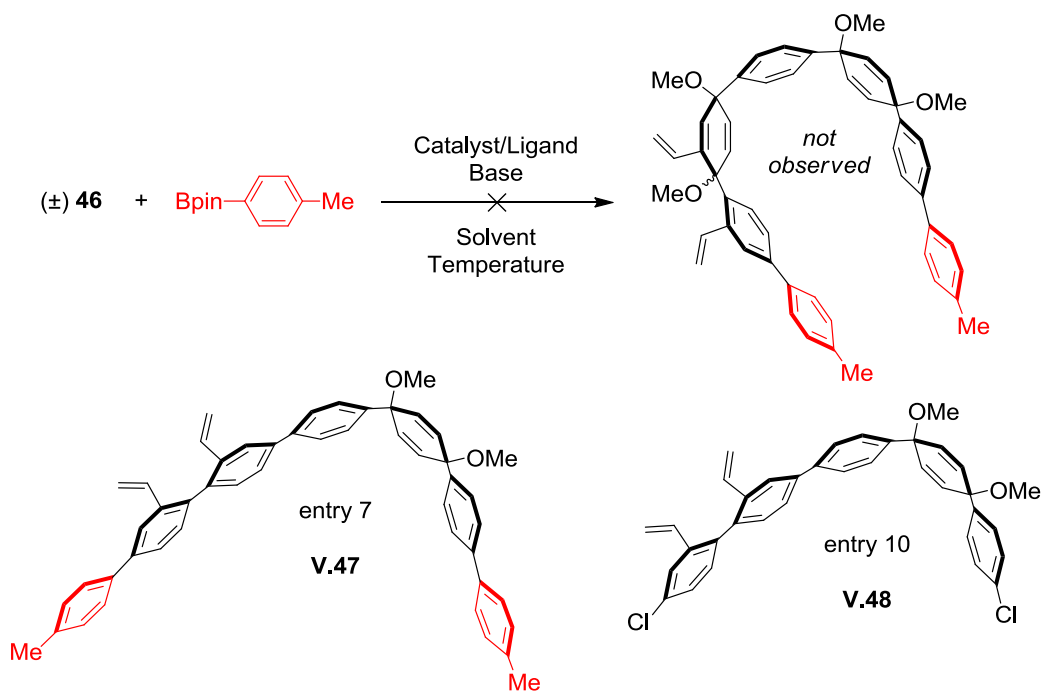
Scheme V.16. Degradation of **V.46** under numerous cross-coupling conditions.

potential decomposition pathway was the observation of the loss of two upfield methyl

ether and three cyclohexadiene resonances to form **V.47** and **V.48**. Interestingly, while

phosphine ligand alone (Table **V.2**, entry 13) does not induce this aromatization event,

Pd(PPh$_3$)$_4$, a catalyst system not capable of oxidatively inserting into the aryl chloride

bonds of **V.46**, does lead to decomposition (Table **V.2**, entry 14). We hypothesize that

decomposition is occurring via an electron-transfer pathway or a π-allyl-like

intermediate, but concrete mechanistic experiments have not been completed at this time.

176

Table V.2. Unsuccessful linear cross-couplings to **V.46**.

Entry	Catalyst	Solvent	T	Base	Outcome
1	Pd(OAc)$_2$/SPhos	PhMe/H$_2$O	70 $^{\circ}$C	K$_3$PO$_4$	**V.46** / decomposition
2	Pd(OAc)$_2$/SPhos	PhMe/H$_2$O	95 $^{\circ}$C	K$_3$PO$_4$	**V.46** / decomposition
3	Pd(OAc)$_2$/SPhos	DMF/H$_2$O	50 $^{\circ}$C	K$_3$PO$_4$	**V.46** / decomposition
4	Pd(OAc)$_2$/SPhos	DMF/H$_2$O	70 $^{\circ}$C	K$_3$PO$_4$	decomposition
5	Pd(OAc)$_2$/SPhos	Dioxane/H$_2$O	50 $^{\circ}$C	K$_3$PO$_4$	**V.46** / decomposition
6	Pd(OAc)$_2$/SPhos	Dioxane/H$_2$O	70 $^{\circ}$C	K$_3$PO$_4$	decomposition
7	Pd(OAc)$_2$/DavePhos	Dioxane/H$_2$O	70 $^{\circ}$C	K$_3$PO$_4$	**V.47**
8	Pd(OAc)$_2$/DavePhos	PhMe/H$_2$O	70 $^{\circ}$C	Cs$_2$CO$_3$	**V.46, V.47, V.48**
9	Pd(OAc)$_2$/JohnPhos	Dioxane/H$_2$O	70 $^{\circ}$C	K$_3$PO$_4$	decomposition
10	Pd(PCy$_3$)$_2$Cl$_2$	Dioxane/H$_2$O	70 $^{\circ}$C	K$_3$PO$_4$	**V.48**
11	Pd(PCy$_3$)$_2$Cl$_2$	DMF/H$_2$O	70 $^{\circ}$C	K$_3$PO$_4$	**V.46** only
12	Pd(PCy$_3$)$_2$Cl$_2$	PhMe/H$_2$O	70 $^{\circ}$C	Cs$_2$CO$_3$	**V.46** only
13	DavePhos only	Dioxane/H$_2$O	70 $^{\circ}$C	K$_3$PO$_4$	**V.46** only
14	Pd(PPh$_3$)$_4$	Dioxane/H$_2$O	70 $^{\circ}$C	K$_3$PO$_4$	decomposition
15[b]	Pd(OAc)$_2$/DavePhos	Dioxane/H$_2$O	70 $^{\circ}$C	K$_3$PO$_4$	**V.46** / decomposition
16[b]	Pd(PCy$_3$)$_2$Cl$_2$	Dioxane/H$_2$O	70 $^{\circ}$C	K$_3$PO$_4$	**V.46** / decomposition

[a] Catalyst loadings were 14 mol% Pd (entries 1-6) or 28 mol% Pd (entries 8 – 12, 14 – 16); ligand:Pd ratio = 3:1. [b] Run without 4-methylphenylboronic acid bis(pinacol)ester.

V.4.2. Modifying Diene Substitution

Despite the difficulties associated with having a single vinyl substituent appended to a cyclohexadiene ring, such as in the case of **V.46**, we next tested if (*E*)- propenyl groups might afford additional stability under Suzuki-Miyuara cross-coupling conditions.

Beginning with **V.49** (E:Z = 5:1), nucleophlic addition of (4-bromophenyl)lithium, followed by acid catalyzed deprotection of the dimethyl ketal, yielded *p*-quinol **V.50** in 72% yield (Scheme **V.17**). Diastereoselective addition of (4-bromophenyl)lithium and subsequent methylation delivered **V.51** in 36% yield (E:Z = 9:1), which was then subjected to Pd(PPh₃)₄ and 4-tolylboronic acid bis(pinacol)ester. While similar conditions decomposed **V.46**, **V.51** was cleanly coupled to deliver **V.52** in 92% yield.
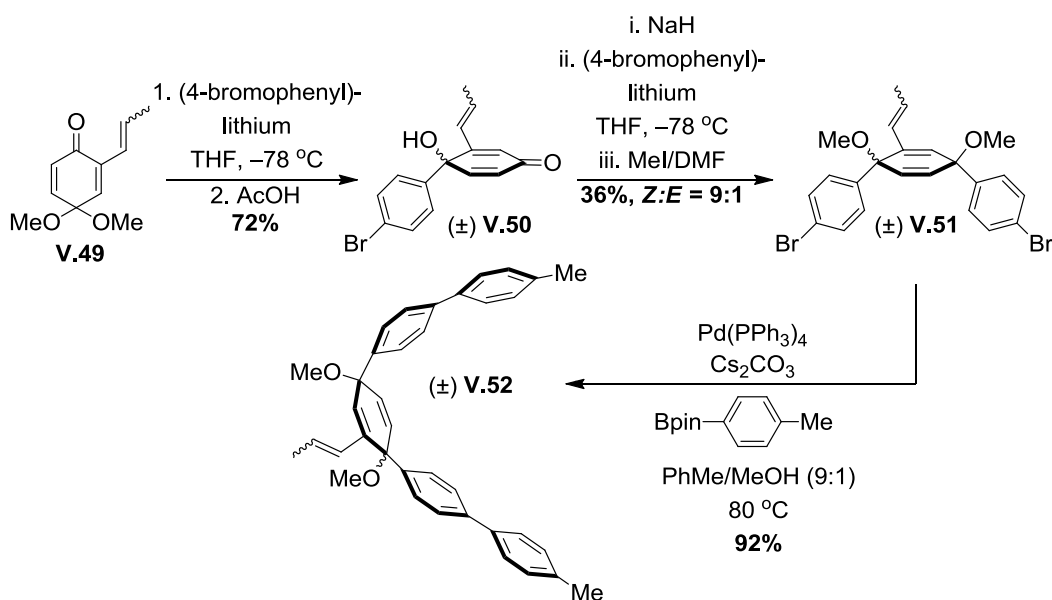
Scheme V.17. Propenyl-substitution provides additional stabilization to access **V.52**.

Attempts to directly incorporate two (*E*)-propenyl groups on the cyclohexadiene ring were less successful, however. Two-fold isomerization of **II.12** with PdCl₂(MeCN) proceeded cleanly to **V.53** in 50% yield, but mono-methylation with catalytic sodium nitrite in acidic methanol led to decomposition rather than **V.54** (Scheme **V.18**). **V.54** could in fact be accessed from *t*BuOK mediated olefin isomerization of **II.13**, but

oxidative dearomatization of **V.54** only produced trace amounts of potential ketal product

V.55. Instead, we turned to some of the advanced allylated intermediates synthetized in

Chapter **II** to serve as models for a later-stage olefin migration event.
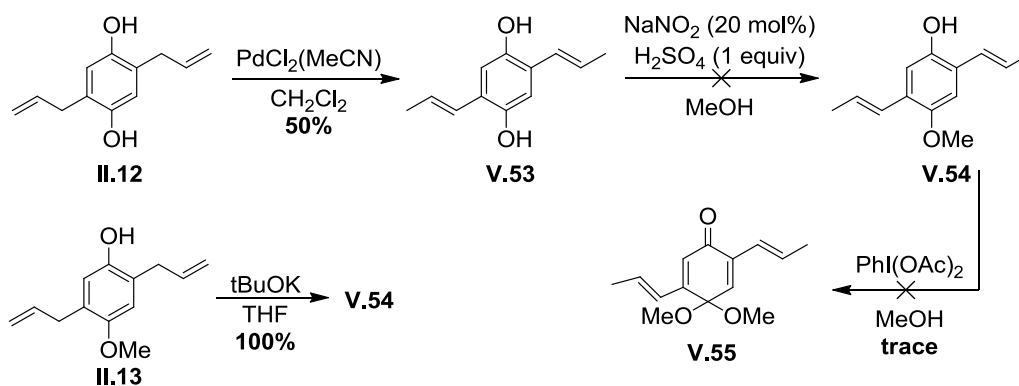
Scheme V.18. Unsuccessful routes to access quinol **V.55**.

In addition to the ease of installation compared to propenyl groups, allyl groups

also have already shown to be robust in early stages of our synthetic sequences. Hence,

although methodology for the diastereoselective synthesis of highly functionalized 1,4-

syn-dimethoxycyclohexa-2,5-dienes is still ongoing, we wanted some insight to the

behavior of intermediates synthesized in Chapter **II** under olefin isomerization

conditions. Subjecting methylated *p*-quinol **II.26** to Grubbs II in methanol under air[33]

afforded two-fold isomerization product **V.56** in 50% yield (Scheme **V.19**). Highly

functionalized methylated *p*-quinol **II.19** decomposed under the same conditions,

however. Allylated anti-adduct **II.21** decomposed with Grubbs II in MeOH, and also with

*t*BuOK in THF, while **II.30** isomerized with Grubbs II in MeOH fairly cleanly (72%

yield, ^{1}H NMR internal standard). Although our attempts were certainly not exhaustive

179

by any means, if a highly allylated 1,4-syn-dihydroxycyclohexa-2,5-diene can be synthesized, revisiting the plethora of olefin isomerization conditions in the literature[34] will certainly be necessary.
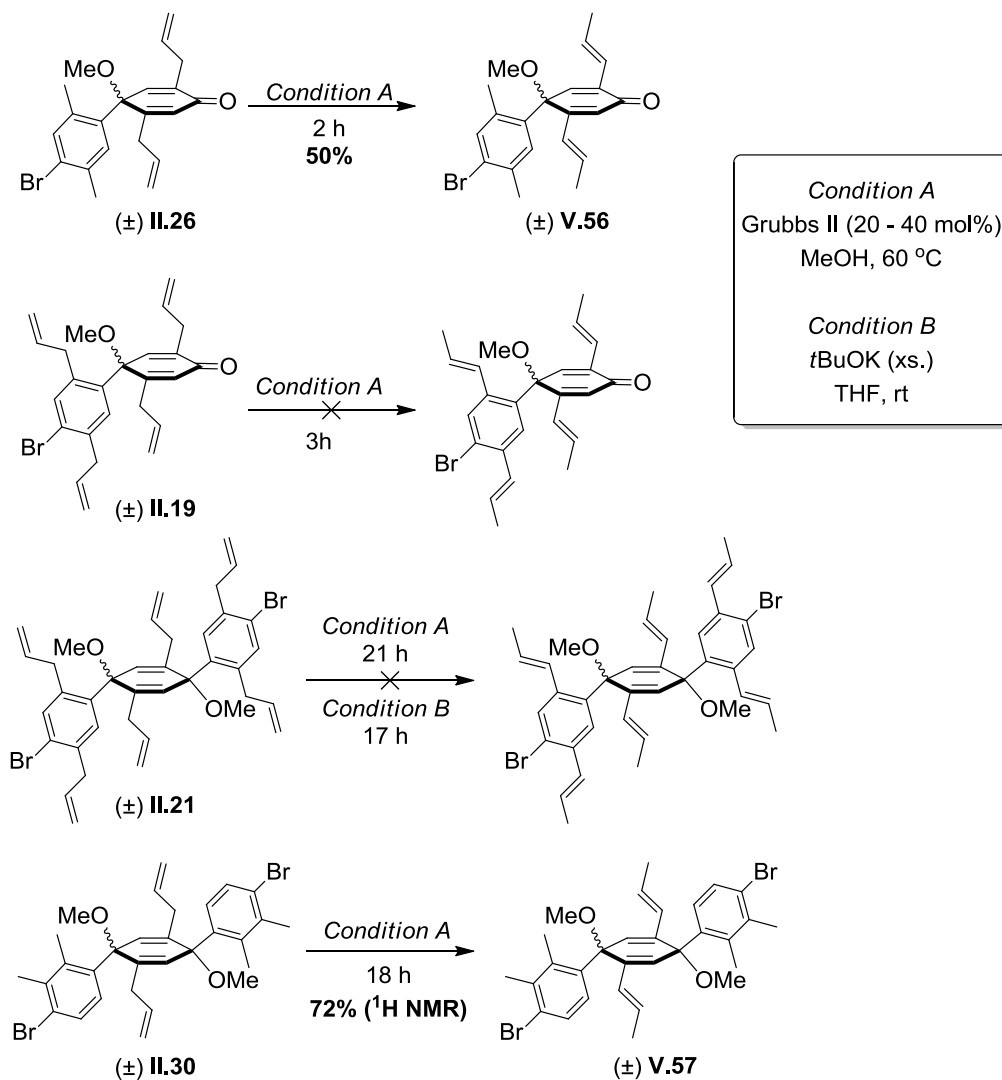
Scheme V.19. Various attempts for late-stage olefin migrations of allyl groups.

V.4.3. A Potential Two-Fold Claisen Rearrangement of 1,4-syn-Dihydroxycyclohexa-2,5-dienes

In a separate attempt to add functionality to the diene moiety, Evan Darzi conceived of the idea to perform tandem [3,3] rearrangements, utilizing the two doubly allylic alcohols of **V.58** as functional handles. Vinylating the alcohols should allow for facile Claisen rearrangements, affording a terphenyl product, upon oxidative dehydrogenation, with *p*-substituted benzylic aldehydes (**V.59**,Scheme **V.20**). If successful, this would completely remove the reductive aromatization reaction as a synthetic step. Treatment of **V.58** with Pd(TFA)$_2$/phenanthroline and triethylamine in *tert*-butyl vinyl ether[35] caused extensive decomposition, while use of Ir[(OMe)(cod)]$_2$ and vinyl acetate in refluxing toluene[36] only afforded starting material. Switching to more classical vinyl transfer conditions, Hg(OAc)$_2$ and ethyl vinyl ether, delivered an interesting and unexpected product, albeit in low yield (**V.60**).
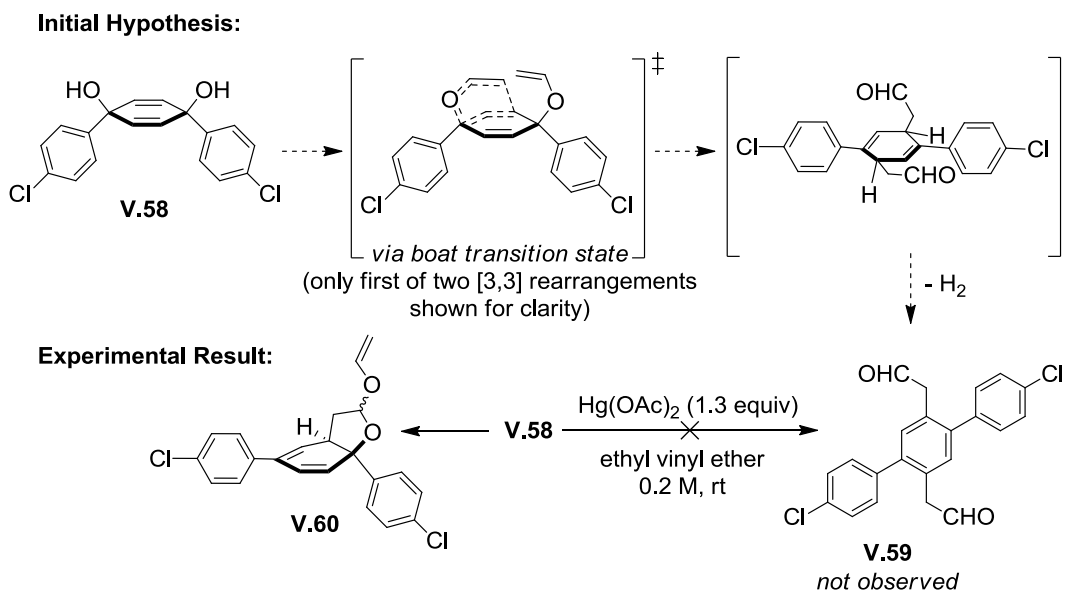
Scheme V.20. A potential two-fold Claisen rearrangement that could provide functionality and an alternative aromatization pathway (**V.59**).

Upon one vinylation/Claisen rearrangement of **V.58**, the resulting benzylic aldehyde is trapped by the second alcohol before another vinylation event can occur (Scheme **V.21**). The resulting heterocycle is then vinylated further to afford **V.60** as a mixture of diastereomers as judged by crude ^{1}H NMR spectroscopy (dr = 4:1). Stereochemical assignment of the major isolable diastereomer ((S) configuration at the alcohol) was done using basic Karplus analysis. The stereogenic hydrogen, if placed in the pseudo-equatorial position, has a dihedral angle with the adjacent pseudo-equatorial hydrogen on the methylene spacer of approximately 83°. Thus, the hydrogen at the chiral center appears as a doublet (J = 4.6 Hz) downfield at 5.50 ppm. Inverting the stereocenter would allow stronger coupling between this hydrogen and the two adjacent methylene hydrogens, causing further splitting beyond a simple doublet. We rationalize the stereochemical outcome of the cyclization by simply placing the carbonyl away from the ring system to alleviate sterics. Although this is certainly not the product that we had hoped to isolate, we are confident that, at least for an acyclic system, appropriate functionalization will allow for two tandem rearrangements to occur. The question still remains if this type of a process can build strain, as would be required in a macrocyclic compound.
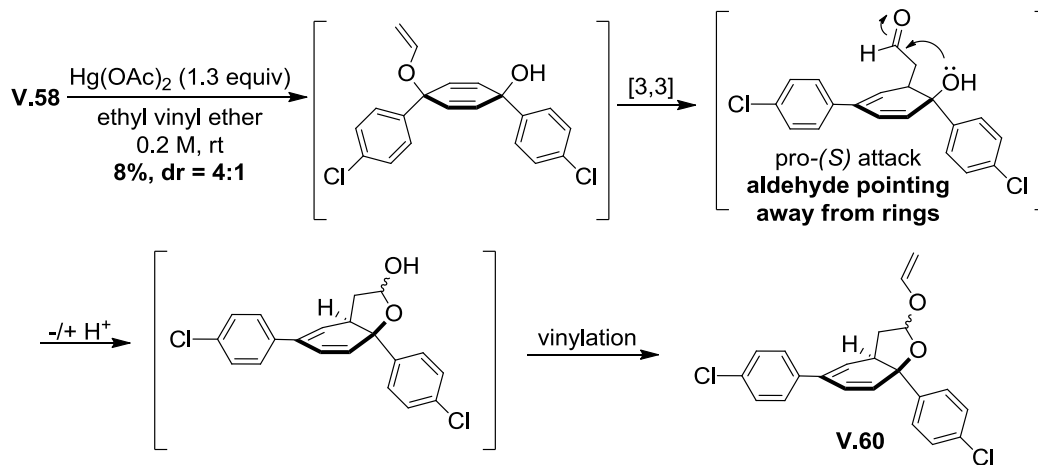
Scheme V.21. Unexpected heterocycle **V.60** formation during an attempted [3,3]-rearrangement of **V.58**.

V.5. Synthesis and Characterization of Dibenzo[a,h]anthracene and Dibenzo[c,m]pentaphene Incorporated CPPs

With the difficulties of previous attempts, we decided to refocus and avoid systems that would require cyclohexadiene functionality. Through more straightforward methodology, we sought a system where RCM reactions could be tested in the context of a macrocycle. Specifically, C-C bond formation would occur between adjacent functionalized aryl rings, rather than between functionalized arenes and cyclohexadienes. We envisioned cyclophane targets **V.61** and **V.62**, which could arise from ring-closing metathesis of appropriately vinylated macrocycles. Thus, the strategic incorporation of olefins into earlier coupling partners would hopefully allow us to rapidly access both macrocycles (Figure **V.3**). It is noteworthy that the final structures **V.61** and **V.62** represent some of the largest polycyclic aromatic hydrocarbons to be incorporated into a fully conjugated macrocycle.
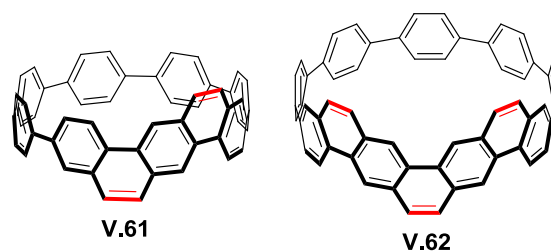
Figure V.3. Graphitic belt fragments **V.61** and **V.62**.

Following up their work with [n](2,7)pyreneophanes,[37-39] Bodwell and co-workers elegantly synthesized a series of [n](2,11) teropyrenophanes that contain equally impressive bent PAHs linked by tethered alkyl chains.[40-42] In particular, [8](2,11)teropyrenophane **V.63** contains an aromatic unit that is bent (θ) almost 180°, which is quite comparable to the bending observed in an armchair SWCNT (Figure **V.4**).[40]
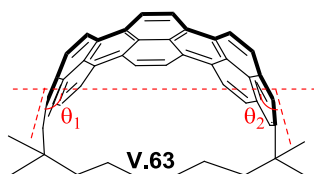
Figure V.4. Bodwell's [8](2,11)teropyreneophane with an aromatic unit that is bent almost 180°. $\theta = 180 - (\theta_1 + \theta_2)$.

In contrast to Bodwell's work, a few smaller PAHs have been incorporated end-to-end to yield conjugated macrocycles, such as [9]cyclo-1,4-naphthalene **V.64**,[43] [4]cyclo-2,7-pyrene **V.65**,[44] and a family of stereoisomeric [4]cyclocrysenylenes (including **V.66**) (Figure **V.5**). Our targets build upon both classes of these recently accessed molecules by incorporating large, bent PAHs into fully conjugated cyclophanes.

184
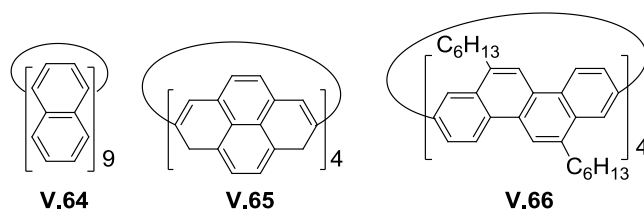
Figure V.5. Macrocycles incorporating small PAHs from the Itami, Yamago, and Isobe laboratories.

V.5.1. Synthesis

Our synthesis commenced with the two-fold lithiation of syn-dibromide **V.67**, followed by addition of benzoquinone monoketal. Following deprotection, diqunol **V.68** was accessed in 44% yield. Previously, we showed that additions of aryl lithium reagents to *p*-quinols in the presence of sodium hydride preferentially affords the syn diastereomer (dr = 19:1) (Scheme **II.3**). Hence, two-fold diastereoselective addition of (((3-OTBS)methyl)-4-chlorophenyl)lithium (derived from **V.69)** to **V.68**, followed by *in-situ* methylation of the resulting tetra-alkoxide, allowed for rapid formation of dichloride **V.70** in 36% yield (dr = 9:1, syn-syn:syn-anti) (Scheme **V.22**). Deprotection with TBAF, followed by oxidation with Dess-Martin periodinane and Wittig olefination afforded dichloride **V.71** in 34% yield over three steps. Attempts to directly access divinyl **V.70** (or its di-(*E*)-propenyl analog) by employing 2-chloro-4-bromostyrene (or (*E*)-2-chloro-4-bromo-β-methylstyrene) as pronucleophiles for two-fold additions to **V.68** were unsuccessful as lithium-bromide exchange could not be affected under a variety of conditions without concurrent anionic polymerization. Having accessed **V.71,** we were now in a position to explore macrocyclization conditions.
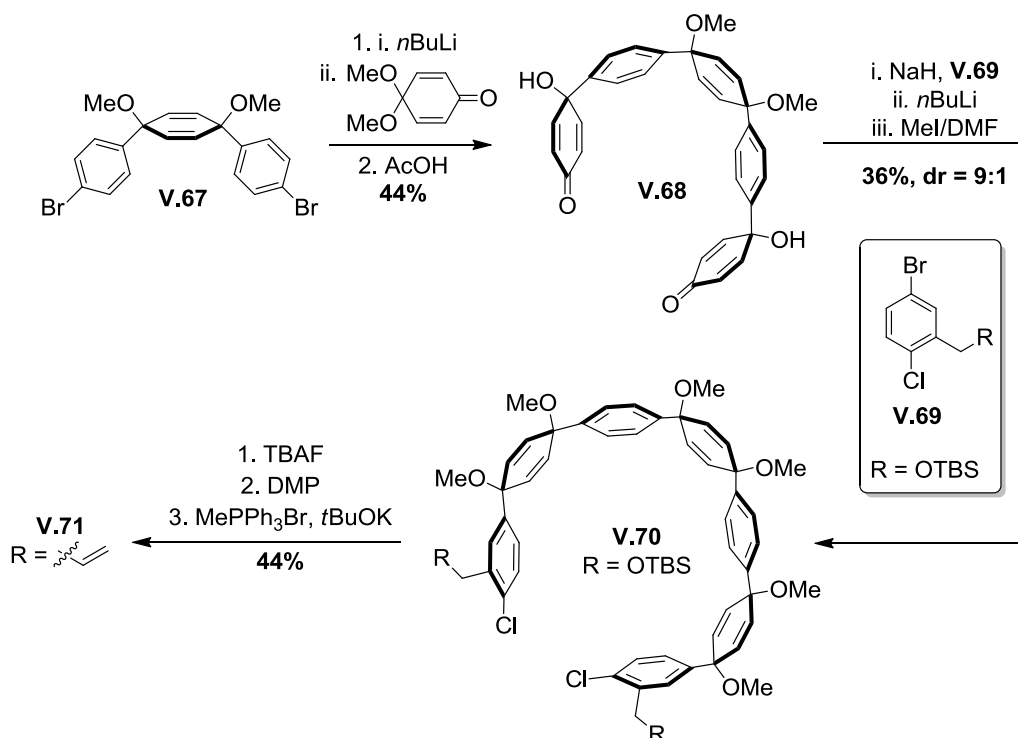
Scheme V.22. Synthesis of divinyl intermediate **V.71**.

Although there are certainly reports of Suzuki-Miyaura cross-couplings between aryl chlorides and aryl boronic acid bis(pinacol)esters that both possess ortho functionality, we had yet to explore these types of substrates for macrocycle generation. Treatment of **V.71** and **V.72**[45] with 20 mol% SPhos-Pd-G2[46] in dioxane/water (9:1, ca. 1 mM) at 80 $^{\circ}$C afforded terphenyl-containing macrocycle **V.73** in 19% yield (Scheme **V.23**). Interestingly, **V.73** exhibits some dynamic behavior in its ^{1}H NMR spectrum (Figure **V.16**). At 25 $^{\circ}$C, **V.73** has extremely sharp resonances indicative of a single, more stable conformation at room temperature. Upon heating to 70 $^{\circ}$C, a terminal olefinic resonance (ca. 5.1 ppm) and the resonance for the proton ortho to the vinyl group in the outer *ABX* system (marked H$_a$, 8.5 ppm) begin to broaden, among several other

186

overlapping resonances. At room temperature, the rigidity of the macrocycle, which in turn breaks the symmetry of the molecule, is also seen with the "W-like" coupling between protons on the top face and the bottom face of the cyclohexadiene diene rings. For example, while *a priori* one might expect H_b/H_b' to be equivalent by symmetry, weak coupling (^4J = 2.2 Hz) is observed.
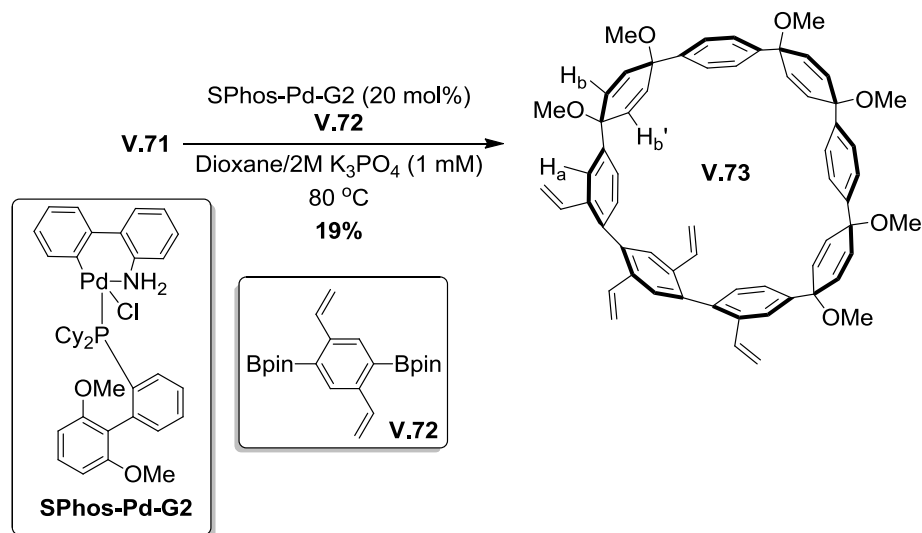
Scheme V.23. Macrocyclization towards tetravinyl macrocycle **V.73**.

Next, we subjected **V.73** to Grubbs 2nd generation catalyst (Grubbs II) in dichloromethane at 40 ^oC. Gratifyingly, **V.73** was cleanly converted to **V.74** in 76% yield in just 30 minutes without evidence of cyclohexadiene degradation or decomposition of the benzylic, doubly allylic methyl ethers (Scheme **V.24**). It seems reasonable that the styrenes react significantly faster than the electron-poor disubstituted cyclohexadiene olefins, though the reaction time can be prolonged to 5 hours without any observable byproducts or decomposition. Subjecting **V.74** to sodium naphthalenide at –78 ^oC afforded racemic aromatic belt fragment (3,10)-dibenzo[*a,h*]anthracene-nanohoop **V.61**. The MALDI-MS spectrum shows a single peak at *m/z* 656.74 (calculated mass: 656.81).

187
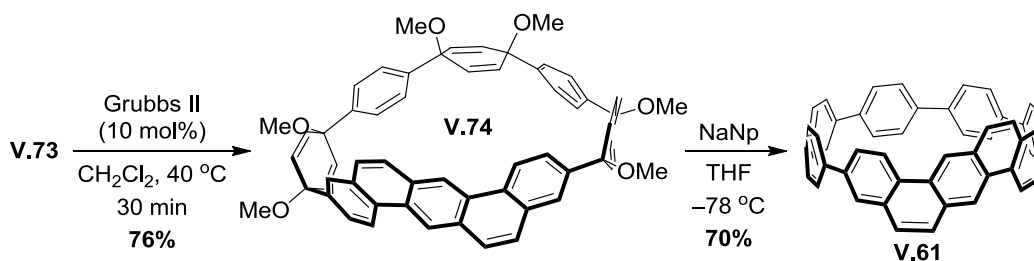
Scheme V.24. End game to synthesize (3,10)-dibenzo[*a,h*]anthracene-nanohoop **V.61**.

To test the limits of this RCM methodology, we aimed to incorporate a quaterphenyl unit into a 9-unit macrocycle. Biphenyl coupling partner **V.79** was envisioned as a precursor to (2,11)-dibenzo[*c,m*]pentaphene-nanohoop **V.62**. We began with benzylic bromination and two-fold olefination of easily accessible 1-bromo-4-chloro-*p*-xylene **V.75** to afford **V.76** in 80% yield. Miyuara borylation of a portion of the aryl bromide (**V.77**), followed by biphenyl formation by coupling **V.76** and **V.77**, and two-fold Miyuara borylation of the resulting aryl chloride **V.78** delivered **V.79** (Scheme **V.25**).
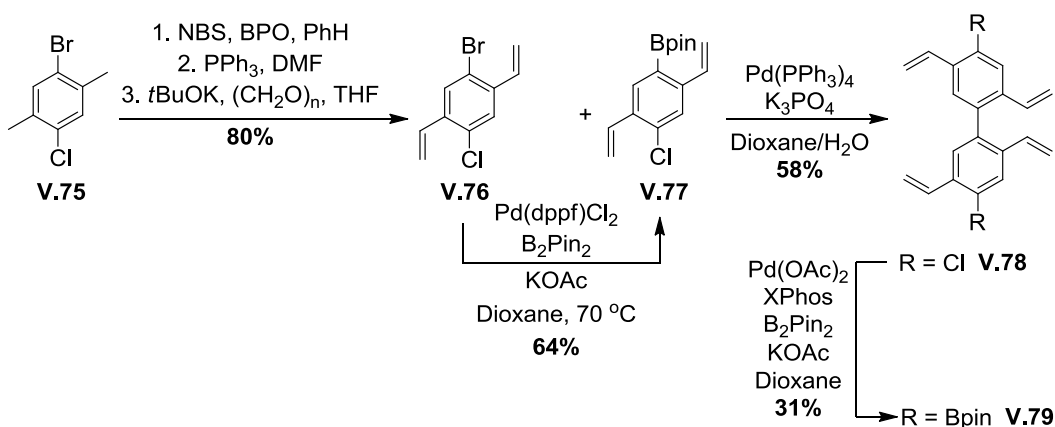
Scheme V.25. Synthesis of biphenyl coupling partner **V.79**.

We could form quaterphenyl-containing macrocycle **V.80** under similar conditions used to synthesize **V.73**, albeit with higher catalyst loadings, in 10% yield (Scheme **V.26**).[*] Like **V.73**, **V.80** also exhibits dynamic behavior in its ^{1}H NMR spectrum (Figure **V.17**). Interestingly, **V.80** has extremely broad resonances at 25 $^\text{o}$C, some of which begin to sharpen with increasing temperature. The differences in dynamic behavior between **V.73** and **V.80** will be discussed in Chapter **V.5.4.1**.
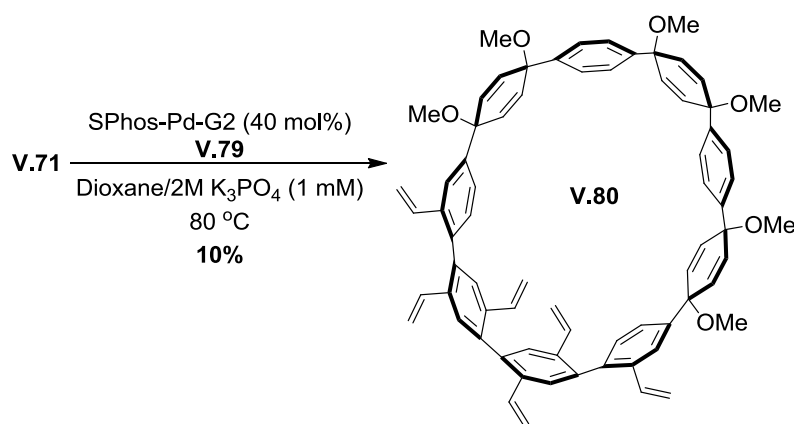
Scheme V.26. Synthesis of hexavinyl macrocycle **V.80**.

We continued by subjecting **V.80** to Grubbs II in dichloromethane at 40 $^\text{o}$C to afford **V.81** in 44% yield after 50 minutes. As was the case for tetravinyl macrocycle **V.73**, the rigidity of **V.81** lends itself to 4-bond coupling between cyclohexadiene protons, such as H_c/H_c'. Aromatization with sodium naphthalenide at -78 $^\text{o}$C delivered (2,11)-dibenzo[*c,m*]pentaphene-nanohoop **V.62** in 21% yield (Scheme **V.27**). The MALDI- spectrum shows a single distinct peak at *m/z* 756.89 (calculated mass: 756.28).

---

[*] We noticed some variability in the catalyst loadings needed to affect macrocyclization using **V.71**. Specifically, certain batches of **V.71** had small amounts of impurities that could not be seen by ^{1}H NMR spectroscopy or GPC. Hence, in some cases we had to increase the catalyst loading to obtain reasonable macrocyclization yields.

To our surprise, **V.62** represents only the second account of a dibenzo[*c,m*]pentaphene synthesis; the first account from Clar included only an electronic absorption spectrum, presumably due to the insolubility of the acyclic parent PAH.[47]
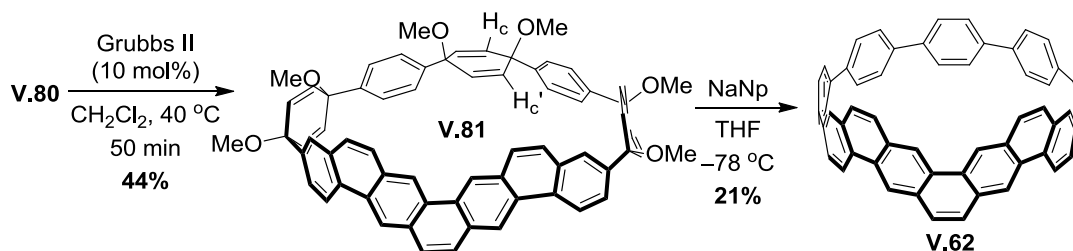
Scheme V.27. End game to synthesize (2,11)-dibenzo[*c,m*]pentaphenene-nanohoop **V.62**.

V.5.2. X-ray Crystallographic Analysis

We were able to obtain single crystals of **V.61** (slow evaporation from a THF/pentane solution, Figure **V.6**) and **V.62** (slow evaporation from a benzene/pentane solution, Figure **V.7**) suitable for X-ray diffraction. Unfortunately, since **V.61** crystallized as a racemate, the dibenzo[*a,h*]anthracene group was disordered over four positions, prohibiting us from extracting structural parameters. Like similarly sized [8]CPP, however, **V.61** packs in a herringbone fashion. In Chapter **V.6.5.**, Figure **V.12.** shows one possible orientation of the dibenzo[*a,h*]anthracene group, while Figure **V.10.** below shows all possible orientations for clarity.

190
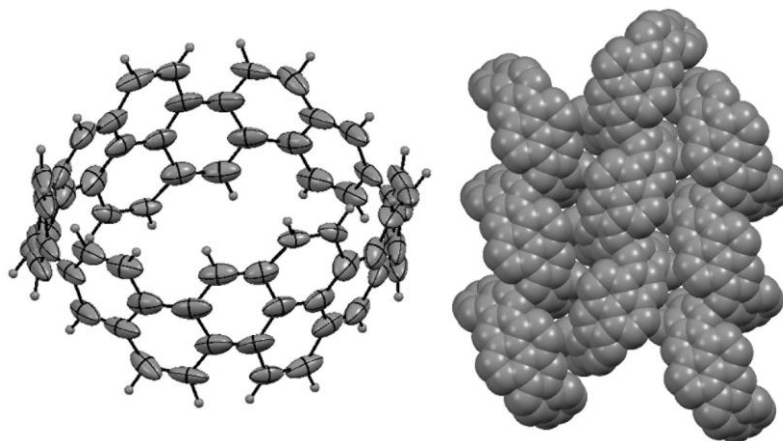
Figure V.6. ORTEP representation (thermal ellipsoids shown at 30% probability), left, and herringbone packing, right, for disordered **V.61**. All four possible orientations of the dibenzo[*a,h*]anthracene group are shown.

On the other hand, **V.62** crystallized with two symmetrically independent molecules in the asymmetric unit. The molecules form "head-to-tail" pairs, which further arrange into layers. From the crystallographic analysis of **V.62**, we determined that despite the incorporation of a large polycyclic aromatic hydrocarbon, some features were still shared between **V.62** and [9]CPP. For example, the average $C_{ipso} - C_{ipso}$ bond length between non-fused phenyl rings is 1.47 Å while the average torsional angle between the same rings is 31.5^o. As a comparison, while [9]CPP has exactly the same average C_{ipso}-C_{ipso} bond length as **V.62** in the solid state, its average torsional angle is significantly reduced to 24.4^o.[48] However, when considering all nine torsional angles in **V.62**, the incorporation of dibenzo[*c,m*]pentaphene causes a slight decrease in the overall average dihedral angle to 20.6^o. The implications of reducing the average dihedral angle upon ring fusion will be briefly discussed in Chapter **V.5.3**.

191
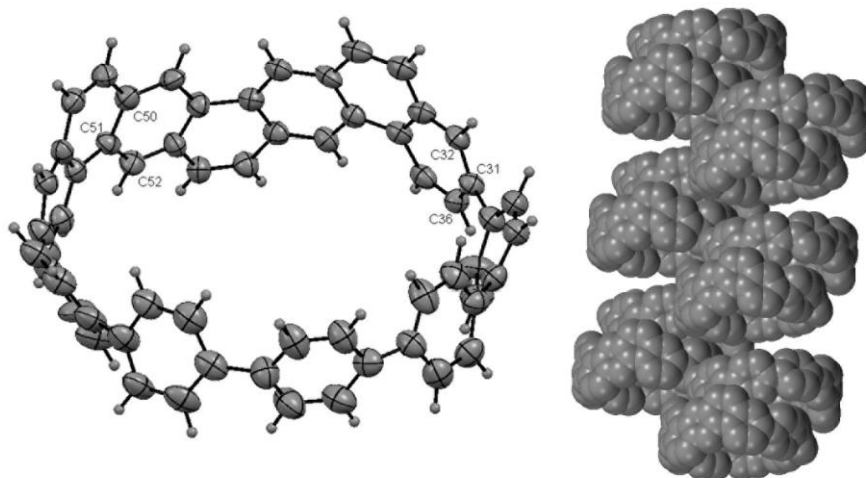
Figure V.7. ORTEP representation (thermal ellipsoids shown at 30% probability), left, and layered packing of "head-to-tail" pairs of nanohoops, right, for **V.62**.

With such a large PAH incorporated into a fully conjuaged cyclophane, we also wanted to evaluate the bending (θ)[38] of the dibenzo[*c,m*]pentaphene group in **V.62**. For a frame of reference, Bodwell's [8](2,11)teropyrenophane **V.63** is bent approximately 167° out of plane.[40] A similar measurement on **V.62**, by determining the angle (θ) between the plane formed by C(57)-C(58)-C(59) and the plane formed by C(31)-C(32)-C(36) revealed that our annulated quaterphenyl was bent by approximately 134°. This is not surprising, due to the shorter cyclophane tether of **V.63** compared to **V.62**. Interestingly, a comparison of the same angle, θ, for the DFT minimized geometry of **V.62** reveals that its dibenzo[*c,m*]pentaphene unit is approximately 34° less distorted from planarity (Scheme **V.28**). From these structural data, it is apparent that we are slowly increasing the degree of dibenzo[*c,m*]pentaphene bending, thus gradually building in the necessary strain to transform **V.81** to **V.62**.

192
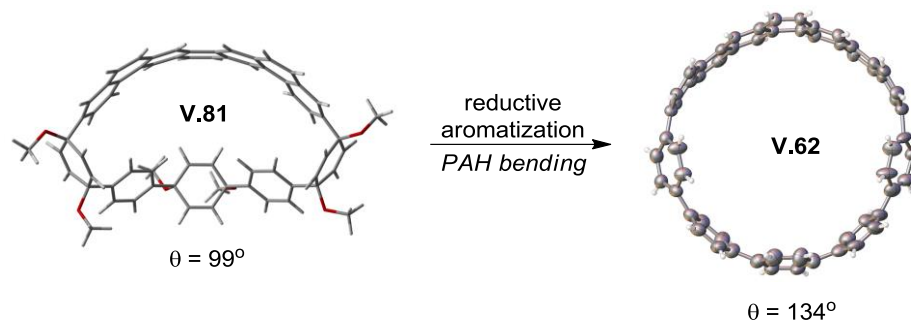
Scheme V.28. Increased PAH bending is predicted to occur from **V.81** (DFT B3LYP/6-31G(d)) to **V.62** (crystal structure) upon reductive aromatization.

V.5.3. Optoelectronic Properties

To investigate the photophysical properties of **V.61** and **V.62**, we obtained their

UV/vis and fluorescence spectra in dichloromethane (Figures **V.8** and **V.9**). Compared to

[8]CPP, **V.61** has a very broad spectrum (λ_{max} = 325 nm) with an additional feature at

350 nm and a weak shoulder around 400 nm representing the HOMO $\rightarrow$ LUMO

transition. Using TD-DFT calculations, we assigned the major transitions (Table **V.3**) to

linear combinations of a variety of orbitals ranging from HOMO $-$ 4 to LUMO $+$ 4. For

V.62, the UV/vis spectrum was reminiscent of the spectrum seen for [9]CPP. Despite

being extremely broad like the spectrum for **V.61**, there is a major absorption at 340 nm.

In addition, there is also an additional feature at 355 nm and a weak shoulder around 400

nm (HOMO $\rightarrow$ LUMO transition). In both **V.61** and **V.62**, the maximum of the HOMO

$\rightarrow$ LUMO transition appears to red-shift slightly compared to those of [8]CPP and

[9]CPP, respectively. Insofar as we have investigated with solid-state analyses of **V.62**

and [9]CPP, the decrease in average dihedral angle by almost 4° upon nearly planarizing

193

four adjacent phenyl rings could be responsible for this (Table **V.9**). This theory would be consistent with the red-shift observed for the HOMO-LUMO maximum absorbance in the [*n*]CPP family with decreasing values of *n*, and therefore decreased torsional angles. Again, we investigated the origin of the major transitions in the context of frontier molecular orbitals with TD-DFT calculations (Table **V.4**).
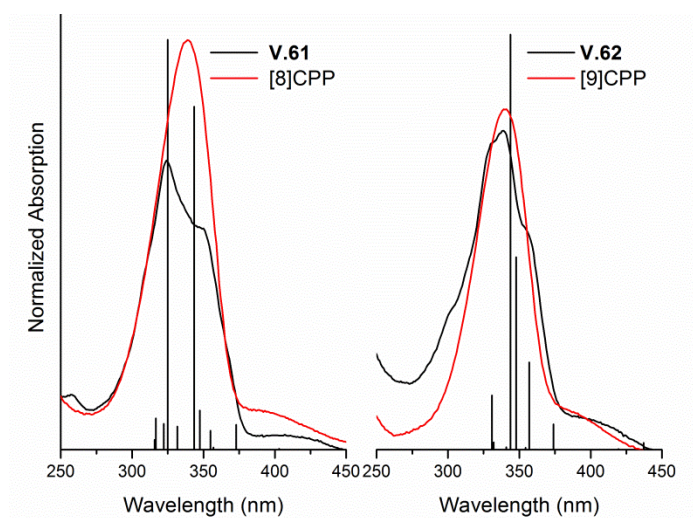
Figure V.8. UV/vis absorption spectra for **V.61**/[8]CPP and **V.62**/[9]CPP. Vertical lines represent TD-DFT transitions (DFT B3LYP/6-31G(d)).

Upon excitation at 340 nm, **V.61** fluoresces at 535 nm ($\Phi = 14\pm5\%$) and **V.62** fluoresces at 500 nm ($\Phi = 15\pm5\%$) (Figure **V.8**). These values are fairly consistent with our measured values for similarly sized [8]CPP ($\lambda_{fl} = 535$ nm, $\Phi = 15\pm5\%$) and [9]CPP ($\lambda_{fl} = 500$ nm, $\Phi = 33\pm5\%$), as well as values reported in the literature.[49-50]
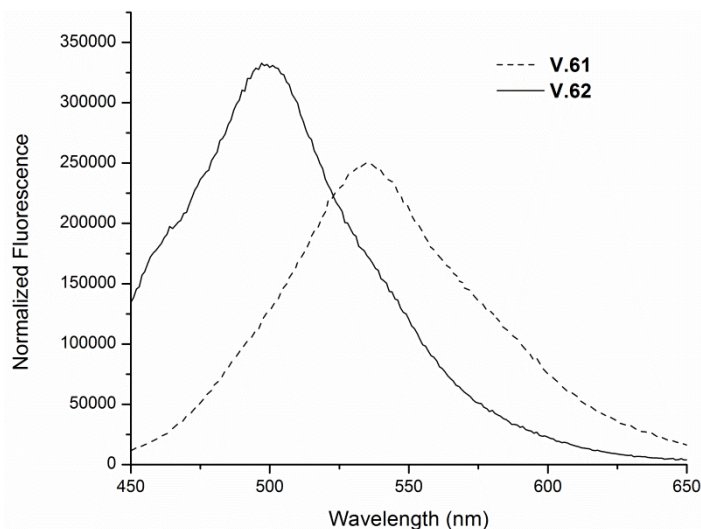
Figure V.9. Fluorescence spectra of **V.61** and **V.62** with excitation at 340 nm.

Unlike [8]- and [9]CPP, which are centrosymmetric molecules, **V.61** and **V.62** have slight dipoles directed away from the PAH units. This is evident in the asymmetric distribution of orbital density in the lower lying occupied orbitals and the higher lying unoccupied orbitals (Figure **V.9**), and may be partly responsible for the broad absorption spectra of these two nanohoops. The calculated HOMO-LUMO levels for **V.61** and **V.62** are very similar to those of closely sized [8]CPP (−1.79 eV / −5.02 eV; HOMO/LUMO gap = 3.23 eV) and [9]CPP (−1.72 eV / −5.12 eV; HOMO/LUMO gap = 3.40 eV), respectively. Importantly, these values indicate that we are not significantly changing the electronic structure, and therefore the potential stability, to any appreciable degree upon ring formation. In these two FMO diagrams, the PAH group is situated at the bottom of each nanohoop, while the phenylene chain is on the top.
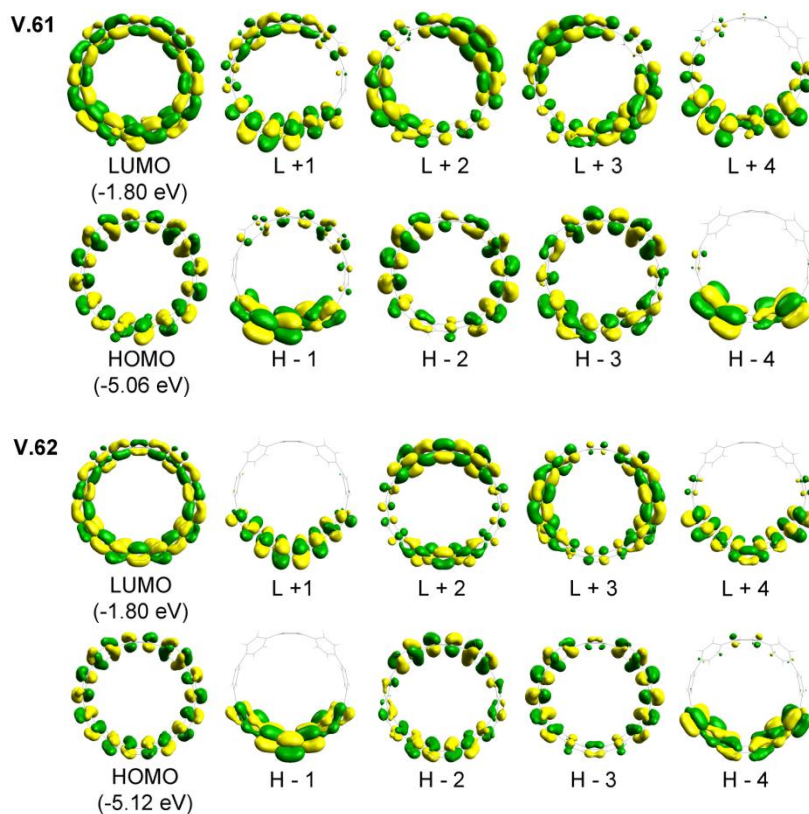
Figure V.10. FMO diagrams[51] for **V.61** (H/L gap = 3.26 eV; top two rows) and **V.62** (H/L gap = 3.32 eV; bottom two rows) (B3LYP/6-31G(d)). H = HOMO, L = LUMO.

V.5.4. DFT Analysis

V.5.4.1. Atropisomers of Vinylated Macrocycles

In order to study the dynamic behavior observed in the ^{1}H NMR spectra of **V.73** and **V.80**, we probed the energies of the macrocycles' various conformations computationally at the RB97D/6-31G(d) level of theory. Upon comparing the ground-state energies of the various atropisomers that **V.73** can adopt, we found that **V.73** has a single, low-lying ground-state conformation that is 1.73 kcal/mol more stable than the next highest energy conformation. Between the lowest energy conformation and the seven other possible conformations, the energy difference between ground-state energies is 1.73 − 5.10 kcal/mol (Table **V.5**). On the other, **V.80** has numerous ground-state

conformations that are close in energy (Table **V.6**). Approximately one-third of the atropisomers are within 1.5 kcal/mol of the lowest-energy conformation, while the highest energy atropisomer is only 3.43 kcal/mol higher in energy. Although we have not investigated the relative transition states between these interconversions within the two molecules, the computational results seem consistent with our VT-NMR experiments. That is, the more disperse ground-states of **V.73** leads to a single major conformation at room temperature and a sharp ^{1}H NMR spectrum. In the case of **V.80**, many closely spaced ground-states of lead to numerous conformations, leading to broadening in the ^{1}H NMR spectrum at room temperature. Based on our experimental RCM data, the varying rigidity of the vinylated macrocycles (i.e. **V.73** and **V.80**) does not seem to influence the outcome of these particular reactions.

V.5.4.2. Strain Analysis

With both final compounds **V.61** and **V.62** in hand, we evaluated their strain energy (at the ωB97x-D level of theory) and compared the values to similarly sized [*n*]CPPs (Chapter **V.6.4.2**). **V.61** has only 79 kcal/mol of strain energy (Scheme **V.31**), while **V.62** has 71 kcal/mol of strain energy (Scheme **V.34**). Interestingly, these values are only 6-7 kcal/mol higher than their [8]- and [9]CPP analogs which have 72 kcal/mol and 66 kcal/mol of strain energy, respectively.[52] More importantly, RCM has shown to complement our already powerful strain-building Suzuki-Miyuara macrocyclization and sodium naphthalenide promoted reductive aromatization methodologies. For example, RCM builds in roughly 24 kcal/mol and 14 kcal/mol of strain energy in the syntheses of **V.74** (Scheme **V.29** and **V.30**) and **V.81** (Scheme **V.32** and **V.33**), respectively. These values amount to approximately 20 – 30% of the total strain energy in final targets **V.61**

and **V.62**, providing a proof of principle that our RCM methodology allows for a gradual increase in strain energy over the course of multiple transformations. As ring formation does not seem to dramatically affect the overall strain energy of **V.61** and **V.62**, reductive aromatization of elaborate macrocycle **V.82** (Figure **V.11**) should be feasible so long as an appropriately vinylated macrocycle can be accessed (Scheme **V.7**, *vide supra*).
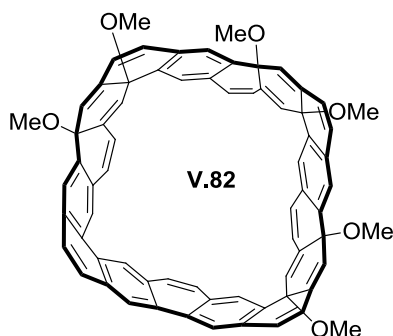
Figure V.11. A potential macrocyclic precursor to [8]cyclophenacene.

V.6. Experimental

V.6.1. General Experimental Considerations

All glassware was oven (140 $^{\circ}$C) or flame dried and cooled under an inert atmosphere of nitrogen unless otherwise noted. Moisture sensitive reactions were carried out under an inert atmosphere of nitrogen using standard syringe/septa technique. Tetrahydrofuran, dichloromethane, 1,4-dioxane, and dimethylformamide were dried by filtration through alumina according to the methods described by Grubbs (JC Meyer).[53] Silica column chromatography was conducted with Zeochem Zeoprep 60 Eco 40-63 µm silica gel. Thin Layer Chromatography (TLC) was performed using Sorbent Technologies Silica Gel XHT TLC plates. Developed plates were visualized using UV light at wavelengths of 254 and 365 nm or by staining with iodine vapor. ^{1}H NMR

spectra were recorded at 600MHz on a Bruker Avance-III, 500 MHz on a Bruker Avance-III, 500 MHz on a Varian VNMRS, 500 MHz on a Varian INOVA, 400 MHz on a Varian VNMRS, or 300 MHz on a Varian INOVA. ^{13}C NMR spectra were recorded at 150 MHz on a Bruker Avance-III, 125 MHz on a Bruker Avance-III, 125 MHz on a Varian VNMRS, 125 MHz on a Varian INOVA, or 100 MHz on a Varian VNMRS. All ^{1}H NMR spectra were taken in CDCl$_3$ (referenced to TMS, δ 0.00 ppm), benzene-*d$_6$* (referenced to residual C$_6$H$_6$, δ 7.16 ppm), acetone-*d$_6$* (referenced to residual acetone, δ 2.05 ppm), or DMSO-*d$_6$* (referenced to residual DMSO, δ 2.50 ppm). All ^{13}C NMR spectra were taken in CDCl$_3$ (referenced to chloroform, δ 77.16 ppm), benzene-*d$_6$* (referenced to benzene, δ 128.06 ppm), acetone-*d$_6$* (referenced to residual acetone, δ 29.84 ppm) or DMSO-*d$_6$* (referenced to DMSO, δ 39.52 ppm). The MALDI matrix, *trans*-2-[3-(4-tert-butylphenyl)-2-methyl-2-propenylidene]malononitrile (DCTB), was obtained from Sigma-Aldrich, and was used as a solution in CH$_2$Cl$_2$. IR spectra were recorded on a Thermo Nicolet 6700 FT-IR. Absorbance and fluorescence spectra were obtained in a 1 cm Quartz cuvette with dichloromethane using a Varian Cary 60 UV-vis spectrometer and a Horiba Jobin Yvon Fluoromax 3 Fluorimeter. Quantum yields were determined using an integrating sphere accessory. Recycling gel permeation chromatography (GPC) was performed using a Japan Analytical Industry LC-9101 with two JIAGEL-2H columns in series. Automated flash chromatography was performed using a Biotage Isolera. NBS was recrystallized from water and dried under high vacuum before use. All reagents were obtained commercially unless otherwise noted.

V.6.2. Synthetic Details

V.32
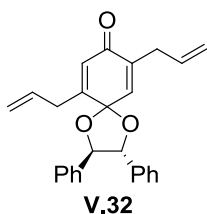
(2R,3R)-6,9-diallyl-2,3-diphenyl-1,4-dioxaspiro[4.5]deca-6,9-dien-8-one **V.32**. To a

solution of **II.14** (0.20 g, 0.85 mmol, 1.0 equiv) and (+)-1,2-diphenylethanediol **V.31**

(0.24 g, 1.1 mmol, 1.3 equiv) in anhydrous THF (2.5 mL) at 0 °C was added freshly

distilled BF_3-Et_2O (0.12 g, 0.10 mL, 0.81 mmol, 0.95 equiv). The resulting red solution

was stirred for 3.5 h before quenching with sat. aq $NaHCO_3$ (2 mL) and extracting with

EtOAc (2 x 5 mL). The combined organics were washed with brine (5 mL), dried over

sodium sulfate, and concentrated on Celite. Purification on silica gel (0 – 5%

EtOAc/hexanes) afforded **V.32** (0.18 g, 54%). ^{1}H NMR (500 MHz, Acetone-d_6) δ(ppm)

7.47 – 7.30 (overlap, 10H), 7.14 (br s, 1H), 6.09 (d, *J* = 1.8 Hz, 2H), 6.09 – 5.89 (overlap,

2H), 5.40 – 5.24 (overlap, 3H), 5.21 – 5.07 (m, 3H), 3.51 (dd, *J* = 17.8, 7.0 Hz, 1H), 3.44

(dd, *J* = 17.8, 7.0 Hz, 1H), 3.11 (dd, *J* = 6.6, 1.5 Hz, 3H); ^{13}C NMR (125 MHz, Acetone-

d_6) δ(ppm) 205.25, 184.36, 157.11, 139.63, 136.29, 136.20, 135.14, 134.91, 133.77,

128.93, 128.64, 128.51, 127.23, 127.08, 127.05, 118.24, 116.39, 100.60, 86.55, 85.45,

33.42, 32.37.

V.33
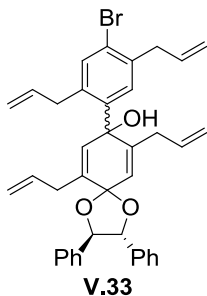
(2R,3R)-6,9-diallyl-8-(2,5-diallyl-4-bromophenyl)-2,3-diphenyl-1,4-dioxaspiro[4.5]deca-6,9-dien-8-ol **V.33**. To a slurry of **V.32** (0.15 g, 0.48 mmol, 1.2 equiv) in anhydrous THF (4 mL) at −78 °C was added *n*BuLi (0.20 mL, 0.48 mmol, 1.2 equiv, 2.4 M in hexanes) dropwise. The aryl lithium reagent was stirred for 5 min before adding **V.32** (0.15 g, 0.40 mmol, 1.0 equiv) in anhydrous THF (2 mL) dropwise via cannula. After stirring for 15 min, the reaction was quenched by the addition of water (5 mL) and the biphasic mixture was extracted with EtOAc (2 x 10 mL). The combined organics were washed with brine (5 mL), dried over sodium sulfate, and concentrated on Celite. Purification on silica gel (0 – 10% EtOAc/hexanes) afforded **V.32** as a white foam (0.20 g, 81%, dr = 1:1). The diastereomeric mixture could not be separate despite exhaustive attempts by silica gel chromatography. The excellent solubility of **V.32** prevented separation by crystallization.
^{1}H NMR (500 MHz, C$_6$D$_6$) δ(ppm) 8.06 (s, 2H), 7.46 (d, J = 15.9 Hz , 2H), 7.35 - 7.02 (overlap, 20H), 6.29 (s, 2H), 6.25 (s, 2H), 6.03 – 5.71 (overlap, 8H), 5.15 (d, J = 17.0 Hz, 2H), 5.12 – 4.86 (m, 16H), 3.59 – 3.22 (overlap, 12H), 3.06 – 2.90 (m, 2H), 2.56 (dt, J = 16.6, 7.7 Hz, 2H); ^{13}C NMR (125 MHz, C$_6$D$_6$) δ(ppm) 144.12, 143.91, 138.59, 137.52, 137.38, 135.90, 135.77, 135.71, 135.24, 135.19, 135.17, 134.40, 134.28, 129.29, 128.50, 128.46, 128.41, 128.38, 128.25, 128.14, 126.90, 126.83, 126.54, 126.42, 124.25, 124.20, 123.98, 117.37, 116.14, 116.11, 115.50, 115.40, 102.42, 102.31, 86.55, 85.41, 85.32, 40.07, 34.96, 34.90, 33.51, 33.46.

Br
||
Cl
V.34
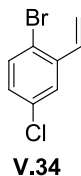
1-bromo-4-chloro-2-vinylbenzene **V.34**. To a solution of 1-bromo-2-(bromomethyl)-4-chlorobenzene[54] (6.2 g, 22 mmol, 1.0 equiv) in toluene (30 mL) was added triphenylphosphine (7.4 g, 28 mmol, 1.3 equiv). The reaction mixture was heated at reflux for 16 h then cooled to rt. The resulting white precipitate was filtered under vacuum, washed with toluene (50 mL) and hexanes (50 mL) then dried under high vacuum. The white phosphonium salt (8.3 g) was used without further purification. To a dry 250 mL RBF was added the phosphonium salt (7.0 g, 13 mmol, 1.0 equiv) and *p*-formaldehyde (9.6 g, 320 mmol, 25 equiv). The solids were suspended in anhydrous THF and the suspension was cooled to 0 ^{o}C. Potassium *tert*-butoxide (41 mL, 21 mmol, 1.6 equiv, 0.50 M in THF) was added via cannula and the reaction was allowed to warm to rt over 30 min. The reaction mixture was filtered through a short plug of Celite (petroleum ether) and the filtrate was concentrated under vacuum. Purification on a short plug of silica gel (petroleum ether) afforded **V.34** (2.2 g, 48%). ^{1}H NMR (400 MHz, CDCl$_3$) δ(ppm) 7.51 (d, *J* = 2.6 Hz, 1H), 7.46 (d, *J* = 8.5 Hz, 1H), 7.09 (dd, *J* = 8.5, 2.6 Hz, 1H), 6.97 (dd, *J* = 17.4, 11.0 Hz, 1H), 5.71 (dd, *J* = 17.4, 0.7 Hz, 1H), 5.41 (dd, *J* = 11.0, 0.7 Hz, 1H); ^{13}C NMR (100 MHz, CDCl$_3$) δ(ppm) 139.10, 134.99, 134.97, 134.04, 133.71, 129.13, 126.85, 121.45, 118.10, 118.07.
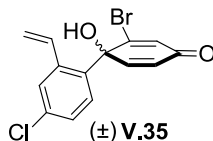
(±)-2-bromo-4'-chloro-1-hydroxy-2'-vinyl-[1,1'-biphenyl]-4(1H)-one **V.35**. To a solution

of *1-bromo-4-chloro-2-vinylbenzene* **V.34** (0.16 g, 0.72 mmol, 1.1 equiv) in anhydrous

Et_2O (8 mL) at −78 $^{\circ}$C was added *t*BuLi (0.97 mL, 1.5 mmol, 2.2 equiv, 1.5 M in

pentane). The resulting yellow solution was stirred for 20 min then 2-bromo-4,4-

dimethoxycyclohexa-2,5-dienone **IV.3** (0.15 g, 0.65 mmol, 1.0 equiv) in anhydrous Et_2O

(2 mL). The reaction mixture was stirred for 2 h then was quenched with 1 M aq HCl (3

mL). The biphasic mixture was stirred rapidly and was allowed to warm to rt for 25 min.

The layers were separated and the aqueous phase was extracted with EtOAc (2 x 10 mL).

The combined organics were washed with sat. aq $NaHCO_3$ (10 mL), water (10 mL), and

brine (10 mL), then dried over sodium sulfate and concentrated onto Celite. Purification

on silica gel (20% EtOAc/hexanes) afforded **V.35** as a white solid (0.10 g, 47%). NOTE:

Attempts to perform lithium halogen exchange on **V.34** in THF with *n*BuLi or *t*BuLi, or

with *n*BuLi in Et_2O lead to decomposition, presumably via an anionic polymerization

pathway. ^{1}H NMR (400 MHz, DMSO-d$_6$) δ(ppm) 7.79 (d, *J* = 8.4 Hz, 1H), 7.48 − 7.42

(overlap, 2H), 7.06 (s, 1H), 6.99 (d, *J* = 9.9 Hz, 1H), 6.81 (d, *J* = 1.7 Hz, 1H), 6.85 − 6.69

(overlap, 1H), 6.27 (dd, *J* = 9.9, 1.7 Hz, 1H), 5.61 (d, *J* = 17.2 Hz, 1H), 5.23 (d, *J* = 11.0

Hz, 1H); ^{13}C NMR (100 MHz, DMSO-d$_6$) δ(ppm) 183.86, 152.55, 150.93, 138.30,

135.30, 133.84, 133.06, 132.32, 129.38, 128.25, 127.39, 125.84, 119.18, 72.20.

MeO   Br   OMe

Cl   Cl

(±) **V.36**
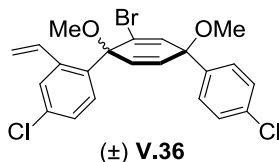
(±)-syn-2'-bromo-4,4''-dichloro-1',4'-dimethoxy-2-vinyl-1',4'-dihydro-1,1':4',1''-terphenyl

V.36. A solution of *(±)-2-bromo-4'-chloro-1-hydroxy-2'-vinyl-[1,1'-biphenyl]-4(1H)-one*

V.35 (0.11 g, 0.34 mmol, 1.0 equiv) in anhydrous THF (5 mL) was added to a slurry of

sodium hydride (68 mg, 1.7 mmol, 5 equiv, 60% suspension in mineral oil) in anhydrous

THF (15 mL) at –78 ^{o}C. Meanwhile, a solution of 1-bromo-4-chlorobenzene in

anhydrous THF (10 mL) was cooled to –78 ^{o}C and *n*BuLi (0.39 mL, 0.99 mmol, 2.9

equiv, 2.5 M in hexanes) was added dropwise. The resulting aryl lithium solution was

allowed to stir for 20 min before quickly transferring it via cannula to the slurry of

sodium hydride and **V.35**. The final reaction mixture was stirred for 1 h 15 min before

quenching with water (5 mL) and warming to rt. The reaction mixture was diluted with

EtOAc (20 mL) and the layers were separated. The aqueous phase was extracted with

EtOAc (2 x 20 mL) and the combined organics were washed with brine (10 mL), dried

over sodium sulfate, and concentrated onto Celite. Purification on silica gel (hexanes then

20 – 30% EtOAc/hexanes) afforded semi-pure diol that was used without further

purification. The semi-pure diol was dissolved in anhydrous THF (5 mL) and transferred

via cannula to a slurry of sodium hydride (0.10 g, 2.5 mmol, 10 equiv, 60% suspension in

mineral oil) in anhydrous THF (15 mL) at 0 ^{o}C. The tan suspension was stirred for 20

min then MeI (0.36 g, 0.16 mL, 2.5 mmol, 10 equiv) was added via syringe and the

reaction mixture was allowed to warm to rt for 16 h. The reaction was quenched by the

addition of water (10 mL) and the mixture was extracted with EtOAc (3 x 15 mL). The

combined organics were washed with brine (10 mL), dried over sodium sulfate and concentrated onto Celite. Purification on silica gel (hexanes then 15% EtOAc/hexanes) afforded **V.36** as a white foam (0.10 g, 63%). ^{1}H NMR (300 MHz, CDCl$_3$) δ(ppm) 7.50 (dd, J = 17.4, 10.9 Hz, 1H), 7.47 (d, J = 2.1 Hz, 1H), 7.34 – 7.19 (overlap, 4H), 7.16 (dd, J = 8.6, 2.1 Hz, 1H), 7.11 (d, J = 8.6 Hz, 1H), 6.67 (d, J = 2.3 Hz, 1H), 6.38 (d, J = 10.2 Hz, 1H), 6.01 (dd, J = 10.2, 2.3 Hz, 1H), 5.51 (dd, J = 17.4, 1.4 Hz, 1H), 5.24 (dd, J = 10.9, 1.4 Hz, 1H), 3.43 (s, 3H), 3.41 (s, 3H).

(±) **V.38**
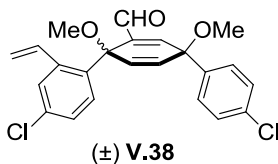
(±)-syn-4,4''-dichloro-1',4'-dimethoxy-2-vinyl-1',4'-dihydro-[1,1':4',1''-terphenyl]-2'-carbaldehyde **V.38**. To a solution of **V.36** (0.12 g, 0.26 mmol, 1.0 equiv) in anhydrous THF (3 mL) at −78 °C was added *n*BuLi (0.16 mL, 0.39 mmol, 1.5 equiv, 2.5 M in hexanes). The brown solution was stirred for 20 min then anhydrous DMF (95 mg, 0.10 mL, 1.3 mmol, 5.0 equiv) was added and the reaction was stirred an additional 30 min. The reaction was quenched by the addition of sat. aq NH$_4$Cl (2 mL) and then warmed to rt. The reaction mixture was extracted with EtOAc (3 x 10 mL) and the combined organics were washed with brine (10 mL), dried over sodium sulfate, and concentrated onto Celite. Purification on silica gel (hexanes then 10% EtOAc/hexanes) afforded **V.38** as a colorless oil (28 mg, 26%, dr = 13:1). Major diastereomer: ^{1}H NMR (400 MHz, CDCl$_3$) δ(ppm) 9.54 (s, 1H), 7.52 (dd, J = 17.4, 10.9 Hz, 1H), 7.50 (d, J = 2.3 Hz, 1H), 7.32 – 7.19 (m, 4H), 7.16 (d, J = 2.5 Hz, 1H), 7.08 (dd, J = 8.5, 2.3 Hz, 1H), 6.79 (d, J =

8.5 Hz, 1H), 6.43 (d, *J* = 10.2 Hz, 1H), 6.06 (dd, *J* = 10.2, 2.5 Hz, 1H), 5.54 (dd, *J* = 17.4, 1.4 Hz, 1H), 5.27 (dd, *J* = 10.9, 1.4 Hz, 1H), 3.40 (s, 3H), 3.33 (s, 3H).

(±) **V.39**
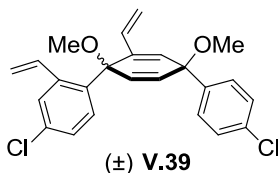
(±)-syn-4,4''-dichloro-1',4'-dimethoxy-2,2'-divinyl-1',4'-dihydro-1,1':4',1''-terphenyl **V.39**.

To a suspension of methyltriphenylphosphonium bromide (0.16 g, 0.45 mmol, 2.2 equiv) in anhydrous THF (5 mL) at 0 °C was added *n*BuLi (0.17 mL, 0.17 mmol, 2.1 equiv, 2.5 M in hexanes). The resulting bright yellow ylide was stirred for 20 min whereupon a solution of **V.38** (85 mg, 0.20 mmol, 1.0 equiv) in anhydrous THF (3 mL) was added via cannula. After warming to rt over 40 min, the reaction mixture was quenched with water (5 mL) and extracted with EtOAc (3 x 10 mL). The combined organics were washed with brine (5 mL), dried over sodium sulfate, and concentrated onto Celite. Purification on silica gel (5% EtOAc/hexanes) afforded **V.39** as an oily colorless solid (50 mg, 60%, dr = 13:1). Major Diastereomer: ^{1}H NMR (400 MHz, CDCl$_3$) δ(ppm) 7.63 (dd, *J* = 17.4, 11.0 Hz, 1H), 7.47 (d, *J* = 2.4 Hz, 1H), 7.30 − 7.17 (m, 9H), 7.04 (dd, *J* = 8.6, 2.4 Hz, 1H), 6.91 (d, *J* = 8.6 Hz, 1H), 6.35 (d, *J* = 10.2 Hz, 1H), 6.27 (d, *J* = 2.5 Hz, 1H), 6.20 (dd, *J* = 17.6, 11.2 Hz, 1H), 5.94 (dd, *J* = 10.2, 2.5 Hz, 1H), 5.48 (overlap, 2H), 5.24 (dd, *J* = 11.0, 1.4 Hz, 1H), 5.11 (dd, *J* = 11.2, 1.4 Hz, 1H), 3.38 (s, 3H), 3.30 (s, 3H).

V.41
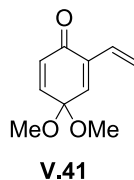
4,4-dimethoxy-2-vinylcyclohexa-2,5-dienone **V.41**. To a methanolic solution (100 mL) of 4-methoxy-2-vinylphenol[55] (3.9 g, 26 mmol, 1 equiv) at 0 °C was added PhI(OAc)$_2$ (10 g, 31 mmol, 1.2 equiv) portionwise over 90 min. The reaction mixture was allowed to warm to rt over 45 min and was quenched with sat. aq NaHCO$_3$ (30 mL) and extracted with MTBE (3 x 40 mL). The combined organics were washed with brine (30 mL), dried over sodium sulfate, and concentrated onto Celite. Purification on silica gel (0 − 15% EtOAc/hexanes w/ ca. 1% Et$_3$N) afforded **V.41** as a yellow oil (1.8 g, 38%). ^{1}H NMR (400 MHz, CDCl$_3$) δ(ppm) 6.84 − 6.79 (overlap, 2H), 6.61 (ddd, *J* = 17.7, 11.2, 0.8 Hz, 1H), 6.29 (d, *J* = 10.2 Hz, 0H), 5.85 (dd, *J* = 17.7, 1.4 Hz, 1H), 5.36 (dd, *J* = 11.2, 1.4 Hz, 1H), 3.39 (s, 6H); ^{13}C NMR (100 MHz, CDCl$_3$) δ(ppm) 184.62, 142.60, 142.58, 136.95, 136.55, 130.41, 129.78, 129.76, 118.95, 118.94, 93.22, 77.48, 77.16, 76.84, 50.50, 50.49.

(±) **V.42**
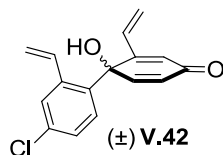
(±)-4'-chloro-1-hydroxy-2,2'-divinyl-[1,1'-biphenyl]-4(1H)-one **V.42**. To a solution of **V.42** (0.39 g, 1.8 mmol, 1.1 equiv) in anhydrous Et$_2$O (18 mL) at −78 °C was added *t*BuLi (2.4 mL, 3.6 mmol, 2.1 equiv, 1.5 M in pentane) over 20 minutes. A solution of **V.41** (0.31 g, 1.7 mmol, 1.0 equiv) in anhydrous Et$_2$O (5 mL) was added via cannula to the orange solution of aryl lithium. The resulting pale yellow solution was stirred for 1 h

then quenched with 1 M aq HCl (15 mL). The reaction mixture was extracted with EtOAc (3 x 20 mL) and the combined organics were washed with sat. aq $NaHCO_3$ (20 mL), water (20 mL), brine (20 mL), dried over sodium sulfate, and concentrated onto Celite. Purification on silica gel (25 – 30% EtOAc/hexanes) afforded **V.42** as an off-white solid (0.21 g, 45%). ^{1}H NMR (400 MHz, Chloroform-d) δ(ppm) 7.82 (br d, J = 8.5 Hz, 1H), 7.39 – 7.30 (overlap, 2H), 6.81 – 6.69 (overlap, 1H), 6.76 (d, J = 9.9 Hz, 1H), 6.37 (d, J = 1.1 Hz, 1H), 6.24 – 6.10 (overlap, 2H), 5.68 (dd, J = 17.7, 0.9 Hz, 2H), 5.41 (dd, J = 17.2, 1.2 Hz, 2H), 5.36 (dd, J = 11.1, 0.9 Hz, 2H), 5.17 (d, J = 10.9 Hz, 1H), 3.34 (s, 1H); ^{13}C NMR (100 MHz, CDCl$_3$) δ(ppm) 186.77, 157.52, 149.71, 138.61, 134.53, 133.94, 133.74, 132.69, 128.18, 128.15, 127.84, 126.42, 124.29, 122.80, 118.20, 70.88.

V.43
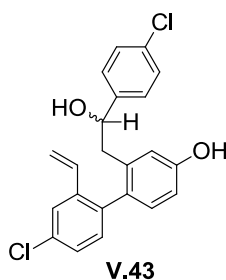
4'-chloro-2-(2-(4-chlorophenyl)-2-hydroxyethyl)-2'-vinyl-[1,1'-biphenyl]-4-ol **V.43**. To a slurry of sodium hydride (73 mg, 1.8 mmol, 2.5 equiv, 60% suspension in mineral oil) in anhydrous Et$_2$O (18 mL) at −78 ^{o}C was added **V.42** (0.20 g, 0.73 mmol, 1.0 equiv) in anhydrous Et$_2$O (10 mL) via cannula. The resulting slurry was stirred for 1 h. Meanwhile, a solution of 1-bromo-4-chlorobenzene (0.42 g, 2.2 mmol, 3.0 equiv) in anhydrous Et$_2$O was cooled to −78 ^{o}C whereupon tBuLi (2.9 mL, 4.4 mmol, 6.0 equiv, 1.5 M in pentane) was added dropwise. The aryl lithium solution was stirred for 20 min before transferring

it to the slurry of sodium hydride and **V.42** via cannula. The final reaction mixture was stirred for 90 min before quenching with water (10 mL) and warming to rt. The reaction mixture was extracted with EtOAc (3 x 20 mL) and the combined organics were washed with brine (10 mL), dried over sodium sulfate, and concentrated onto Celite. Purification on silica gel (DCM then 0 – 20% EtOAc/DCM) afforded the undesired 1,4 addition byproduct **V.43** as a white solid after crystallization from cold DCM (70 mg, 25%). The more polar desired 1,2 addition product could not be completely purified. ^{1}H NMR (400 MHz, DMSO-d$_6$) δ(ppm) 11.47 (s, 1H), 7.90 (br, 1H), 7.44 (d, J = 8.8 Hz, 1H), 7.38 (d, J = 2.4 Hz, 1H), 7.30 (d, J = 8.4 Hz, 1H), 7.15 (d, J = 8.4 Hz, 2H), 6.91 (br, 1H), 6.82 – 6.63 (overlap, 2H), 6.25 (d, J = 2.0 Hz, 1H), 6.15 (dd, J = 9.9, 2.0 Hz, 1H), 5.48 (d, J = 17.4 Hz, 1H), 5.11 (d, J = 11.1 Hz, 1H), 4.16 (d, J = 9.0 Hz, 1H), 3.34 – 3.22 (overlap, 1H), 2.66 (dd, J = 14.9, 9.0 Hz, 1H).

(±) **V.44**
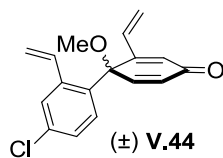
(±)-4'-chloro-1-methoxy-2,2'-divinyl-[1,1'-biphenyl]-4(1H)-one **V.44**. To a solution of *1-bromo-4-chloro-2-vinylbenzene* **V.34** (0.18 g, 0.82 mmol, 1.1 equiv) in anhydrous Et$_2$O (8 mL) at −78 ^{o}C was added *t*BuLi (1.1 mL, 1.6 mmol, 2.1 equiv, 1.5 M in pentane) dropwise. A solution of **V.41** (0.31 g, 1.7 mmol, 1.0 equiv) in anhydrous Et$_2$O (5 mL) was added slowly via cannula to the orange solution of aryl lithium after 5 min. The resulting pale yellow solution was stirred for 2 h then quenched with MeI (5.8 g, 2.5 mL, 41 mmol, 50 equiv) and anhydrous DMF (5 mL). The solution was warmed to rt over 16

h before carefully quenching with water (5 mL) The reaction mixture was extracted with Et$_2$O (2 x 10 mL) and the combined organics were washed with 5% aq LiCl (5 x 5 mL), water (2 x 5 mL), and brine (5 mL) then concentrated under vacuum. The resulting crude yellow oil was dissolved in acetone (4 mL) to which 10% aq AcOH (4 mL) was added. The reaction mixture immediately became cloudy white. After stirring for 20 min, water (10 mL) was added and the reaction mixture was extracted with Et$_2$O (3 x 10 mL). The combined organics were washed with water (10 mL) and brine (10 mL), dried over sodium sulfate, and concentrated under vacuum to a yellow oil which was dissolved in minimal hexanes. Purification on silica gel (0 – 10% EtOAc/hexanes) afforded **V.44** as a pale yellow oil (76 mg, 34%). ^{1}H NMR (500 MHz, CDCl$_3$) δ(ppm) 7.71 (br, 1H), 7.37 – 7.19 (overlap, 2H), 6.86 (br, 1H), 6.59 (br d, J = 1.8, 0.7 Hz, 1H), 6.55 (d, J = 10.0 Hz, 1H), 6.38 (dd, J = 10.0, 1.8 Hz, 1H), 6.11 (dd, J = 17.6, 11.2 Hz, 1H), 5.70 (dd, J = 17.6, 1.0 Hz, 1H), 5.37 (dd, J = 17.2, 1.4 Hz, 1H), 5.31 (dd, J = 11.2, 1.0 Hz, 1H), 5.16 (dd, J = 10.9, 1.4 Hz, 1H), 3.19 (s, 3H); ^{13}C NMR (125 MHz, CDCl$_3$) δ(ppm) 186.27, 154.25, 147.55, 139.14, 134.43, 134.36, 134.07, 132.69, 129.91, 128.46, 128.11, 128.10, 128.06, 127.95, 122.54, 117.81, 50.81.

(±) **V.46**
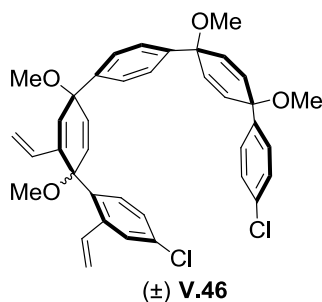
(±)-syn-4,4''''-dichloro-1',1''',4',4'''-tetramethoxy-2,2'-divinyl-1',1'''-tetrahydro-1,1':4',1'':4'',1''':4''',1''''-quinquephenyl **V.46**. To a solution of syn-4-bromo-4''-chloro-

210

1',4'-dimethoxy-1',4'-dihydro-1,1':4',1''-terphenyl **II.6**[56] (0.80 g, 2.0 mmol, 2.0 equiv) in

anhydrous THF (20 mL) was added tBuLi (2.6 mL, 4.0 mmol, 4.0 equiv, 1.5 M in

pentane) dropwise at −78 $^{\circ}$C. After stirring for 20 min, a solution of **V.44** (0.29 g, 0.94

mmol, 1.0 equiv) was added in anhydrous THF (10 mL) via cannula. The reaction

mixture darkened to green and was quenched by the addition of water (10 mL) after 25

min. The resulting biphasic mixture was warmed to rt and extracted with EtOAc (3 x 15

mL). The combined organics were washed with brine (10 mL), dried over sodium sulfate,

and concentrated onto Celite. Purification on silica gel (0 − 20% EtOAc/hexanes)

afforded the semi-pure addition product (360 mg) as a single diastereomer. The alcohol

was dissolved in anhydrous THF (10 mL) and was added to a slurry of sodium hydride

(0.12 g, 2.9 mmol, 5.0 equiv, 60% suspension in mineral oil) in THF (15 mL) at 0 $^{\circ}$C.

After stirring for 15 min, MeI (0.37 mL, 0.83 g, 5.9 mmol, 10 equiv) was added and the

reaction mixture was allowed to warm to rt. After stirring for 16 h, the reaction was

quenched by the addition of water (10 mL). The biphasic mixture was extracted with

EtOAc (3 x 15 mL) and the combined organics were washed with brine (10 mL), dried

over sodium sulfate, and concentrated onto Celite. Purification on silica gel (hexanes then

40% EtOAc/hexanes) afforded **V.46** as a white foam (0.30 g, 47%). ^{1}H NMR (400 MHz,

CDCl$_3$) δ(ppm) 7.62 (dd, J = 17.4, 10.9 Hz, 1H), 7.49 − 7.23 (overlap, 10H), 7.16 (dd, J =

8.5, 2.3 Hz, 1H), 6.38 (d, J = 2.2 Hz, 1H), 6.24 − 5.93 (overlap, 7H), 5.49 (dd, J = 17.4,

1.6 Hz, 1H), 5.44 (dd, J = 17.6, 1.5 Hz, 1H), 5.26 (dd, J = 10.9, 1.6 Hz, 1H), 5.09 (dd, J =

11.1, 1.5 Hz, 1H), 3.43 (overlap, 6H), 3.20 (s, 3H), 3.12 (s, 3H); ^{13}C NMR (100 MHz,

CDCl$_3$) δ(ppm) 143.02, 142.82, 142.09, 139.96, 139.27, 137.61, 136.76, 134.54, 133.78,

133.68, 133.61, 133.52, 133.38, 133.27, 133.02, 131.71, 129.22, 128.61, 128.28, 127.59, 127.14, 126.43, 126.26, 118.00, 116.07, 75.01, 74.71, 74.59, 52.20, 52.18, 52.01, 51.04.

V.49
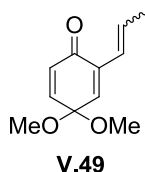
4,4-dimethoxy-2-(prop-1-en-1-yl)cyclohexa-2,5-dienone **V.49**. To a methanolic solution (35 mL) of 4-methoxy-2-(prop-1-en-1-yl)phenol[57] (1.7 g, 10 mmol, 1.0 equiv) was added PhI(OAc)$_2$ (4.0 g, 12 mmol, 1.2 equiv) portionwise at 0 °C. After stirring for 30 min upon completion of PIDA addition, the reaction was quenched with sat. aq NaHCO$_3$ (30 mL). The reaction mixture was extracted with Et$_2$O (3 x 40 mL) and the combined organics were washed with sat. aq NaHCO$_3$ (30 mL), water (30 mL), brine (30 mL), and were dried over sodium sulfate. Concentration under vacuum afforded a crude orange oil that was purified on silica gel (4 cm x 8 cm, hexanes then 15% EtOAc/hexanes) to afford **V.49** as a yellow oil (1.5 g, 75%, E:Z = 5:1). Major Diastereomer: ^{1}H NMR (500 MHz, CDCl$_3$) δ(ppm) 6.82 (dd, J = 10.4, 3.2 Hz, 1H), 6.67 (d, J = 3.2 Hz, 1H), 6.31 (d, J = 10.4 Hz, 1H), 6.25 (m, 1H), 5.95 (dq, J = 11.5, 7.1 Hz, 1H), 3.40 (s, 6H), 1.83 (dd, J = 7.1, 2.0 Hz, 5H).

(±) **V.50**
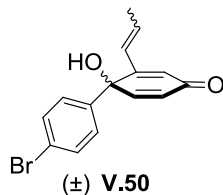
(±)-4'-bromo-1-hydroxy-2-(prop-1-en-1-yl)-[1,1'-biphenyl]-4(1H)-one **V.50**. To a

solution of 1,4-dibromobenzene (2.0 g, 8.5 mmol, 1.1 equiv) in anhydrous THF (35 mL)

at −78 °C was added *n*BuLi (3.9 mL, 9.2 mmol, 1.2 equiv, 2.4 M in hexanes) dropwise.

The milky white suspension was stirred for 10 min then a solution of **V.49** (1.5 g, 7.7

mmol, 1.0 equiv) was added in anhydrous THF (10 mL). The reaction was quenched after

40 min by the addition of water (10 mL) and it was allowed to warm to rt. The reaction

mixture was extracted with EtOAc (2 x 40 mL) and the combined organics were washed

with brine (20 mL), dried over sodium sulfate, and concentrated to yield a viscous oil.

The crude ketal product was dissolved in acetone (7.5 mL) to which 10% aq AcOH (7.5

mL) was added. After stirring at rt for 90 min, sat. aq $NaHCO_3$ (50 mL) was added and

the reaction mixture was extracted with EtOAc (2 x 20 mL). The combined organics were

washed with brine (20 mL), dried over sodium sulfate, and concentrated onto Celite.

Purification on silica gel (2 cm x 8 cm, hexanes then 20 − 35% EtOAc/hexanes) afforded

V.50 as an off-white waxy solid (1.7 g, 72%). ^{1}H NMR (300 MHz, $CDCl_3$) δ(ppm) 7.48

(d, *J* = 8.6 Hz, 1H), 7.30 (d, *J* = 8.6 Hz, 1H), 6.78 (d, *J* = 10.0 Hz, 1H), 6.29 (br s, 1H),

6.18 (dd, *J* = 10.0, 1.9 Hz, 1H), 5.99 (dd, *J* = 12.1, 7.2 Hz, 1H), 5.81 (d, *J* = 12.1 Hz, 1H),

2.79 (s, 1H), 1.85 (dd, *J* = 7.2, 1.9 Hz, 3H); ^{13}C NMR (125 MHz, $CDCl_3$) δ(ppm) 186.89,

157.48, 151.34, 138.12, 134.96, 131.85, 127.23, 125.92, 125.54, 124.90, 122.16, 72.43,

15.67.

(±) **V.51**
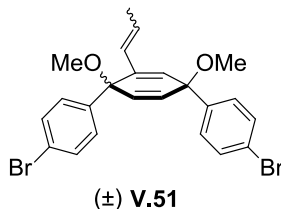
(±)-syn-4,4''-dibromo-1',4'-dimethoxy-2'-(prop-1-en-1-yl)-1',4'-dihydro-1,1':4',1''-terphenyl **V.51**. To a solution of **V.50** (1.2 g, 4.0 mmol, 1.0 equiv) in anhydrous THF (20 mL) at −78 °C was added sodium hydride (0.21 g, 5.2 mmol, 1.3 equiv). The resulting yellow suspension was stirred for 1 h. Meanwhile, 1,4-dibromobenzene was dissolved in anhydrous THF (10 mL) and cooled to −78 °C, whereupon *n*BuLi (3.9 mL, 9.3 mmol, 2.4 M in hexanes) was added dropwise. After stirring the aryl lithium reagent for 10 min, it was transferred via cannula to the mixture of sodium hydride and **V.50**. After stirring for 4 h, MeI (3.4 g, 1.5 mL, 24 mmol, 6.0 equiv) and anhydrous DMF (5 mL) were added and the reaction was allowed to warm to rt. After 15 h, the reaction mixture was quenched with water (15 mL) and was extracted with EtOAc (2 x 25 mL). The combined organics were washed with 1% aq LiCl (5 x 5 mL) and brine (10 mL), then were dried over sodium sulfate and concentrated onto Celite. Purification on silica gel (4 cm x 10 cm, 0 − 3 − 5% EtOAc/hexanes) afforded a semi-pure product that was again concentrated onto Celite. Purification on silica gel (0 − 20 − 50% benzene/hexanes) afforded **V.51** as a white solid after washing with minimal hexanes (0.72 g, 36%, E:Z = 9: 1). ^{1}H NMR (300 MHz, CDCl$_3$) δ(ppm) 7.47 (d, J = 8.6 Hz, 2H), 7.37 (d, J = 8.6 Hz, 1H), 7.33 (d, J = 8.6 Hz, 1H), 7.15 (d, J = 8.6 Hz, 2H), 6.11 − 6.00 (overlap, 2H), 5.96 (d, J = 10.7 Hz, 1H), 5.71 − 5.62 (overlap, 2H), 3.44 (s, 3H), 3.33 (s, 3H), 1.77 (d, J = 5.2 Hz, 3H); ^{13}C NMR (125 MHz, CDCl$_3$) δ(ppm) 143.03, 142.06, 138.01, 135.38, 133.20,

214

131.64, 131.28, 131.24, 129.14, 128.05, 126.18, 121.91, 121.48, 76.70, 75.47, 52.12, 51.72, 15.31.

(±) **V.52**
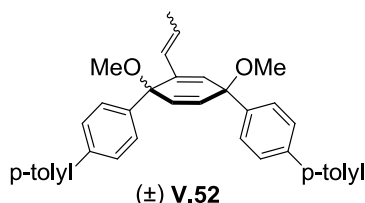
(±)-syn-1'',4''-dimethoxy-4,4''''-dimethyl-2''-(prop-1-en-1-yl)-1'',4''-dihydro-1,1':4',1'':4'',1''':4''',1''''-quinquephenyl **V.52**. To a 100 mL Schlenk tube was added **V.51** (50 mg, 0.10 mmol, 1.0 equiv), 4,4,5,5-tetramethyl-2-(p-tolyl)-1,3,2-dioxaborolane (49 mg, 0.22 mmol, 2.2 equiv), Pd(PPh$_3$)$_4$ (12 mg, 0.10 mmol, 10 mol%), and Cs$_2$CO$_3$ (0.16 g, 0.51 mmol, 6.0 equiv). The vessel was sealed with a rubber septum and evacuated/backfilled (3x) with N$_2$. Degassed (sparged 1 h) toluene (40 mL) and methanol (4 mL) were added. The reaction mixture was heated to 80 ^{o}C under an N$_2$ atmosphere for 19 h, before concentrating onto Celite. Purification on silica gel (1 cm x 5 cm, 0 − 5% EtOAc/hexanes) afforded **V.52** as a white foam (47 mg, 92%, E:Z = 9:1). ^{1}H NMR (300 MHz, CDCl$_3$) δ(ppm) 7.54 − 7.36 (overlap, 10H), 7.28 − 7.14 (overlap, 6H), 6.19 (d, J = 2.4 Hz, 1H), 6.15 (dd, J = 10.0, 2.4 Hz, 1H), 6.05 (d, J = 10.0 Hz, 1H), 5.83 − 5.68 (overlap, 2H), 3.51 (s, 3H), 3.40 (s, 3H), 2.39 (s, 3H), 2.37 (s, 3H), 1.86 (d, J = 5.1 Hz, 3H); ^{13}C NMR (125 MHz, CDCl$_3$) δ(ppm) 142.69, 141.78, 140.47, 139.96, 138.08, 137.91, 137.90, 137.12, 136.98, 135.34, 133.33, 133.32, 131.24, 129.51, 129.44, 128.60, 127.01, 126.97, 126.90, 126.64, 126.62, 126.55, 75.72, 52.07, 52.05, 51.67, 51.65, 21.13, 15.27.

V.53
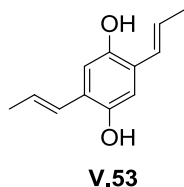
2,5-di((E)-prop-1-en-1-yl)benzene-1,4-diol **V.53**. To a dry 25 mL RBF was added **II.12**

(0.10 g, 0.53 mmol, 1.0 equiv) and $PdCl_2(MeCN)$ (13 mg, 0.053 mmol, 10 mol%). The

vessel was purged with N_2 whereupon anhydrous DCM (2.5 mL) was added. The slurry

was heated to reflux for 15 h, then was cooled to rt, diluted with EtOAc, and filtered

through a short pad of Celite (EtOAc). The filtrate was concentrated onto Celite and

purification on silica gel (1 cm x 6 cm, $10 - 30\%$ acetone/hexanes) afforded **V.53** as an

off-white solid (50 mg, 50%). ^{1}H NMR (300 MHz, Acetone-d_6) δ(ppm) 7.73 (s, 1H), 6.87

(s, 1H), $6.72 - 6.56$ (m, 1H), 6.14 (dq, $J = 15.9$, 6.6 Hz, 1H), 1.83 (dd, $J = 6.6$, 1.8 Hz,

3H).

V.54
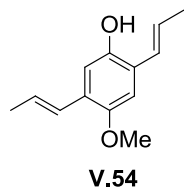
4-methoxy-2,5-di((E)-prop-1-en-1-yl)phenol **V.54**. To a solution of **II.13** (0.50 g, 2.5

mmol, 1.0 equiv) in anhydrous THF (20 mL) was added potassium *tert*-butoxide (2.8 g,

25 mmol, 10 equiv). The reaction mixture was stirred under N_2 at rt for 17 h before

quenching with sat. aq NH_4Cl (10 mL) and extracting with EtOAc (3 x 20 mL). The

combined organics were washed with brine (10 mL), dried over sodium sulfate, and

concentrated onto Celite. Purification on silica gel (2 cm x 5 cm, 15% acetone/hexanes)

afforded **V.54** as a white solid (500 mg, 100%). ^{1}H NMR (300 MHz, $CDCl_3$) δ(ppm) 6.84

(s, 1H), 6.79 (s, 1H), 6.68 – 6.10 (overlap, 2H), 6.26 – 6.08 (overlap, 2H), 4.55 (s, 1H),

3.80 (s, 3H), 1.91 (dd, *J* = 6.8, 1.8 Hz, 3H), 1.88 (dd, *J* = 6.7, 1.7 Hz, 3H); ^{13}C NMR (150

MHz, CDCl$_3$) δ(ppm) 146.50, 127.68, 126.99, 126.72, 126.71, 125.13, 124.03, 113.53,

109.86, 109.86, 56.40, 19.05, 19.04.

(±) **V.56**
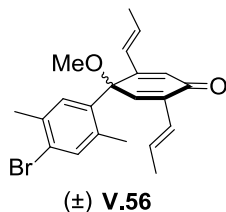
(±)-4'-bromo-1-hydroxy-2',3'-dimethyl-2,5-di((E)-prop-1-en-1-yl)-[1,1'-biphenyl]-4(1H)-

one **V.56**. To a methanolic solution (1.5 mL) of ketone **II.26** (22 mg, 0057 mmol, 1.0

equiv) was added Grubbs II (9.6 mg, 0.011 mmol, 20 mol%). The reaction mixture was

heated to 60 °C for 2 h then concentrated onto Celite. Purification on silica gel (1 cm x 5

cm, 0 – 5% EtOAc/hexanes) afforded **V.56** as a pale yellow oil (11 mg, 50%). ^{1}H NMR

(300 MHz, CDCl$_3$) δ(ppm) 7.75 (s, 1H), 7.22 (s, 1H), 6.54 (s, 1H), 6.43 – 6.18 (overlap,

4H), 5.80 (d, *J* = 15.9 Hz, 1H), 3.15 (s, 3H), 2.41 (s, 3H), 2.03 (s, 3H), 1.81 (d, *J* = 5.3

Hz, 3H), 1.73 (dd, *J* = 6.8, 1.8 Hz, 3H).

V.60
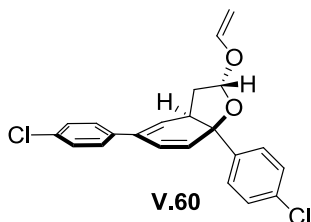
(2R,7aS)-5,7a-bis(4-chlorophenyl)-2-(vinyloxy)-2,3,3a,7a-tetrahydrobenzofuran **V.60**.

To a 2 dram vial was added **V.58** (0.21 g, 0.62 mmol, 1.0 equiv), Hg(OAc)$_2$ (0.26 g, 0.80

mmol, 1.3 equiv) and ethyl vinyl ether (3 mL). The vial was capped and stirred at rt for 20 h. The reaction was quenched by the addition of 10% aq KOH (3 mL) and the resulting mixture was filtered through a short plug of basic alumina then concentrated onto Celite. Purification on silica gel (0 – 5% EtOAc/hexanes) afforded **V.60** as a colorless oil (20 mg, 8%, dr > 19:1). NOTE: The cleanliness of the crude ^{1}H NMR spectrum of this reaction varied based on the source of Hg(OAc)$_2$ used. ^{1}H NMR (400 MHz, CDCl$_3$) δ(ppm) 7.42 – 7.30 (overlap, 6H), 7.29 – 7.20 (overlap, 2H), 6.53 (dd, $J =$ 14.2, 6.6 Hz, 1H), 6.38 (dd, $J =$ 9.9, 1.7 Hz, 1H), 6.23 (br d, $J =$ 6.2 Hz, 1H), 5.78 (d, $J =$ 9.9 Hz, 1H), 5.50 (d, $J =$ 4.6 Hz, 1H), 4.55 (dd, $J =$ 14.2, 1.6 Hz, 1H), 4.25 (dd, $J =$ 6.6, 1.6 Hz, 1H), 3.20 (dd, $J =$ 12.5, 6.8 Hz, 1H), 2.56 (dd, $J =$ 12.5, 6.8 Hz, 1H), 2.11 (ddd, J = 12.5, 12.5, 4.6 Hz, 1H); ^{13}C NMR (125 MHz, CDCl$_3$) δ(ppm) 149.32, 143.55, 138.04, 133.65, 133.34, 132.76, 130.82, 128.92, 128.56, 127.00, 126.26, 124.52, 122.33, 99.46, 91.51, 85.96, 44.37, 41.86.
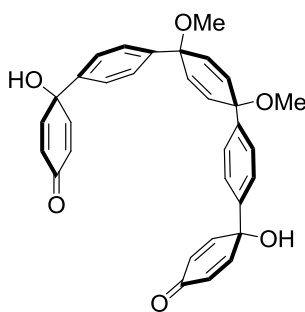
V.68

(1"s,4"s)-1,1""-dihydroxy-1",4"-dimethoxy-1",4"-dihydro-[1,1':4',1":4",1"':4"',1""-quinquephenyl]-4,4""(1H,1""H)-dione **V.68** To a solution of dibromide **V.67** (9.0 g, 20 mmol, 1.0 equiv) in anhydrous THF (175 mL) at −78 °C was added *n*BuLi (17 mL, 42

218

mmol, 2.1 equiv, 2.5 M in hexanes) over ca. 5 min. Upon completion of nBuLi addition, benzoquinone monoketal (6.8 g, 44 mmol, 2.2 equiv) was added immediately as a single stream. The reaction mixture became extremely viscous and stirring stopped at this time. The bath was removed and the reaction mixture was allowed to warm to rt over 3 h. The reaction was then quenched with water (50 mL) and diluted with DCM (100 mL). The layers were separated and the aqueous phase was extracted with DCM (2 x 100 mL). The combined organics were washed with water (1 x 50 mL) and brine (1 x 50 mL) then dried over sodium sulfate and concentrated under vacuum to a dark yellow oil. To the crude oil was added acetone (150 mL) and 10% aq acetic acid (55 mL). The solution was stirred at rt and became cloudy after 20 min. After stirring for 30 min, the solid was collected by vacuum filtration and was washed with MeOH (3 x 50 mL). The resulting solid was dried under high vacuum to afford diquinol **V.68** as an off-white solid (4.5 g, 44%). ^{1}H NMR (500 MHz, CDCl$_3$): δ(ppm) 4.41 (s, 8H), 6.87 (d, J = 9.8 Hz, 4H), 6.23 (d, J = 9.8 Hz, 4H), 6.09 (s, 4H), 3.42 (s, 6H), 2.42 (2H); ^{13}C NMR (150 MHz, DMSO-d_6): δ(ppm) 185.50, 152.51, 142.99, 139.57, 133.03, 126.12, 125.55, 125.38, 73.86, 69.91, 51.49. HRMS (FAB+) (m/z): [M]$^+$ calcd. for C$_{32}$H$_{28}$O$_6$, 508.1886; found, 508.1897. IR (neat): 665.96, 700.79, 735.09, 764.23, 833.02, 859.16, 948.54, 1015.94, 1027.50, 1078.34, 1171.62, 1227.79, 1226.22, 1395.25, 1448.72, 1461.42, 1500.16, 1621.32, 1665.36, 2823.69, 2936.05, 3400.15 cm^{-1}.

V.69
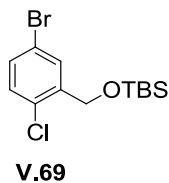
((5-bromo-2-chlorobenzyl)oxy)(tert-butyl)dimethylsilane **V.69**. To a solution of (5-bromo-2-chlorophenyl)methanol (13 g, 57 mmol, 1.0 equiv) and imidazole (6.2 g, 91 mmol, 1.6 equiv) in anhydrous DCM (50 mL) at 0 $^{\circ}$C was added solid TBS-Cl (11 g, 74 mmol, 1.3 equiv). The resulting slurry was allowed to slowly warm to rt. After stirring at rt for 14 h, the reaction mixture was filtered through a short plug of silica gel (DCM). The filtrate was concentrated under vacuum to afford **V.69** as a colorless oil (19 g, quant). ^{1}H NMR (300 MHz, CDCl$_3$): δ(ppm) 7.69 (dd, *J*= 2.4, 1.1 Hz, 1H), 7.31 (dd, *J*= 8.4, 2.4 Hz, 1H), 7.16 (d, *J*= 8.4 Hz, 1H), 4.74 (d, *J*= 1.0 Hz, 2H), 0.97 (s, 9H), 0.14 (s, 6H); ^{13}C NMR (125 MHz, CDCl$_3$) δ(ppm) 141.12, 130.87, 130.52, 130.30, 130.18, 120.88, 62.04, 26.07, 18.54, -5.22. HRMS (FAB+) (*m/z*): [M]$^{+}$ calcd. for C$_{13}$H$_{19}$OSiBrCl, 333.0077; found, 333.0102. IR (neat): 620.65, 668.89, 775.35, 807.69, 833.33, 938.45, 1005.08, 1039.84, 1079.25, 1105.59, 1195.10, 1253.26, 1395.05, 1470.97, 2856.37, 2928.26, 2954.01 cm^{-1}.

V.70
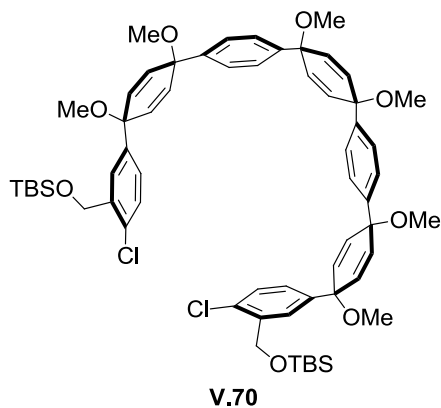
disilylether **V.70**. To a dry 500 mL RBF charged with a magnetic stir bar was added solid diquinol **V.68** (1.9 g, 3.7 mmol, 1.0 equiv) and **V.69** (8.7 g, 26 mmol, 7.0 equiv). The mixture was evacuated/backfilled with N$_2$ (3x) and fitted with a rubber septum under N$_2$.

Anhydrous THF (50 mL) was added and the slurry was cooled to $-78\ ^{\circ}$C. Solid sodium hydride (0.74 g, 19 mmol, 5.0 equiv, 60% suspension in mineral oil) was added and the reaction mixture was stirred 1 h at $-78\ ^{\circ}$C. Next, *n*BuLi was added dropwise (10 mL, 26 mmol, 7.0 equiv, 2.5 M in hexanes). The reaction mixture became extremely viscous and stirring became sluggish. After 10 min, the tan suspension was slowly warmed to rt and stirred for 90 min before quenching with MeI (5.2 g, 2.3 mL, 37 mmol, 10 equiv) and anhydrous DMF (10 mL). The solution was stirred for 16 h before quenching with water (25 mL) and diluting with Et$_2$O (30 mL). The layers were separated and the aqueous phase was extracted with Et$_2$O (2 x 30 mL). The combined organics were washed with water (10 x 10 mL) and brine (10 mL) then were dried over sodium sulfate and concentrated onto Celite. Purification on silica gel (4 cm x 9 cm, 0 – 20% EtOAc/hexanes) afforded a semi-pure off-white foam that was concentrated onto Celite again. Purification on silica gel (3 cm x 9 cm, 5 – 20% EtOAc/hexanes) afforded **V.70** as a white foam (1.7 g, 43%). ^{1}H NMR (300 MHz, CDCl$_3$, major diastereomer): δ(ppm) 7.77 (d, *J*= 2.3 Hz, 2H), 7.33 – 7.29 (overlap, 8H), 7.22 (d, *J*= 8.3 Hz, 2H), 7.10 (dd, *J*= 8.3, 2.3 Hz, 2H), 6.11 – 6.02 (overlap, 12H), 4.76 (s, 4H), 3.41 (s, 6H), 3.41 (s, 6H), 3.40 (s, 6H), 0.92 (s, 18H), 0.08 (s, 12H); ^{13}C NMR (125 MHz, CDCl$_3$): δ(ppm) 142.57, 142.31, 142.04, 138.60, 133.40, 133.05, 132.72, 130.42, 128.47, 125.84, 125.81, 125.71, 125.52, 125.32, 74.39, 74.29, 74.16, 62.19, 51.69, 31.50, 25.67, 18.09, -5.54. MALDI-TOF (*m/z*): [M - OMe]$^+$ calcd. for C$_{61}$H$_{75}$O$_7$Cl$_2$Si$_2$, 1045.44, found 1044.98. IR (neat): 663.90, 814.18, 834.94, 1041.67, 1085.95, 1196.50, 1256.21, 1462.86, 2855.45, 2933.08, 2954.67 cm^{-1}.

V.71
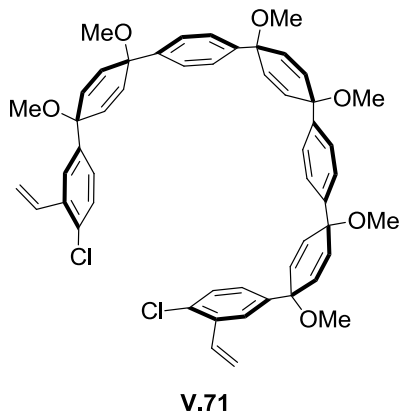
dichloride **V.71**. To a dry RBF charged with a magnetic stirbar was added **V.70** (0.93 g, 0.86 mmol, 1.0 equiv). The flask was purged with N_2 and anhydrous THF (8 mL) was added under an N_2 atmosphere. The reaction mixture was cooled to 0 °C whereupon TBAF (2.2 mL, 2.2 mmol, 2.5 equiv, 1.0 M in THF) was added dropwise. The resulting solution was allowed to slowly warm to rt over 2 h before quenching with sat. aq NH_4Cl (5 mL) and diluting with EtOAc (20 mL). The layers were separated and the aqueous phase was extracted with EtOAc (2 x 20 mL). The combined organics were washed with water (3 x 10 mL) and brine (10 mL) then were dried over sodium sulfate and concentrated under vacuum. The resulting crude foam was passed through a plug of silica gel (30% EtOAc/DCM) to afford a semi-pure diol (0.42 g, 0.49 mmol) that was added to a dry RBF charged with a magnetic stirbar and $NaHCO_3$ (0.25 g, 3.0 mmol, 6 equiv). The flask was purged with N_2 and anhydrous DCM (25 mL) was added under an N_2 atmosphere. The reaction mixture was cooled to 0 °C whereupon Dess-Martin Periodinane (0.48 g, 1.1 mmol, 2.3 equiv) was added. The resulting slurry was allowed to slowly warm to rt over 90 min and was then quenched by the addition sat. aq $NaHCO_3$ (10 mL) and sat. aq $Na_2S_2O_3$ (10 mL). The biphasic mixture was stirred for 1 h and the layers were separated. The aqueous phase was extracted with DCM (2 x 20 mL) and the

222

combined organic were washed with brine (10 mL), dried over sodium sulfate, and concentrated under vacuum. The resulting crude white solid dialdehyde (0.41 g) was used immediately without purification by first dissolving it in anhydrous THF (10 mL). In a separate dry RBF, methyltriphenylphosphonium bromide (0.67 g, 1.9 mmol, 4.0 equiv) was suspended in anhydrous THF (10 mL) and cooled to 0 °C. Solid potassium *tert*-butoxide (0.32 g, 2.9 mmol, 6.0 equiv) was added and the resulting bright yellow ylide solution was stirred for 10 min. The solution of dialdehyde was added to the solution of ylide via cannula and the reaction mixture was allowed to stir at rt for 15 min. Acetone (1 mL) was added and the reaction mixture was concentrated under vacuum. The crude material was loaded onto silica gel in DCM; purification on silica gel (3 cm x 7 cm, 0 − 5% EtOAc/DCM) afforded dichloride **V.71** as a white foam (0.32 g, 44%). ^{1}H NMR (500 MHz, CDCl$_3$): δ(ppm) 7.53 (d, J = 2.2 Hz, 2H), 7.40 − 7.35 (overlap, 8H), 7.30 (d, J = 8.6 Hz, 2H), 7.27 (dd, J = 8.6, 2.2 Hz, 2H), 7.04 (dd, J = 17.5, 10.9 Hz, 2H), 6.17 (d, J = 10.2 Hz, 4H), 6.09 (s, 3H), 6.07 (d, J = 10.2 Hz, 4H), 5.51 (d, J = 17.5 Hz, 2H), 5.25 (d, J = 10.9 Hz, 2H), 3.46 (s, 6H), 3.44 (s, 12H); ^{13}C NMR (125 MHz, CDCl$_3$) δ(ppm) 143.01, 142.53, 142.29, 135.40, 133.65, 133.24, 133.15, 132.87, 132.17, 129.56, 126.43, 126.18, 126.06, 124.20, 116.74, 74.60, 74.55, 74.48, 52.05, 52.03, 51.98. MALDI-TOF (*m/z*): [M − OMe + H]$^+$ calcd. for C$_{51}$H$_{48}$O$_5$Cl$_2$, 810.29, found 810.55. IR (neat): 752.26, 831.60, 1079.88, 1228.92, 1365.36, 1467.32, 1737.30, 2821.77, 2937.70 cm^{-1}.

V.73
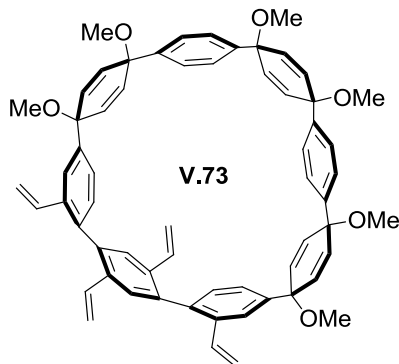
tetravinyl macrocycle **V.73**. To a dry 250 mL Schlenk flask charged with a magnetic

stirbar was added dichloride **V.71** (0.14 g, 0.16 mmol, 1.0 equiv), diboronate **V.72** (76

mg, 0.20 mmol, 1.2 equiv), and SPhos-Pd-G2 (24 mg, 0.033 mmol, 20 mol%). The vessel

was fitted with a rubber septum and evacuated/backfilled with N_2 (3x) before the addition

of anhydrous dioxane (150 mL) under an N_2 atmosphere. The reaction mixture was

heated to 85 $^{\circ}$C for ca. 10 min whereupon degassed (sparged 1 h) 2 M aq K_3PO_4 (17 mL)

was added via cannula. The resulting dark yellow solution was heated under N_2 for 19.5

h. Upon cooling to rt, the brown reaction mixture was filtered through a short plug of

Celite (EtOAc) and the layers were separated. The aqueous phase was extracted with

EtOAc (2 x 50 mL) and the combined organics were washed with brine (20 mL), dried

over sodium sulfate, and concentrated under vacuum to a brown foam. This brown foam

was redissolved in DCM and pass through a silica plug (4 cm x 3 cm) topped with Celite

(50% EtOAc/DCM). The filtrate was concentrated under vacuum and purified by

preparative recycling GPC (t_R = 43 min, collected on 2nd cycle) to afford an off-white

solid that could be washed with minimal acetone to afford tetravinyl macrocycle **V.73** as

a while solid (25 mg, 17%). ^{1}H NMR (400 MHz, CDCl$_3$): δ(ppm) 8.03 (d, J = 1.8 Hz,

2H), 7.49 – 7.32 (overlap, 10H), 6.98 (dd, J = 17.6, 11.0 Hz, 2H), 6.78 (dd, J = 8.2, 1.8

Hz, 2H), 6.52 – 6.40 (overlap, 4H), 6.32 – 6.16 (overlap, 8H), 6.10 (dd, J = 10.2, 2.2 Hz,

2H), 6.04 (dd, J = 10.2, 2.2 Hz, 2H), 5.89 (d, J = 17.5 Hz, 2H), 5.58 (d, J = 17.5 Hz, 2H), 5.30 (d, J = 11.0 Hz, 2H), 5.07 (d, J = 11.1 Hz, 2H), 3.54 (s, 6H), 3.39 (s, 6H), 3.18 (s, 6H); ^{13}C NMR (125 MHz, CDCl$_3$): δ(ppm) 143.51, 142.89, 142.13, 139.83, 139.19, 135.88, 135.36, 135.16, 135.03, 134.87, 134.27, 134.11, 133.74, 133.56, 133.17, 131.24, 128.23, 126.83, 126.66, 125.62, 121.27, 115.30, 114.77, 75.95, 74.65, 72.43, 52.66, 51.79, 51.47; MALDI-TOF (*m/z*): [M - OMe]$^+$ calcd. for C$_{61}$H$_{55}$O$_5$, 867.40; found, 867.92. IR (neat): 754.83, 828.35, 907.32, 948.53, 1084.65, 1226.47, 1377.55, 1410.43, 1466.49, 1661.06, 1737.12, 2853.29, 2924.08, 3363.89 cm^{-1}.
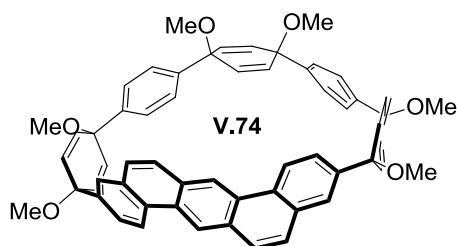
dibenzo[a,h]anthracene macrocycle **V.74**. To a dry 2 dram vial with a septum cap and magnetic stirbar was added tetravinyl macrocycle **V.73** (25 mg, 0.027 mmol, 1.0 equiv) and Grubbs II (2.4 mg, 0.0027 mmol, 10 mol%). The vial was sealed and evacuated/backfilled with N$_2$ (3x) before the addition of anhydrous DCM (1.5 mL) under an N$_2$ atmosphere. The reaction mixture was heated to 40 ^{o}C for 30 min then concentrated under reduced pressure. Meanwhile, to a second dry 2 dram vial with a septum cap and magnetic stir bar was added macrocycle **V.73** (44 mg, 0.049 mmol, 1.0 equiv) and Grubbs II (4.1 mg, 0.0049 mmol, 10 mol%). The vial was sealed and evacuated/backfilled with N$_2$ (3x) before the addition of anhydrous DCM (2 mL) under an N$_2$ atmosphere. The reaction mixture was heated to 40 ^{o}C for 30 min then concentrated

under reduced pressure. The two crude solids were redissolved in DCM, combined, and concentrated onto Celite. Purification on silica gel (1 cm x 5 cm, 20% EtOAc/DCM) afforded an off-white solid that was washed several times with minimal acetone to afford dibenza[*a,h*]anthracene macrocycle **V.74** as a white solid (55 mg, 86% combined). ^{1}H NMR (400 MHz, CDCl$_3$): δ(ppm) 9.04 (s, 2H), 8.59 (d, *J* = 8.8 Hz, 2H), 7.92 (d, *J* = 9.0 Hz, 2H), 7.64 (s, 2H), 7.57 – 7.39 (overlap, 4H), 6.88 (d, *J* = 8.2 Hz, 4H), 6.62 (d, *J* = 8.2 Hz, 4H), 6.33 (overlap, 4H), 6.13 (d, *J* = 10.3 Hz, 2H), 6.09 (d, *J* = 10.3 Hz, 2H), 6.04 – 5.94 (overlap, 4H), 3.56 (s, 6H), 3.36 (s, 12H); ^{13}C NMR (125 MHz, CDCl$_3$): δ(ppm) 142.96, 140.40, 139.70, 133.57, 133.50, 133.30, 133.17, 133.06, 131.89, 131.27, 130.09, 128.90, 127.33, 127.12, 126.73, 126.30, 125.91, 125.68, 123.13, 122.16, 76.08, 75.56, 72.60, 52.58, 51.79, 51.40. MALDI-TOF (*m/z*): [M – 3OMe]$^+$ calcd. for C$_{55}$H$_{41}$O$_3$, 749.03; found, 749.81. IR (neat): 752.34, 1082.39, 1217.14, 1365.34, 1736.81, 3600.67, 3626.27, 3702.45, 3726.69 cm^{-1}.
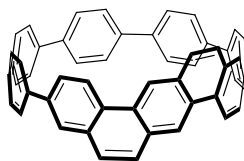
V.61

(3,10)-dibenzo[a,h]anthracene-nanohoop **V.61**. To a dry 25 mL RBF charged with a magnetic stirbar was added dibenza[*a,h*]anthracene macrocycle **V.74** (11 mg, 0.013 mmol, 1.0 equiv). The vessel was sealed with a rubber septum and evacuated/backfilled with N$_2$ (3x) before adding anhydrous THF (2 mL). The solution was cooled to −78 $^{\circ}$C, whereupon sodium naphthalenide (1 mL, 0.50 mmol, 40 equiv) was added dropwise via

syringe. During the addition process, the reaction mixture first became dark red, then eventually purple. After stirring for 30 min, a solution of I_2 in anhydrous THF (1 mL, 1 M) was added via syringe and the resulting dark red solution was stirred at -78 ^{o}C for 15 min. Sat. aq $Na_2S_2O_3$ (3 mL) was then added and the reaction mixture was allowed to warm to rt. The yellow biphasic mixture was extracted with DCM (2 x 25 mL) and the combined organics were washed with brine, dried over sodium sulfate, and concentrated under vacuum. Meanwhile, to a dry 50 mL RBF charged with a magnetic stirbar was added dibenza[a,h]anthracene macrocycle **V.74** (31 mg, 0.037 mmol, 1.0 equiv). The vessel was sealed with a rubber septum and evacuated/backfilled with N_2 (3x) before adding anhydrous THF (10 mL). The solution was cooled to -78 ^{o}C, whereupon sodium naphthalenide (3 mL, 1.5 mmol, 40 equiv) was added dropwise via syringe. After stirring for 30 min, a solution of I_2 in anhydrous THF (3 mL, 1 M) was added via syringe and the resulting dark red solution was stirred at -78 ^{o}C for 15 min. Sat. aq $Na_2S_2O_3$ (9 mL) was then added and the reaction mixture was allowed to warm to rt. The yellow biphasic mixture was extracted with DCM (2 x 40 mL) and the combined organics were washed with brine, dried over sodium sulfate, and concentrated under vacuum. The two crude solids were concentrated onto Celite and purified on silica gel (2 cm x 9 cm, hexanes then 30 – 40% DCM/hexanes). The bright yellow fractions containing product were pooled and further purified using preparative recycling GPC (t_R = 53 min, collected on 2nd cycle) to afford (3,10)-dibenzo[*a,h*]anthracene-nanohoop **V.61** (23 mg, 70% combined). ^{1}H NMR (500 MHz, CDCl$_3$): δ(ppm) 8.63 (s, 2H), 8.42 (d, *J* = 9.1 Hz, 2H), 7.88 (dd, *J* = 9.1, 2.1 Hz, 2H), 7.86 (d, *J* = 2.1 Hz, 2H), 7.72 (d, *J* = 9.2 Hz, 2H), 7.66 (d, *J* = 8.4 Hz, 4H), 7.54 (d, *J* = 9.2 Hz, 2H), 7.49 (overlap, 16H); ^{13}C NMR (125 MHz, CDCl$_3$): δ(ppm)

137.78, 137.58, 137.56, 136.66, 135.57, 132.83, 132.11, 129.58, 129.06, 127.72, 127.65, 127.43, 127.39, 127.26, 127.17, 126.69, 126.40, 125.32, 123.84, 122.71. MALDI-TOF (m/z): $[M]^+$ calcd. for $C_{52}H_{32}$, 656.81; found, 656.74. IR (neat): 720.43, 810.94, 886.03, 1217.18, 1365.34, 1485.57, 1583.43, 1737.78, 3021.78 cm^{-1}.

V.75
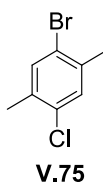
1-bromo-4-chloro-2,5-dimethylbenzene **V.75**. To a 3N 500 mL RBF charged with a magnetic stirbar and fitted with a septum, a condenser, and an addition funnel was added a solution of 2-chloro-*p*-xylene (56 g, 0.40 mol, 1.0 equiv) in glacial AcOH (180 mL). The solution was cooled to 0 °C and a solution of bromine (71 g, 23 mL, 0.44mol, 1.1 equiv) in glacial AcOH (180 mL) was added over ca. 1 h via addition funnel. Upon completion of the addition, the reaction mixture was heated to 60 °C for 21 h. The reaction mixture was cooled to rt whereupon 1 M aq NaOH (400 mL) was slowly added. When gas evolution stopped, sat. aq $Na_2S_2O_3$ (50 mL) was added to quench excess bromine. The solution was extracted with Et_2O (3 x 200 mL) and the combined organic were dried over sodium sulfate. Concentration under vacuum gave a white solid that was washed with ice cold MeOH to afford **V.75** as a crystalline white sold (44 g, 50%). ^{1}H NMR (500 MHz, CDCl$_3$) δ(ppm) 7.37 (s, 1H), 7.19 (s, 1H), 2.32 (s, 3H), 2.30 (s, 3H); ^{13}C NMR (125 MHz, CDCl$_3$) δ(ppm) 136.82, 135.22, 134.22, 133.20, 130.91, 122.56, 22.36, 19.43. HRMS (EI+) (m/z): $[M]^+$ calcd. for C_8H_8BrCl, 217.9498; found, 217.9493.

IR(neat): 741.48, 755.97, 877.81, 987.66, 1037.51, 1185.14, 1265.43, 1348.02, 1379.99, 1451.71, 1477.79, 1745.77, 2851.62, 2920.24, 2952.89, 2984.20 cm^{-1}.

V.76
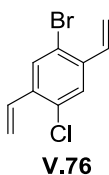
1-bromo-4-chloro-2,5-divinylbenzene **V.76**. To a solution of **V.75** (44 g, 0.20 mol, 1.0 equiv) in benzene (1000 mL) was added *N*-bromosuccinimide (78 g, 0.44 mol, 2.2 equiv) and benzoyl peroxide (2.2 g, 10 mmol, 0.050 equiv, wet with 25% water). The reaction mixture was heated to 80 °C for 20 h, then another portion of benzoyl peroxide (1.0 g, 4.5 mmol, 0.023 equiv, wet with 25% water) and stirring was continued for another 20 h. Upon cooling to rt, the reaction mixture was diluted with EtOAc (300 mL) and was washed with 1 M aq NaOH (3 x 200 mL), water (200 mL) and brine (100 mL). The organics were dried over sodium sulfate and concentrated to afford an off white solid that was crystallized from 95% EtOH to yield crystalline white tetrabromide (21 g) that was then dissolved in DMF (250 mL). To this solution was added triphenylphosphine (37 g, 139 mmol, 2.5 equiv). The resulting mixture was heated to 120 °C for 16 h. Upon cooling to room temperature, the solid white precipitate was collected by vacuum filtration and was washed with EtOAc (2 x 50 mL) and hexanes (2 x 50 mL). The diphosphonium salt was then dried under high vacuum and suspended in THF (200 mL). *p*-Formaldehyde (22 g, 748 mmol, 15 equiv) was added to the suspension, followed by the portion-wise addition of potassium *tert*-butoxide (11 g, 200 mmol, 4.0 equiv). The reaction mixture turned brown initially, and slowly became yellow. After 90 min, the reaction mixture was

229

milky white and was filtered through a short plug of Celite (hexanes). The filtrate was concentrated under vacuum and purified on silica gel by loading the crude product as a slurry in hexanes (4 cm x 6 cm, hexanes) to afford **V.76** as a white solid (9.7 g, 20%). ^{1}H NMR (300 MHz, CDCl$_3$): δ(ppm) 7.74 (s, 1H), 7.53 (s, 1H), 7.00 (dd, $J = 17.5$, 11.2 Hz, 1H), 6.96 (dd, $J = 17.4$, 11.2 Hz, 1H), 5.75 (d, $J = 17.5$ Hz, 1H), 5.72 (d, $J = 17.4$ Hz, 1H), 5.42 (d, $J = 11.2$ Hz, 1H), 5.42 (d, $J = 11.2$ Hz, 1H); ^{13}C NMR (125 MHz, CDCl$_3$) δ(ppm) 137.92, 136.46, 134.61, 132.46, 131.90, 130.52, 127.46, 121.79, 117.78, 117.72. HRMS (EI+) (*m/z*): [M]$^+$ calcd. for C$_{10}$H$_8$BrCl, 241.9498; found, 241.9489. IR (neat): 720.10, 741.59, 886.65, 988.01, 1032.20, 1069.82, 1365.54, 1416.16, 1469.64, 1620.32, 1843.07, 3094.60 cm^{-1}.

V.77
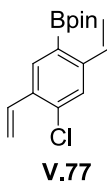
2-(4-chloro-2,5-divinylphenyl)-4,4,5,5-tetramethyl-1,3,2-dioxaborolane **V.**77. To a dry 100 mL Schlenk flask charged with a large magnetic stirbar was added freshly ground anhydrous potassium acetate (3.1 g, 32mmol, 3.0 equiv), **V.76** (2.6 g, 11 mmol, 1.0 equiv), freshly ground bis(pinacolato)diboron (3 g, 12 mmol, 1.1 equiv), and Pd(dppf)Cl$_2$ (0.26 g, 0.30 mmol, 3.0 mol%). The vessel was fitted with a rubber septum and evacuated/backfilled with N$_2$ (3x) before the addition of anhydrous dioxane (30 mL) under an N$_2$ atmosphere. The resulting dark red suspension was heated to 80 ^{o}C for 20 h. Upon cooling to rt, the reaction mixture was concentrated onto Celite. Automated flash

chromatography (100 g KP-Sil, 3 – 5% EtOAc/hexanes) afforded **V.77** as a pale yellow oil that solidified upon standing (2.0 g, 64%). ^{1}H NMR (300 MHz, CDCl$_3$): δ(ppm) 7.98 (s, 1H), 7.61 (s, 1H), 7.46 (dd, J = 17.6, 10.9 Hz, 1H), 7.06 (dd, J = 17.6, 11.1 Hz, 1H), 5.83 (dd, J = 17.6, 1.2 Hz, 1H), 5.70 (dd, J = 17.6, 1.2 Hz, 1H), 5.37 (dd, J = 11.1, 1.2 Hz, 1H), 5.30 (dd, J = 10.9, 1.2 Hz, 1H), 1.35 (s, 12H); ^{13}C NMR (125 MHz, C$_6$D$_6$) δ(ppm) 145.07, 136.52, 136.20, 135.00, 134.24, 132.58, 125.78, 116.30, 115.49, 83.52, 24.45 (C-B not observed). HRMS (FAB+) (*m/z*): [M]$^+$ calcd. for C$_{16}$H$_{20}$O$_2$BCl, 290.1245; found, 290.1256. IR (neat): 668.17, 731.73, 855.35, 912.12, 966.99, 987.91, 1040.83, 1083.18, 1110.69, 1212.77, 1256.31, 1299.87, 1314.58, 1329.48, 1388.76, 1477.54, 1529.56, 1586.82, 1623.78, 2929.50, 2977.71, 3086.38 cm^{-1}.

V.78
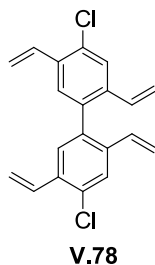
4,4'-dichloro-2,2',5,5'-tetravinyl-1,1'-biphenyl **V.78**. To a 50 mL Schlenk flask charged with a magnetic stirbar was added **V.77** (1.8 g, 7.3 mmol, 1.0 equiv), **V.76** (2.3 g, 8.0 mmol, 1.1 equiv), Pd(PPh$_3$)$_4$ (0.37 g, 0.32 mmol, 4.5 mol%), and freshly ground K$_3$PO$_4$ (4.6 g, 22 mmol, 3.0 equiv). The vessel was sealed with a rubber septum and evacuated/backfilled with N$_2$ (3x) before adding degassed (sparged 1 h) dioxane (12 mL) and water (2 mL) under an N$_2$ atmosphere. The bright yellow reaction mixture was heated in the dark to 70 °C. After stirring for 20 h, the reaction mixture was cooled to rt and diluted with EtOAc (20 mL). The layers were separated and the aqueous layer was

extracted with EtOAc (2 x 20 mL). The combined organics were washed with brine (20

mL), dried over sodium sulfate, and concentrated onto Celite. Purification on silica gel (3

cm x 10 cm, hexanes) afforded **V.78** as a viscous, colorless oil that solidified to a white

solid upon standing (1.0 g, 42%). ^{1}H NMR (500 MHz, CDCl$_3$): δ(ppm) 7.65 (s, 1H), 7.36

(s, 1H), 7.11 (dd, J = 17.6, 11.1 Hz, 1H), 6.31 (dd, J = 17.5, 11.0 Hz, 1H), 5.72 (d, J =

17.5 Hz, 1H), 5.67 (d, J = 17.6 Hz, 1H), 5.37 (d, J = 11.1 Hz, 1H), 5.16 (d, J = 11.0 Hz,

1H); ^{13}C NMR (125 MHz, CDCl$_3$): δ(ppm) 137.26, 137.21, 134.70, 133.55, 133.03,

132.59, 128.35, 126.08, 117.01, 116.36; LRMS (FAB+) (m/z): [M]$^+$ calcd. for C$_{20}$H$_{16}$Cl$_2$,

326.06; found, 326.10. IR(neat): 681.12, 880.49, 898.06, 985.63, 1029.19, 1041.91,

1216.46, 1260.44, 1372.48, 1415.59, 1472.13, 1622.27, 2987.93, 3017.88, 3086.40 cm^{-1}.

V.79
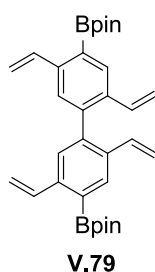
2,2'-(2,2',5,5'-tetravinyl-[1,1'-biphenyl]-4,4'-diyl)bis(4,4,5,5-tetramethyl-1,3,2-

dioxaborolane) **V.79**. To a dry 50 mL RBF was added **V.78** (0.46 g, 1.4 mmol, 1.0

equiv), freshly ground anhydrous potassium acetate (0.84 g, 8.5 mmol, 6.0 equiv), freshly

ground bis(pinacolato)diboron (2.2 g, 8.5 mmol, 6.0 equiv), XPhos (81 mg, 0.17 mmol,

12 mol%), and Pd(OAc)$_2$ (19 mg, 0.028 mmol, 2.0 mol%). The vessel was fitted with a

rubber septum and evacuated/backfilled with N$_2$ (3x) before the addition of anhydrous

dioxane (10 mL) under an N$_2$ atmosphere. The brown reaction mixture was heated to 75

°C for 19 h. Upon cooling to rt, the crude reaction mixture was filtered through a short pad of Celite (EtOAc) then concentrated onto Celite. Purification on silica gel (3 cm x 9 cm, 3% EtOAc/hexanes) afforded **V.79** as a white solid after washing with minimal hexanes (350 mg, 48%). ^{1}H NMR (300 MHz, CDCl$_3$): δ(ppm) 8.09 (s, 1H), 7.55 (dd, J = 17.5, 11.0 Hz, 1H), 7.44 (s, 1H), 6.37 (dd, J = 17.6, 11.1 Hz, 1H), 5.72 (dd, J = 17.6, 1.3 Hz, 1H), 5.66 (dd, J = 17.5, 1.4 Hz, 1H), 5.25 (dd, J = 11.1, 1.3 Hz, 1H), 5.07 (dd, J = 11.0, 1.4 Hz, 1H), 1.38 (s, 12H); ^{13}C NMR (125 MHz, CDCl$_3$): δ(ppm) 142.70, 142.22, 137.02, 134.81, 134.61, 132.86, 126.32, 115.04, 114.97, 83.98, 25.06 (C-B not observed). HRMS (FAB+) [M]$^+$ calcd. for C$_{32}$H$_{40}$B$_2$O$_4$, 510.3113; found, 510.3141. IR(neat): 854.14, 909.77, 964.87, 991.92, 1041.91, 1084.58, 1110.49, 1143.47, 1214.40, 1273.43, 1329.85, 1389.91, 1590.34, 1737.03, 2930.22, 2977.37, 3085.05 cm^{-1}.
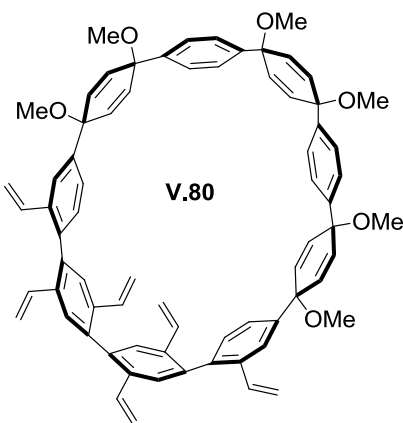
hexavinyl macrocycle **V.80**. To a dry 200 mL Schlenk flask charged with a magnetic stirbar was added dichloride **V.71** (95 mg, 0.11 mmol, 1.0 equiv), diboronate **V.79** (63 mg, 0.12 mmol, 1.1 equiv), and SPhos-Pd-G2 (75 mg, 0.33 mmol, 40 mol%). The vessel was fitted with a rubber septum and evacuated/backfilled with N$_2$ (3x) before the addition

of anhydrous dioxane (160 mL) under an N_2 atmosphere. The reaction mixture was heated to 80 °C for ca. 10 min whereupon degassed (sparged 1 h) 2 M aq K_3PO_4 (20 mL) was added via cannula. The resulting dark yellow solution was heated under N_2 for 15 h. Upon cooling to rt, the brown reaction mixture was diluted with EtOAc and water. The aqueous phase was extracted with EtOAc (2 x 50 mL) and the combined organics were washed with brine (20 mL), dried over sodium sulfate, and concentrated onto Celite. Purification on silica gel (3 cm x 6 cm, 15 – 20% THF/hexanes) afforded hexavinyl macrocycle **V.80** as a white solid (27 mg, 10%). ^{1}H NMR (500 MHz, C_6D_6, 70 °C) δ(ppm) 8.26 (br s, 2H), 7.62 (s, 2H), 7.53 – 7.39 (overlap, 10H), 7.10 – 6.97 (overlap, 4H), 6.87 – 6.78 (overlap, 4H), 6.53 - 6.40 (br m, 2H), 6.18 (s, 4H), 6.01 - 5.92 (overlap, 8H), 5.78 (d, J = 17.7 Hz, 2H), 5.59 (d, J = 17.6 Hz, 2H), 5.41 (d, J = 17.5 Hz, 2H), 5.11 (d, J = 11.0 Hz, 2H), 5.04 (d, J = 11.1 Hz, 2H), 4.86 (d, J = 11.0 Hz, 2H), 3.37 (s, 6H), 3.23 (s, 6H), 3.10 (s, 6H); ^{13}C NMR (125 MHz, C_6D_6, 70 °C) δ(ppm) 144.30, 143.63, 143.40, 140.18, 140.01, 139.62, 136.67, 136.46, 136.07, 135.71, 135.31, 134.49, 133.11, 127.28, 126.94, 126.39, 122.88, 115.62, 115.46, 115.39, 76.17, 75.00, 72.70, 52.27, 51.48, 51.20. MALDI-TOF (m/z): $[M + H]^+$ calcd. for $C_{72}H_{66}O_6$, 1027.50, found 1027.10. IR(neat): 668.11, 828.08, 904.69, 1083.50, 1226.97, 1365.37, 1462.32, 1737.13, 2854.81, 2926.83 cm^{-1}.
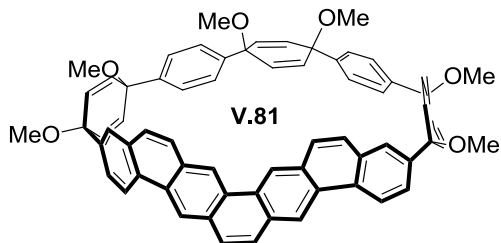
dibenzo[c,m]pentaphene macrocycle **V.81**. To a dry 4 dram vial with a septum cap and magnetic stirbar was added hexavinyl macrocycle **V.80** (32 mg, 0.031 mmol, 1.0 equiv) and Grubbs II (4.0 mg, 0.0047 mmol, 15 mol%). The vial was sealed and evacuated/backfilled with N_2 (3x) before the addition of anhydrous DCM (1.5 mL) under an N_2 atmosphere. The reaction mixture was heated to 40 ^{o}C for 90 min then concentrated onto Celite. Purification on silica gel (1 cm x 7 cm, 25 − 35% THF/hexanes) afforded dibenzo[*c,m*]pentaphene macrocycle **V.81** as a pale yellow solid, that was further purified by washing with minimal acetone (12.5 mg, 43%). ^{1}H NMR (500 MHz, CDCl$_3$): δ(ppm) 9.15 (s, 2H), 8.93 (s, 2H), 8.64 (d, *J* = 8.9 Hz, 2H), 7.89 (s, 2H), 7.81 (d, *J* = 8.9 Hz, 2H), 7.77 (dd, *J* = 8.8, 1.9 Hz, 2H), 7.25 − 7.21 (overlap, 4H), 6.60 (d, *J* = 8.5 Hz, 4H), 6.53 (d, *J* = 8.5 Hz, 4H), 6.52 − 6.48 (overlap, 2H), 6.33 (dd, *J* = 10.3, 2.2 Hz, 2H), 6.29 (dd, *J* = 10.2, 2.2 Hz, 2H), 5.91 (d, *J* = 2.2 Hz, 2H), 5.81 (d, *J* = 2.2 Hz, 2H), 5.74 (dd, *J* = 10.2, 2.2 Hz, 2H), 3.53 (s, 6H), 3.27 (s, 6H), 3.26 (s, 6H); ^{13}C NMR (125 MHz, CDCl$_3$) δ(ppm) 142.18, 140.73, 139.36, 136.25, 136.18, 133.51, 132.59, 131.90, 131.57, 131.36, 130.69, 130.41, 130.03, 129.39, 128.91, 127.56, 127.48, 126.84, 126.13, 126.11, 123.62, 122.70, 122.58, 75.95, 75.42, 71.87, 52.77, 51.85, 51.47. MALDI-TOF (*m/z*): [M - OMe]$^+$ calcd. for C$_{72}$H$_{51}$O$_5$, 911.37, found 911.74. IR(neat): 824.49, 954.80, 1076.42, 1217.26, 1375.31, 1458.12, 1738.04, 2853.55, 2923.05, 2953.07 cm^{-1}.
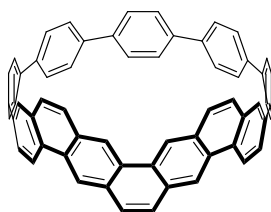
V.62

(2,11)-dibenzo[c,m]pentaphene-nanohoop **V.62**. To a dry 50 mL RBF charged with a magnetic stirbar was added dibenza[*c*,*m*]pentaphene macrocycle **V.81** (3 mg, 0.0030 mmol, 1.0 equiv). The vessel was sealed with a rubber septum and evacuated/backfilled with N_2 (3x) before adding anhydrous THF (1 mL). The solution was cooled to $-78\ ^{\circ}$C, whereupon sodium naphthalenide (0.5 mL, 0.13 mmol, 1 M in THF, 40 equiv) was added dropwise via syringe. After stirring for 30 min, a solution of I_2 (1 mL, 1 M in THF) was added via syringe and the resulting dark red solution was stirred at $-78\ ^{\circ}$C for 15 min. Sat. aq $Na_2S_2O_3$ (2 mL) was then added and the reaction mixture was allowed to warm to rt. The yellow biphasic mixture was extracted with DCM (2 x 20 mL) and the combined organics were washed with brine (10 mL), dried over sodium sulfate, and concentrated onto Celite. Purification using preparative recycling GPC (t_R = 53 min, collected on 2nd cycle) to afford (2,11)-dibenzo[*c*,*m*]pentaphene-nanohoop **V.62** (0.5 mg, 21%). ^{1}H NMR (500 MHz, CDCl$_3$): δ(ppm) 8.73 (s, 2H), 8.60 (s, 2H), 8.42 (d, *J* = 9.1 Hz, 2H), 7.84 (dd, *J* = 9.1, 2.0 Hz, 2H), 7.80 (d, *J* = 2.0 Hz, 2H), 7.73 (d, *J* = 9.2 Hz, 2H), 7.65 (s, 2H), 7.59 (d, *J* = 8.7 Hz, 4H), 7.52 (d, *J* = 9.2 Hz, 2H), 7.48 – 7.39 (overlap, 16H). MALDI-TOF (*m/z*): [M]$^+$ calcd. for $C_{60}H_{36}$, 756.28, found 756.89. IR(neat): 703.43, 811.72, 891.82, 1012.39, 1263.66, 1377.32, 1458.54, 1662.05, 1737.14, 2853.18, 2923.55 cm^{-1}.

V.6.3. Optoelectronic Characterization

Table V.3. Optical predictions for **V.61** via TD-DFT at the B3LYP/6-31G(d) level of theory.

Energy (cm⁻¹)	Wavelength (nm)	Osc. Strength	Major contributions
22181.20656	450.832103	0.0115	HOMO→LUMO (96%)
24811.39872	403.0405586	0.0033	H-1→LUMO (52%), HOMO→L+1 (29%)
26811.66752	372.9719531	0.0791	H-1→LUMO (32%), HOMO→L+1 (52%)
28019.8944	356.8892822	0.0065	H-3→LUMO (48%), HOMO→L+2 (12%), HOMO→L+3 (16%)
28171.52768	354.9683252	0.0605	H-2→LUMO (64%), HOMO→L+2 (23%)
28778.0608	347.48693	0.1244	H-3→LUMO (17%), H-1→L+1 (31%), HOMO→L+2 (20%), HOMO→L+3 (20%)
29110.36352	343.5202722	1.0903	H-2→LUMO (24%), HOMO→L+2 (34%), HOMO→L+3 (36%)
30141.1472	331.7723753	0.0736	H-4→LUMO (13%), H-2→L+1 (27%), H-1→L+2 (19%), H-1→L+3 (10%), HOMO→L+4 (15%)
30774.2968	324.9464989	1.3025	H-3→LUMO (13%), H-1→L+1 (51%), HOMO→L+3 (10%)
31045.30096	322.1099391	0.0818	H-3→L+1 (29%), H-1→L+2 (26%), H-1→L+3 (26%)
31580.05024	316.6556077	0.0998	H-2→L+1 (49%), HOMO→L+4 (15%)
31678.45056	315.6720049	0.0309	H-3→L+1 (44%), H-2→L+2 (18%), H-1→L+2 (16%)

Table V.4. Optical predictions for **V.62** via TD-DFT at the B3LYP/6-31G(d) level of theory.
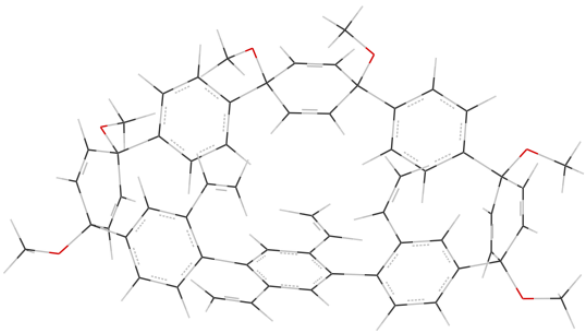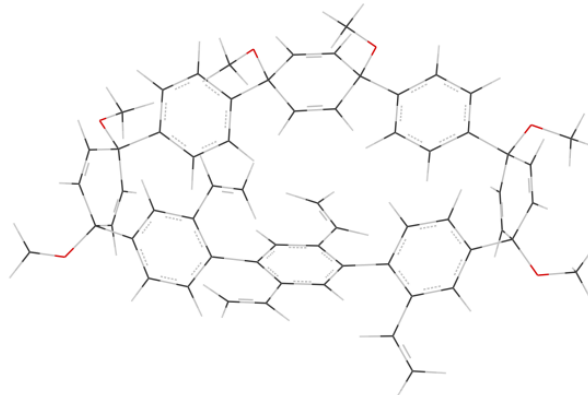
Energy (cm⁻¹)	Wavelength (nm)	Osc. Strength	Major contributions
22875.65472	437.1459581	0.0264	HOMO→LUMO (95%)
23841.9136	419.4294203	0.0025	H-1→LUMO (58%), HOMO→L+1 (29%)
26418.8728	378.5172848	0.0002	H-2→LUMO (18%), H-1→L+1 (65%), HOMO→L+2 (12%)
26745.5296	373.8942601	0.0963	H-1→LUMO (34%), HOMO→L+1 (63%)
27694.85072	361.0779528	0.0006	H-4→LUMO (15%), H-2→LUMO (23%), H-1→L+3 (10%), HOMO→L+2 (25%), HOMO→L+4 (11%)
28016.66816	356.9303795	0.3326	H-3→LUMO (93%)
28222.34096	354.3292179	0.0069	H-4→LUMO (15%), H-3→L+1 (10%), H-2→LUMO (29%), H-1→L+3 (10%), HOMO→L+2 (20%), HOMO→L+4 (10%)

28750.63776	347.8183713	0.7339	HOMO→L+3 (91%)
29091.81264	343.7393236	1.5827	H-2→LUMO (26%), H-1→L+1 (29%), HOMO→L+2 (38%)
29331.36096	340.9320152	0.0094	H-2→L+1 (39%), H-1→L+2 (49%)
30120.9832	331.9944749	0.028	H-3→L+1 (72%), H-1→L+3 (11%)
30230.67536	330.7898312	0.2072	H-4→LUMO (25%), H-1→L+3 (60%)

V.6.4. Computational Analysis

V.6.4.1. Vinylated Macrocycle Atropisomers

Table V.5. Calculated energies of **V.73** conformers (RB97D/6-31G(d)).

Atropisomer	Energy (kcal/mol)	Relative Energy (kcal/mol)
	-1793331.913	0.00
	-1793330.180	1.73

238
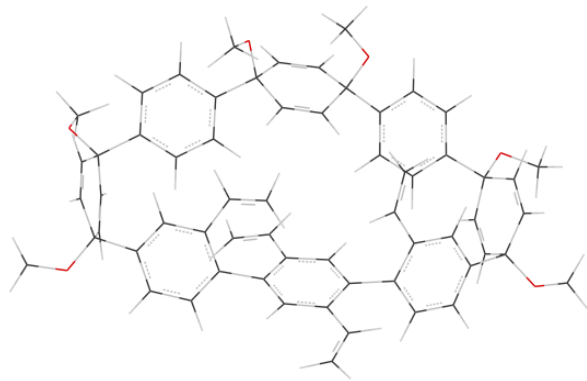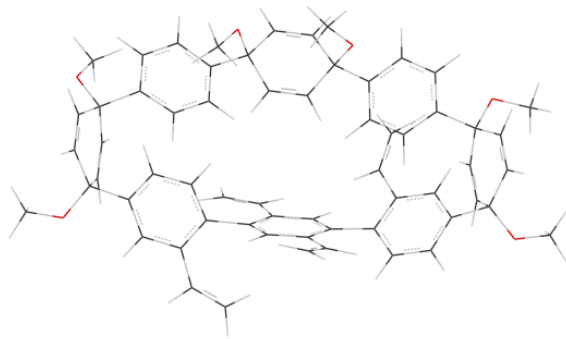
-1793330.058	1.85
-1793328.902	3.01
-1793328.577	3.33
-1793327.840	4.07
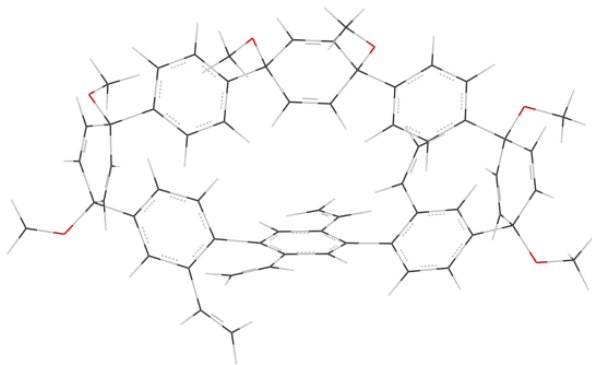
239
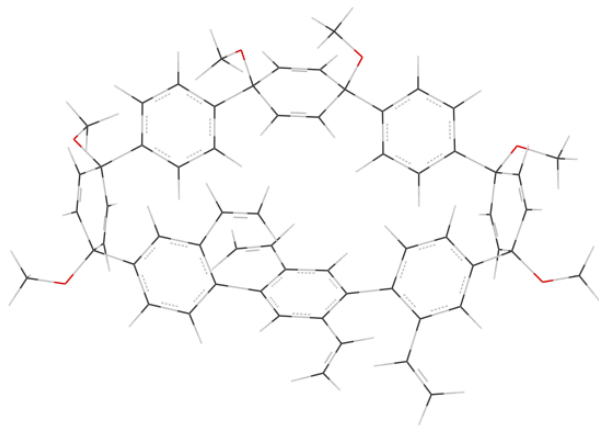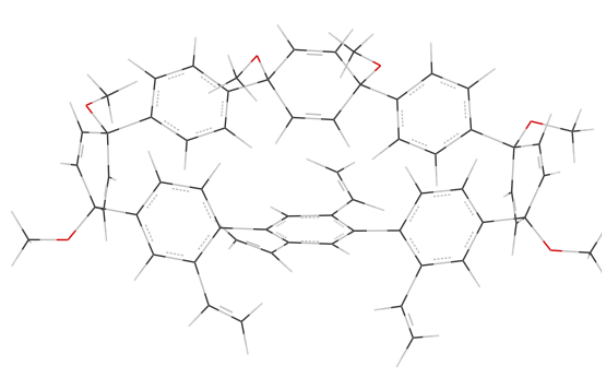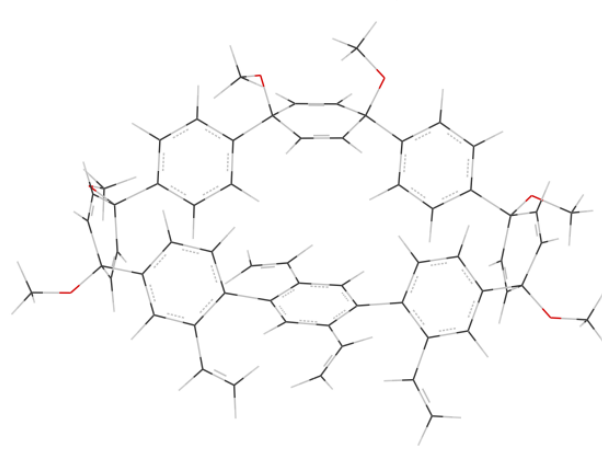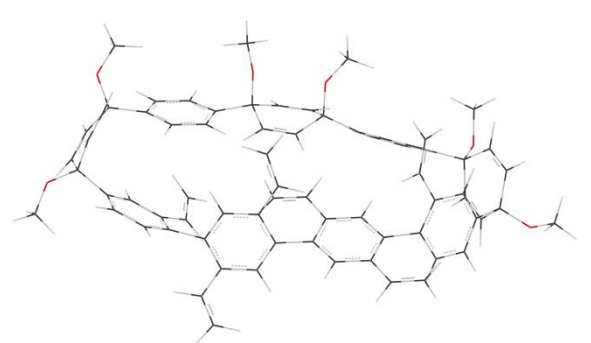
	Energy	Relative Energy
	-1793327.628	4.29
	-1793326.813	5.10

Table V.6. Calculated energies of **V.80** conformers (RB97D/6-31G(d)).

Atropisomer	Energy (kcal/mol)	Relative Energy (kcal/mol)
	-2036217.532	0.00
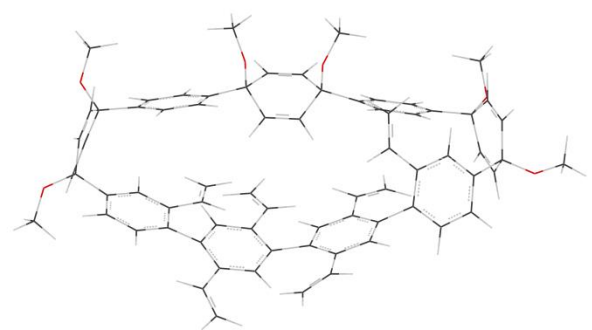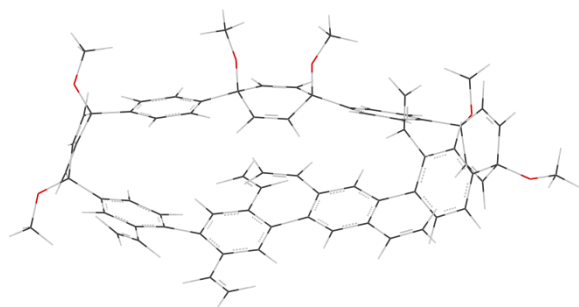
-2036216.478	1.05
-2036216.28	1.25
-2036216.259	1.27
-2036216.175	1.35
-2036215.683	1.85
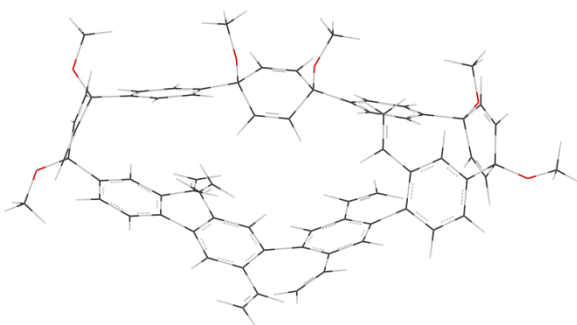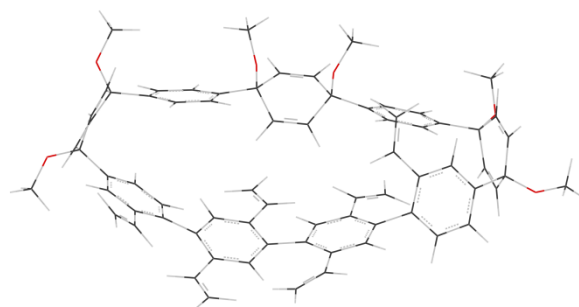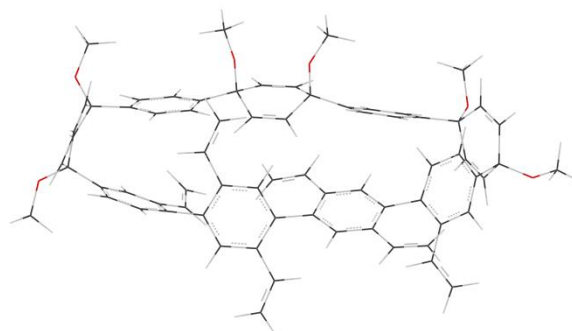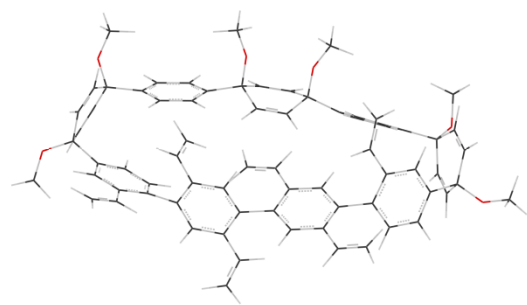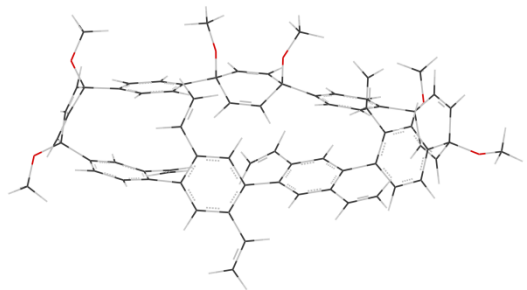
	-2036215.614	1.91
	-2036215.604	1.92
	-2036215.562	1.97
	-2036214.891	2.64
	-2036214.850	2.68
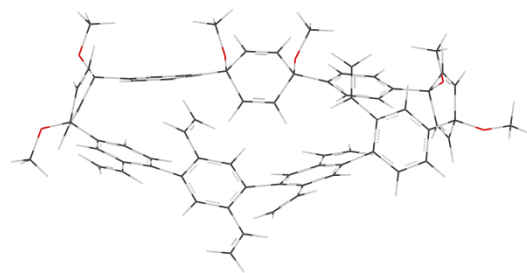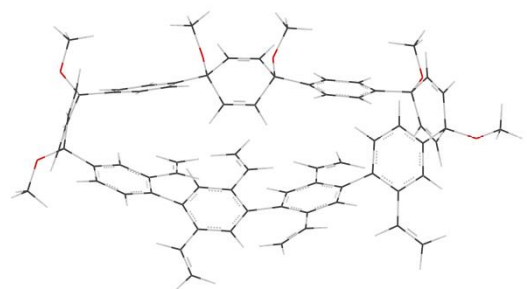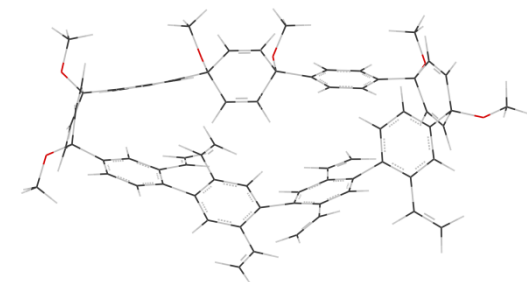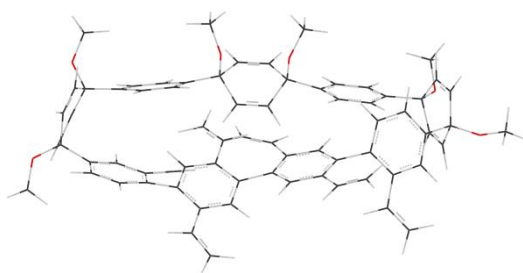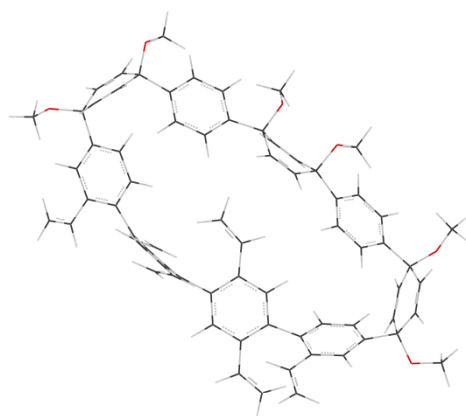
-2036214.755	2.78
-2036214.706	2.83
-2036214.664	2.87
-2036214.173	3.36
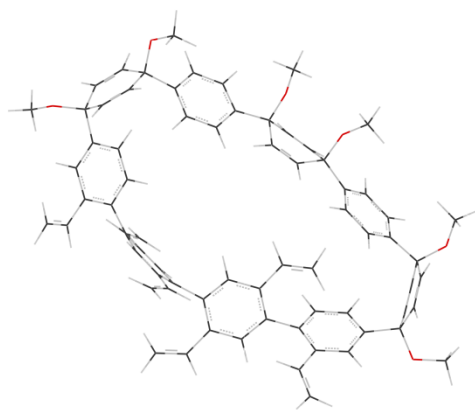
243
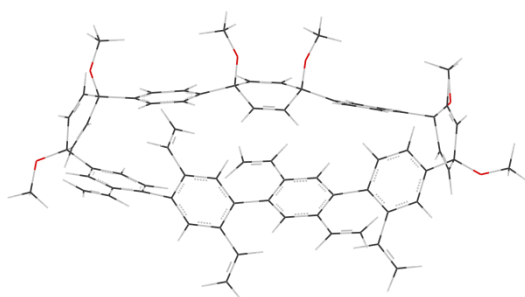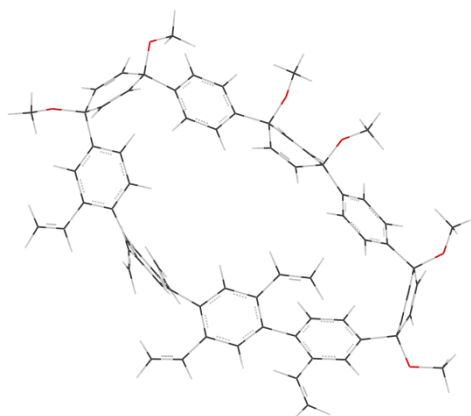
| | -2036214.102 | 3.43 |

V.6.4.2. Homodesmotic Reactions
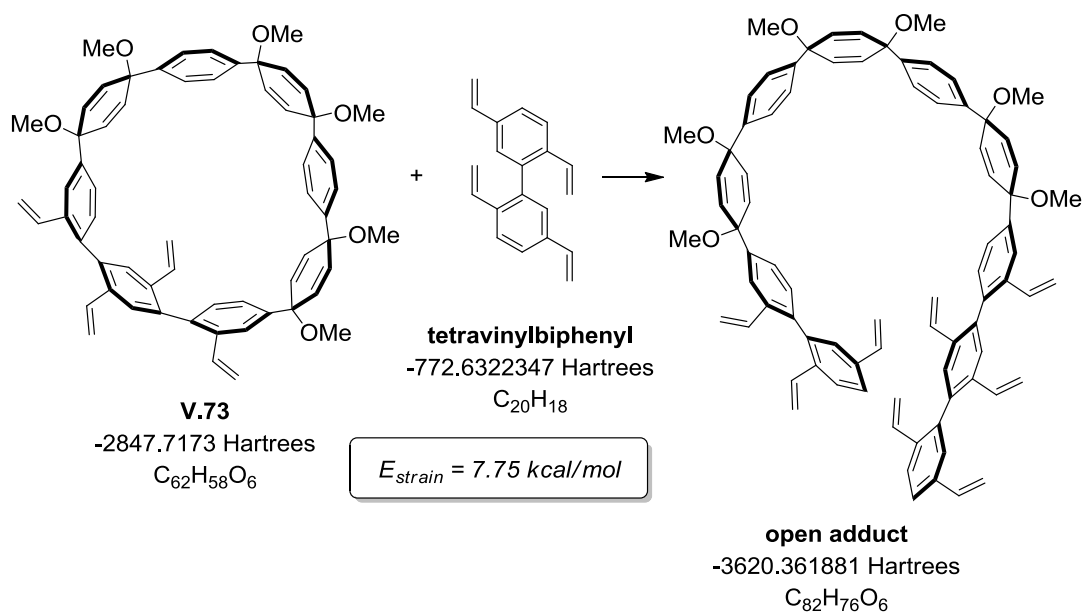
Scheme V.29. Homodesmotic reaction to access strain energy of **V.73** calculated at the ωB97x-D/6-31G(d) level of theory.

244
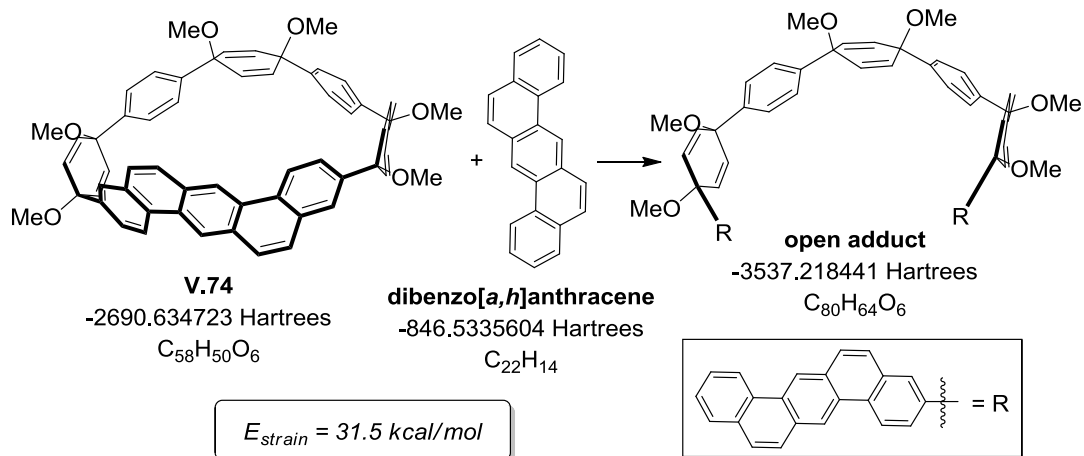
Scheme V.30. Homodesmotic reaction to access strain energy of **V.74** calculated at the ωB97x-D/6-31G(d) level of theory.
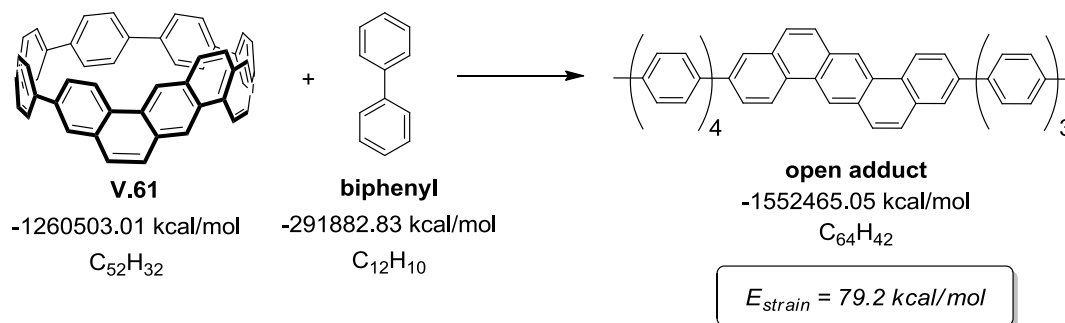
Scheme V.31. Homodesmotic reaction to access strain energy of **V.61** calculated at the ωB97x-D/6-31G(d) level of theory.
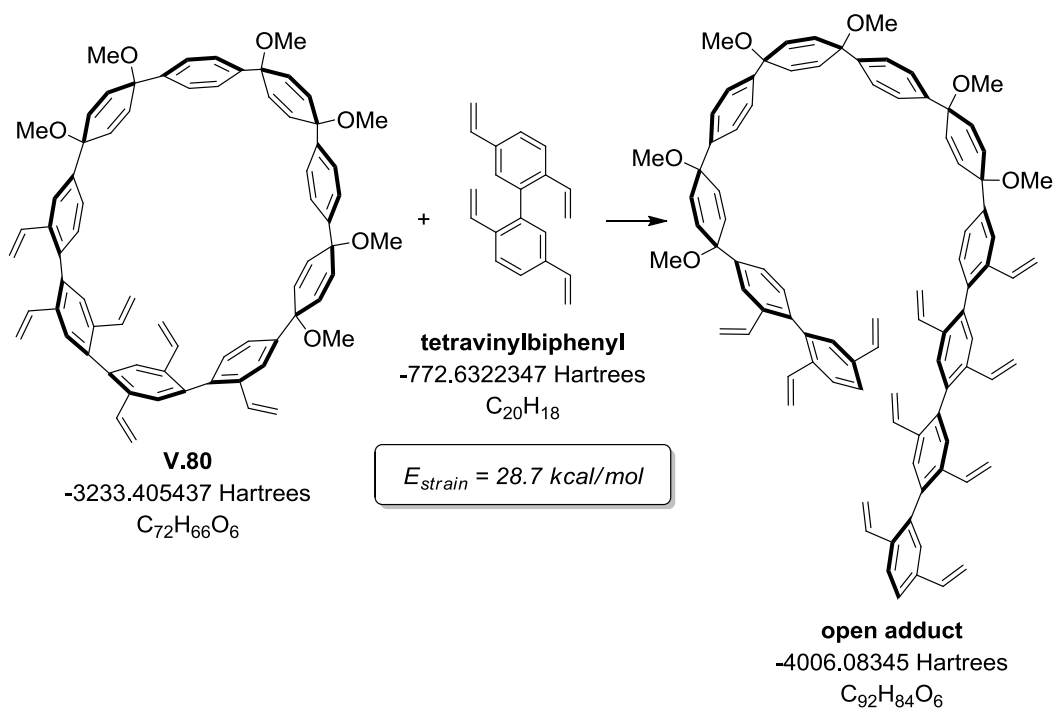
Scheme V.32. Homodesmotic reaction to access strain energy of **V.80** calculated at the ωB97x-D/6-31G(d) level of theory.
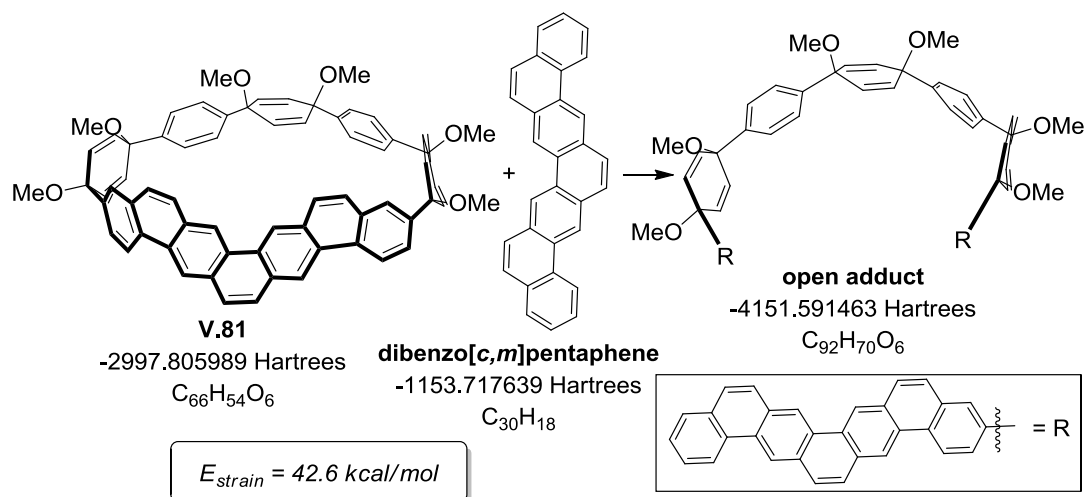
Scheme V.33. Homodesmotic reaction to access strain energy of **V.81** calculated at the ωB97x-D/6-31G(d) level of theory.
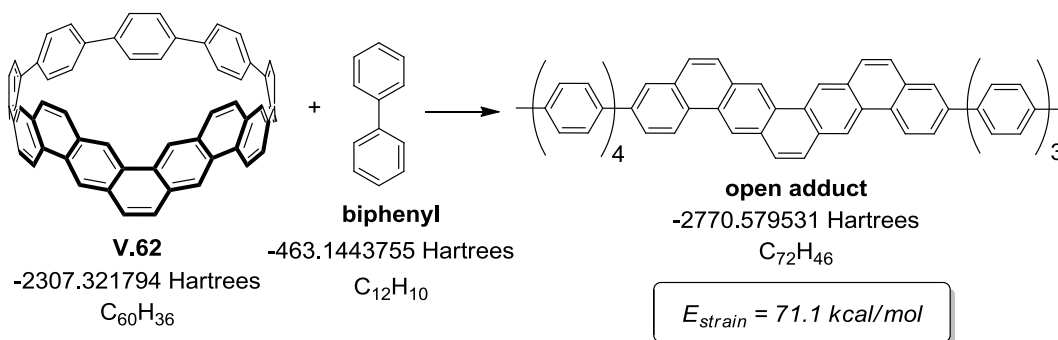
Scheme V.34. Homodesmotic reaction to access strain energy of **V.62** calculated at the ωB97x-D/6-31G(d) level of theory.

V.6.5. X-ray Crystallographic Analysis

Diffraction intensities were collected at 173 K on a Bruker Apex2 Duo CCD diffractometer with a micro-focus Incoatec *IμS* Cu source, CuKα radiation, λ= 1.54178 Å. Space groups were determined based on systematic absences (**V.61**) and intensity statistics (**V.62**). Absorption corrections were applied by SADABS.[58] Structures were solved by direct methods and Fourier techniques and refined on F^2 using full matrix least-squares procedures. All non-H atoms were refined with anisotropic thermal parameters. H atoms in all structures were refined in calculated positions in a rigid group model. Single crystals of racemic **V.61** were grown from slow evaporation of a pentane/THF solution. Single crystals of **V.62** were grown from slow evaporation of a pentane/benzene solution. ORTEP representations (Figures **V.12** and **V.13**) and relevant X-ray crystallographic data (Tables **V.7.** and **V.8**) are presented below.
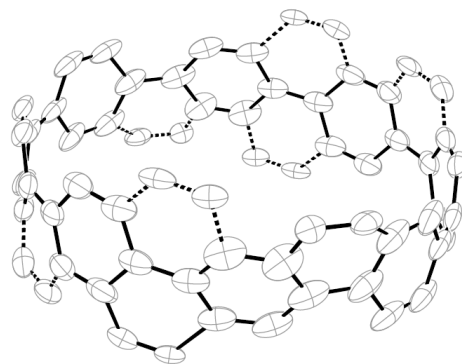
Figure V.12. ORTEP representation (thermal ellipsoids shown at 30% probability) of **V.61** with one possible orientation of the disordered dibenzo[*a,h,*]anthracene unit indicated with solid lines. Dotted lines represent all other possible orientations of this group. Hydrogen atoms are omitted for clarity.

The main molecule in **V.61** is disordered over several different positions having different orientation of two additional C_6-rings. The structure was determined in a centro-symmetrical space group with centro-symmetrical main molecules disordered over four different positions. Two additional THF solvent molecules fill out a space inside the main molecule. Positions of some weak peaks (less 1 e$Å^3$) on the residual density map show that disorder of the main molecule in the crystal structure could be even more complicated than given in the final refined structure and may consist of eight positions of the main molecule with different orientations. Some of the disordered C_6-rings in **V.61** were refined with restrictions; the distance of 1.39 Å was used in the refinement as a target for the corresponding C-C bonds.

Table V.7. X-ray crystallographic parameters for **V.61**.

Identification code	cu_jasti32_0m_a
Empirical formula	$C_{60}H_{48}O_2$
Formula weight	800.98
Temperature/K	173(2)
Crystal system	monoclinic
Space group	$P2_1/c$
a/Å	13.3012(7)
b/Å	9.9339(5)
c/Å	17.0395(6)
α/°	90
β/°	110.381(3)
γ/°	90
Volume/Å^3	2110.53(18)
Z	2
ρ_{calc}g/cm^3	1.26
μ/mm^{-1}	0.572
F(000)	848
Crystal size/mm^3	$0.150 \times 0.120 \times 0.100$
Radiation	CuKα ($\lambda = 1.54178$)
2Θ range for data collection/°	7.09 to 133.284
Index ranges	$-15 \le h \le 14, -10 \le k \le 11, -20 \le l \le 19$
Reflections collected	11828
Independent reflections	3706 [$R_{int} = 0.0426$, $R_{sigma} = 0.0372$]
Data/restraints/parameters	3706/34/334
Goodness-of-fit on F^2	1.015
Final R indexes [I>=2σ (I)]	$R_1 = 0.1024$, w$R_2 = 0.3416$
Final R indexes [all data]	$R_1 = 0.1330$, w$R_2 = 0.4100$
Largest diff. peak/hole / e Å^{-3}	0.31/-0.38
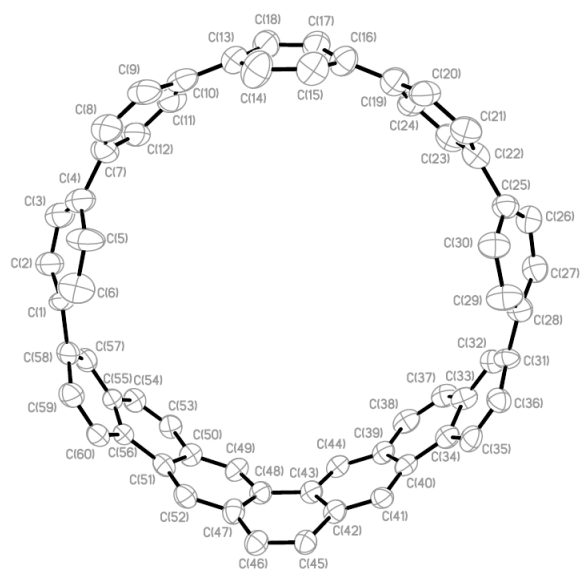
Figure V.13. ORTEP representation (thermal ellipsoids shown at 30% probability) of **V.62**. Hydrogen atoms are omitted for clarity.

In the crystal structure of **V.62** there are two benzene and five pentane solvent molecules which fill out an empty space in the packing. Two benzene molecules were located and refined and five highly disordered pentane solvent molecules were treated with SQUEEZE.[59] Correction of the X-ray data by SQUEEZE, 557 electron/cell, is higher versus the required values of 420 electron/cell for ten pentane molecules in the full unit cells indicating that number of solvent molecules could be slightly bigger and benzene and pentane molecules could share the same disordered positions as well. Crystals of **V.62** suitable for data collection were very small and diffraction at high angles was very weak. Even using a strong micro-focus Incoatec *IμS* Cu source intensities were collected only up to $2\theta_{max} = 50.256°$. The collected data provided an appropriate number of measured reflections per refined parameters. All calculations were performed with the Bruker SHELXL-2013 package.[60]

Table V.8. X-ray crystallographic parameters for **V.62**.

Identification code	cu_jasti43_0m_sqd
Empirical formula	$C_{78.5}H_{72}$
Formula weight	1015.36
Temperature/K	173(2)
Crystal system	triclinic
Space group	P-1
a/Å	15.8435(7)
b/Å	19.3722(9)
c/Å	20.9937(10)
α/°	94.124(3)
β/°	90.490(3)
γ/°	105.769(3)
Volume/Å^3	6182.3(5)
Z	4
ρ_{calc}g/cm^3	1.091
μ/mm^{-1}	0.46
F(000)	2172
Crystal size/mm^3	$0.100 \times 0.070 \times 0.020$
Radiation	CuKα ($\lambda = 1.54178$)
2Θ range for data collection/°	4.222 to 100.512
Index ranges	$-15 \leq h \leq 15, -19 \leq k \leq 19, -20 \leq l \leq 20$
Reflections collected	45042
Independent reflections	12774 [$R_{int} = 0.0802$, $R_{sigma} = 0.1146$]
Data/restraints/parameters	12774/0/1165
Goodness-of-fit on F^2	1.009
Final R indexes [I>=2σ (I)]	$R_1 = 0.0807$, w$R_2 = 0.2119$
Final R indexes [all data]	$R_1 = 0.1678$, w$R_2 = 0.2404$
Largest diff. peak/hole / e Å^{-3}	0.41/-0.24

Table V.9. Dihedral angles between adjacent rings from X-ray crystal structure of **V.62**.

Center C-C Bond[a]	Molecule 1 (deg)[b]	Molecule 2 (deg)[b]
C(1) – C(58)	8.9	28.3
C(4) – C(7)	36.5	39.4
C(10) – C(13)	34.0	23.9
C(16) – C(19)	20.4	25.0
C(22) – C(25)	34.8	38.5
C(28) – C(31)	35.6	25.5
C(34) – C(40)	7.2	0.6
C(43) – C(48)	3.1	2.9
C(51) – C(56)	5.3	1.9
Average	20.6	20.6

[a]Measured dihedral angles are defined around the given central C-C bonds. [b]Angles are an average of the two dihedral angles defined by each C-C bond.

V.6.6. Selected NMR Spectra
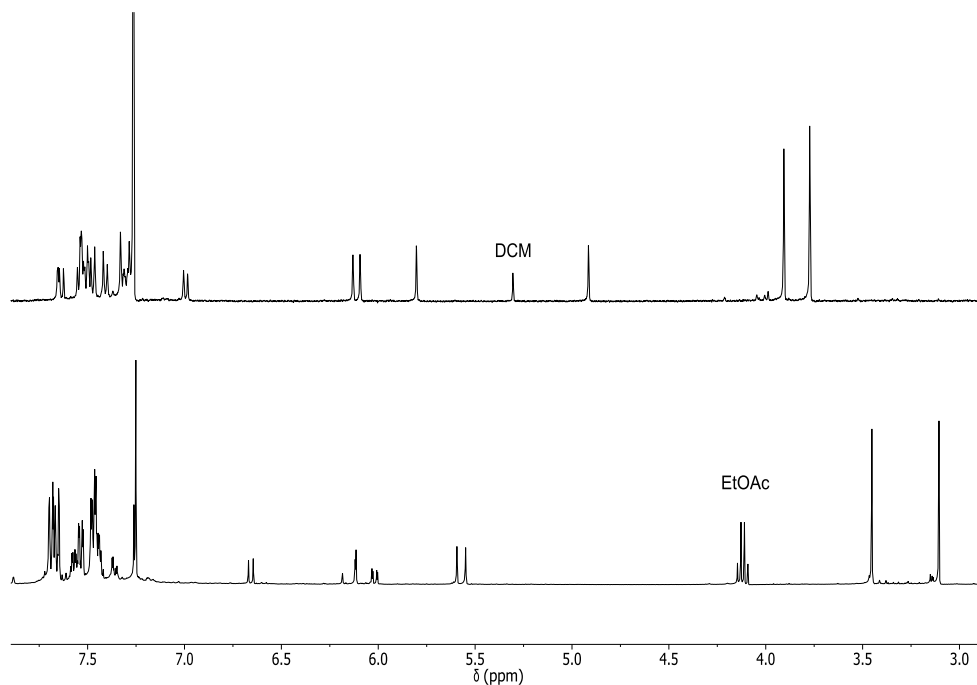
Figure V.14. ^{1}H NMR spectra of 5-*exo-trig* cyclization of **V.36** before (bottom) and after (top) SiO$_2$ chromatography in CDCl$_3$ (400 MHz).
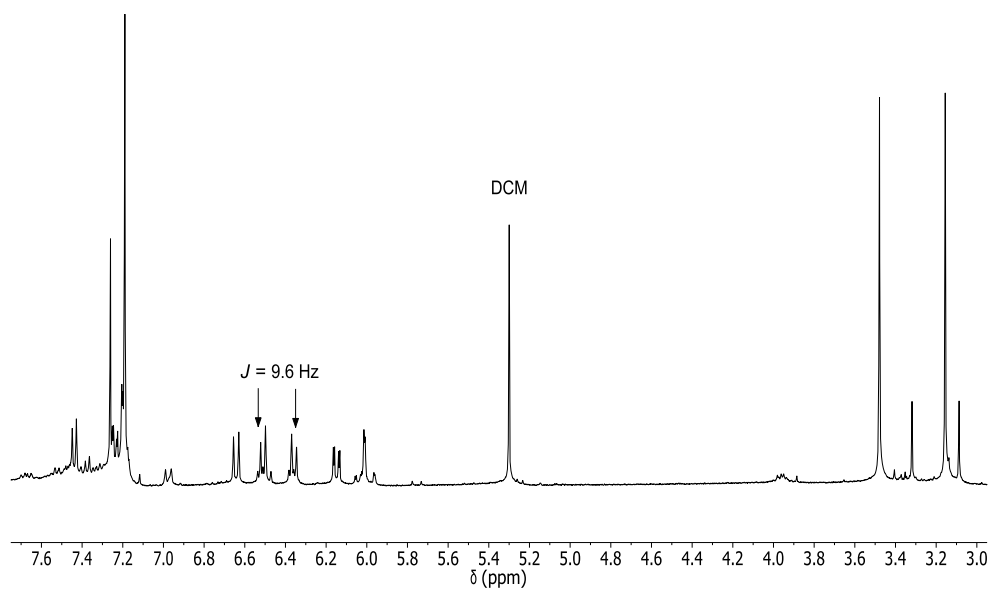
Figure V.15. Crude ^{1}H NMR spectrum (CDCl$_3$) of **V.40** after treating **V.39** with 10 mol% Grubbs II (400 MHz).
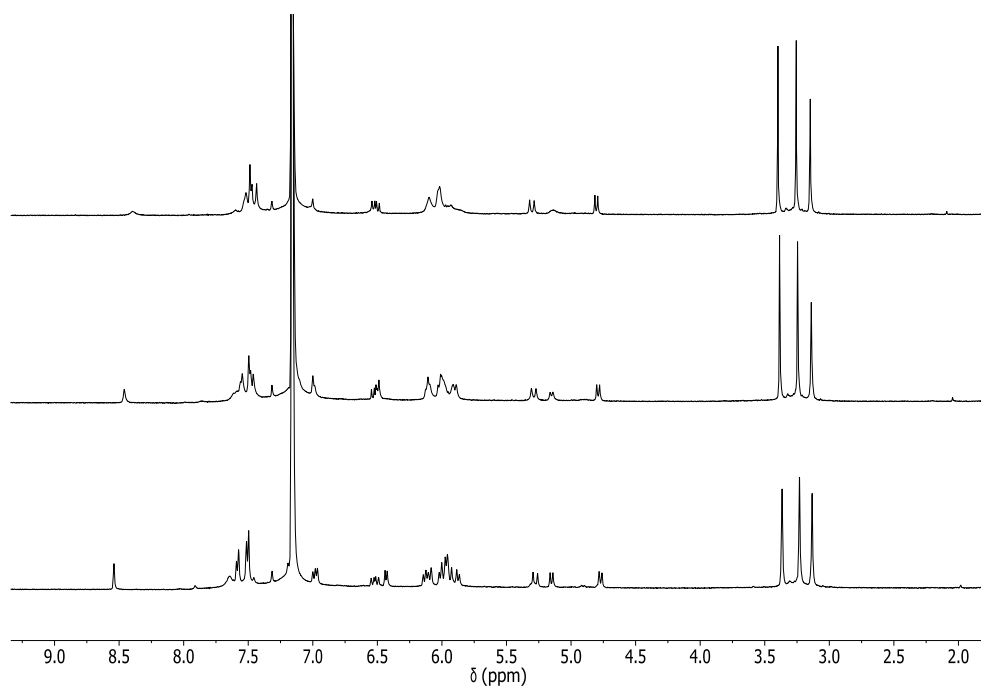
Figure V.16. ^{1}H NMR spectra of **V.73** at 25 ^{o}C, 50 ^{o}C, and 70 ^{o}C in C$_6$D$_6$ (500 MHz).
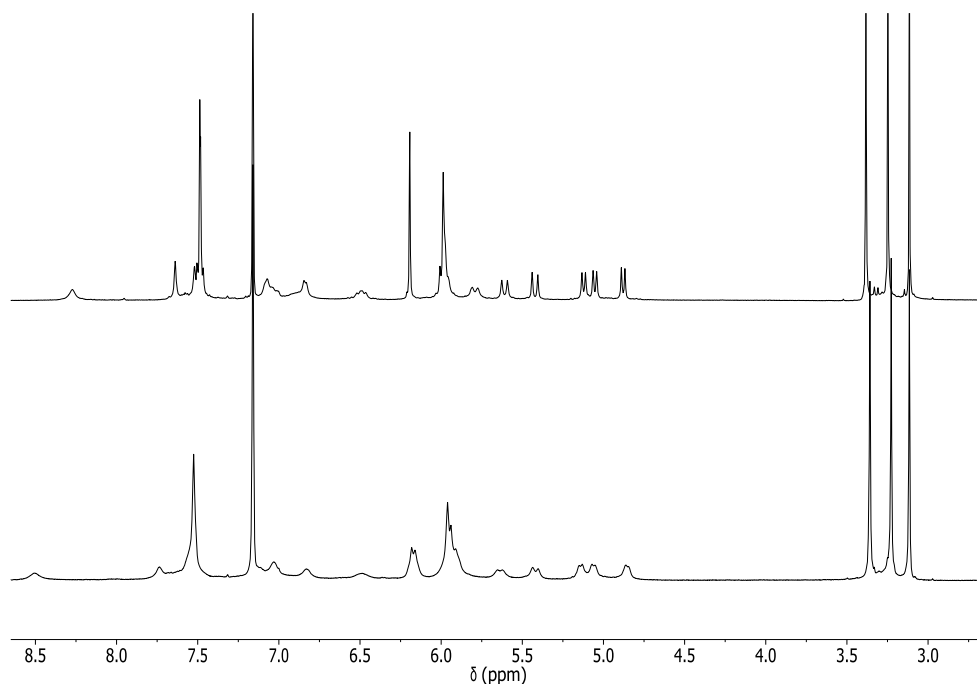
Figure V.17. ^{1}H NMR spectra of **V.80** at 25 $^\circ$C and 70 $^\circ$C in C_6D_6 (500 MHz).

V.7. Conclusion

In this chapter, we have detailed our efforts towards the synthesis of [*n*]cyclophenacenes thus far. Our studies are all based on a ring-closing metathesis strategy, stemming from an appropriately functionalized [*n*]CPP or [*n*]CPP macrocyclic precursor. As RCM offers mild, redox-neutral conditions, we envisioned building in macrocyclic strain via an [*n*]CPP synthesis, with RCM acting as a strain-free ring-forming method. We soon discovered that simply synthesizing the necessary model substrates was not as trivial as originally expected, and even a simple vinyl group could cause intractable decomposition even before a macrocycle was reached. We were later able to validate RCM methodology as a viable strategy towards [*n*]cyclophenacenes in the synthesis of (3,10)-dibenzo[*a,h*]anthracenyl-nanohoop **V.61** and (2,11)-

254

dibenzo[*c,m*]pentapheneyl-nanohoop **V.62**. Importantly, we found that even in the presence of strained 1,4 -dimethoxycyclohexa-2,5-dienes, Grubbs II only leads to the desired ring-closed product, without concomitant decomposition. Then, alluding to work previously discussed in Chapter **II**, several allylated intermediates were subjected to olefin isomerization conditions, only to find that the more highly allylated compounds decomposed under the conditions employed. In conjunction with the future work associated with Chapter **II** in developing methods to access the functionalized 1,4-syn-dimethoxycyclohexa-2,5-dienes, the synthesis of [*n*]cyclophenacenes also relies on ongoing work to efficiently incorporate vinyl group surrogates and cleanly affect their transformation to olefins capable of undergoing RCM.

REFERENCES CITED

Chapter I

1.   Hoffmann, R., Molecular Beauty. *J Aesthetics Art Criticism* **1990,** *48*, 191-204.

2.   Hoffmann, R.; Hopf, H., Learning from Molecules in Distress. *Angew. Chem. Int. Ed.* **2008,** *47*, 4474-4481.

3.   Eaton, P. E.; Cole, T. W., The Cubane System. *J. Am. Chem. Soc.* **1964,** *86*, 962-964.

4.   Paquette, L. A.; Ternansky, R. J.; Balogh, D. W.; Kentgen, G., Total synthesis of dodecahedrane. *J. Am. Chem. Soc.* **1983,** *105*, 5446-5450.

5.   Woodward, R. B.; Cava, M. P.; Ollis, W. D.; Hunger, A.; Daeniker, H. U.; Schenker, K., The Total Synthesis Of Styrchnine. *J. Am. Chem. Soc.* **1954,** *76*, 4749-4751.

6.   Eschenmoser, A.; Wintner, C., Natural product synthesis and vitamin B12. *Science* **1977,** *196*, 1410-1420.

7.   Nicolaou, K. C.; Petasis, N. A.; Zipkin, R. E., The endiandric acid cascade. Electrocyclizations in organic synthesis. 4. "Biomimetic" approach to endiandric acids A-G. Total synthesis and thermal studies. *J. Am. Chem. Soc.* **1982,** *104*, 5560-5562.

8.   Trauner, D., Finding function and form. *Nat. Prod. Rep.* **2014,** *31*, 411-413.

9.   Jasti, R.; Bertozzi, C. R., Progress and challenges for the bottom-up synthesis of carbon nanotubes with discrete chirality. *Chem. Phys. Lett.* **2010,** *494*, 1-7.

10.   Tian, X.; Jasti, R., Synthesis of Cycloparaphenylenes: The Shortest-Possible Segments of Armchair Carbon Nanotubes. In *Fragments of Fullerenes and Carbon Nanotubes: Designed Synthesis, Unusual Reactions, and Coordination Chemistry*, Petrukhina, M. A.; Scott, L. T., Eds. Wiley: 2011.

11.   Hirst, E. S.; Jasti, R., Bending Benzene: Syntheses of [*n*]Cycloparaphenylenes. *J. Org. Chem.* **2012,** *77*, 10473-10478.

12.   Parekh, V. C.; Guha, P. C., Synthesis of *p,p*'-diphenylene disulfide. *J. Indian. Chem. Soc.* **1934,** *11*, 95-100.

13.   Jasti, R.; Chattacharjee, J.; Neaton, J. B.; Bertozzi, C. R., Synthesis, Characterization, and Theory of [9]-, [12]-, and [18]Cycloparaphenylene: Carbon Nanohoop Structures. *J. Am. Chem. Soc.* **2008,** *130*, 17646-17647.

14.   Barth, W. E.; Lawton, R. G., Dibenzo[*ghi,mno*]fluoranthene. *J. Am. Chem. Soc.* **1966,** *88*, 380-381.

15.   Lawton, R. G.; Barth, W. E., Synthesis of corannulene. *J. Am. Chem. Soc.* **1971,** *93*, 1730-1745.

16.   Scott, L. T.; Cheng, P.-C.; Hashemi, M. M.; Bratcher, M. S.; Meyer, D. T.; Warren, H. B., Corannulene. A Three-Step Synthesis. *J. Am. Chem. Soc.* **1997,** *119*, 10963-10968.

17.   Butterfield, A. M.; Bruno, G.; Siegel, J. S., Kilogram-Scale Production of Corannulene. *Org. Process Res. Dev.* **2012,** *16*, 664-676.

18.   Iijima, S., Helical microtubulues of graphitic carbon. *Nature* **1991,** *354*, 56-58.

19.   Prasek, J.; Drbohlavova, J.; Chomoucka, J.; Hubalek, J.; Jasek, O.; Adam, V.; Kizek, R., Methods for carbon nanotubes synthesis-review. *J. Mater. Chem.* **2011,** *21*, 15872-15884.

20.   Kroto, H. W.; Heath, J. R.; O'Brien, S. C.; Curl, R. F.; Smalley, R. E., C60: Buckminsterfullerene. *Nature* **1985,** *318*, 162-163.

21.   Scott, L. T.; Boorum, M. M.; McMahon, B. J.; Hagen, S.; Mack, J.; Blank, J.; Wegner, H.; de Meijere, A., A Rational Chemical Synthesis of C60. *Science* **2002,** *295*, 1500-1503.

22.   Tsefrikas, V. M.; Scott, L. T., Geodesic Polyarenes by Flash Vacuum Pyrolysis. *Chem. Rev.* **2006,** *106*, 4868-4884.

23.   Scott, L. T., Polycyclic Aromatic Hydrocarbon Bowls, Baskets, Balls, and Tubes: Challenging Targets for Chemical Synthesis. *Polycyclic Aromat. Compd.* **2010,** *30*, 247-259.

24.   Steinberg, B.; Scott, L., New strategies for synthesizing short sections of carbon nanotubes. *Angew. Chem. Int. Ed.* **2009,** *48*, 5400-5402.

25.   Scott, L. T., Conjugated Belts and Nanorings with Radially Oriented p Orbitals. *Angew. Chem. Int. Ed.* **2003,** *42*, 4133-4135.

26.   Nishiuchi, T.; Feng, X.; Enkelmann, V.; Wagner, M.; Müllen, K., Three-Dimensionally Arranged Cyclic p-Hexaphenylbenzene: Toward a Bottom-Up Synthesis of Size-Defined Carbon Nanotubes. *Chem. Eur. J.* **2012,** *18*, 16621-16625.

27.   Schwab, M. G.; Narita, A.; Hernandez, Y.; Balandina, T.; Mali, K. S.; De Feyter, S.; Feng, X.; Müllen, K., Structurally Defined Graphene Nanoribbons with High Lateral Extension. *J. Am. Chem. Soc.* **2012,** *134*, 18169-18172.

28.   Chen, L.; Hernandez, Y.; Feng, X.; Müllen, K., From Nanographene and Graphene Nanoribbons to Graphene Sheets: Chemical Synthesis. *Angew. Chem. Int. Ed.* **2012,** *51*, 7640-7654.

29.   Talirz, L.; Söde, H.; Cai, J.; Ruffieux, P.; Blankenburg, S.; Jafaar, R.; Berger, R.; Feng, X.; Müllen, K.; Passerone, D.; Fasel, R.; Pignedoli, C. A., Termini of Bottom-Up Fabricated Graphene Nanoribbons. *J. Am. Chem. Soc.* **2013,** *135*, 2060-2063.

30.   Kunz, H.; Müllen, K., Natural Product and Material Chemistries—Separated Forever? *J. Am. Chem. Soc.* **2013,** *135*, 8764-8769.

31.   Friederich, R.; Nieger, M.; Vögtle, F., Auf dem Weg zu makrocyclischen para-Phenylenen. *Chem. Ber.* **1993,** *126*, 1723-1732.

32.   Omachi, H.; Segawa, Y.; Itami, K., Synthesis of Cycloparaphenylenes and Related Carbon Nanorings: A Step toward the Controlled Synthesis of Carbon Nanotubes. *Acc. Chem. Res.* **2012**, 1378-1389.

33. Kammermeier, S.; Jones, P. G.; Herges, R., Ring-Expanding Metathesis of Tetradehydro-anthracene—Synthesis and Structure of a Tubelike, Fully Conjugated Hydrocarbon. *Angew. Chem. Int. Ed.* **1996,** *35*, 2669-2671.

34. Kammermeier, S.; Jones, P. G.; Herges, R., Beltlike Aromatic Hydrocarbons by Metathesis Reaction with Tetradehydrodianthracene. *Angew. Chem. Int. Ed.* **1997,** *36*, 2200-2202.

35. Nakamura, E.; Tahara, K.; Matsuo, Y.; Sawamura, M., Synthesis, Structure, and Aromaticity of a Hoop-Shaped Cyclic Benzenoid [10]Cyclophenacene. *J. Am. Chem. Soc.* **2003,** *125*, 2834-2835.

36. Matsuo, Y.; Tahara, K.; Sawamura, M.; Nakamura, E., Creation of Hoop- and Bowl-Shaped Benzenoid Systems by Selective Detraction of [60]Fullerene Conjugation. [10]Cyclophenacene and Fused Corannulene Derivatives. *J. Am. Chem. Soc.* **2004,** *126*, 8725-8734.

37. Kawase, T.; Darabi, H. R.; Oda, M., Cyclic [6]- and [8]Paraphenylacetylenes. *Angew. Chem. Int. Ed.* **1996,** *35*, 2664-2666.

38. Srinivasan, M.; Sankararaman, S.; Hopf, H.; Varghese, B., Synthesis of Buta-1,3-diyne-Bridged Macrocycles with (Z)-1,4-Diethynyl1,4-dimethoxycyclohexa-2,5-diene as the Building Block. *Eur. J. Org. Chem.* **2003**, 660-665.

39. Alonso, F.; Yus, M., Reactivity of 3,6-dimethoxy-3,6-dimethylcyclohexa-1,4-diene (Part 2). Regioselective arylation of electron-rich aromatic compounds. *Tetrahedron* **1991,** *47*, 313-316.

40. Morrow, G. W.; Schwind, B., Syntheses of Para-Terphenyl via Reductive Deoxygenation of Quinol Derivatives. *Synth. Commun.* **1995,** *25*, 269-276.

41. Liu, H.-J.; Yip, J.; Shia, K.-S., Reductive cleavage of benzyl ethers with lithium naphthalenide. A convenient method for debenzylation. *Tetrahedron Lett.* **1997,** *38*, 2253-2256.

42. Iwamoto, T.; Watanabe, Y.; Sakamoto, Y.; Suzuki, T.; Yamago, S., Selective and Random Syntheses of [*n*]Cycloparaphenylenes (*n* = 8–13) and Size Dependence of Their Electronic Properties. *J. Am. Chem. Soc.* **2011,** *133*, 8354-8361.

43. Wong, B. M., Optoelectronic Properties of Carbon Nanorings: Excitonic Effects from Time-Dependent Density Functional Theory. *J. Phys. Chem. C* **2009,** *113*, 21921-21927.

44. Segawa, Y.; Fukazawa, A.; Matsuura, S.; Omachi, H.; Yamaguchi, S.; Irle, S.; Itami, K., Combined experimental and theoretical studies on the photophysical properties of cycloparaphenylenes. *Org. Biomol. Chem.* **2012,** *10*, 5979-5984.

45. Sisto, T. J.; Golder, M. R.; Hirst, E. S.; Jasti, R., Selective Synthesis of Strained [7]Cycloparaphenylene: An Orange-Emitting Fluorophore. *J. Am. Chem. Soc.* **2011,** *133*, 15800-15802.

46. Sisto, T. J.; Tian, X.; Jasti, R., Synthesis of Tetraphenyl-Substituted [12]Cycloparaphenylene: Toward a Rationally Designed Ultrashort Carbon Nanotube. *J. Org. Chem.* **2012,** *77*, 5857-5860.

47. Xia, J.; Bacon, J. W.; Jasti, R., Gram-Scale Synthesis and Crystal Structures of [8]- and [10]CPP, and the Solid-State Structure of C60@[10]CPP. *Chem. Sci.* **2012,** *3*, 3018-3021.

48. Xia, J.; Jasti, R., Synthesis, Characterization, and Crystal Structure of [6]Cycloparaphenylene. *Angew. Chem. Int. Ed.* **2012,** *51*, 2474-2476.

49. Xia, J.; Golder, M. R.; Foster, M. E.; Wong, B. M.; Jasti, R., Synthesis, Characterization, and Computational Studies of Cycloparaphenylene Dimers. *J. Am. Chem. Soc.* **2012,** *134*, 19709-19715.

50. Darzi, E. R.; Sisto, T. J.; Jasti, R., Selective Syntheses of [7]–[12]Cycloparaphenylenes Using Orthogonal Suzuki–Miyaura Cross-Coupling Reactions. *J. Org. Chem.* **2012,** *77*, 6624-6628.

51. Golder, M. R.; Wong, B. M.; Jasti, R., Photophysical and theoretical investigations of the [8]cycloparaphenylene radical cation and its charge-resonance dimer. *Chem. Sci.* **2013,** *4*, 4285-4291.

52. Evans, P. J.; Darzi, E. R.; Jasti, R., Efficient Room-Temperature Synthesis of a Highly Strained Carbon Nanohoop Fragment of Buckminsterfullerene. *Nature Chem.* **2014,** *6*, 404-408.

53.   Omachi, H.; Matsuura, S.; Segawa, Y.; Itami, K., A Modular and Size-Selective Synthesis of [*n*]Cycloparaphenylenes: A Step toward the Selective Synthesis of [*n,n*] Single-Walled Carbon Nanotubes. *Angew. Chem. Int. Ed.* **2010**, *49*, 10202-10205.

54.   Yamago, S.; Watanabe, Y.; Iwamoto, T., Synthesis of [8]Cycloparaphenylene from a Square-Shaped Tetranuclear Platinum Complex. *Angew. Chem. Int. Ed.* **2010**, *49*, 757-759.

55.   Eiichi, K.; Takahiro, I.; Toshiyasu, S.; Shigeru, Y., Selective Synthesis of [6]-, [8]-, and [10]Cycloparaphenylenes. *Chem. Lett.* **2013**, *42*, 621-623.

56.   Takaba, H.; Omachi, H.; Yamamoto, Y.; Bouffard, J.; Itami, K., Selective Synthesis of [12]Cycloparaphenylene. *Angew. Chem. Int. Ed.* **2009**, *48*, 6112-6116.

57.   Jagadeesh, M. N.; Makur, A.; Chandrasekhar, J., The Interplay of Angle Strain and Aromaticity: Molecular and Electronic Structures of [0n]Paracyclophanes. *J. Mol. Mod.* **2000**, *6*, 226-233.

58.   Segawa, Y.; Omachi, H.; Itami, K., Theoretical Studies on the Structures and Strain Energies of Cycloparaphenylenes. *Org. Lett.* **2010**, *12*, 2262-2265.

59.   Tahara, K.; Tobe, Y., Molecular Loops and Belts. *Chem. Rev.* **2006**, *106*, 5274-5290.

60.   Bunz, U.; Menning, S.; Martín, N., para-Connected Cyclophenylenes and Hemispherical Polyarenes: Building Blocks for Single-Walled Carbon Nanotubes. *Angew. Chem. Int. Ed.* **2012**, *51*, 7094-7101.

61.   Wipf, P.; Jung, J.-K., Nucleophilic Additions to 4,4-Disubstituted 2,5-Cyclohexadienones: Can Dipole Effects Control Facial Selectivity? *Chem. Rev.* **1999**, *99*, 1469-1480.

62.   Barder, T. E.; Walker, S. D.; Martinelli, J. R.; Buchwald, S. L., Catalysts for Suzuki−Miyaura Coupling Processes: Scope and Studies of the Effect of Ligand Structure. *J. Am. Chem. Soc.* **2005**, *127*, 4685-4696.

63.   Fujitsuka, M.; Cho, D.; Iwamoto, T.; Yamago, S.; Majima, T., Size-dependent fluorescence properties of [*n*]cycloparaphenylenes (n = 8-13), hoop-shaped π-conjugated molecules. *Phys. Chem. Chem. Phys.* **2012,** *14*, 14585-14588.

64.   Reddy, V. S.; Camacho, C.; Xia, J.; Jasti, R.; Irle, S., Quantum Dynamics Simulations Reveal Vibronic Effects on the Optical Properties of [*n*]Cycloparaphenylenes. *J. Chem. Theory Comput.* **2014,** *10*, 4025-4036.

65.   Adamska, L.; Nayyar, I.; Chen, H.; Swan, A. K.; Oldani, N.; Fernandez-Alberti, S.; Golder, M. R.; Jasti, R.; Doorn, S. K.; Tretiak, S., Self-Trapping of Excitons, Violation of Condon Approximation, and Efficient Fluorescence in Conjugated Cycloparaphenylenes. *Nano Lett.* **2014,** *14*, 6539-6546.

66.   Li, P.; Sisto, T. J.; Darzi, E. R.; Jasti, R., The Effects of Cyclic Conjugation and Bending on the Optoelectronic Properties of Paraphenylenes. *Org. Lett.* **2014,** *16*, 182-185.

67.   Since our initial report, Itami has also reported on the selective synthesis of [7]CPP: Sibbel, F.; Matsui, K.; Segawa, Y.; Studer, A.; Itami, K., Selective synthesis of [7]- and [8]cycloparaphenylenes. Chem. Commun. 2014, 50, 954-956.

68.   Zabula, A. V. F., A. S.; Xia, J.; Jasti, R.; Petrukhina, M. A., Tightening the Nanobelt Upon Multi-Electron Reduction. *Angew. Chem. Int. Ed.* **2013,** *52*, 5033-5036.

69.   Sibbel, F.; Matsui, K.; Segawa, Y.; Studer, A.; Itami, K., Selective synthesis of [7]- and [8]cycloparaphenylenes. *Chem. Commun.* **2014,** *50*, 954-956.

70.   Segawa, Y.; Šenel, P.; Matsuura, S.; Omachi, H.; Itami, K., [9] Cycloparaphenylene: Nickel-mediated Synthesis and Crystal Structure. *Chem. Lett.* **2011,** *40*, 423-425.

71.   Kayahara, E.; Sakamoto, Y.; Suzuki, T.; Yamago, S., Selective Synthesis and Crystal Structure of [10]Cycloparaphenylene. *Org. Lett.* **2012,** *14*, 3284-3287.

72.   Segawa, Y.; Miyamoto, S.; Omachi, H.; Matsuura, S.; Šenel, P.; Sasamori, T.; Tokitoh, N.; Itami, K., Concise Synthesis and Crystal Structure of [12]Cycloparaphenylene. *Angew. Chem. Int. Ed.* **2011,** *50*, 3244-3248.

73.	Punna, S.; Díaz, D. D.; Finn, M. G., Palladium-Catalyzed Homocoupling of Arylboronic Acids and Esters Using Fluoride in Aqueous Solvents. *Synlett* **2004,** *2004*, 2351-2354.

74.	Kayahara, E.; Patel, V. K.; Yamago, S., Synthesis and Characterization of [5]Cycloparaphenylene. *J. Am. Chem. Soc.* **2014,** *136*, 2284-2287.

75.	Baran, P. S.; Burns, N. Z., Total synthesis of (±)-haouamine A. *J. Am. Chem. Soc.* **2006,** *128*, 3908-3909.

76.	Takiguchi, H.; Ohmori, K.; Suzuki, K., Synthesis and determination of the absolute configuration of cavicularin by a symmetrization/asymmetrization approach. *Angew. Chem. Int. Ed.* **2013,** *52*, 10472-10476.

77.	Tobe, Y.; Ueda, K.; Kakiuchi, K.; Odaira, Y.; Kai, Y.; Kasai, N., Synthesis, Structure and Reactivities of [6]Paracyclophanes. *Tetrahedron* **1986,** *42*, 1851-1857.

78.	Allinger, N. L.; Walter, T. J.; Newton, M. G., Synthesis, structure, and properties of the [7]paracyclophane ring system. *J. Am. Chem. Soc* **1974,** *96*, 4588-4597.

79.	Kawai, H.; Suzuki, T.; Ohkita, M.; Tsuji, T., Kinetic Stabilization of the [1.1]Paracyclophane System: Isolation and X-ray Structural Analysis of a [1.1]Paracyclophane Derivative and Its Interconversion with the Transannular Adduct. *Chem. Eur. J.* **2000,** *6*, 4177-4187.

80.	Bodwell, G. J.; Bridson, J. N.; Houghton, T. J.; Kennedy, J. W. J.; Mannion, M. R., 1,7-Dioxa[7](2,7)pyrenophane: The Pyrene Moiety Is More Bent than That of C70. *Chem. Eur. J.* **1999,** *5*, 1823-1827.

81.	Dobrowolski, M. A.; Cyrański, M. K.; Merner, B. L.; Bodwell, G. J.; Wu, J. I.; Schleyer, P. v. R., Interplay of π-Electron Delocalization and Strain in [*n*](2,7)Pyrenophanes. *J. Org. Chem.* **2008,** *73*, 8001-8009.

82.	Tsuji, T.; Okuyama, M.; Ohkita, M.; Kawai, H.; Suzuki, T., Functionalization and Kinetic Stabilization of the [4]Paracyclophane System and Aromaticity of Its Extremely Bent Benzene Ring. *J. Am. Chem. Soc.* **2003,** *125*, 951-961.

83. Rice, J. E.; Lee, T. J.; Remington, R. B.; Allen, W. D.; Clabo, D. A.; Schaefer, H. F., [5]Paracyclophane. An important example of ring strain and aromaticity in hydrocarbon compounds. *J. Am. Chem. Soc.* **1987,** *109*, 2902-2909.

84. Fort, E. H.; Donovan, P. M.; Scott, L. T., Diels−Alder Reactivity of Polycyclic Aromatic Hydrocarbon Bay Regions: Implications for Metal-Free Growth of Single-Chirality Carbon Nanotubes. *J. Am. Chem. Soc.* **2009,** *131*, 16006-16007.

85. Fort, E. H.; Scott, L. T., Carbon nanotubes from short hydrocarbon templates. Energy analysis of the Diels-Alder cycloaddition/rearomatization growth strategy. *J. Mater. Chem.* **2011,** *21*, 1373-1381.

86. Omachi, H.; Nakayama, T.; Takahashi, E.; Segawa, Y.; Itami, K., Initiation of carbon nanotube growth by well-defined carbon nanorings. *Nature Chem.* **2013,** *5*, 572-576.

87. Iwamoto, T.; Watanabe, Y.; Sadahiro, T.; Haino, T.; Yamago, S., Size-Selective Encapsulation of C60 by [10]Cycloparaphenylene: Formation of the Shortest Fullerene-Peapod. *Angew. Chem. Int. Ed.* **2011,** *50*, 8342-8344.

Chapter II

1. Cram, D. J.; Elhafez, F. A. A., Studies in Stereochemistry. X. The Rule of "Steric Control of Asymmetric Induction" in the Syntheses of Acyclic Systems. *J. Am. Chem. Soc.* **1952,** *74*, 5828-5835.

2. Anh, N. T.; Eisenstein, O., Induction asymetrique 1−2: comparaison ab initio des modeles de cram, de cornforth, de karabatsos et de felkin. *Tetrahedron Lett.* **1976,** *17*, 155-158.

3. Evans, D. A., Stereoselective Organic Reactions: Catalysts for Carbonyl Addition Processes. *Science* **1988,** *240*, 420-426.

4. Wipf, P.; Jung, J.-K., Nucleophilic Additions to 4,4-Disubstituted 2,5-Cyclohexadienones: Can Dipole Effects Control Facial Selectivity? *Chem. Rev.* **1999,** *99*, 1469-1480.

5. Swiss, K. A.; Liotta, D. C.; Maryanoff, C. A., Mechanistic aspects of the ligand-assisted nucleophilic addition reaction. *J. Am. Chem. Soc.* **1990,** *112*, 9393-9394.

6.   Swiss, K. A.; Hinkley, W.; Maryanoff, C. A.; Liotta, D. C., Complementary Facial Selectivity in Conjugate Additions to γ-Hydroxyenones. *Synthesis* **1992,** *1992*, 127-131.

7.   Wipf, P.; Kim, Y., π-Facial Selectivity in Nucleophilic Additions to 4,4-Disubstituted Dienones: Experimental Support for Electrostatic Control. *J. Am. Chem. Soc.* **1994,** *116*, 11678-11688.

8.   Jasti, R.; Chattacharjee, J.; Neaton, J. B.; Bertozzi, C. R., Synthesis, Characterization, and Theory of [9]-, [12]-, and [18]Cycloparaphenylene: Carbon Nanohoop Structures. *J. Am. Chem. Soc.* **2008,** *130*, 17646-17647.

9.   Sisto, T. J.; Golder, M. R.; Hirst, E. S.; Jasti, R., Selective Synthesis of Strained [7]Cycloparaphenylene: An Orange-Emitting Fluorophore. *J. Am. Chem. Soc.* **2011,** *133*, 15800-15802.

10.   Evans, P. J.; Darzi, E. R.; Jasti, R., Efficient Room-Temperature Synthesis of a Highly Strained Carbon Nanohoop Fragment of Buckminsterfullerene. *Nature Chem.* **2014,** *6*, 404-408.

11.   Xia, J.; Jasti, R., Synthesis, Characterization, and Crystal Structure of [6]Cycloparaphenylene. *Angew. Chem. Int. Ed.* **2012,** *51*, 2474-2476.

12.   Darzi, E. R.; Sisto, T. J.; Jasti, R., Selective Syntheses of [7]–[12]Cycloparaphenylenes Using Orthogonal Suzuki–Miyaura Cross-Coupling Reactions. *J. Org. Chem.* **2012,** *77*, 6624-6628.

13.   Yagi, A.; Segawa, Y.; Itami, K., Synthesis and properties of [9]cyclo-1,4-naphthylene: a π-extended carbon nanoring. *J. Am. Chem. Soc.* **2012,** *134*, 2962-2965.

14.   Chattopadhyay, S. K.; Pal, B. K.; Maity, S., Combined Multiple Claisen Rearrangement and Ring-closing Metathesis as a Route to Naphthalene, Anthracene, and Anthracycline Ring Systems. *Chem. Lett.* **2003,** *32*, 1190-1191.

15.   Majumdar, K. C.; Chattopadhyay, B.; Chakravorty, S., An Expedient Synthesis of Bis-Fused Benzofuran and a Two-Directional Ring-Closing Metathesis for the Synthesis of Bisbenzoxepines and Bisbenzoxocines. *Synthesis* **2009,** *2009*, 674-680.

16.   Gambarotti, C.; Melone, L.; Punta, C.; Shisodia, S. U., Selective Monoetherification of 1,4-Hydroquinone Promoted by NaNO$_2$. *Curr. Org. Chem.* **2013,** *17*, 1108-1113.

17.   Bosch, E.; Rathore, R.; Kochi, J. K., Novel Catalysis of Hydroquinone Autoxidation with Nitrogen Oxides. *J. Org. Chem.* **1994,** *59*, 2529-2536.

18.   Bonifacio, M. C.; Robertson, C. R.; Jung, J.-Y.; King, B. T., Polycyclic Aromatic Hydrocarbons by Ring-Closing Metathesis. *J. Org. Chem.* **2005,** *70*, 8522-8526.

19.   Martin, H. J.; Drescher, M.; Kählig, H.; Schneider, S.; Mulzer, J., Synthesis of the C1–C13 Fragment of Kendomycin: Atropisomerism around a C−Aryl Glycosidic Bond. *Angew. Chem. Int. Ed.* **2001,** *40*, 3186-3188.

20.   Casarini, D.; Lunazzi, L.; Mazzanti, A., Correlated Rotations in Benzylfluorene Derivatives: Structure, Conformation, and Stereodynamics. *J. Org. Chem.* **2008,** *73*, 2811-2818.

21.   Casarini, D.; Lunazzi, L.; Mazzanti, A., Stereomutation of Conformational Enantiomers of 9-Isopropyl-9-formylfluorene and Related Acyl Derivatives. *J. Org. Chem.* **2008,** *73*, 6382-6385.

22.   Bowden, K.; Cook, R. S., Reactions in strongly basic solutions. Part VI. Correlation of the rates of rearrangement of weak carbon acids in aqueous dimethyl sulphoxide with an acidity function. Substituent and kinetic isotope effects. *J. Chem. Soc., Perkin Trans. 2* **1972**, 1407-1411.

23.   Lai, Y.-H.; Yap, A. H.-T., Synthesis and rigid conformers of 14,15-dimethyl-2,11-dithia[3.3](1,3)(1,4)cyclophane and 12,13-dimethyl[2.2](1,3)(1,4)cyclophane. *J. Chem. Soc., Perkin Trans. 2* **1993**, 1373-1377.

24.   Spring, D. R.; Krishnan, S.; Blackwell, H. E.; Schreiber, S. L., Diversity-Oriented Synthesis of Biaryl-Containing Medium Rings Using a One Bead/One Stock Solution Platform. *J. Am. Chem. Soc.* **2002,** *124*, 1354-1363.

25.   Pangborn, A. B.; Giardello, M. A.; Grubbs, R. H.; Rosen, R. K.; Timmers, F. J., Safe and Convenient Procedure for Solvent Purification. *Organometallics* **1996,** *15*, 1518-1520.

Chapter III

1.   Lewis, I. C.; Singer, L. S., Electron Spin Resonance of Radical Cations Produced by the Oxidation of Aromatic Hydrocarbons with SbCl$_5$. *J. Chem. Phys.* **1965,** *43*, 2712-2727.

2.   Badger, B.; Brocklehurst, B., Formation of Dimer Cations of Aromatic Hydrocarbons. *Nature* **1968,** *219*, 263.

3.   Miller, L. L.; Mann, K. R., π-Dimers and π-Stacks in Solution and in Conducting Polymers. *Acc. Chem. Res.* **1996,** *29*, 417-423.

4.   Sullivan, P. A.; Dalton, L. R., Theory-Inspired Development of Organic Electro-optic Materials. *Acc. Chem. Res.* **2009,** *43*, 10-18.

5.   Baumgarten, M.; Müllen, K., Radical ions: Where organic chemistry meets materials sciences. *Top. Curr. Chem.* **1994,** *169*, 1-103.

6.   Law, K. Y., Organic photoconductive materials: recent trends and developments. *Chem. Rev.* **1993,** *93*, 449-486.

7.   Hellstrom, S. L.; Vosgueritchian, M.; Stoltenberg, R. M.; Irfan, I.; Hammock, M.; Wang, Y. B.; Jia, C.; Guo, X.; Gao, Y.; Bao, Z., Strong and Stable Doping of Carbon Nanotubes and Graphene by MoOx for Transparent Electrodes. *Nano Lett.* **2012,** *12*, 3574-3580.

8.   Chandra, B.; Afzali, A.; Khare, N.; El-Ashry, M. M.; Tulevski, G. S., Stable Charge-Transfer Doping of Transparent Single-Walled Carbon Nanotube Films. *Chem. Mater.* **2010,** *22*, 5179-5183.

9.   Hicks, R. G., What's new in stable radical chemistry? *Org. Biomol. Chem.* **2007,** *5*, 1321-1338.

10. Rathore, R.; Kochi, J. K., Isolation of Novel Radical Cations from Hydroquinone Ethers. Conformational Transition of the Methoxy Group upon Electron Transfer. *J. Org. Chem.* **1995,** *60*, 4399-4411.

11. Rathore, R.; Kumar, A. S.; Lindeman, S. V.; Kochi, J. K., Preparation and Structures of Crystalline Aromatic Cation-Radical Salts. Triethyloxonium Hexachloroantimonate as a Novel (One-Electron) Oxidant. *J. Org. Chem.* **1998,** *63*, 5847-5856.

12. Rathore, R.; Burns, C. L.; Deselnicu, M. I., Multiple-Electron Transfer in a Single Step. Design and Synthesis of Highly Charged Cation-Radical Salts. *Org. Lett.* **2001,** *3*, 2887-2890.

13. Rathore, R.; Burns, C. L., A Practical One-Pot Synthesis of Soluble Hexa-peri-hexabenzocoronene and Isolation of Its Cation-Radical Salt. *J. Org. Chem.* **2003,** *68*, 4071-4074.

14. Rathore, R.; Burns, C. L.; Abdelwahed, S., Hopping of a single hole in hexakis[4-(1,1,2-triphenyl-ethenyl)phenyl]benzene cation radical through the hexaphenylbenzene propeller. *Org. Lett.* **2004,** *6*, 1689-1692.

15. Banerjee, M.; Lindeman, S.; Rathore, R., Structural characterization of quaterphenyl cation radical: X-ray crystallographic evidence of quinoidal charge delocalization in poly-p-phenylene cation radicals. *J. Am. Chem. Soc.* **2007,** *129*, 8070-8071.

16. Ferraris, J.; Cowan, D. O.; Walatka, V.; Perlstein, J. H., Electron transfer in a new highly conducting donor-acceptor complex. *J. Am. Chem. Soc.* **1973,** *95*, 948-949.

17. Yoshizawa, M.; Kumazawa, K.; Fujita, M., Room-Temperature and Solution-State Observation of the Mixed-Valence Cation Radical Dimer of Tetrathiafulvalene, $[(TTF)_2]^{+\bullet}$, within a Self-Assembled Cage. *J. Am. Chem. Soc.* **2005,** *127*, 13456-13457.

18. Aprahamian, I.; Olsen, J.-C.; Trabolsi, A.; Stoddart, J. F., Tetrathiafulvalene Radical Cation Dimerization in a Bistable Tripodal [4]Rotaxane. *Chem. Eur. J.* **2008,** *14*, 3889-3895.

19. Hasegawa, M.; Daigoku, K.; Hashimoto, K.; Nishikawa, H.; Iyoda, M., Face-to-Face Dimeric Tetrathiafulvalenes and Their Cation Radical and Dication Species as Models of Mixed Valence and π-Dimer States. *Bull. Chem. Soc. Jpn.* **2012,** *85*, 51-60.

20.   Graf, D. D.; Campbell, J. P.; Miller, L. L.; Mann, K. R., Single-Crystal X-ray Structure of the Cation Radical of 3',4'-Dibutyl-2,5"-diphenyl-2,2':5',2"-terthiophene: Definitive Evidence for π-Stacked Oxidized Oligothiophenes. *J. Am. Chem. Soc.* **1996,** *118*, 5480-5481.

21.   Graf, D. D.; Duan, R. G.; Campbell, J. P.; Miller, L. L.; Mann, K. R., From Monomers to π-Stacks. A Comprehensive Study of the Structure and Properties of Monomeric, π-Dimerized, and π-Stacked Forms of the Cation Radical of 3',4'-Dibutyl-2,5"-diphenyl-2,2':5',2"-terthiophene. *J. Am. Chem. Soc.* **1997,** *119*, 5888-5899.

22.   Takita, R.; Song, C.; Swager, T. M., π-Dimer Formation in an Oligothiophene Tweezer Molecule. *Org. Lett.* **2008,** *10*, 5003-5005.

23.   Shomura, R.; Sugiyasu, K.; Yasuda, T.; Sato, A.; Takeuchi, M., Electrochemical Generation and Spectroscopic Characterization of Charge Carriers within Isolated Planar Polythiophene. *Macromolecules* **2012,** *45*, 3759-3771.

24.   Janata, J.; Gendell, J.; Ling, C.-Y.; Barth, W. E.; Backes, L.; Mark, H. B.; Lawton, R. G., Concerning the anion and cation radicals of corannulene. *J. Am. Chem. Soc.* **1967,** *89*, 3056-3058.

25.   Morita, Y.; Suzuki, S.; Sato, K.; Takui, T., Synthetic organic spin chemistry for structurally well-defined open-shell graphene fragments. *Nature Chem.* **2011,** *3*, 197-204.

26.   Dessau, R. M.; Shih, S.; Heiba, E. I., Oxidation by Metal Salts. VI. A New Chemical Method for the Generation of Aromatic Radical Cations. *J. Am. Chem. Soc.* **1970,** *92*, 412-413.

27.   Becker, H.; Javahery, G.; Petrie, S.; Cheng, P. C.; Schwarz, H.; Scott, L. T.; Bohme, D. K., Gas-phase ion/molecule reactions of corannulene, a fullerene subunit. *J. Am. Chem. Soc.* **1993,** *115*, 11636-11637.

28.   Baumgarten, M.; Gherghel, L.; Wagner, M.; Weitz, A.; Rabinovitz, M.; Cheng, P.-C.; Scott, L. T., Corannulene Reduction: Spectroscopic Detection of All Anionic Oxidation States. *J. Am. Chem. Soc.* **1995,** *117*, 6254-6257.

29.   Galue, H. A.; Rice, C. A.; Steill, J. D.; Oomens, J., Infrared spectroscopy of ionized corannulene in the gas phase. *J. Chem. Phys.* **2011,** *134*, 054310-11.

30. Krusic, P. J.; Wasserman, E.; Keizer, P. N.; Morton, J. R.; Preston, K. F., Radical Reactions of C60. *Science* **1991,** *254*, 1183-1185.

31. Morita, Y.; Ueda, A.; Nishida, S.; Fukui, K.; Ise, T.; Shiomi, D.; Sato, K.; Takui, T.; Nakasuji, K., Curved Aromaticity of a Corannulene-Based Neutral Radical: Crystal Structure and 3 D Unbalanced Delocalization of Spin. *Angew. Chem. Int. Ed.* **2008,** *47*, 2035-2038.

32. Rath, H.; Tokuji, S.; Aratani, N.; Furukawa, K.; Lim, J. M.; Kim, D.; Shinokubo, H.; Osuka, A., A Stable Organic Radical Delocalized on a Highly Twisted π System Formed Upon Palladium Metalation of a Möbius Aromatic Hexaphyrin. *Angew. Chem. Int. Ed.* **2010,** *49*, 1489-1491.

33. Jasti, R.; Chattacharjee, J.; Neaton, J. B.; Bertozzi, C. R., Synthesis, Characterization, and Theory of [9]-, [12]-, and [18]Cycloparaphenylene: Carbon Nanohoop Structures. *J. Am. Chem. Soc.* **2008,** *130*, 17646-17647.

34. Xia, J.; Bacon, J. W.; Jasti, R., Gram-Scale Synthesis and Crystal Structures of [8]- and [10]CPP, and the Solid-State Structure of C60@[10]CPP. *Chem. Sci.* **2012,** *3*, 3018-3021.

35. Takaba, H.; Omachi, H.; Yamamoto, Y.; Bouffard, J.; Itami, K., Selective Synthesis of [12]Cycloparaphenylene. *Angew. Chem. Int. Ed.* **2009,** *48*, 6112-6116.

36. Ishii, Y.; Nakanishi, Y.; Omachi, H.; Matsuura, S.; Matsui, K.; Shinohara, H.; Segawa, Y.; Itami, K., Size-selective synthesis of [9]–[11] and [13]cycloparaphenylenes. *Chem. Sci.* **2012,** *3*, 2340-2345.

37. Yamago, S.; Watanabe, Y.; Iwamoto, T., Synthesis of [8]Cycloparaphenylene from a Square-Shaped Tetranuclear Platinum Complex. *Angew. Chem. Int. Ed.* **2010,** *49*, 757-759.

38. Iwamoto, T.; Watanabe, Y.; Sakamoto, Y.; Suzuki, T.; Yamago, S., Selective and Random Syntheses of [n]Cycloparaphenylenes (n = 8–13) and Size Dependence of Their Electronic Properties. *J. Am. Chem. Soc.* **2011,** *133*, 8354-8361.

39. Hitosugi, S.; Nakanishi, W.; Yamasaki, T.; Isobe, H., Bottom-up synthesis of finite models of helical (n,m)-single-wall carbon nanotubes. *Nat. Commun.* **2011,** *2*, 492-496.

40. Nishiuchi, T.; Feng, X.; Enkelmann, V.; Wagner, M.; Müllen, K., Three-Dimensionally Arranged Cyclic p-Hexaphenylbenzene: Toward a Bottom-Up Synthesis of Size-Defined Carbon Nanotubes. *Chem. Eur. J.* **2012,** *18*, 16621-16625.

41. Jasti, R.; Bertozzi, C. R., Progress and challenges for the bottom-up synthesis of carbon nanotubes with discrete chirality. *Chem. Phys. Lett.* **2010,** *494*, 1-7.

42. Hirst, E. S.; Jasti, R., Bending Benzene: Syntheses of [n]Cycloparaphenylenes. *J. Org. Chem.* **2012,** *77*, 10473-10478.

43. Omachi, H.; Segawa, Y.; Itami, K., Synthesis of Cycloparaphenylenes and Related Carbon Nanorings: A Step toward the Controlled Synthesis of Carbon Nanotubes. *Acc. Chem. Res.* **2012**, 1378-1389.

44. Iwamoto, T.; Watanabe, Y.; Sadahiro, T.; Haino, T.; Yamago, S., Size-Selective Encapsulation of C60 by [10]Cycloparaphenylene: Formation of the Shortest Fullerene-Peapod. *Angew. Chem. Int. Ed.* **2011,** *50*, 8342-8344.

45. Zabula, A. V. F., A. S.; Xia, J.; Jasti, R.; Petrukhina, M. A., Tightening the Nanobelt Upon Multi-Electron Reduction. *Angew. Chem. Int. Ed.* **2013,** *52*, 5033-5036.

46. Kochi, J. K.; Rathore, R.; Maguères, P. L., Stable Dimeric Aromatic Cation−Radicals. Structural and Spectral Characterization of Through-Space Charge Delocalization. *J. Org. Chem.* **2000,** *65*, 6826-6836.

47. Chen, J.; Klinke, C.; Afzali, A.; Avouris, P., Self-aligned carbon nanotube transistors with charge transfer doping. *Appl. Phys. Lett.* **2005,** *86*, 123108-3.

48. Marchetti, F.; Pinzino, C.; Zacchini, S.; Pampaloni, G., Long-Lived Radical Cations of Monocyclic Arenes at Room Temperature Obtained by NbF5 Acting as an Oxidizing Agent and Counterion Precursor. *Angew. Chem. Int. Ed.* **2010,** *49*, 5268-5272.

49. Chen, X.; Wang, X.; Sui, Y.; Li, Y.; Ma, J.; Zuo, J.; Wang, X., Synthesis, Characterization, and Structures of a Persistent Aniline Radical Cation. *Angew. Chem. Int. Ed.* **2012,** *51*, 11878-11881.

271

50.   Navale, T. S.; Thakur, K.; Vyas, V. S.; Wadumethrige, S. H.; Shukla, R.; Lindeman, S. V.; Rathore, R., Charge Delocalization in Self-Assembled Mixed-Valence Aromatic Cation Radicals. *Langmuir* **2012,** *28*, 71-83.

51.   Rieger, P. H., *Electron Spin Resonance: Analysis and Interpretation*. RSC Publishing: 2007.

52.   Takase, M.; Narita, T.; Fujita, W.; Asano, M. S.; Nishinaga, T.; Benten, H.; Yoza, K.; Müllen, K., Pyrrole-Fused Azacoronene Family: The Influence of Replacement with Dialkoxybenzenes on the Optical and Electronic Properties in Neutral and Oxidized States. *J. Am. Chem. Soc.* **2013,** *135*, 8031-8040.

53.   Ueda, H., Formation and Decay of the Transient Species in Radiation Chemistry. Radiolysis of Alkyl Halide Systems. *Bull. Chem. Soc. Jpn.* **1968,** *41*, 2578-2586.

54.   Mah, S.; Yamamoto, Y.; Hayashi, K., Effects of salts having complex metal halide anions on formation and decay of biphenyl radical cations studied by pulse radiolysis. *J. Phys. Chem.* **1983,** *87*, 297-300.

55.   Lin, C.; Endo, T.; Takase, M.; Iyoda, M.; Nishinaga, T., Structural, Optical, and Electronic Properties of a Series of 3,4-Propylenedioxythiophene Oligomers in Neutral and Various Oxidation States. *J. Am. Chem. Soc.* **2011,** *133*, 11339-11350.

56.   Zhang, F.; Gotz, G.; Mena-Osteritz, E.; Weil, M.; Sarkar, B.; Kaim, W.; Bauerle, P., Molecular and electronic structure of cyclo[10]thiophene in various oxidation states: polaron pair vs. bipolaron. *Chem. Sci.* **2011,** *2*, 781-784.

57.   Rose, J., *Molecular Complexes*. Pergamon Press: New York, 1967.

58.   Benesi, H. A.; Hildebrand, J. H., A Spectrophotometric Investigation of the Interaction of Iodine with Aromatic Hydrocarbons. *J. Am. Chem. Soc.* **1949,** *71*, 2703-2707.

59.   Rodgers, M. A. J., Nanosecond pulse radiolysis of acetone. Kinetic and thermodynamic properties of some aromatic radical cations. *J. Chem. Soc., Faraday Trans. 1* **1972,** *68*, 1278-1286.

60.   Ayalon, A.; Sygula, A.; Cheng, P.-C.; Rabinovitz, M.; Rabideau, P. W.; Scott, L. T., Stable High-Order Molecular Sandwiches: Hydrocarbon Polyanion Pairs with Multiple Lithium Ions Inside and Out. *Science* **1994,** *265*, 1065-1067.

61.   Aprahamian, I.; Eisenberg, D.; Hoffman, R. E.; Sternfeld, T.; Matsuo, Y.; Jackson, E. A.; Nakamura, E.; Scott, L. T.; Sheradsky, T.; Rabinovitz, M., Ball-and-Socket Stacking of Supercharged Geodesic Polyarenes: Bonding by Interstitial Lithium Ions. *J. Am. Chem. Soc.* **2005,** *127*, 9581-9587.

62.   Zabula, A.; Filatov, A.; Spisak, S.; Rogachev, A.; Petrukhina, M., A main group metal sandwich: five lithium cations jammed between two corannulene tetraanion decks. *Science* **2011,** *333*, 1008-1011.

63.   Zabula, A. V.; Spisak, S. N.; Filatov, A. S.; Petrukhina, M. A., Self-Assembly of Charged Supramolecular Sandwiches Formed by Corannulene Tetraanions and Lithium Cations. *Organometallics* **2012,** *31*, 5541-5545.

64.   Shorafa, H.; Mollenhauer, D.; Paulus, B.; Seppelt, K., The Two Structures of the Hexafluorobenzene Radical Cation $C_6F_6^{+\bullet}$ *Angew. Chem. Int. Ed.* **2009,** *48*, 5845-5847.

65.   Frisch, M. J.; Trucks, G. W.; Schlegel, H. B.; Scuseria, G. E.; Robb, M. A.; Cheeseman, J. R.; Scalmani, G.; Barone, V.; Mennucci, B.; Petersson, G. A.; Nakatsuji, H.; Caricato, M.; Li, X.; Hratchian, H. P.; Izmaylov, A. F.; Bloino, J.; Zheng, G.; Sonnenberg, J. L.; Hada, M.; Ehara, M.; Toyota, K.; Fukuda, R.; Hasegawa, J.; Ishida, M.; Nakajima, T.; Honda, Y.; Kitao, O.; Nakai, H.; Vreven, T.; Montgomery, J. A.; Peralta, J. E.; Ogliaro, F.; Bearpark, M.; Heyd, J. J.; Brothers, E.; Kudin, K. N.; Staroverov, V. N.; Kobayashi, R.; Normand, J.; Raghavachari, K.; Rendell, A.; Burant, J. C.; Iyengar, S. S.; Tomasi, J.; Cossi, M.; Rega, N.; Millam, J. M.; Klene, M.; Knox, J. E.; Cross, J. B.; Bakken, V.; Adamo, C.; Jaramillo, J.; Gomperts, R.; Stratmann, R. E.; Yazyev, O.; Austin, A. J.; Cammi, R.; Pomelli, C.; Ochterski, J. W.; Martin, R. L.; Morokuma, K.; Zakrzewski, V. G.; Voth, G. A.; Salvador, P.; Dannenberg, J. J.; Dapprich, S.; Daniels, A. D.; Farkas; Foresman, J. B.; Ortiz, J. V.; Cioslowski, J.; Fox, D. J., Gaussian 09, Revision B.01. Wallingford CT, 2009.

66.   Nelsen, S.; Weaver, M.; Yamazaki, D.; Komatsu, K.; Rathore, R.; Bally, T., Calculations of the optical spectra of hydrocarbon radical cations based on Koopmans' theorem. *J. Phys. Chem. A.* **2007,** *111*, 1667-1676.

67.   Xia, J.; Golder, M. R.; Foster, M. E.; Wong, B. M.; Jasti, R., Synthesis, Characterization, and Computational Studies of Cycloparaphenylene Dimers. *J. Am. Chem. Soc.* **2012,** *134*, 19709-19715.

68.   Hanwell, M.; Curtis, D.; Lonie, D.; Vandermeersch, T.; Zurek, E.; Hutchison, G., Avogadro: An advanced semantic chemical editor, visualization, and analysis platform. *J. Chem. Inf.* **2012,** *4*, 17.

69.   Chai, J.-D.; Head-Gordon, M., Systematic optimization of long-range corrected hybrid density functionals. *J. Chem. Phys.* **2008,** *128*, 084106-15.

70.   Chai, J.-D.; Head-Gordon, M., Long-range corrected hybrid density functionals with damped atom-atom dispersion corrections. *Phys. Chem. Chem. Phys.* **2008,** *10*, 6615-6620.

71.   Stephan, N. S.; Cyril, P.; Aurore, D.; Clemence, C., Why are the Interaction Energies of Charge-Transfer Complexes Challenging for DFT? *J. Chem. Theory Comput.* **2012,** *8*, 1629-1640.

72.   Dag, S.; Senger, R. T.; Ciraci, S., Theoretical study of crossed and parallel carbon nanotube junctions and three-dimensional grid structures. *Phys. Rev. B* **2004,** *70*, 205407.

73.   Fuhrer, M. S.; Nygård, J.; Shih, L.; Forero, M.; Yoon, Y.-G.; Mazzoni, M. S. C.; Choi, H. J.; Ihm, J.; Louie, S. G.; Zettl, A.; McEuen, P. L., Crossed Nanotube Junctions. *Science* **2000,** *288*, 494-497.

74.   Margulis, V.; Pyataev, M., Electron transport in crossed nanotubes with a point contact. *Phys. Rev. B* **2007,** *76*, 085411-085417.

75.   Fuhrer, M. S.; Lim, A. K. L.; Shih, L.; Varadarajan, U.; Zettl, A.; McEuen, P. L., Transport through crossed nanotubes. *Physica E* **2000,** *6*, 868-871.

76.   Hecht, D.; Hu, L.; Gruner, G., Conductivity scaling with bundle length and diameter in single walled carbon nanotube networks. *Appl. Phys. Lett.* **2006,** *89*, 133112-3.

77. Kayahara, E.; Kouyama, T.; Kato, T.; Takaya, H.; Yasuda, N.; Yamago, S., Isolation and Characterization of the Cycloparaphenylene Radical Cation and Dication. *Angew. Chem. Int. Ed.* **2013,** *52*, 13722-13726.

78. Toriumi, N.; Muranaka, A.; Kayahara, E.; Yamago, S.; Uchiyama, M., In-Plane Aromaticity in Cycloparaphenylene Dications: A Magnetic Circular Dichroism and Theoretical Study. *J. Am. Chem. Soc.* **2015,** *137*, 82-85.

79. Tahara, K.; Tobe, Y., Molecular Loops and Belts. *Chem. Rev.* **2006,** *106*, 5274-5290.

80. Golder, M. R.; Wong, B. M.; Jasti, R., Photophysical and theoretical investigations of the [8]cycloparaphenylene radical cation and its charge-resonance dimer. *Chem. Sci.* **2013,** *4*, 4285-4291.

81. Darzi, E. R.; Sisto, T. J.; Jasti, R., Selective Syntheses of [7]–[12]Cycloparaphenylenes Using Orthogonal Suzuki–Miyaura Cross-Coupling Reactions. *J. Org. Chem.* **2012,** *77*, 6624-6628.

82. Pangborn, A. B. G., M. A; Grubbs, R. H.; Rosen, R. K.; Timmers, F. J. , *Organometallics* **1996,** *15*, 1518-1520.

83. Becke, A. D., Density-functional thermochemistry. III. The role of exact exchange. *J. Chem. Phys.* **1993,** *98*, 5648-5652.

84. Grimme, S., Semiempirical GGA-type density functional constructed with a long-range dispersion correction. *J. Comput. Chem.* **2006,** *27*, 1787-1799.

Chapter IV

1. Iijima, S., Helical microtubulues of graphitic carbon. *Nature* **1991,** *354*, 56-58.

2. Dresselhaus, M. S. D., G.; Avouris, P, *Carbon Nanotubes: Synthesis, Structure, Properties and Applications*. Springer-Verlag: Berlin, 2001.

3. Jose-Yacaman, M.; Miki-Yoshida, M.; Rendon, L.; Santiesteban, J. G., Catalytic growth of carbon microtubules with fullerene structure. *Appl. Phys. Lett.* **1993,** *62*, 657-659.

4.   Thess, A.; Lee, R.; Nikolaev, P.; Dai, H.; Petit, P.; Robert, J.; Xu, C.; Lee, Y. H.; Kim, S. G.; Rinzler, A. G.; Colbert, D. T.; Scuseria, G. E.; Tománek, D.; Fischer, J. E.; Smalley, R. E., Crystalline Ropes of Metallic Carbon Nanotubes. *Science* **1996,** *273*, 483-487.

5.   Prasek, J.; Drbohlavova, J.; Chomoucka, J.; Hubalek, J.; Jasek, O.; Adam, V.; Kizek, R., Methods for carbon nanotubes synthesis-review. *J. Mater. Chem.* **2011,** *21*, 15872-15884.

6.   Bodwell, G., Carbon nanotubes: growth potential. *Nat. Nanotechnol.* **2010,** *5*, 103-104.

7.   Jasti, R.; Bertozzi, C. R., Progress and challenges for the bottom-up synthesis of carbon nanotubes with discrete chirality. *Chem. Phys. Lett.* **2010,** *494*, 1-7.

8.   Tian, X.; Jasti, R., Synthesis of Cycloparaphenylenes: The Shortest-Possible Segments of Armchair Carbon Nanotubes. In *Fragments of Fullerenes and Carbon Nanotubes: Designed Synthesis, Unusual Reactions, and Coordination Chemistry*, Petrukhina, M. A.; Scott, L. T., Eds. Wiley: 2011.

9.   Scott, L. T., Polycyclic Aromatic Hydrocarbon Bowls, Baskets, Balls, and Tubes: Challenging Targets for Chemical Synthesis. *Polycyclic Aromat. Compd.* **2010,** *30*, 247-259.

10.   Fort, E. H.; Donovan, P. M.; Scott, L. T., Diels−Alder Reactivity of Polycyclic Aromatic Hydrocarbon Bay Regions: Implications for Metal-Free Growth of Single-Chirality Carbon Nanotubes. *J. Am. Chem. Soc.* **2009,** *131*, 16006-16007.

11.   Steinberg, B.; Scott, L., New strategies for synthesizing short sections of carbon nanotubes. *Angew. Chem. Int. Ed.* **2009,** *48*, 5400-5402.

12.   Fort, E. H.; Scott, L. T., One-Step Conversion of Aromatic Hydrocarbon Bay Regions into Unsubstituted Benzene Rings: A Reagent for the Low-Temperature, Metal-Free Growth of Single-Chirality Carbon Nanotubes. *Angew. Chem.* **2010,** *122*, 6776-6778.

13.   Fort, E. H.; Scott, L. T., Carbon nanotubes from short hydrocarbon templates. Energy analysis of the Diels-Alder cycloaddition/rearomatization growth strategy. *J. Mater. Chem.* **2011,** *21*, 1373-1381.

14.   Li, H.-B.; Page, A.; Irle, S.; Morokuma, K., Theoretical insights into chirality-controlled SWCNT growth from a cycloparaphenylene template. *ChemPhysChem* **2012,** *13*, 1479-1485.

15.   Kim, J.; Page, A.; Irle, S.; Morokuma, K., Dynamics of local chirality during SWCNT growth: armchair versus zigzag nanotubes. *J. Am. Chem. Soc.* **2012,** *134*, 9311-9319.

16.   Omachi, H.; Segawa, Y.; Itami, K., Synthesis of Cycloparaphenylenes and Related Carbon Nanorings: A Step toward the Controlled Synthesis of Carbon Nanotubes. *Acc. Chem. Res.* **2012**, 1378-1389.

17.   Bunz, U.; Menning, S.; Martín, N., para-Connected Cyclophenylenes and Hemispherical Polyarenes: Building Blocks for Single-Walled Carbon Nanotubes. *Angew. Chem. Int. Ed.* **2012,** *51*, 7094-7101.

18.   Schrettl, S.; Frauenrath, H., Elements for a rational polymer approach towards carbon nanostructures. *Angew. Chem. Int. Ed.* **2012,** *51*, 6569-6571.

19.   Page, A.; Ohta, Y.; Irle, S.; Morokuma, K., Mechanisms of single-walled carbon nanotube nucleation, growth, and healing determined using QM/MD methods. *Acc. Chem. Res.* **2010,** *43*, 1375-1385.

20.   Segawa, Y.; Fukazawa, A.; Matsuura, S.; Omachi, H.; Yamaguchi, S.; Irle, S.; Itami, K., Combined experimental and theoretical studies on the photophysical properties of cycloparaphenylenes. *Org. Biomol. Chem.* **2012,** *10*, 5979-5984.

21.   Iwamoto, T.; Watanabe, Y.; Sakamoto, Y.; Suzuki, T.; Yamago, S., Selective and Random Syntheses of [n]Cycloparaphenylenes (n = 8–13) and Size Dependence of Their Electronic Properties. *J. Am. Chem. Soc.* **2011,** *133*, 8354-8361.

22.   Jasti, R.; Chattacharjee, J.; Neaton, J. B.; Bertozzi, C. R., Synthesis, Characterization, and Theory of [9]-, [12]-, and [18]Cycloparaphenylene: Carbon Nanohoop Structures. *J. Am. Chem. Soc.* **2008,** *130*, 17646-17647.

23.   Sisto, T. J.; Golder, M. R.; Hirst, E. S.; Jasti, R., Selective Synthesis of Strained [7]Cycloparaphenylene: An Orange-Emitting Fluorophore. *J. Am. Chem. Soc.* **2011,** *133*, 15800-15802.

24.   Xia, J.; Jasti, R., Synthesis, Characterization, and Crystal Structure of [6]Cycloparaphenylene. *Angew. Chem. Int. Ed.* **2012,** *51*, 2474-2476.

25.   Xia, J.; Bacon, J. W.; Jasti, R., Gram-Scale Synthesis and Crystal Structures of [8]- and [10]CPP, and the Solid-State Structure of C60@[10]CPP. *Chem. Sci.* **2012,** *3*, 3018-3021.

26.   Wong, B. M., Optoelectronic Properties of Carbon Nanorings: Excitonic Effects from Time-Dependent Density Functional Theory. *J. Phys. Chem. C* **2009,** *113*, 21921-21927.

27.   Iwamoto, T.; Watanabe, Y.; Sadahiro, T.; Haino, T.; Yamago, S., Size-Selective Encapsulation of C60 by [10]Cycloparaphenylene: Formation of the Shortest Fullerene-Peapod. *Angew. Chem. Int. Ed.* **2011,** *50*, 8342-8344.

28.   Parekh, V. C.; Guha, P. C., Synthesis of p,p'-diphenylene disulfide. *J. Indian. Chem. Soc.* **1934,** *11*, 95-100.

29.   Friederich, R.; Nieger, M.; Vögtle, F., Auf dem Weg zu makrocyclischen para-Phenylenen. *Chem. Ber.* **1993,** *126*, 1723-1732.

30.   Darzi, E. R.; Sisto, T. J.; Jasti, R., Selective Syntheses of [7]–[12]Cycloparaphenylenes Using Orthogonal Suzuki–Miyaura Cross-Coupling Reactions. *J. Org. Chem.* **2012,** *77*, 6624-6628.

31.   Takaba, H.; Omachi, H.; Yamamoto, Y.; Bouffard, J.; Itami, K., Selective Synthesis of [12]Cycloparaphenylene. *Angew. Chem. Int. Ed.* **2009,** *48*, 6112-6116.

32.   Omachi, H.; Matsuura, S.; Segawa, Y.; Itami, K., A Modular and Size-Selective Synthesis of [n]Cycloparaphenylenes: A Step toward the Selective Synthesis of [n,n] Single-Walled Carbon Nanotubes. *Angew. Chem. Int. Ed.* **2010,** *49*, 10202-10205.

33.   Segawa, Y.; Miyamoto, S.; Omachi, H.; Matsuura, S.; Šenel, P.; Sasamori, T.; Tokitoh, N.; Itami, K., Concise Synthesis and Crystal Structure of [12]Cycloparaphenylene. *Angew. Chem. Int. Ed.* **2011,** *50*, 3244-3248.

34.   Segawa, Y.; Šenel, P.; Matsuura, S.; Omachi, H.; Itami, K., [9]
        Cycloparaphenylene: Nickel-mediated Synthesis and Crystal Structure. *Chem. Lett.* **2011,** *40*, 423-425.

35.   Ishii, Y.; Nakanishi, Y.; Omachi, H.; Matsuura, S.; Matsui, K.; Shinohara, H.;
        Segawa, Y.; Itami, K., Size-selective synthesis of [9]–[11] and
        [13]cycloparaphenylenes. *Chem. Sci.* **2012,** *3*, 2340-2345.

36.   Yamago, S.; Watanabe, Y.; Iwamoto, T., Synthesis of [8]Cycloparaphenylene
        from a Square-Shaped Tetranuclear Platinum Complex. *Angew. Chem. Int. Ed.*
        2010, *49*, 757-759.

37.   Kayahara, E.; Sakamoto, Y.; Suzuki, T.; Yamago, S., Selective Synthesis and
        Crystal Structure of [10]Cycloparaphenylene. *Org. Lett.* **2012,** *14*, 3284-3287.

38.   Hitosugi, S.; Nakanishi, W.; Yamasaki, T.; Isobe, H., Bottom-up synthesis of
        finite models of helical (*n,m*)-single-wall carbon nanotubes. *Nat Commun* **2011,** *2*,
        492-496.

39.   Hitosugi, S.; Yamasaki, T.; Isobe, H., Bottom-up Synthesis and Thread-in-Bead
        Structures of Finite (*n*,0)-Zigzag Single-Wall Carbon Nanotubes. *J. Am. Chem.
        Soc.* **2012,** *134*, 12442-12445.

40.   Sato, S.; Yamasaki, T.; Isobe, H., Solid-state structures of peapod bearings
        composed of finite single-wall carbon nanotube and fullerene molecules. *Proc.
        Natl. Acad. Sci. U. S. A.* **2014,** *111*, 8374-8379.

41.   Matsuno, T.; Sato, S.; Iizuka, R.; Isobe, H., Molecular recognition in curved π-
        systems: effects of π-lengthening of tubular molecules on thermodynamics and
        structures. *Chem. Sci.* **2015,** *6*, 909-916.

42.   Yagi, A.; Segawa, Y.; Itami, K., Synthesis and properties of [9]cyclo-1,4-
        naphthylene: a π-extended carbon nanoring. *J. Am. Chem. Soc.* **2012,** *134*, 2962-
        2965.

43.   Matsui, K.; Segawa, Y.; Itami, K., Synthesis and properties of
        cycloparaphenylene-2,5-pyridylidene: a nitrogen-containing carbon nanoring.
        Org. Lett. **2012,** *14*, 1888-1891.

44. Matsui, K.; Segawa, Y.; Namikawa, T.; Kamada, K.; Itami, K., Synthesis and properties of all-benzene carbon nanocages: a junction unit of branched carbon nanotubes. *Chem. Sci.* **2013,** *4*, 84-88.

45. Matsui, K.; Segawa, Y.; Itami, K., All-Benzene Carbon Nanocages: Size-Selective Synthesis, Photophysical Properties, and Crystal Structure. *J. Am. Chem. Soc.* **2014,** *136*, 16452-16458.

46. Iwamoto, T.; Kayahara, E.; Yasuda, N.; Suzuki, T.; Yamago, S., Synthesis, Characterization, and Properties of [4]Cyclo-2,7-pyrenylene: Effects of Cyclic Structure on the Electronic Properties of Pyrene Oligomers. *Angew. Chem. Int. Ed.* **2014,** *53*, 6430-6434.

47. Golling, F. E.; Quernheim, M.; Wagner, M.; Nishiuchi, T.; Müllen, K., Concise Synthesis of 3D π-Extended Polyphenylene Cylinders. *Angew. Chem. Int. Ed.* **2014,** *53*, 1525-1528.

48. Quernheim, M.; Golling, F. E.; Zhang, W.; Wagner, M.; Räder, H.-J.; Nishiuchi, T.; Müllen, K., The Precise Synthesis of Phenylene-Extended Cyclic Hexa-peri-hexabenzocoronenes from Polyarylated [*n*]Cycloparaphenylenes by the Scholl Reaction. *Angew. Chem. Int. Ed.* **2015,** *54*, 10341-10346.

49. Sisto, T. J.; Tian, X.; Jasti, R., Synthesis of Tetraphenyl-Substituted [12]Cycloparaphenylene: Toward a Rationally Designed Ultrashort Carbon Nanotube. *J. Org. Chem.* **2012,** *77*, 5857-5860.

50. He, Z.; Xu, X.; Zheng, X.; Ming, T.; Miao, Q., Conjugated macrocycles of phenanthrene: a new segment of [6,6]-carbon nanotube and solution-processed organic semiconductors. *Chem. Sci.* **2013,** *4*, 4525-4531.

51. Neuhaus, P.; Cnossen, A.; Gong, J. Q.; Herz, L. M.; Anderson, H. L., A Molecular Nanotube with Three-Dimensional π-Conjugation. *Angew. Chem. Int. Ed.* **2015,** *54*, 7344-7348.

52. Chuang, K. V.; Navarro, R.; Reisman, S. E., *Chem. Sci.* **2011,** *2*, 1086-1089.

53. Mo, F.; Jiang, Y.; Qiu, D.; Zhang, Y.; Wang, J., Direct Conversion of Arylamines to Pinacol Boronates: A Metal-Free Borylation Process. *Angew. Chem. Int. Ed.* **2010,** *49*, 1846-1849.

54.   Gómez-López, M.; Preece, J. A.; Stoddart, J. F., The art and science of self-assembling molecular machines. *Nanotechnology* **1996,** *7*, 183.

55.   Balzani, V.; Credi, A.; Raymo, F. M.; Stoddart, J. F., Artificial Molecular Machines. *Angew. Chem. Int. Ed.* **2000,** *39*, 3348-3391.

56.   Pease, A. R.; Jeppesen, J. O.; Stoddart, J. F.; Luo, Y.; Collier, C. P.; Heath, J. R., Switching Devices Based on Interlocked Molecules. *Acc. Chem. Res.* **2001,** *34*, 433-444.

57.   Tseng, H.-R.; Vignon, S. A.; Stoddart, J. F., Toward Chemically Controlled Nanoscale Molecular Machinery. *Angew. Chem. Int. Ed.* **2003,** *42*, 1491-1495.

58.   Badjić, J. D.; Balzani, V.; Credi, A.; Silvi, S.; Stoddart, J. F., A Molecular Elevator. *Science* **2004,** *303*, 1845-1849.

59.   Moonen, N.; Flood, A.; Fernández, J.; Stoddart, J., Towards a Rational Design of Molecular Switches and Sensors from their Basic Building Blocks Molecular Machines. *Top. Curr. Chem.* **2005,** *262*, 99-132.

60.   Landge, S. M.; Aprahamian, I., A pH Activated Configurational Rotary Switch: Controlling the *E/Z* Isomerization in Hydrazones. *J. Am. Chem. Soc.* **2009,** *131*, 18269-18271.

61.   Wong, B. M., *Comput. Chem.* **2009,** *30*, 51-56.

62.   Osuna, S.; Swart, M.; Solà, M., *J. Phys. Chem. A* **2011,** *115*, 3491-3496.

63.   Zambrini, L.; Fabris, F.; De, O.; Gardenal, G.; Visentin, F.; Canovese, L., Heck self-condensation of polycyclic haloalkenes: the case of (1R)-2-iodobornene. *Tetrahedron* **2001,** *57*, 8719-8724.

64.   Fabris, F.; Zambrini, L.; Rosso, E.; De Lucchi, O., Comparative Cyclotrimerisation of Enantiopure vic-Bromo(trimethylstannyl)bicycloalkenes Derived from (+)-Camphor, (+)-Fenchocamphorone and (−)-Epicamphor: Effect of the Bridgehead Methyl Group on the syn/anti Product Ratios. *Eur. J. Org. Chem.* **2004,** *2004*, 3313-3322.

65. Fabris, F.; Leoni, L.; De Lucchi, O., Synthesis and cycloaddition reactions of 1,1′-dimenthene. *Tetrahedron Lett.* **1999,** *40*, 1223-1226.

66. Ishii, Y.; Matsuura, S.; Segawa, Y.; Itami, K., Synthesis and Dimerization of Chloro[10]cycloparaphenylene: A Directly Connected Cycloparaphenylene Dimer. *Org. Lett.* **2014,** *16*, 2174-2176.

67. Pangborn, A. B.; Giardello, M. A.; Grubbs, R. H.; Rosen, R. K.; Timmers, F. J., Safe and Convenient Procedure for Solvent Purification. *Organometallics* **1996,** *15*, 1518-1520.

68. Chuang, K. V.; Navarro, R.; Reisman, S. E., Benzoquinone-derived sulfinyl imines as versatile intermediates for alkaloid synthesis: Total synthesis of (-)-3-demethoxyerythratidinone. *Chem. Sci.* **2011,** *2*, 1086-1089.

69. Williams, A. T. R.; Winfield, S. A.; Miller, J. N., Relative fluorescence quantum yields using a computer-controlled luminescence spectrometer. *Analyst* **1983,** *108*, 1067-1071.

70. Frisch, M. J.; Trucks, G. W.; Schlegel, H. B.; Scuseria, G. E.; Robb, M. A.; Cheeseman, J. R.; Scalmani, G.; Barone, V.; Mennucci, B.; Petersson, G. A.; Nakatsuji, H.; Caricato, M.; Li, X.; Hratchian, H. P.; Izmaylov, A. F.; Bloino, J.; Zheng, G.; Sonnenberg, J. L.; Hada, M.; Ehara, M.; Toyota, K.; Fukuda, R.; Hasegawa, J.; Ishida, M.; Nakajima, T.; Honda, Y.; Kitao, O.; Nakai, H.; Vreven, T.; Montgomery, J. A.; Peralta, J. E.; Ogliaro, F.; Bearpark, M.; Heyd, J. J.; Brothers, E.; Kudin, K. N.; Staroverov, V. N.; Kobayashi, R.; Normand, J.; Raghavachari, K.; Rendell, A.; Burant, J. C.; Iyengar, S. S.; Tomasi, J.; Cossi, M.; Rega, N.; Millam, J. M.; Klene, M.; Knox, J. E.; Cross, J. B.; Bakken, V.; Adamo, C.; Jaramillo, J.; Gomperts, R.; Stratmann, R. E.; Yazyev, O.; Austin, A. J.; Cammi, R.; Pomelli, C.; Ochterski, J. W.; Martin, R. L.; Morokuma, K.; Zakrzewski, V. G.; Voth, G. A.; Salvador, P.; Dannenberg, J. J.; Dapprich, S.; Daniels, A. D.; Farkas; Foresman, J. B.; Ortiz, J. V.; Cioslowski, J.; Fox, D. J., Gaussian 09, Revision B.01. Wallingford CT, 2009.

71. Becke, A. D., Density-functional thermochemistry. III. The role of exact exchange. *J. Chem. Phys.* **1993,** *98*, 5648-5652.

72. Grimme, S., Semiempirical GGA-type density functional constructed with a long-range dispersion correction. *J. Comput. Chem.* **2006,** *27*, 1787-1799.

Chapter V

1.   Scott, L. T., Conjugated Belts and Nanorings with Radially Oriented p Orbitals. *Angew. Chem. Int. Ed.* **2003,** *42*, 4133-4135.

2.   Tahara, K.; Tobe, Y., Molecular Loops and Belts. *Chem. Rev.* **2006,** *106*, 5274-5290.

3.   Eisenberg, D.; Shenhar, R.; Rabinovitz, M., Synthetic approaches to aromatic belts: building up strain in macrocyclic polyarenes. *Chem. Soc. Rev.* **2010,** *39*, 2879-2890.

4.   Evans, P. J.; Jasti, R., Molecular Belts. *Top. Curr. Chem.* **2013**, 1-42.

5.   Nakamura, E.; Tahara, K.; Matsuo, Y.; Sawamura, M., Synthesis, Structure, and Aromaticity of a Hoop-Shaped Cyclic Benzenoid [10]Cyclophenacene. *J. Am. Chem. Soc.* **2003,** *125*, 2834-2835.

6.   Choi, H. S.; Kim, K. S., Structures, Magnetic Properties, and Aromaticity of Cyclacenes. *Angew. Chem. Int. Ed.* **1999,** *38*, 2256-2258.

7.   Kohnke, F. H.; Slawin, A. M. Z.; Stoddart, J. F.; Williams, D. J., Molecular Belts and Collars in the Making: A Hexaepoxyoctacosahydro[12]cyclacene Derivative. *Angew. Chem. Int. Ed.* **1987,** *26*, 892-894.

8.   Ashton, P. R.; Isaacs, N. S.; Kohnke, F. H.; Slawin, A. M. Z.; Spencer, C. M.; Stoddart, J. F.; Williams, D. J., Towards the Making of [12]Collarene. *Angew. Chem. Int. Ed.* **1988,** *27*, 966-969.

9.   Girreser, U.; Giuffrida, D.; Kohnke, F. H.; Mathias, J. P.; Philp, D.; Stoddart, J. F., The structure-directed synthesis of cyclacene and polyacene derivatives. *Pure Appl. Chem.* **1993,** *65*, 119-119.

10.   Cory, R. M.; McPhail, C. L.; Dikmans, A. J.; Vittal, J. J., Macrocyclic cyclophane belts via double Diels-Alder cycloadditions: Macroannulation of bisdienes by bisdienophiles. Synthesis of a key precursor to an [8]cyclacene. *Tetrahedron Lett.* **1996,** *37*, 1983-1986.

11.   Cory, R. M.; McPhail, C. L., Transformations of a macrocyclic cyclophane belt into advanced [8]cyclacene and [8]cyclacene triquinone precursors. *Tetrahedron Lett.* **1996,** *37*, 1987-1990.

12.   Wolf Dietrich, N.; Dieter, L.; Maribel, A.; Schlüter, A. D., The Carbon Skeleton of the Belt Region of Fullerene C_{84} (*D₂*). *Chem. Eur. J.* **2003,** *9*, 2745-2757.

13.   Stuparu, M.; Gramlich, V.; Stanger, A.; Schlüter, A. D., Double-Stranded Cycles: Toward C_{84}'s Belt Region. *J. Org. Chem.* **2007,** *72*, 424-430.

14.   Mihaiela, S.; Dieter, L.; Heinz, R.; Schlüter, A. D., Exploring the Chemistry of a Double-Stranded Cycle with the Carbon Skeleton of the Belt Region of the C_{84} Fullerene. *Eur. J. Org. Chem.* **2007,** *2007*, 88-100.

15.   Chagit, D.; Alexander, E.; Walter, A.; Amnon, S.; Mihaiela, S.; Schlüter, A. D., Towards a Fully Conjugated, Double-Stranded Cycle: A Mass Spectrometric and Theoretical Study. *Chem. Eur. J.* **2008,** *14*, 1628-1637.

16.   Iyoda, M.; Kuwatani, Y.; Yamauchi, T.; Oda, M., A simple and efficient synthesis of cisoid, transoid, transoid- and all-cisoid-trimers of benzocyclobutene; a novel formation of *Z,Z,Z*-tribenz[12]annulene from the latter trimer. *J. Chem. Soc., Chem. Commun.* **1988**, 65-66.

17.   Diercks, R.; Vollhardt, K. P. C., Tris(benzocyclobutadieno)benzene, the Triangular [4]Phenylene with a Completely Bond-Fixed Cyclohexatriene Ring: Cobalt-Catalyzed Synthesis from Hexaethynylbenzene and Thermal Ring Opening to 1,2:5,69,10-Tribenzo-3,4,7,8,11,12-hexadehydro[12]-annulene *J. Am. Chem. Soc.* **1986,** *108*, 3150-3152.

18.   Debra, L. M.; Vollhardt, K. P. C.; Stefan, W., Facile Hydrogenation of the Central Cyclohexatriene of Tris(benzocyclobutadieno)benzene: Synthesis, Structure, and Thermal and Photochemical Isomerization of all cis Tris(benzocyclobuta)cyclohexane. *Angew. Chem. Int. Ed.* **1990,** *29*, 1151-1154.

19.   Deichmann, M.; Näther, C.; Herges, R., Pyrolysis of a tubular aromatic compound. *Org. Lett.* **2003,** *5*, 1269-1271.

20.   Kammermeier, S.; Jones, P. G.; Herges, R., Ring-Expanding Metathesis of Tetradehydro-anthracene—Synthesis and Structure of a Tubelike, Fully Conjugated Hydrocarbon. *Angew. Chem. Int. Ed.* **1996,** *35*, 2669-2671.

21.   Kammermeier, S.; Jones, P. G.; Herges, R., Beltlike Aromatic Hydrocarbons by Metathesis Reaction with Tetradehydrodianthracene. *Angew. Chem. Int. Ed.* **1997,** *36*, 2200-2202.

22.   Nishiuchi, T.; Feng, X.; Enkelmann, V.; Wagner, M.; Müllen, K., Three-Dimensionally Arranged Cyclic *p*-Hexaphenylbenzene: Toward a Bottom-Up Synthesis of Size-Defined Carbon Nanotubes. *Chem. Eur. J.* **2012,** *18*, 16621-16625.

23.   Golling, F. E.; Quernheim, M.; Wagner, M.; Nishiuchi, T.; Müllen, K., Concise Synthesis of 3D π-Extended Polyphenylene Cylinders. *Angew. Chem. Int. Ed.* **2014,** *53*, 1525-1528.

24.   Quernheim, M.; Golling, F. E.; Zhang, W.; Wagner, M.; Räder, H.-J.; Nishiuchi, T.; Müllen, K., The Precise Synthesis of Phenylene-Extended Cyclic Hexa-peri-hexabenzocoronenes from Polyarylated [*n*]Cycloparaphenylenes by the Scholl Reaction. *Angew. Chem. Int. Ed.* **2015**, *54*, 10341-10346.

25.   Bonifacio, M. C.; Robertson, C. R.; Jung, J.-Y.; King, B. T., Polycyclic Aromatic Hydrocarbons by Ring-Closing Metathesis. *J. Org. Chem.* **2005,** *70*, 8522-8526.

26.   Sakurai, H.; Daiko, T.; Hirao, T., A Synthesis of Sumanene, a Fullerene Fragment. *Science* **2003,** *301*, 1878.

27.   Kumar, B.; Viboh, R. L.; Bonifacio, M. C.; Thompson, W. B.; Buttrick, J. C.; Westlake, B. C.; Kim, M.-S.; Zoellner, R. W.; Varganov, S. A.; Mörschel, P.; Teteruk, J.; Schmidt, M. U.; King, B. T., Septulene: The Heptagonal Homologue of Kekulene. *Angew. Chem. Int. Ed.* **2012,** *51*, 12795-12800.

28.   Kalstabakken, K. A.; Harned, A. M., Asymmetric transformations of achiral 2,5-cyclohexadienones. *Tetrahedron* **2014,** *70*, 9571-9585.

29.   Harned, A. M., Asymmetric oxidative dearomatizations promoted by hypervalent iodine(III) reagents: an opportunity for rational catalyst design? *Tetrahedron Lett.* **2014,** *55*, 4681-4689.

30.   Molander, G. A.; Rivero, M. R., Suzuki Cross-Coupling Reactions of Potassium Alkenyltrifluoroborates†. *Org. Lett.* **2002,** *4*, 107-109.

31.   Molander, G. A.; Bernardi, C. R., Suzuki−Miyaura Cross-Coupling Reactions of Potassium Alkenyltrifluoroborates. *J. Org. Chem.* **2002,** *67*, 8424-8429.

32.   Molander, G. A.; Felix, L. A., Stereoselective Suzuki−Miyaura Cross-Coupling Reactions of Potassium Alkenyltrifluoroborates with Alkenyl Bromides. *J. Org. Chem.* **2005,** *70*, 3950-3956.

33.   Hanessian, S.; Giroux, S.; Larsson, A., Efficient Allyl to Propenyl Isomerization in Functionally Diverse Compounds with a Thermally Modified Grubbs Second-Generation Catalyst. *Org. Lett.* **2006,** *8*, 5481-5484.

34.   Hassam, M.; Taher, A.; Arnott, G. E.; Green, I. R.; van Otterlo, W. A. L., Isomerization of Allylbenzenes. *Chem. Rev.* **2015,** *115*, 5462-5569.

35.   Bosch, M.; Schlaf, M., Synthesis of Allyl and Alkyl Vinyl Ethers Using an in Situ Prepared Air-Stable Palladium Catalyst. Efficient Transfer Vinylation of Primary, Secondary, and Tertiary Alcohols. *J. Org. Chem.* **2003,** *68*, 5225-5227.

36.   Okimoto, Y.; Sakaguchi, S.; Ishii, Y., Development of a Highly Efficient Catalytic Method for Synthesis of Vinyl Ethers. *J. Am. Chem. Soc.* **2002,** *124*, 1590-1591.

37.   Bodwell, G. J.; Bridson, J. N.; Houghton, T. J.; Kennedy, J. W. J.; Mannion, M. R., 1,7-Dioxa[7](2,7)pyrenophane: The Pyrene Moiety Is More Bent than That of C70. *Chem. Eur. J.* **1999,** *5*, 1823-1827.

38.   Bodwell, G. J.; Fleming, J. J.; Miller, D. O., Non-planar aromatic compounds. Part 4: Fine tuning the degree of bend in the pyrene moiety of [7](2,7)pyrenophanes by modifying the nature of the bridge. *Tetrahedron* **2001,** *57*, 3577-3585.

39.   Dobrowolski, M. A.; Cyrański, M. K.; Merner, B. L.; Bodwell, G. J.; Wu, J. I.; Schleyer, P. v. R., Interplay of π-Electron Delocalization and Strain in [*n*](2,7)Pyrenophanes. *J. Org. Chem.* **2008,** *73*, 8001-8009.

40.   Merner, B. L.; Dawe, L. N.; Bodwell, G. J., 1,1,8,8-Tetramethyl[8](2,11)teropyrenophane: Half of an Aromatic Belt and a Segment of an (8,8) Single-Walled Carbon Nanotube. *Angew. Chem. Int. Ed.* **2009,** *48*, 5487-5491.

41. Merner, B. L.; Unikela, K. S.; Dawe, L. N.; Thompson, D. W.; Bodwell, G. J., 1,1,*n,n*-Tetramethyl[*n*](2,11)teropyrenophanes (*n* = 7-9): a series of armchair SWCNT segments. *Chem. Commun.* **2013,** *49*, 5930-5932.

42. Ghasemabadi, P. G.; Yao, T.; Bodwell, G. J., Cyclophanes containing large polycyclic aromatic hydrocarbons. *Chem. Soc. Rev.* **2015**.

43. Yagi, A.; Segawa, Y.; Itami, K., Synthesis and properties of [9]cyclo-1,4-naphthylene: a π-extended carbon nanoring. *J. Am. Chem. Soc.* **2012,** *134*, 2962-2965.

44. Iwamoto, T.; Kayahara, E.; Yasuda, N.; Suzuki, T.; Yamago, S., Synthesis, Characterization, and Properties of [4]Cyclo-2,7-pyrenylene: Effects of Cyclic Structure on the Electronic Properties of Pyrene Oligomers. *Angew. Chem. Int. Ed.* **2014,** *53*, 6430-6434.

45. Vermeulen, N. A.; Karagiaridi, O.; Sarjeant, A. A.; Stern, C. L.; Hupp, J. T.; Farha, O. K.; Stoddart, J. F., Aromatizing Olefin Metathesis by Ligand Isolation inside a Metal– Organic Framework. *J. Am. Chem. Soc.* **2013,** *135*, 14916-14919.

46. Kinzel, T.; Zhang, Y.; Buchwald, S. L., A New Palladium Precatalyst Allows for the Fast Suzuki−Miyaura Coupling Reactions of Unstable Polyfluorophenyl and 2-Heteroaryl Boronic Acids. *J. Am. Chem. Soc.* **2010,** *132*, 14073-14075.

47. Clar, E.; John, F.; Avenarius, R., Benzologen des Pentaphens und ihre Abkömmlinge. *Ber. dtsch. chem. Ges.* **1939,** *72*, 2139-2147.

48. Segawa, Y.; Šenel, P.; Matsuura, S.; Omachi, H.; Itami, K., [9] Cycloparaphenylene: Nickel-mediated Synthesis and Crystal Structure. *Chem. Lett.* **2011,** *40*, 423-425.

49. Iwamoto, T.; Watanabe, Y.; Sakamoto, Y.; Suzuki, T.; Yamago, S., Selective and Random Syntheses of [*n*]Cycloparaphenylenes (*n* = 8–13) and Size Dependence of Their Electronic Properties. *J. Am. Chem. Soc.* **2011,** *133*, 8354-8361.

50. Darzi, E. R.; Sisto, T. J.; Jasti, R., Selective Syntheses of [7]–[12]Cycloparaphenylenes Using Orthogonal Suzuki–Miyaura Cross-Coupling Reactions. *J. Org. Chem.* **2012,** *77*, 6624-6628.

51.   Hanwell, M.; Curtis, D.; Lonie, D.; Vandermeersch, T.; Zurek, E.; Hutchison, G., Avogadro: An advanced semantic chemical editor, visualization, and analysis platform. *J. Chem. Inf.* **2012,** *4*, 17.

52.   Segawa, Y.; Omachi, H.; Itami, K., Theoretical Studies on the Structures and Strain Energies of Cycloparaphenylenes. *Org. Lett.* **2010,** *12*, 2262-2265.

53.   Pangborn, A. B.; Giardello, M. A.; Grubbs, R. H.; Rosen, R. K.; Timmers, F. J., Safe and Convenient Procedure for Solvent Purification. *Organometallics* **1996,** *15*, 1518-1520.

54.   Spring, D. R.; Krishnan, S.; Blackwell, H. E.; Schreiber, S. L., Diversity-Oriented Synthesis of Biaryl-Containing Medium Rings Using a One Bead/One Stock Solution Platform. *J. Am. Chem. Soc.* **2002,** *124*, 1354-1363.

55.   Hu, J.; Hirao, H.; Li, Y.; Zhou, J., Palladium-Catalyzed Asymmetric Intermolecular Cyclization. *Angew. Chem. Int. Ed.* **2013,** *52*, 8676-8680.

56.   Sisto, T. J.; Golder, M. R.; Hirst, E. S.; Jasti, R., Selective Synthesis of Strained [7]Cycloparaphenylene: An Orange-Emitting Fluorophore. *J. Am. Chem. Soc.* **2011,** *133*, 15800-15802.

57.   Daniels, R. N.; Fadeyi, O. O.; Lindsley, C. W., A New Catalytic Cu(II)/Sparteine Oxidant System for β,β-Phenolic Couplings of Styrenyl Phenols: Synthesis of Carpanone and Unnatural Analogs. *Org. Lett.* **2008,** *10*, 4097-4100.

58.   Sheldrick, G. M. *Bruker/Siemens Area Detector Absorption Correction Program*, Bruker AXS: Madison, WI, 1998.

59.   Sluis, P. V. d.; Spek, A. L., BYPASS: an effective method for the refinement of crystal structures containing disordered solvent regions. *Acta Cryst.* **1990,** *A46*, 194-201.

60.   Sheldrick, G. M., A short history of SHELX. *Acta Cryst.* **2008,** *A64*, 112-122.